A PETROLOGIC INVESTIGATION OF DEEP-CRUSTAL AND UPPER-MANTLE XENOLITHS FROM THE SIERRA NEVADA, CALIFORNIA; CONSTRAINTS ON LITHOSPHERIC COMPOSITION BENEATH CONTINENTAL ARCS AND THE ORIGIN OF CORDILLERAN BATHOLITHS

Thesis by

Mihai Nicolae Ducea

in Partial Fulfillment of the Requirements

for the Degree of

Doctor of Philosophy

California Institute of Technology

Pasadena, California

1998

(submitted April 30, 1998)

Chapter 2 reprinted from *Journal of Geophysical Research volume **101**,*

Mihai N. Ducea and Jason B. Saleeby, "Buoyancy sources for a large, unrooted mountain

range, the Sierra Nevada, California; Evidence from xenolith thermobarometry,"

pages 8029-8044, © 1996

with kind permission from the American Geophysical Union,

2000 Florida Avenue, NW, Washington, D.C. 20009, USA

Chapter 3 in press at *Contributions to Mineralogy and Petrology*,

Mihai N. Ducea and Jason B. Saleeby, "The age and origin of a thick mafic-ultramafic root

from beneath the Sierra Nevada batholith, California," © 1998, Springer Verlag, Berlin.

Chapter 6 reprinted from *Earth and Planetary Sciences Letters,* volume **156**,

Mihai Ducea and Jason Saleeby, "Crustal recycling beneath continental arcs: silica-rich

glass inclusions in ultramafic xenoliths from the Sierra Nevada, California,"

pages 101-116, © 1998,

with kind permission from Elsevier Science Ltd.,

Sara Burgerhartstraat 25, 1055 KV Amsterdam, The Netherlands

Chapter 7 reprinted from *International Geology Review*, volume **40**,

Mihai Ducea and Jason Saleeby, "A case for delamination of the deep batholithic crust

beneath the Sierra Nevada, California," pages 78-93, © 1998

with kind permission from V.H. Winston & Son, Inc. and Belwether Publishing, Ltd.,

8640 Guilford Road, 200, Columbia, MD 21045, USA

Acknowledgements

Abstract

There are few direct observations constraining the vertical extent of the large Cordilleran granitic batholiths and their composition at depths greater than 30 km. I present evidence for a ~ 100 km thick sequence of cogenetic rocks which together comprise the Sierra Nevada batholith of California (SNB). The SNB magmatism produced tonalitic and granodioritic magmas which reside in the Sierra Nevada upper- to mid-crust as well as deep crust/upper mantle mafic-ultramafic cumulates. Samples of the mafic-ultramafic sequence are preserved only as xenoliths in Miocene volcanics which erupted through the central part of the batholith. Sm-Nd and Rb-Sr mineral geochronologic analyses were performed on fresh, cumulate textured, garnet pyroxenite, eclogite and gabbroic xenoliths with large grainsize. All samples equilibrated between ~35 and 100 km beneath the batholith and yield Sm-Nd mineral ages between 81 and 136 Ma, broadly coincident with the previously established period of most voluminous batholithic magmatism in the Sierra Nevada.

The whole rock initial $^{87}Sr/^{86}Sr$, $^{143}Nd/^{144}Nd$, $^{206}Pb/^{204}Pb$, $^{207}Pb/^{204}Pb$, $^{208}Pb/^{204}Pb$ and the δ ^{18}O ratios of the igneous xenoliths are similar to the ratios published for the outcrops of the central SNB. I interpret these xenoliths to be magmatically related to the upper- and mid-crustal granitoids, as cumulates and/or restites. This more complete view of the vertical dimension in a batholith demonstrates that a large mass of mafic-ultramafic residue at depth complements the predominantly granitic batholiths, as predicted by mass balance calculations and experimental studies. The SNB magmatism was a large scale process responsible for efficiently segregating a ~30-35 km thick column consisting predominantly of granitoids from a ~ 70 km mafic-ultramafic, mainly eclogite facies root.

Trace element data indicate that these garnet-rich assemblages were in equilibrium at depths of 45 km or more with SNB-like tonalitic-granodioritic melts. I propose that the petrologic mechanisms responsible for "distillation" of large scale granitoids in the central Sierra Nevada are similar to the ones which led to the extraction of the voluminous granitoids that make up the cratonic nucleii of the continents. The large magnitude isotopic

heterogeneity observed in the xenoliths, and the similar range of isotopic ratios measured in surface granitoids, suggest that the compositional variability observed in the surface granitods is primarily inherited from the source rocks in the deeper parts of the lithosphere. The isotopic ratios of the deep-seated residues/cumulates require the existence of three source components for the batholith: (1) a young supracrustal component, represented by Mesozoic accreted arc rocks, (2) a Proterozoic lower crustal (+old lithospheric mantle) component, and (3) a Phanerozoic depleted mantle component. Xenolith data support the hypothesis of lithospheric scale thrusting of accreted masses over the autochtonous crust of western North-America prior to the generation of large volume granitic magmatism in the Sierra Nevada region.

Batholith cumulates/residues resided under the batholith as eclogite facies rocks for at least 70 My after magmatism shutoff. However, mantle xenoliths sampled in younger, Pliocene volcanic rocks contain spinel peridotites which equilibrated over the same depth interval as the garnet pyroxenite assemblages from Miocene pipes. Futhermore, no garnet-bearing samples have been recovered from the Pliocene volcanics. Silica-rich glass inclusions, trapped along grain boundaries of peridotites from Pliocene volcanics, have isotopic compositions similar to the eclogitic keel. These geologic observations as well as geophysical constraints suggest that the thick and dense "eclogitic" root may have foundered in the mantle between Mid- Miocene and Pliocene.

Table of Contents

LIST OF FIGURES

LIST OF TABLES

CHAPTER 1

Introduction

1.1. Background and motivation

Observations of magmatism in continental arcs and granitic batholiths come principally from upper- to mid-crustal levels exposed at the Earth's surface (e.g., Pitcher, 1993). These observations are complemented by experimental studies of the plausible sources and liquid line of descent of arc magmas. A number of first order questions regarding the large scale petrology and tectonics of granitic batholiths cannot be answered by these constraints, owing to the general lack of direct access to the roots of batholiths, the deep crustal counterparts of the plutons exposed at the surface. An outstanding task in continental arc tectonics is to constrain the vertical composition of the continental lithosphere beneath batholiths. This would provide important information necessary to: (1) unambiguously identify the mechanisms and source rocks generating batholithic magmatism, (2) understand the fate of postulated large volume sub-batholith ultramafic residues, and (3) determine the extent to which large volume granitoids represent continental crust internally differentiated through arc magmatism or generated by extraction from the mantle.

The Mesozoic and Cenozoic batholiths found throughout the western U.S. Cordillera (Figure 1-1) formed as a product of the prolonged ocean floor subduction beneath the western margin of the north-American continent (Dickinson, 1981). The Sierra Nevada batholith of California (Figure 1-1) is the type-Cordilleran batholith. The igneous crystallization depths of the rocks presently exposed vary from 0 km represented by large ~100 My caldera deposits preserved in the high Sierra Nevada (Saleeby, 1990), to ~ 30 km in the southernmost Sierra Nevada (Pickett and Saleeby, 1993). Overall, the Sierra Nevada has been preserved as a tilted, but coherent block providing almost continuous exposures of the upper 30 km of a gigantic Mesozoic batholith. There is no

direct information on the composition and vertical extent of the batholith at depths exceeding the equivalent of 1.0 GPa equilibration pressures. Hence, the extent and composition of the batholith at depths greater than ~30-35 km was so far inferred only indirectly from: (1) petrologic constraints borne out of studies of the granitoid outcrops and (2) geophysical observations.

The Cenozoic collapse of the Cordillera at the latitude of the Sierra Nevada and the high magnitude extension to the east of the batholith in the Basin and Range province was accompanied by significant volcanism, which extended into the Sierra Nevada mountain range. As many as 150 small volume flows, pipes and dikes of mafic to intermediate compositions have erupted through the central and southern Sierra Nevada batholith during the Late Cenozoic (Moore and Dodge, 1980). Nineteen of these volcanic occurrences contain upper mantle and/or lower crustal xenoliths (Wilshire et al., 1988; this study).

These xenoliths provide physical evidence for the composition of the deep lithosphere beneath a young continental convergent plate margin, accompanied by large scale magmatism. Deep lithospheric xenoliths, although relatively common in continental environments (Nixon, 1987; Rudnick, 1992), are rarely found in volcanic rocks erupted in continental margin settings, particularly from beneath large Cordilleran (Andean) batholiths. Preliminary petrologic studies of the Sierra Nevada xenolith populations (Domenick et al., 1983; Dodge et al., 1986, 1988; Mukhopadhyay, 1989) suggested that many of the Sierra Nevada nodules may represent the deep counterparts of the composite Mesozoic batholith. One could aquire direct geologic information on the vertical composition of batholiths at significant depths using these xenoliths, if their petrography, depth of residence, age, chemical composition and petrologenesis would be constrained.

This dissertation is a petrologic study of the representative Sierra Nevada xenolith suites. It represents a three-folded effort aimed at: (1) constraining the vertical

Figure 1-1. Location of major batholiths of the North American Cordillera (after Anderson, 1990).

Coast batholith

Idaho batholith

Sierra Nevada
batholith

Peninsular Ranges
batholith

400 km
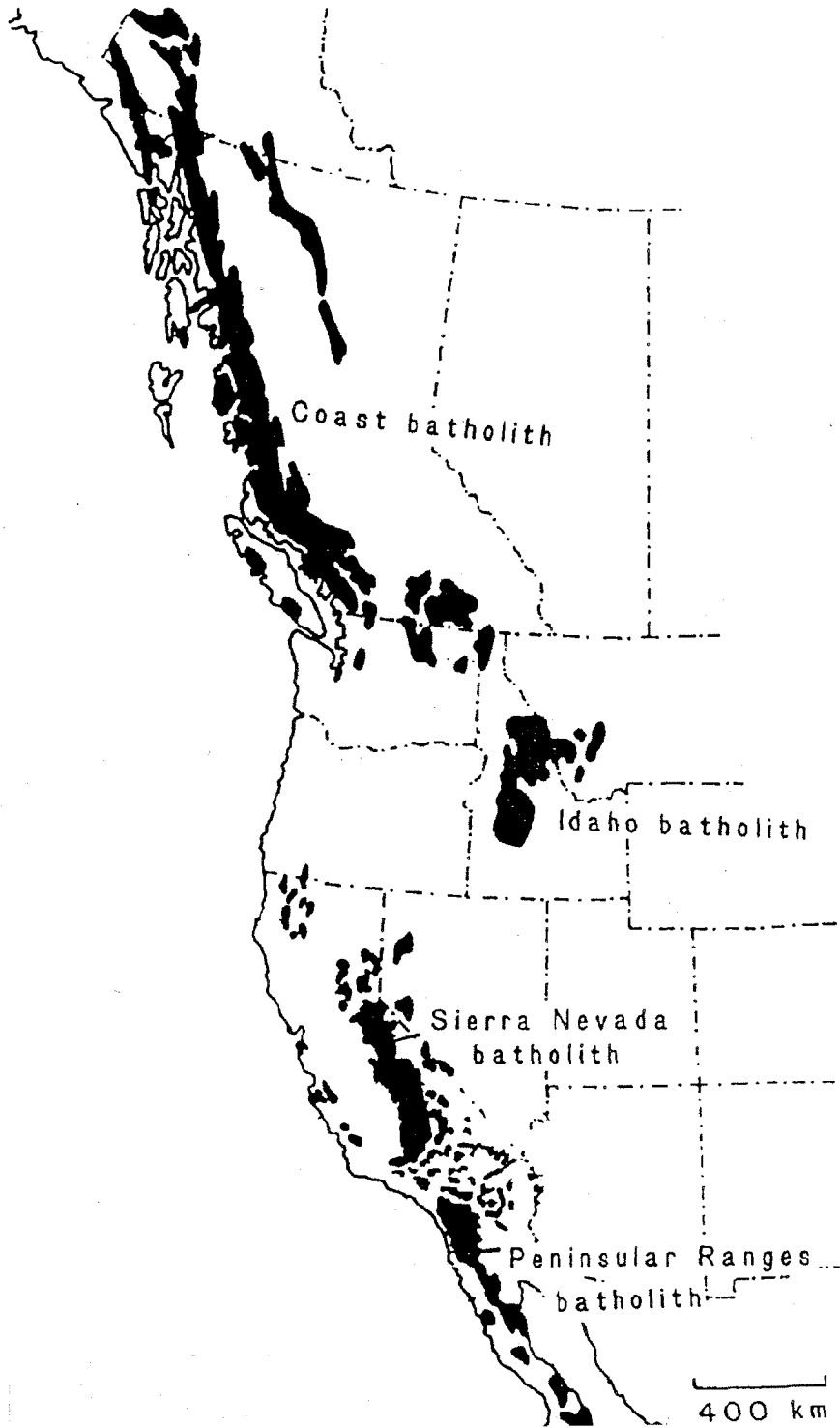
composition of the lithosphere in the central Sierra Nevada region, (2) testing, using the petrologic and geochemical data from (1), various hypotheses proposed to be responsible for the formation of the Sierra Nevada batholith, and (3) deciphering tectonic processes which appear to have triggered a fundamental change in the composition of the sub-batholith lithosphere after the region ceased to be an active magmatic arc and later, also a convergent margin.

1.2. Thesis Outline

This thesis has been organized in seven chapters, including this introduction; the other chapters were written as separate manuscripts. The first two appendices accompany these chapters. Chapter 2 presents an overview of xenolith-bearing volcanic rocks from the central and eastern Sierra Nevada regions, describes the petrography and mineral chemistry of sampled xenoliths, and the results of quantitative thermobarometric determinations performed on selected samples. The thermobarometric results are then used to put some constraints on the vertical composition of the Sierra Nevada lithosphere and determine the sources of buoyancy for the modern Sierra Nevada mountain range.

Chapters 3-5 focus on xenoliths found in Miocene volcanic rocks from the central Sierra Nevada. Chapter 3 presents Sm-Nd and Rb-Sr mineral geochronologic results performed on representative samples of lower crustal and upper mantle xenoliths, in order to elucidate the age of the deep lithosphere beneath the Mesozoic batholith. The geochronologic results suggest batholith consanguinity for the lower Sierran lithosphere and are used to put constraints on the vertical composition of a Cordilleran batholith. In addition, some tectonic implications for various tectonic models concerning the Mesozoic and Cenozoic evolution of central California are discussed. Chapter 4 presents the major, trace element and oxygen isotopic compositions of pyroxenites, the most abundant xenoliths from beneath the Sierra Nevada batholith. The results are used to argue that the

1-6

pyroxenites are residual assemblages after granitoid (batholith) extraction from an original basaltic protolith. It is also proposed in Chapter 4 that the petrologic processes which led to the extraction of Archean granitoids were similar to the ones responsible for the generation of the Sierra Nevada batholith. Chapter 5 reports whole rock Sr, Nd, Pb, and O isotopic compositions measured in all xenolith petrographic types. End member components involved in the batholith formation are being identified based on the isotopic heterogeneities measured in the central Sierra Nevada xenoliths, as proxies for the deeper parts of the lithosphere in this region. The tectonic significance of these end members is also discussed.

Chapter 6 and 7 are studies of Pliocene and Quaternary xenolith localities from the central and eastern Sierra Nevada regions, and address the importance of lower crustal foundering as a mechanism potentially responsible for returning large volumes of batholith residues into the underlying mantle. Chapter 6 is a study of silica-rich glass inclusions found in mantle-derived peridotitic xenoliths from central Sierra Nevada Pliocene volcanic rocks. Major, trace element and isotopic compositions of the glass inclusions and host peridotites are used to argue for a continental crustal origin of the glasses, indicative of crustal recycling in the Sierra Nevada lithospheric mantle. The eclogite facies batholith root represent plausible source rocks of the glass inclusions. The hypothesis of crustal root foundering is further developed in Chapter 7. In this chapter, a number of geologic and geophysical lines of evidence are used to substantiate the model of batholith eclogitic root foundering into the underlying mantle.

Appendix 1 describes the xenolith localities investigated for this thesis. Brief geographic localization, petrographic description of host volcanic rocks and xenoliths are provided for each locality. Appendix 2 contains information important for the acquisition of radiogenic isotopic data in Dr. Saleeby's laboratory during the course of this study (1994-1998): new procedures, analytical results for standards, and blanks.

Finally, Appendices 3 and 4 contain the results of a project unrelated to the main subject of this thesis, a recognizance study of sulfur solubility in magmatic rocks as a function of melt alkalinity, at elevated oxygen fugacities. This study was carried out under the supervision of Dr. Peter Wyllie as part of the qualifying exam requirements in the Division of Geological and Planetary Sciences at Caltech. Appendix 3 presents a review of sulfur concentrations in undegassed volcanic products from worldwide locations and interprets the correlations between sulfur and other chemical components, particularly the alkalis. Appendix 4 reports preliminary experimental results on sulfate solubility in quartz-normative and nepheline-normative oxidized granitic melts at ~1.5 kbar.

Note: Chapters 2-7, and Appendices 3-4 of this thesis were written as manucripts publishable in scholarly journals, and therefore should stand as independent materials. This accounts for some degree of overlap between these chapters.

References

Anderson, J. L., 1990, The nature and origin of Cordilleran magmatism, Geol. Soc. Am. Mem., 174, 414 p.

Dickinson, W., Plate tectonics and the continental margin of California, in Ernst W.G. (ed.) *The geotectonic development of California*, Prentice-Hall, Englewood Cliffs, N.J., 1-28, 1981.

Dodge, F. C. W., L. C. Calk, and R. W. Kistler, Lower crustal xenoliths, Chinese Peak lava flow, Central Sierra Nevada, *Jour. Petrol.*, 27, 1277-1304, 1986.

Dodge, F. C. W., J. P. Lockwood, and L. C. Calk, Fragments of the mantle and crust beneath the Sierra Nevada batholith: xenoliths in a volcanic pipe near Big Creek, California, *Geol. Soc. Am. Bull.*, 100, 938-947, 1988.

Domenick, M. A., R. W. Kistler, F. C. W. Dodg,e and M. Tatsumoto, Nd and Sr isotopic study of crustal and mantle inclusions from the Sierra Nevada and implications for batholith petrogenesis, *Geol. Soc. Am. Bull., 94*, 713-719, 1983.

Moore, J.G. and Dodge F.C.W., Late Cenozoic volcanic rocks of the Southern Sierra Nevada, California; I. Geology and petrology: Summary, *Geol. Soc. Am. Bull.*, 91: 515-518, 1980.

Mukhopadhyay, B., Petrology and geochemistry of mafic and ultramafic xenoliths from the Sierra Nevada batholith, Part 1, Ph.D. dissertation, *University of Texas at Dallas*, 215 p, 1989.

Nixon, P.H., Mantle xenoliths, John Wiley and Sons, New York, 844 p.

Pickett, D. A. and J. B. Saleeby, Thermobarometric constraints on the depth of exposure and conditions of plutonism and metamorphism at deep levels of the Sierra Nevada batholith, Tehachapi Mountains, California, *Jour. Geophys. Res., 98, no. B1*, 609-629, 1993.

Pitcher, W.S. The nature and origin of granite, Blackdie Acad.& Prof., London, 321 p, 1993.

Rudnick, R. L., Xenoliths, samples of the lower continental crust, in *Lower continental crust*, D. M. Fountain, ed., 137-158, 1993.

Saleeby, J. B., Progress in tectonic and petrogenetic studies in an exposed cross-section of young (C.100 Ma) continental crust, southern Sierra Nevada, California, in *Exposed Crustal Sections of the Continental Crust*, M. H. Salisbury and D. M. Fountain, eds., pp. 137-158, Kluwer Academic Publishers, Norwell, Mass, 1990.

Wilshire, H. G., C. E Meyer, J. K. Nakata, L. C. Calk, J. W. Shervais, J. E. Nielson, and E. C. Schwarzman, Mafic and ultramafic xenoliths from volcanic rocks of the western United States, *U. S. Geol. Surv. Prof. Pap., 1443*, 179 p., 1988.

CHAPTER 2

Buoyancy Sources for a Large, Unrooted Mountain Range, the Sierra Nevada; Evidence From Xenolith Petrography and Thermobarometry

Mihai N. Ducea and Jason B. Saleeby

paper published in *Journal of Geophysical Research*

Abstract

Xenoliths hosted by Cenozoic volcanic flows and plugs from the Central Sierra Nevada and Eastern Sierra Nevada, Owens Valley and Inyo Mountains were studied for petrography and thermobarometry. The Central Sierra Nevada suite consists of abundant feldspathic granulites, garnet clinopyroxenites, garnet websterites and peridotites. Olivine-free mafic and ultramafic assemblages occur down to >70 km, although below 35-40 km they are mainly in the eclogite facies. In contrast, the Eastern Sierra Region suites show peridotitic, pyroxenitic and harzburgitic assemblages at depths of ≥~35-40 km. They define an adiabat in P-T space (T ~1180-1250 ^{0}C), suggesting the presence of the asthenospheric upper mantle close to the base of the crust. The ultramafic mantle rocks from the Central Sierra Nevada also define an adiabatic slope in P-T space, possibly an artifact of side heating from the east. There is xenolith evidence that the Sierra Nevada lost about half of its original crust on the eastern side of the range. Regardless of the actual mechanism of crustal thinning, the loss of the eclogitic lowermost crust and replacement by peridotite in the eastern Sierra Nevada is a process accompanied by a substantial density decrease (>100 kg/m^3). Overall, if the mechanism of eclogitic lowermost crust removal is viable, there are enough buoyancy sources to explain topographic differences between the Sierra Nevada and the adjacent Basin and Range assuming isostatic equilibrium.

2.1. Introduction

The Southern Sierra Nevada, California, is a high standing mountain range (2800 m mean elevation) relative to the adjacent Basin and Range province (1000 m mean elevation) to the east and the Great Valley (sea level elevation) to the west. The Sierra Nevada is composed primarily of a large, Cordilleran-type batholith (Saleeby, 1990), a Mesozoic magmatic arc similar to the modern Andes. The Sierra Nevada was traditionally believed to have a thick, ~55 km root (Bateman and Eaton, 1967) which compensates the mountain range's elevation. Recent teleseismic results (Jones et al., 1994) and active and passive seismic experiments (Wernicke et al., 1996; Park et al., 1995a), in contrast, show that the Southern Sierra Nevada is underlain by a relatively thin, ~35 km thick crust. In light of these results, a different mechanism of compensation of the Sierra Nevada must be found. The upper mantle has to be buoyant enough to explain much of a ~150 mgal negative Bouguer anomaly (Oliver, 1977) that characterizes the Sierra Nevada. The Sierra Nevada mountain range is located at the edge of a rift province (the Basin and Range). The topography support mechanisms may be related to heating of this rift "shoulder" and upwelling of hot asthenosphere (Crough and Thompson, 1977).

The only direct samples of the lower crust and the uppermost mantle in the region are represented by xenoliths hosted by numerous young volcanic flows and plugs. In this paper, we are exploring the source(s) of upper mantle/lower crustal buoyancy in the area, based on xenolith evidence as a proxy for the Sierra Nevada lithospheric structure. The crustal and upper mantle compositions derived from xenolith studies are very different in the central part and the eastern side of the mountain range. These differences permit us to assess the possible mechanisms of support for the Sierra Nevada. Two potential mechanisms for lowering the density in the uppermost seismologically-defined mantle are discussed in detail: (1) the replacement of lithosphere with asthenosphere, and (2), eclogite removal during crustal thinning.

2.2. Location and Age of Xenolith Bearing Flows and Plugs in the Sierra Nevada; Xenolith Petrography

Lower crustal and upper mantle xenoliths from young basaltic volcanic rocks in the Sierra Nevada and Owens Valley were previously described by Domenick et al. (1983), Dodge et al. (1986, 1988), Mukhopadhyay (1989, 1991b), Mukhopadhyay and Manton (1994), Ducea and Saleeby (1994), Wilshire et al. (1988) and Beard and Glazner (1995). In this paper we use all previous reports on thermobarometry of the Sierra Nevada xenoliths, in addition to our results. The xenolith-bearing localities used in this study are shown in Figure A1-1 and the compositions and ages of the host volcanics are given in Table A1-1. The xenolith-bearing volcanics can be divided in two broad groups based on location and age. One suite located in the central Sierra Nevada consists mainly of Miocene volcanics (which will be named "Central Sierra Nevada" throughout the paper) and the other consists of Quaternary volcanics of the eastern Sierra Nevada, Owens Valley and Inyo Mountains (the "Eastern Sierra Region suite"). Figure 2-1 is a histogram of petrographic compositions of xenoliths sampled from both the Central Sierra Nevada and the Eastern Sierra Region, and includes data from Mukhopadhyay (1989), our collection, and Frank Dodge's collection, which is stored at the Smithsonian Institution.

There are significant compositional and equilibration temperature differences between the xenoliths of the two groups. An average age difference of ~8 Ma between the Central Sierra Nevada and the Eastern Sierra Region xenolith-bearing volcanics is a serious limitation in our attempt to infer in a static manner any lateral variations in the Sierran lithosphere from the xenolith petrology, especially because the eastern Sierra was probably subject to significant extension in the past 10 Ma. This age difference, however, sheds light on the recent dynamical evolution of the Sierra Nevada.

Below, we will describe the petrography of the two distinct suites.

Figure 2-1. Lithologic types and abundance of sampled xenoliths from the Central Sierra Nevada (CS) (a) and Eastern Sierra Region (ES) (b) present in the Ducea and Saleeby collection, the Dodge collection stored at the Smithsonian Institution, as well as the samples studied by Mukhopadhyay (1989).

Central Sierra Nevada Lithologic Types
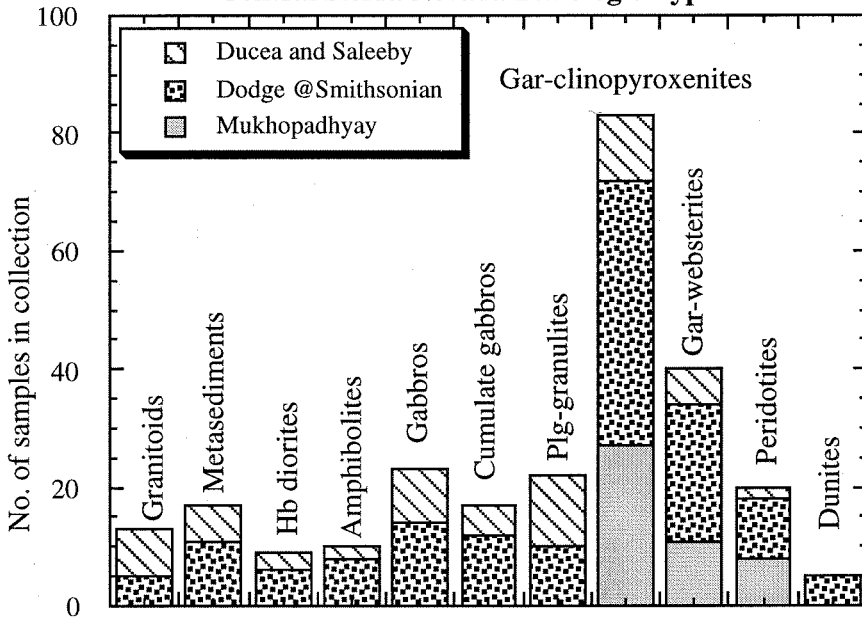
Eeastern Sierra Region Lithologic Types
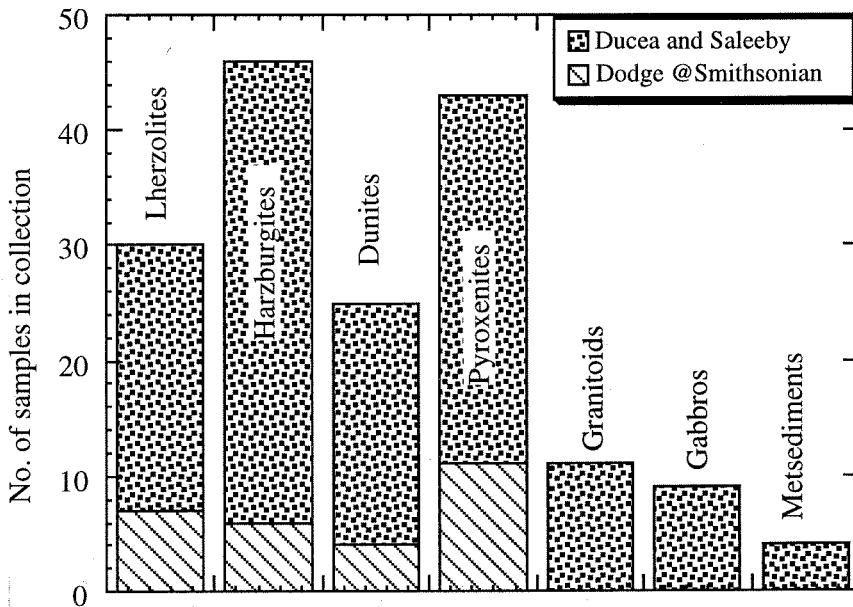
Central Sierra Nevada suite petrography

The Central Sierra Nevada suite is rich in both crustal and mantle xenoliths (Figure 2-1). Most of the crustal xenoliths are mafic in composition. Other compositions, such as metasediments, diorites, and amphibolites, are sparse and have not been investigated in detail in this study.

The mafic xenoliths are gabbros, cumulate gabbros, feldspathic granulites, garnet clinopyroxenites, and websterites. Many of the mafic xenoliths have igneous textures. The gabbros (Figure 2-2a) consist of plagioclase, clinopyroxene, orthopyroxene, hornblende and biotite. Accessory phases include magnetite, ilmenite, quartz, sphene, apatite, zircon, and orthoclase. Commonly, the gabbros have cumulate textures; these rocks are centimeter scale layered rocks. The size of the xenolith is comparable to the scale of layering which makes textural identification difficult. Clinopyroxene and orthopyroxene form the mafic layers and are commonly rimmed by hornblende. Many samples also have garnet as a cumulus phase (Figure 2-2b). Garnet crystals crystallized within the plagioclase intercumulus layers. The presence of garnet is an indication of the deep provenance of most of the xenolithic gabbros, although textural and mineralogical evidence show that the gabbros are not very different lithologically from some of the western Sierra Nevada mafic plutons (Saleeby and Sharp, 1982; Clemens-Knott, 1992), which formed at depths shallower than 15 km.

Granulite xenoliths vary from 20 to 80% plagioclase with mafic phases dominated by two pyroxenes and garnet. Accessory quartz is common. Textures are granoblastic and some xenoliths display a distinct, sub-parallel alignment of tabular laths of plagioclase. Banding is suggestive of metamorphic gneissic texture but could well be inherited igneous lamination (Dodge et al., 1986). The phase mineralogy and bulk composition reconstructed from point counting suggest that the gabbros, cumulate gabbros and mafic feldspathic granulites share a common origin, and are most likely deep batholithic rocks. Preliminary

Figure 2-2. Microphotographs of representative central Sierra Nevada xenoliths. The long dimension is 5 mm in each photograph.

a. top page 2-8; hornblende gabbro, crossed polars. Dark phase - amphibole, light phase - plagioclase.

b. bottom page 2-8; cumulate gabbro. Large isometric crystals of garnet, with dark kelyphitic rims along the rims, are enclosed in a plagioclase matrix.

c. top page 2-9; composite granulite-pyroxenite xenolith. Photograph is taken near the border between the two distinct compositions and shows a layered zone alternating dark regions (garnet and pyroxenes) with white regions (plagioclase-rich).

d. bottom page 2-9; garent pyroxenite. Photograph of a large crystal of garnet (light color), in which darker crystals of clinopyroxenes are included, forming a poikilitic texture.
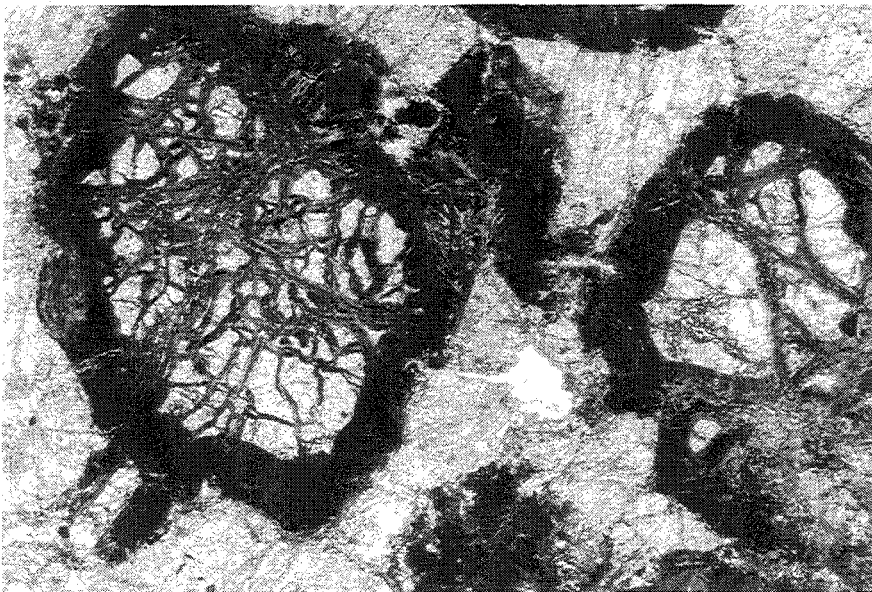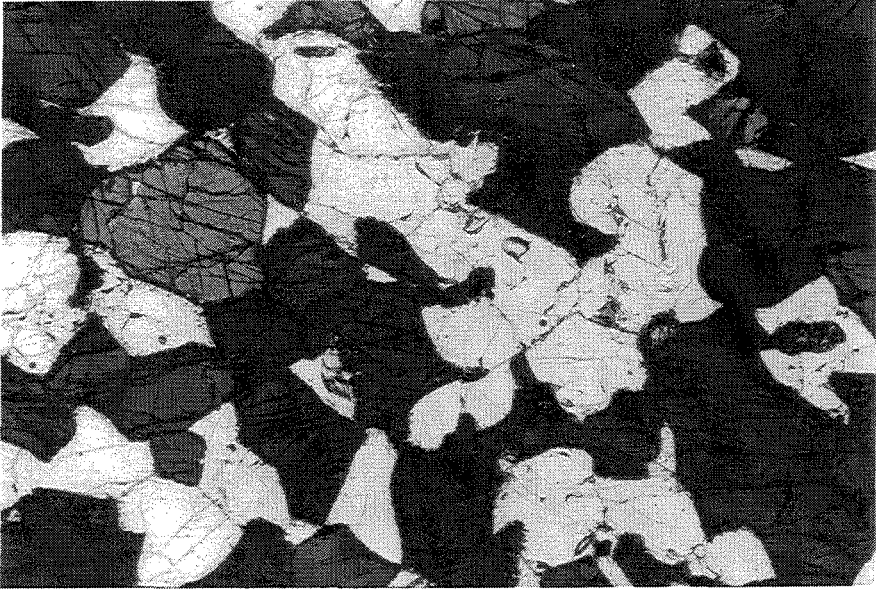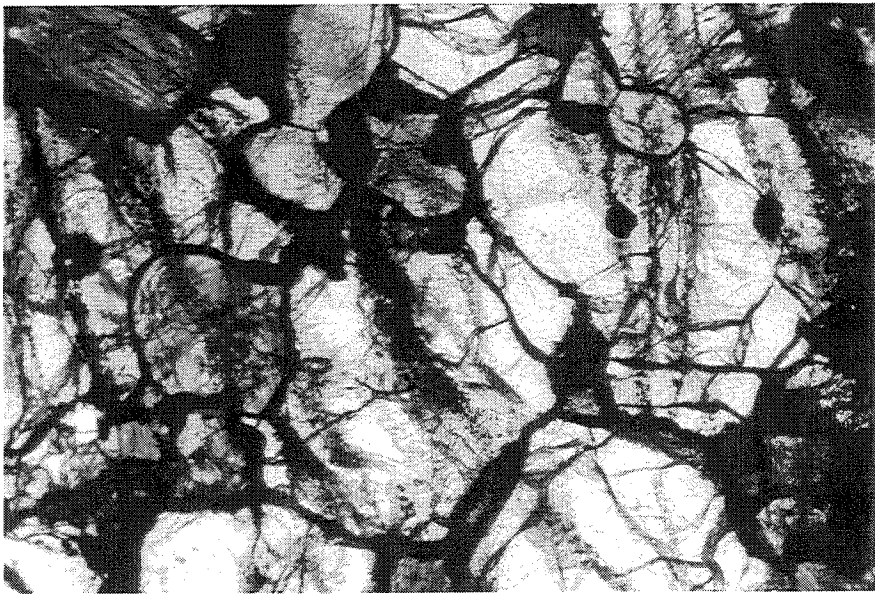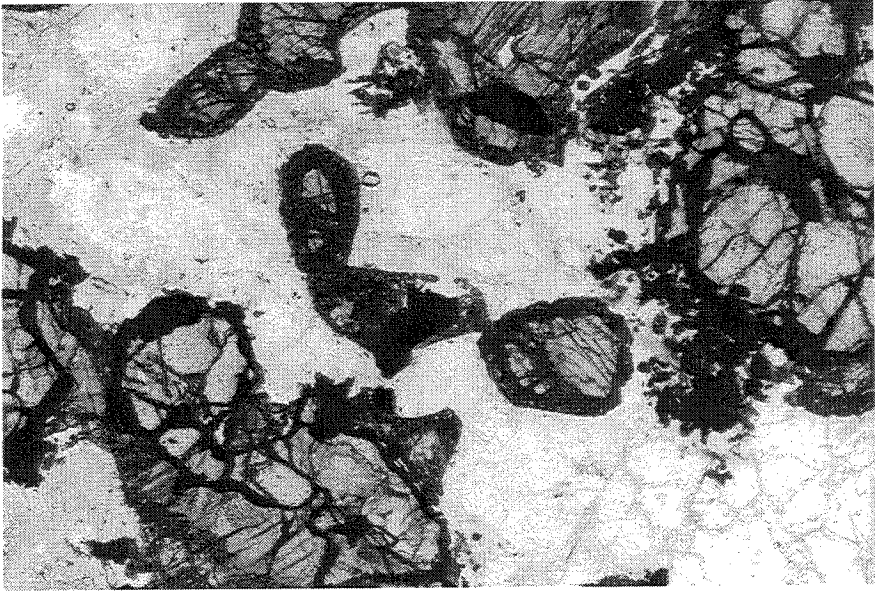
trace element studies on these rocks (Ducea et al., 1995) are consistent with a residual/cumulate origin of the mafic feldspathic rocks of the Central Sierra Nevada suite.

A distinct petrographic group is represented by the garnet clinopyroxenites. They have been identified at the Big Creek, Chinese Peak, Pick and Shovel, and Hume Lake locations. The garnet clinopyroxenites (Figure 2-2d) represent an ubiquitous assemblage in the Central Sierra xenoliths. They have also been called "granulites" or "eclogites" by Dodge et al. (1986) and Dodge and Bateman (1988). They have equigranular, bimineralic, clinopyroxene-garnet assemblages varying in composition from garnetites to clinopyroxenites. Coarse, subidioblastic to rounded garnets are enclosed in a xenomorphic matrix of clinopyroxenes. Minor amounts of rutile, spinels and secondary amphiboles are present. Commonly, the garnet is replaced by fine grained secondary assemblages consisting of rutile, two phase Fe-Ti oxides, secondary amphibole, and rare biotite which is replaced by opaque pseudomorphs (see also Mukhopadhyay, 1989). Dodge and others (1986) described sporadic layered xenoliths which consist of bands of garnet clinopyroxenite which show granoblastic mosaic textures interlayered with feldspathic-rich zones containing subordinate amounts of garnet, identical in composition with the granulites described above. Given the geological framework of the Sierra Nevada, garnet clinopyroxenite xenoliths can be cognate inclusions, subordinate mafic material (e.g., veins) within an ultramafic upper mantle, batholith-related cumulates, former mafic liquids frozen in the lower crust, partial melting residues, older continental crust or subducted oceanic crust. The above textural evidence, as well as preliminary REE investigations (Ducea et al., 1995), suggest a cumulate origin for most of the mafic lower crustal xenoliths of the Central Sierra, including the garnet clinopyroxenites. The focus of this paper is on the thermobarometry of the different xenolith assemblages; testing petrogenetic hypotheses for the garnet clinopyroxenites and their link with the other mafic assemblages is currently under investigation. However, we point out here the similarity in the average major element

Table 2-1. Average major element composition of various mafic xenoliths of the Central Sierra Nevada suite.

Oxide (wt. %)	Gabbro	Cumulate gabbro	Feldspathic granulite	Garnet clinopyroxenite
SiO_2	49.7	51.5	50.3	45.1
Al_2O_3	11.8	19.5	10.3	15.1
FeO_{tot}	8.9	5.1	7.2	8.9
MgO	12.7	7.6	13.1	14.2
CaO	13.3	11.4	14.3	15.4
Na_2O	3.2	1.6	2.3	0.9
K_2O	0.3	-	0.4	0.3

chemistry of the gabbros, cumulate gabbros, granulites and garnet clinopyroxenites (Table 2-1).

Another distinct group of xenoliths of the Central Sierra Nevada is represented by garnet websterites. The garnet grains are commonly clouded with inclusions, whereas clinopyroxene has local orthopyroxene exsolution lamellae. The texture is granoblastic characterized by polygonization of large, centimeter-size grains into smaller millimeter-size grains with abundant triple point and equigranular mosaic aspect. Accessory minerals include Cu-Fe sulfides (mainly chalcopyrite), rutile and amphibole.

Garnet peridotites, spinel-garnet peridotites and spinel peridotites (Dodge et al., 1988; Mukhopadhyay and Manton, 1994) were previously described in the Central Sierra suite. We sampled a few garnet peridotites and spinel peridotites with granoblastic polygonal to allotriomorphic granular textures. Typically, the ultramafic xenoliths were recovered as samples smaller than 5 cm in diameter.

Eastern Sierra Nevada Region suite petrography

The Eastern Sierra Region suite is very rich in upper mantle assemblages (Figure 2-1) and is very different from the Central Sierra suite. No garnet has been recorded in any of the Eastern Sierra Region xenoliths, nor have mafic granulites been identified.

Xenoliths of granodioritic compositions from Golden Trout, Oak Creek and Aberdeen resemble batholithic rocks of the eastern Sierra Nevada in composition and texture. Some of them, however, have a distinct gneissic texture, commonly displaying a mylonitic texture with the mafic minerals (hornblende and biotite) stretched in foliation planes.

Gabbroic xenoliths are layered cumulates having green, 2-5 cm bands of augite alternating with plagioclase layers. Sparse hornblende diorites grading to hornblendites

with pegmatitic textures are present as well. The typical size of these xenoliths is 2-40 cm in diameter.

Clinopyroxenites, orthopyroxenites and spinel websterites are very common in the Eastern Sierra Region suite (Figure 2-1). They contain rare olivine and small amounts of anorthitic plagioclase. The textures are metamorphic and are usually porphyroblastic. Accessory phases include Fe-Ti oxides and sulfides.

Spinel lherzolites are common. There are two textural types, an allotriomorphic type, with grain size up to 0.5 cm and a porphyroclastic type, sometimes completely annealed with grain size typically on the order of a few millimeters. Larger, clastic olivine and orthopyroxene grains are occasionally present as relics within the finer grained porphyroclastic peridotites.

Harzburgites and spinel dunites with minor amounts of orthopyroxene are texturally very similar to the porphyroclastic lherzolites. The ultramafic lithologies described above are end-member rocks and transitions between them are common. Most of the ultramafic xenoliths are small samples, 1-4 cm in diameter.

2.3. Mineral chemistry

Analytical Methods

The mineral chemistry of each petrographic type was investigated. Polished rock thin sections were analyzed on a JEOL 733 electron microprobe fitted with five wavelength spectrometers. The accelerating voltage was 15 keV, the probe current was 25 nA (measured on brass), count time was 60-80 sec and probe diameter was 10 μm^2. Sodium was analyzed first in order to reduce alkali migration. At least 5 grains of each mineral phase were analyzed in every thin section to check for equilibrium attainment. Cores, rims and spots on the extreme outer limit of grains ("extreme rims") were measured for each

Table 2-2. Major element compositions (wt. %) of phases used for thermobarometric determinations.

a. Garnet compositions

Sample	7	9	25	293	295	35	222	297	36	207
	Feldspathic xenoliths							Quartzite	Eclogites	
SiO_2	40.49	38.20	39.39	39.87	40.53	39.57	39.94	40.50	38.51	38.87
TiO_2	0.01	0.39	0.01	0.01	0.01	0.03	0.12	0.20	0.22	0.27
Al_2O_3	23.56	20.56	21.46	22.78	23.88	21.93	21.51	21.71	22.17	19.42
Cr_2O_3	0.00	0.00	0.15	0.23	0.02	0.25	0.02	0.28	1.05	0.09
FeO	15.04	16.37	23.63	17.35	15.29	16.05	22.32	20.86	20.45	9.32
MnO	0.55	1.98	1.58	1.30	0.53	1.50	0.39	0.58	0.45	1.93
MgO	15.87	9.64	9.32	7.97	13.82	8.31	7.56	10.10	6.21	0.56
CaO	5.79	13.80	4.17	10.14	5.84	11.66	9.19	5.17	10.19	29.03
Na_2O	0.25	0.00	0.13	0.29	0.36	0.02	0.03	0.25	0.02	0.04
Total	101.56	100.94	99.84	99.94	100.28	99.32	101.08	99.65	100.27	99.53

a. Garnet compositions, continued.

Sample	39	218	300	CaS3	227	216	34	221	CaS8	U9	1
	Garnet Clinopyroxenites						Garnet Websterites				Peridotite
SiO_2	40.87	40.61	39.80	40.81	41.26	39.36	42.51	42.17	41.31	42.22	40.55
TiO_2	0.00	0.07	0.09	0.00	0.13	0.11	0.16	0.23	0.06	0.15	0.21
Al_2O_3	22.25	22.11	21.84	22.37	22.10	21.63	22.43	21.70	22.03	22.55	22.67
Cr_2O_3	0.05	0.00	0.05	0.03	0.03	0.02	0.55	0.14	0.99	0.89	1.02
FeO	18.20	21.59	21.57	15.46	17.95	21.66	7.45	16.38	9.45	9.43	6.78
MnO	0.60	0.26	0.28	0.41	0.48	0.29	0.34	0.58	0.45	0.87	0.33
MgO	13.28	10.86	10.16	14.77	9.28	10.34	21.87	13.88	19.21	20.15	22.35
CaO	5.24	6.25	6.22	5.64	9.32	6.22	5.43	4.39	6.19	4.97	5.11
Na_2O	0.06	0.01	0.00	0.03	0.02	0.00	0.02	0.13	0.02	0.12	0.22
Total	100.55	99.76	100.01	99.52	100.57	99.63	100.76	99.60	99.71	101.35	99.24

b. Orthopyroxene compositions

Sample	7	9	25	293	295	CaS3	39	218
		Feldspathic xenoliths				Garnet clinopyroxenites		
SiO_2	52.85	51.24	52.31	51.00	50.81	55.07	55.94	55.26
TiO_2	0.00	0.25	0.01	0.00	0.21	0.04	0.01	0.04
Al_2O_3	3.25	2.33	2.77	1.17	2.00	1.44	1.34	1.67
Cr_2O_3	0.16	0.00	0.01	0.00	0.00	0.02	0.02	0.00
FeO	11.96	25.55	14.07	27.26	23.27	11.77	13.05	12.55
MnO	0.00	0.75	0.01	0.67	0.73	0.14	0.15	0.21
MgO	32.42	17.84	28.93	19.88	22.31	31.14	30.31	30.75
CaO	0.00	0.52	1.07	0.59	0.41	0.26	0.27	0.33
Total	99.64	98.48	99.18	100.57	99.74	99.88	101.09	100.81

b. Othopyroxene compositions, continued.

Sample	221	34	CaS8	U9	1	212	loc11	ocx	wc1
		Garnet Websterites			Garnet Peridotite		Spinel Peridotites		
SiO2	53.80	53.85	55.04	56.12	55.12	57.00	53.90	54.05	53.16
TiO2	0.12	0.00	0.03	0.02	0.03	0.07	0.27	0.25	0.11
Al2O3	2.62	2.37	3.10	3.58	4.22	2.12	4.88	3.72	4.67
Cr2O3	0.04	0.36	0.50	0.57	0.76	0.58	0.45	0.43	0.33
FeO	13.24	6.29	6.44	6.22	5.45	6.10	6.52	7.20	11.47
MnO	0.21	0.13	0.19	0.16	0.10	0.13	0.00	0.00	0.00
MgO	29.85	35.29	33.87	33.27	34.07	33.34	33.66	32.49	28.82
CaO	0.18	0.31	0.46	0.22	0.03	0.43	0.76	1.03	1.15
Total	100.06	98.60	99.63	100.16	99.78	99.77	100.44	99.17	99.71

c. Clinopyroxene compositions.

Sample	25	35	293	295	222	207	36	205	218	300	227
	Feldspathic Xenoliths					Eclogites		Quartzite	Garnet Clinopyroxenites		
SiO_2	50.12	51.89	49.29	51.63	49.01	53.03	51.87	52.92	52.57	55.36	52.66
TiO_2	0.37	0.22	0.43	0.42	1.01	0.00	0.00	0.05	0.45	0.47	0.16
Al_2O_3	2.36	1.49	1.00	2.94	7.41	3.14	2.33	0.50	5.11	5.41	3.85
Cr_2O_3	0.00	0.37	0.13	0.00	0.01	0.02	0.05	0.04	0.03	0.03	0.02
FeO	12.65	13.02	15.74	9.17	9.63	9.04	12.4	9.77	6.72	6.61	4.68
MnO	0.46	0.58	0.77	0.32	0.06	0.23	0.33	0.48	0.02	0.04	0.01
MgO	10.67	12.80	10.01	12.46	10.30	10.77	8.55	15.85	12.75	12.66	14.17
CaO	21.81	19.34	21.88	21.32	21.03	20.92	20.92	19.83	20.55	19.41	21.91
Na_2O	1.55	0.39	0.54	0.77	1.62	2.29	2.76	0.35	1.64	1.04	1.58
Total	99.99	100.10	99.80	99.03	100.08	99.44	99.21	99.79	99.84	101.03	99.04

c. Clinopyroxene compositions, continued.

Sample	39	CaS3	216	CaS8	34	221	U9	1	bc212	loc 11	ocx	wc1
	Garnet clinopyroxenites			Websterites				Garnet Peridotite		Spinel Peridotites		
SiO_2	54.13	53.58	53.92	51.82	52.96	53.89	53.00	52.15	55.26	51.51	51.28	49.06
TiO_2	0.16	0.17	0.11	0.09	0.11	0.00	0.09	0.22	0.06	0.62	0.60	1.37
Al_2O_3	3.26	4.07	3.99	3.56	2.24	1.03	1.51	2.76	2.09	7.37	5.50	5.35
Cr_2O_3	0.22	0.01	0.55	0.76	0.63	0.14	0.37	0.55	0.96	0.60	0.83	0.88
FeO	3.76	4.63	4.30	2.19	1.68	4.21	3.98	2.16	1.94	3.78	3.64	4.96
MnO	0.05	0.05	0.04	0.06	0.04	0.06	0.15	0.04	0.12	0.00	0.21	0.22
MgO	14.86	13.94	14.16	16.63	19.00	16.47	17.49	18.22	15.25	15.27	15.90	13.79
CaO	22.63	20.60	21.81	21.26	22.07	22.78	23.10	23.76	23.09	18.81	20.27	22.77
Na_2O	1.29	1.97	1.45	0.55	0.50	0.76	0.44	0.55	0.80	1.48	1.78	1.34
Total	100.36	99.02	100.33	96.92	99.23	99.34	100.13	100.41	99.57	99.44	100.01	99.74

d. Plagioclase compositions.

Sample	35	7	9	25	293	295	222
				Feldpathic xenoliths			
SiO_2	56.03	56.60	59.14	53.56	55.50	54.73	61.95
Al_2O_3	26.12	26.56	24.41	26.56	28.92	28.76	23.51
CaO	11.21	10.66	6.86	8.37	10.00	10.39	5.29
Na_2O	5.89	5.67	5.01	5.26	5.76	5.44	8.07
K_2O	0.21	0.10	4.20	1.81	0.36	0.42	0.99
Total	99.46	99.59	99.62	95.56	100.54	99.74	99.81

e. Olivine compositions.

Sample	1	212	loc 11	OCX	wc1	bb2
	Garnet Peridotite			Spinel Peridotites		
SiO2	40.77	40.83	40.20	39.84	39.04	39.23
FeO	7.80	9.12	9.87	10.68	14.41	11.54
MgO	51.02	49.57	49.38	48.67	45.88	48.91
CaO	0.12	0.14	0.15	0.09	0.35	0.10
NiO	0.12	0.00	0.00	0.48	0.00	0.10
Total	99.73	99.53	99.60	99.76	99.68	99.88

analyzed grain, usually averaged from 2-5 analyses. Several traverses were performed across the most important phases. Only the granulites showed noticeable compositional gradients, whereas most of the garnet clinopyroxenites as well as the high temperature rocks showed uniform compositions. The extreme rim compositions were not used in interpretations because they systematically showed effects of heating due to entrapment in the host melt. We used the chemistry of the phases in conjunction with point countings on thin sections to calculate the major element chemistry of some of the xenoliths (reported in Table 2-1).

Described below are the compositions of the mineral phases involved in the thermobarometric calculations. Representative analyses given in Table 2-2 are average values for mineral rims consisting of 2-5 spots.
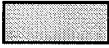
Central Sierra Nevada Suite mineral compositions

Granulites and gabbros. Clinopyroxenes are diopsidic. In thin section, they show weak pleochroism and are often twinned. The magnesium number (Mg/Mg+Fe) varies between 0.42 and 0.7. The $^{IV}Al/^{VI}Al$ ratios vary from 1/2 to 2 but are commonly close to 1. The Fe^{3+} calculated using the method of Papike et al. (1974) is less than 10% of the total Fe. The Na_2O varies between 0.39 and 1.75%; none of the pyroxenes have a significant jadeitic component.

Orthopyroxenes consist of bronzite and hypersthene compositions. In thin section, they show weak green-pink pleochroism. Al_2O_3 content is normally less than 5%. However, some orthopyroxenes have up to 15-16 % Al_2O_3. This feature was observed in both orthopyroxene extreme rims and sometimes in single grains and is probably a pyrometamorphic product due to xenolith heating in the host magma (Zhang et al., 1993). These Al-orthopyroxenes are not pure phases and were not used for thermobarometry.

Figure 2-3. Summary of garnet compositions from various Sierra Nevada deep samples. Prp- pyrope component; Alm+Sps- almandine and grossular component; Gros-grossular component. Data on amphibolites and gneisses from the Tehachapi Mts., Southern Sierra Nevada are from Pickett and Saleeby (1993). Peridotites, websterites, granulites, clinopyroxenites, gabbros and grospydites are xenoliths; their analyses are from this study, Mukhopadhyay (1989) and Dodge et al. (1986, 1988). Fields "A," "B," and "C" are defined in Coleman et al. (1965); "A" is typical for garnets in kimberlites, "B" corresponds to deep crustal garnets metamorphosed in the amphibolite or granulite facies, and "C" corresponds to garnets from subduction-related complexes.
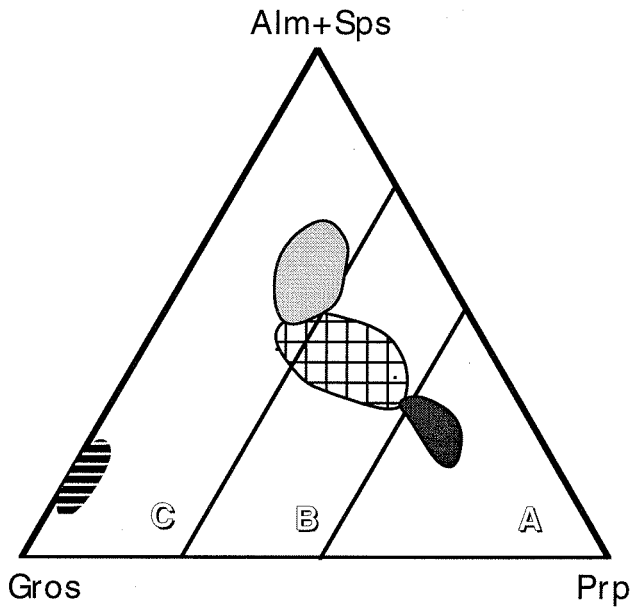
amphibolites & gneisses, Southern Sierra Nevada.

garnet peridotites and websterites

feldspathic granulites and garnet clinopyroxenites

gabbros, grospydites

Garnet compositions are shown in Figure 2-3. The garnet clinopyroxenites (see below) are richer in the grossular component than the feldspathic granulites garnets, but they all fall in the group B compositional range of Coleman et al. (1965). The garnet in rocks with igneous textures (gabbros) is very rich in the grossular component (Figure 2-3), and grew at the expense of An-rich plagioclase, perhaps upon cooling, and at high pressure. The garnets are commonly surrounded by thick kelyphititc rims (see Mukhopadhyay, 1991b).

Plagioclase compositions vary from 95.5% to 38% anorthite (An). The An content obtained from electron probe data has also been determined with optical methods; the values agree to within 5%.

Garnet clinopyroxenites. Clinopyroxenes in the garnet clinopyroxenites are very similar in composition to those in the feldspathic granulites (in excellent agreement with data from Mukhopadhyay, 1989). They are almost always unzoned. Amphiboles formed locally along rims. Their chemistry is dominated by quadrilateral components (i.e., have a low jadeitic component). The chemistry of the clinopyroxenes from granulites and garnet clinopyroxenites form continuous trends for all major oxides and elements. In the quadrilateral diagram, clinopyroxenes from the granulites and garnet clinopyroxenites display a continuous linear trend suggesting a common origin (Figure 2-4). In Figure 2-4 we plot the Ca content vs. the Mg# (Mg/(Mg+Fe)) in clinopyroxenes from both types of rocks. This suggests a common origin for the two groups.

Garnets have group B composition (Figure 2-3, Coleman et al., 1965). Mukhopadhyay (1989) observed similar compositions but with a wider range; some of his garnet compositions plot outside the Group B garnet field. Garnets do not exhibit chemical zoning except for the kelyphitization.

Peridotites and websterites. The chemistry of minerals from these rocks is also shown in Table 2-2. The very similar chemistry of the garnets, clinopyroxene and orthopyroxene for both rock types is an argument for chemical equilibration between them.

Again, none of the clinopyroxenes are rich in jadeitic component. Garnets plot in the group A field of Coleman and others (1965) resembling kimberlitic garnets (Figure 2-3). This is not surprising since some of these rocks are unusually deep samples for alkali-basalt hosted-xenoliths (3.5 GPa).

Eastern Sierra Nevada Suite mineral compositions

Spinel peridotites and pyroxenites. No significant differences between the allotriomorphic and porphyroclastic types peridotites are apparent in the olivine and pyroxene phase chemistry (Table 2-2). Pyroxenites, olivine pyroxenites, lherzolites and harzburgites exhibit very similar major element compositions for all major phases present. We describe below the mineral phases of the Eastern Sierra Region as a group.

Olivines from Eastern Sierra Region peridotites, olivine pyroxenites, and olivine xenocrysts are Fo_{87}-Fo_{90}. There is a significant variation in the CaO content in olivines (0-0.8 wt. %) indicative of a wide equilibration pressure range for these rocks (Kohler and Brey, 1990). Zoning is rare in the olivines.

Orthopyroxene compositions are on average En_{88} and are relatively uniform in all lithologic types. Mineralogically, some of the magnesian pyroxenes are clinoenstatites with somewhat higher Al and Ti contents, perhaps also a measure of a range of equilibration pressures.

Clinopyroxenes are on average $En_{50}Fs_6Wo_{44}$, very similar to values reported by Beard and Glazner (1995). The Al_2O_3 content varies from 6 to over 8 wt. %. Zoning is uncommon in the pyroxenes.

2.4. Equilibration Pressures and Temperatures

Figure 2-4. Quadrilateral components of clinopyroxenes in the Central Sierra Nevada feldspathic granulites and garnet clinopyroxenites. Mg # represents the Mg/ (Mg+Fe) ratio in clinopyroxenes. The two petrographic groups display a coherent trend, and significant overlap.
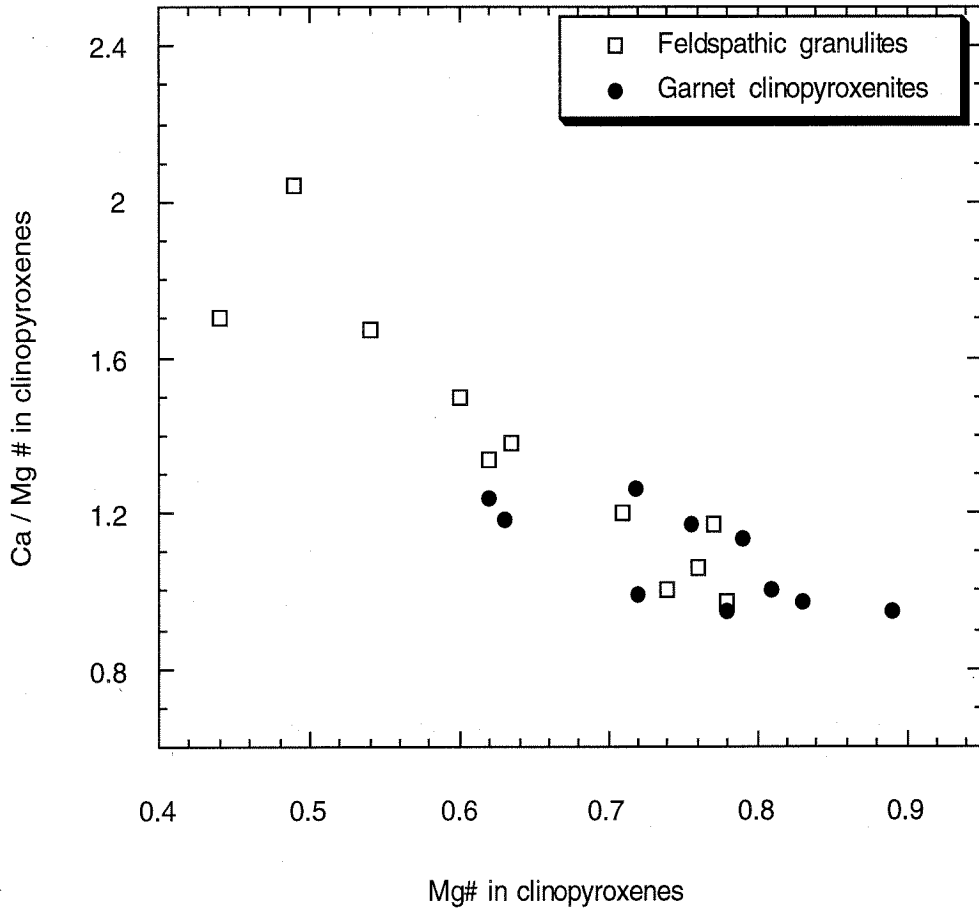
For many of the investigated xenoliths, we calculated the temperatures and pressures at which they equilibrated. We will describe below the thermometers and barometers that we used, the results of the pressure-temperature calculations, and the interpretation of the obtained geotherms (paleogeotherms and pseudogeotherms). The results are shown in Figure 2-5.

Methods. The equilibration temperatures for the granulites and garnet clinopyroxenites were determined using a single thermometer (Ellis and Green, 1979) and a single method of calculating the Fe^{3+} in the pyroxenes (Papike et al., 1974). Several barometric calibrations are available for the feldspathic lower crustal lithologies (e.g., garnet-clinopyroxene-plagioclase-quartz). The equilibration pressures from different barometers applied on each feldspathic granulite sample (Perkins and Newton, 1981; Harley, 1984; Harley and Green, 1982; Perkins and Chipera, 1985) did not differ by more than 0.2 GPa. The equilibration pressures of the garnet clinopyroxenites were calculated using the Mukhopadhyay (1991a) barometer. To our data we added thermobarometric results from Mukhopadhyay (1989) on the Big Creek and the Pick and Shovel garnet clinopyroxenites. In order to check consistency between the two types of barometers applied on the two different groups of rocks, we did two tests: 1) we calculated pressures of the clinopyroxene- and garnet-bearing feldspathic granulites using the Mukhopadhyay (1991a) barometer and compared these values with the much more reliable plagioclase-garnet-pyroxene-quartz barometers (e.g., Perkins and Newton, 1981) and 2) we calculated the CaO/(CaO+MgO) ratios for garnets coexisting with pyroxenes for all xenoliths. The lower ratios of the garnet clinopyroxenites prove that they represent rocks that equilibrated at consistently higher pressures (Brey et al., 1986). We observed that the pressures obtained on feldspathic samples with the Mukhopadhyay (1991a) barometer show consistently ~0.1-0.2 GPa higher pressure than the typical feldspathic granulite barometers (e.g., Newton and Perkins, 1982) and corrected the values obtained for garnet clinopyroxenites by subtracting 0.15 GPa from the values calculated using the

Figure 2-5. Equilibration temperatures and pressures for the Sierra Nevada xenoliths, including data from this study, Dodge et al. (1986, 1988), and Mukhopadhyay (1989). Error bars include experimental and analytical uncertainties. Trends "A", "B", and "C" are explained in the text. Curve "1" represents the garnet breakdown reaction described in text (reaction 1), calculated with the thermodynamic data set of Powell and Holland (1988). Curve "2" is the spinel to garnet peridotite transition, based on BVSP (1981), curve "4" and "5" are the "wet"- and "dry" solidus for mantle peridotite (BVSP, 1981). Curve "3" is the low crustal geothermal gradient of the western Sierra Nevada, based on the heat flow measurements of Lachenbruch and Sass (1977), perhaps the typical thermal gradient of the entire Sierra Nevada for Cenozoic times, before the Basin and Range extension (see Dumitru, 1990).

Eastern Sierra Nevada Region

■ Spinel peridotites
+ Gabbros

1 σ errors in P-T determinations
for different rock types (scale as
in figure)

⊕ feldspathic granulites

◇ all garnet clinopyroxenites and eclogites

◣ garnet websterites and garnet peridotites

■ spinel peridotites and gabbros

Central Sierra Nevada

○ Feldspathic granulites
□ Grossular-albite quartzite
◇ Garnet clinopyroxenites

▲ Peridotite (Dodge et al., 1986)
▽ Eclogite (Dodge et al., 1986)
□ Garnet clinopyroxenites (Mukhopahdyay, 1989)

▼ Garnet peridotites
▲ Garnet websterites
▨ Field of garnet peridotites and websterites (Mukhopadhyay and Manton, 1994)

Temperature (°C)
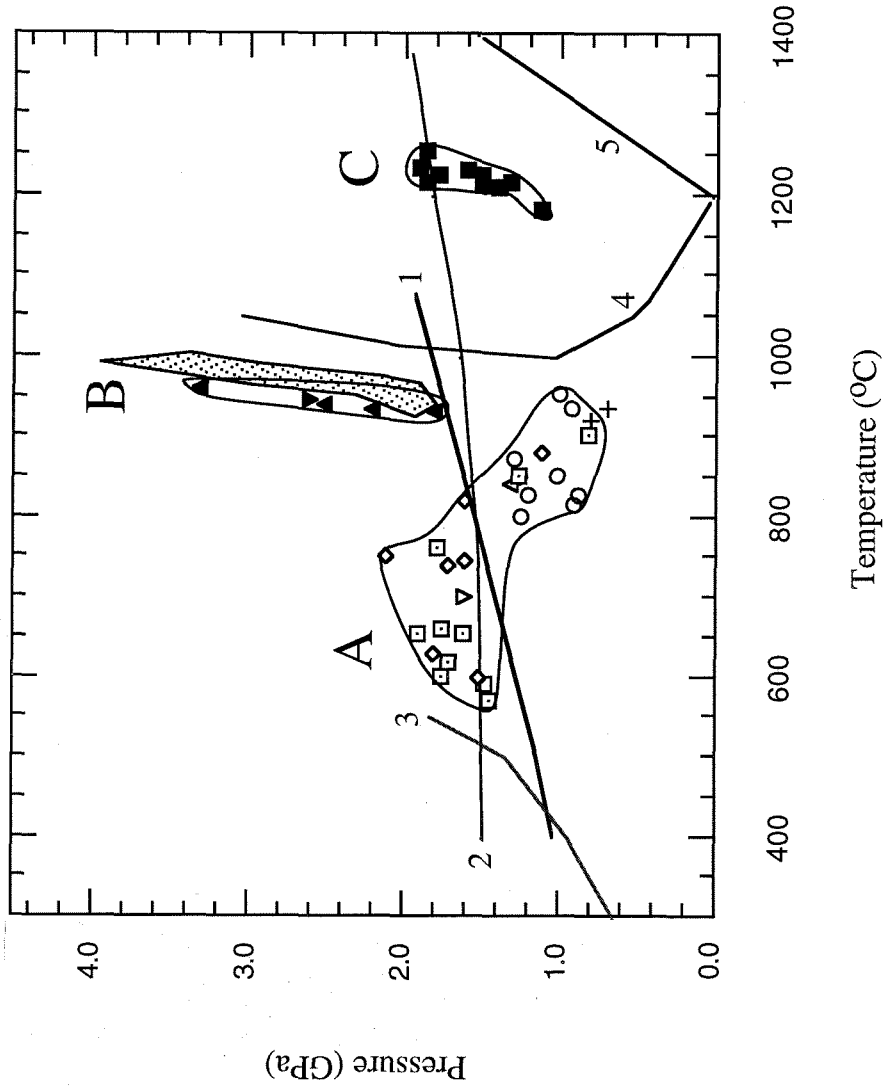
Pressure (GPa)

Mukhopadhyay (1991a) calibration. The pressure data points in Figure 2-5 represent averages of the barometers for the feldspathic granulites and the Mukhopadhyay (1991a)-corrected values for the garnet clinopyroxenites. We applied this correction also for the Big Creek and the Pick and Shovel data obtained by Mukhopadhyay (1989) using his calibration.

We analyzed four garnet websterites and one garnet peridotite and added the analyses on similar rocks from Mukhopadhyay and Manton (1994). Temperatures are calculated with the Harley (1984) garnet-orthopyroxene thermometer for both the peridotites and websterites. Temperatures are ~100 °C higher when using the Ellis and Green (1979) calibration. Pressures were obtained by the Harley (1984) Al-in-orthopyroxene coexisting with garnet barometer. The difference between the results obtained with the Harley (1984) barometer on garnet websterites and the Mukhopadhyay (1991a) barometer on garnet clinopyroxenites was nonsystematic, as large as 0.35 GPa.

The temperatures for the spinel peridotites, spinel dunites and olivine clinopyroxenites were determined using the following thermometers: two-pyroxene (Wells, 1977; Brey and Kohler, 1990), Ca-in orthopyroxene, the partitioning of Na between the two pyroxenes (both described by Brey and Kohler, 1990), and the Mg-Fe exchange between olivine and spinel (Sack and Ghiorso, 1991). All determined temperatures, including those lacking barometric data and not represented in Figure 2-6, fall between 1180-1250 °C. The pressures were determined on lherzolites and olivine clinopyroxenites using the Ca-in-olivine coexisting with clinopyroxene barometer (Kohler and Brey, 1990).

Results. The thermobarometric results are shown in Figure 2-5. Two pressure-temperature trends, "A" and "B," are characteristic for the Central Sierra Nevada and a third one, "C" for the Eastern Sierra Region.

Interpretation. Trend "A." The results shown in Figure 2-5 reveal that the garnet clinopyroxenites show consistently higher equilibration pressures than the feldspathic

granulites. A value of ~ 1.2 GPa would correspond to the transition from feldspar-bearing to the feldspar-absent lithologies.

The negative slope in the P-T diagram for trend "A" needs further explanation. One possible explanation is the presence of an inverted metamorphic gradient in the Sierra Nevada deep crust due to the presence of a shallow Cenozoic subducted slab, postulated by previous theoretical studies (e.g., Atwater and Molnar, 1973) and favored by thermochronologic (Dumitru, 1990) and geophysical data (Henyey and Lee, 1976). If this is the case, the trend, although probably transient, would reflect P-T conditions attained at some point in the Sierra Nevada. Such an interpretation would be bolstered if some or all of the eclogite facies xenoliths from the Central Sierra represent fragments of oceanic crust, as suggested by Dodge et al. (1986).

Alternatively, this slope might be an artifact of the conductive cooling underwent by the Sierra Nevada after the period of batholith generation. Deeper rocks in the suite cooled more slowly and can potentially equilibrate at lower temperatures (Frost and Chacko, 1989). The effect should be significant, because the deepest garnet clinopyroxenites equilibrated at 2 GPa, almost twice as high pressure as most of the feldspathic samples. Therefore, they cooled ~ 4 times slower, based on the assumption of one-dimensional conductive cooling of the crust. We prefer the later hypothesis because all the current evidence on the origin of the rocks that define trend "A" (Ducea et al., 1995; Mukhopadhyay and Manton, 1994; Dodge et al., 1988) suggest a common, most likely batholithic origin for the garnet clinopyroxenites, gabbros and mafic granulites. However, the very low temperatures recorded at deep levels in the batholith might overall be the result of the Cenozoic "slab refrigeration" advocated by Dumitru (1990).

Trend "B" resembles a solid adiabat. Our results are remarkably similar to those of Mukhopadhyay and Manton (1994), confirming that the garnet websterites of the Central Sierra Nevada are the deepest rocks in the suite, associated with the mantle peridotites rather than with the crustal garnet clinopyroxenites.

Trend "C" characterizes the Eastern Sierra Region for which both thermometric and barometric determinations were possible. It has also an adiabatic slope and is defined to depths as shallow as 35-40 km, which corresponds to the base of the crust in the area. This implies that the convective mantle upper boundary is close to or at the base of the crust in the eastern Sierra-Owens Valley region. The error bars on this barometer are ~ 0.3 GPa. Nevertheless, the consistent pressure variation at nearly constant temperature suggest that the adiabatic, asthenospheric-like slope in P-T space is probably real.

The xenolith thermometry also suggest a Late Cenozoic lateral temperature variation in the sub-Sierra upper mantle (trends "B" and "C"). The recorded difference in the xenolith assemblage is ~ 250 ^{0}C, but this can be higher than the real lateral temperature difference in the Sierra Nevada lithosphere because it was recorded at different times.

One important problem with the thermobarometry is the timing of the equilibration. Geochronometric work is in progress. As a working model based on the geologic history of the Sierra Nevada and adjacent Basin and Range, we hypothesize that trend "A" is a cooling slope for the deep batholithic rocks and was probably attained between 100 and 80 Ma. This hypothesis is consistent with a 100 Ma zircon U/Pb data from a granulite xenolith from Chinese Peak (Dodge et al., 1986). Trends "B" and "C" are possibly related to the young (post 20 Ma) extension in the Basin and Range and formation of the eastern Sierra Nevada range front. Lack of timing information for the described trends leaves several unanswered questions; for example, if the rocks forming trend "A" were at their equilibration depths during establishment of trend "B," why did they fail to re-equilibrate at higher temperatures?

Another potential problem with the high temperatures of trends "B" and "C" is to what extent they have been influenced by the presence of magmas similar to the xenoliths' hosts. Are we looking at P-T trends indeed representative for the Sierra Nevada mantle at a regional scale or at an uppermost mantle that was anomalous because of the very existence of magmatism? For example, the temperatures of trend "B" imply a relatively high heat

flow in recent past, in contrast with present day measurements of heat flow in the same region (Lachenbruch and Sass, 1977). Yet, the differences between the mantle compositional properties in the central vs. the eastern part of the range exist and they need to be interpreted.

2.5. Implications for the composition and structure of the Sierra Nevada

We will use the petrographic and thermobarometric results to constrain: (1) the composition and crustal thickness of the Sierra Nevada during batholith generation, (2) the present day composition and crustal thickness, and (3) the position of the lithosphere-asthenosphere boundary during late Cenozoic times beneath the Sierra Nevada.

Composition and thickness of the Sierra Nevada crust before Basin and Range extension. The central region of the Sierra Nevada batholith is exposed to an average crustal depth of ~10 km (Ague and Brimhall, 1988) and has an average tonalitic composition for the upper to mid-crustal levels (Saleeby, 1990), typical of the Circum-Pacific Cordilleran-type batholiths.

The composition of the lower continental crust is a subject of intense controversy (e.g., Kay and Kay, 1986; Meissner, 1986; Rudnick and Taylor, 1987; and Hanchar et al., 1994 for the southwestern U.S.). Geochemical calculations based on planetary models and evidence from crustal xenoliths point to a mafic composition (~48-50 wt. % SiO_2, Rudnick, 1993; Griffin and O'Reilly, 1986), while exposed lower crustal terranes suggest a more intermediate, andesitic composition (up to 55-60 % wt. SiO_2, Taylor and McLennan, 1985; Saleeby, 1990). Several hypotheses have been proposed to explain this difference: mafic compositions may be more resistant as xenoliths, exposed deep crustal terrains may represent anomalously buoyant lower crust, or since exposed lower crustal fragments are often Precambrian in age, they might be representative of a different, more silicic lower crustal composition of the early Earth (e.g., Rudnick, 1993)

In the case of the deep exposure of the southernmost Sierra Nevada, tonalite (~55% SiO_2) with subordinate mafic-ultramafic cumulates of the primary batholithic crust equilibrated from 27 to 35 km depth, equivalent to pressures of 0.8 GPa to 1 GPa (Pickett and Saleeby, 1993). We note that the mafic feldspathic granulite xenoliths of the Central Sierra Nevada suite yield pressures of 0.8 to 1.2 GPa which overlap this depth range. Additionally, there are tonalite xenoliths from the Central Sierra Nevada suite which could have likewise formed at 0.8 to 1 GPa pressures, but useful barometric indicators have yet to be found. Overall, the average composition of the xenoliths that equilibrated at ~1 GPa in the Sierra suites is more mafic than the average xenoliths equilibrated at ~1 GPa in the nearby Mojave desert (Hanchar et al., 1994).

We tentatively interpret the above relations to indicate that at ~1 GPa the primary batholithic composition graded upwards from predominantly mafic (48-50% SiO_2) to predominantly tonalitic (55-60% SiO_2). The Central Sierra Nevada xenolith data further suggest that the deep mafic batholith extends or extended downwards to ~65-70 km (pressures of 2 GPa). At the time of xenolith entrapment, depths corresponding to pressures greater than 1.2 GPa within this layer were in the eclogitic facies. The rocks are garnet clinopyroxenites which fall in the group B eclogites of Coleman et al. (1965) and are different from the eclogites described in kimberlites and subduction complexes. They resemble granulite-facies to eclogite facies assemblages and some may be high pressure magmatic eclogitic assemblages (Mukhopadhyay, 1991 b). These eclogites are mafic rocks, part of the petrologically-defined crust, but are also dense and have high seismic velocities yielding properties of the seismic mantle. The Moho discontinuity would correspond in these situations with the basalt-eclogite transition, a phase change rather than a chemical boundary (Wyllie, 1963; Ito and Kennedy, 1970, Dewey et al., 1993).

Preliminary trace element (Ducea et al., 1995) and isotopic (Mukhopadhyay, 1989) data on the feldspathic granulites and the garnet clinopyroxenites support the above proposition that these assemblages represent a coherent mafic igneous protolith suite

directly related to the overlying batholith. A close relationship between the feldspar-free and feldspar-bearing deep mafic rocks is further suggested by the recovery of a few composite granulite-garnet clinopyroxenite layered xenoliths (Dodge et al., 1988).

A bulk mafic composition of the lower crustal xenoliths would undergo a basalt-eclogite transition following the garnet breakdown reaction:

pyrope + grossular = anorthite + 2 diopside + spinel   (1)
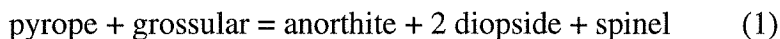
This univariant reaction, although a simplified one, uses the rough composition of the garnets in the xenoliths. We calculated the P-T position of this univariant curve (labeled "1" in Figure 2-5) using the thermodynamic data set of Powell and Holland (1988). The calculated pressures-temperatures from xenoliths are consistent with the reaction (1). It should be noticed that during high heat flow periods, such as batholith formation, little if any mafic crust would be in eclogite facies down to ~70 km depths. In contrast, the extremely low heat flow regime which followed batholith generation in the Cenozoic (Dumitru, 1990) strongly favors eclogitic conditions for the deep mafic batholithic rocks, below ~35 km (Figure 2-6).

Given the rapid increase in cooling rates following the Cretaceous batholith emplacement at ~0.4 GPa pressure (Renne et al., 1993), the batholith exhumation must have been rapid and on the order of 0.2-0.3 GPa. This is further supported by the thick, Cretaceous stratigraphy with a batholithic source in the Great Valley (Mansfield, 1979) and leaves very little exhumation as a result of the commonly presumed Late Cenozoic uplift. From the above observations we can speculate about the original thickness of the Sierra Nevada batholithic crust: the abundant growth of garnet in the lower crustal rocks took place during cooling of the batholith, most likely after the initial rapid exhumation of the batholith which followed its emplacement. Therefore, to the pressures recorded we could add ~0.3 GPa, the average pressure of exposure in the batholith today (Ague and Brimhall, 1988), which corresponds to ~11-12 km erosional removal from its top. The implied total of ~75-80 km thick batholithic crust would be very similar with the modern day Andes, the

Figure 2-6. Schematic cross section (not at scale) of the composition and structure of the Sierra Nevada, (a) at the time of batholith formation (~Cretaceous), and (b), during the Cenozoic, but prior to the extension of the westernmost Basin and Range. The figure emphasizes the existence of a thick (~80 km) crust, generated mainly during batholith-related magmatism. Ten kilometers of the crustal section were lost during the late-Cretaceous rapid exhumation of the batholith (e.g., Renne et al., 1993). The temperature-depth schematic diagrams show how an average basalt-eclogite univariant curve would intersect the geothermal gradients typical for the Sierra Nevada during batholith generation and, the low Cenozoic heat flow, respectively. The mafic "root" of the batholith was probably metamorphosed in the eclogite facies for most of the Cenozoic.

a

Sierra Nevada (Cretaceous)
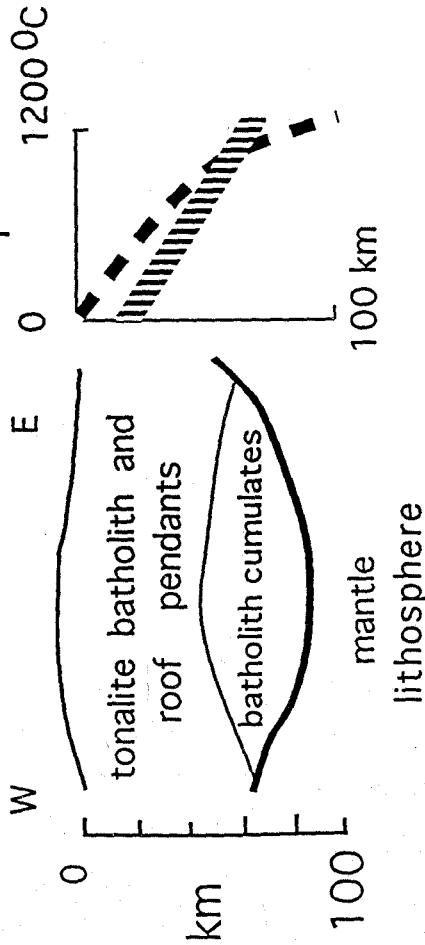
b

Sierra Nevada (Cenozoic, pre-Basin and Range extension)

tonalite batholith and roof pendants

batholith cumulates

mantle lithosphere

eclogite facies mafic rocks
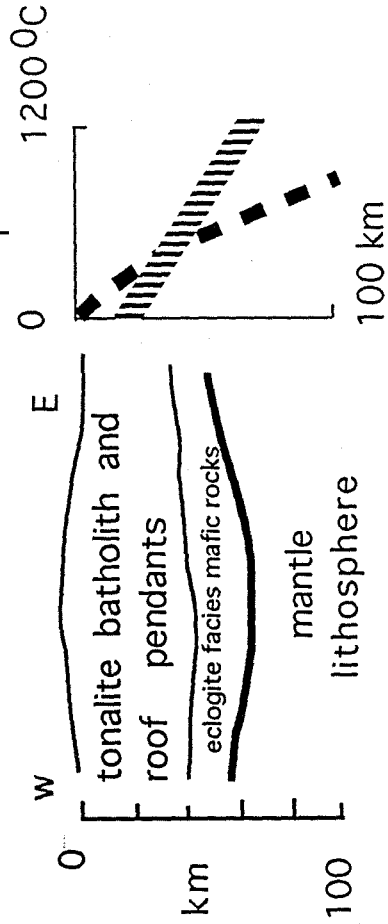
crust-mantle boundary

thermal gradient

basalt-eclogite phase change

type active Cordilleran magmatic arc (Isacks, 1988). Given the coherency of the surface batholith, we will assume that this primary batholith "thickness" applies to the entire Sierra Nevada crustal section before extension (Figure 2-6).

Modern crustal thickness of the Sierra Nevada. The modern Sierra Nevada has a thin, ~ 35 km thick crust (Figure 2-7, Wernicke et al., 1996), which is on average only 5 km thicker than the Basin and Range crust (Ruppert and Fliedner, 1995; Mooney and Weaver, 1989). The seismic results show a slight westward thickening (35 to 42 km) within the Sierra Nevada and also a change from a sharp Moho in the east, beneath the Sierra Nevada crest to a diffuse Moho under the western side of the Range (Ruppert and Fliedner, 1995). The recorded crustal thickness and the sharpness of Moho is in agreement with the transition from mafic to ultramafic assemblages found in Eastern Sierra Region xenoliths and also with the granulite-eclogite facies transition suggested by the Central Sierra Nevada xenolith petrography and thermobarometry. Therefore, the recorded Moho can be a phase change in the western side of the batholith and a chemical change on the eastern side. The two important implications of these observations are: (1) the seismologically defined crust under the western-central Sierra Nevada *may* be ~ 25 km thinner than the petrologically defined crust and (2) the lowermost batholithic crust has been replaced by peridotitic upper mantle rocks under the high part of the range, the eastern Sierra Nevada (Figure 2-7). Possible mechanisms of removal will be addressed below. Recent investigations of younger than 3.5 Ma xenolith-bearing volcanics from the central Sierra Nevada (Ducea and Saleeby, work in progress) show that garnet is absent in the lower crustal lithologies. It is therefore possible that the lower crust was removed from the central Sierra Nevada, as well, since the time when the xenoliths reported in this study were sampled by their host ~Miocene volcanics.

The lithosphere-asthenosphere boundary. Several geophysical studies of the Sierra Nevada (Crough and Thompson, 1977; Jones, 1987, etc.) postulate a shallow lithosphere-asthenosphere boundary beneath the easternmost part of the range. The thermobarometry

Figure 2-7. Schematic cross section (not at scale) of the recent to present day composition and structure of the Sierra Nevada. The depth and sharpness of Moho are based on the results of the Sierra Nevada Continental Dynamics Project seismic refraction study (Ruppert and Fliedner, 1995). It is possible that the mafic lower crust was also removed from the western Sierra Nevada.
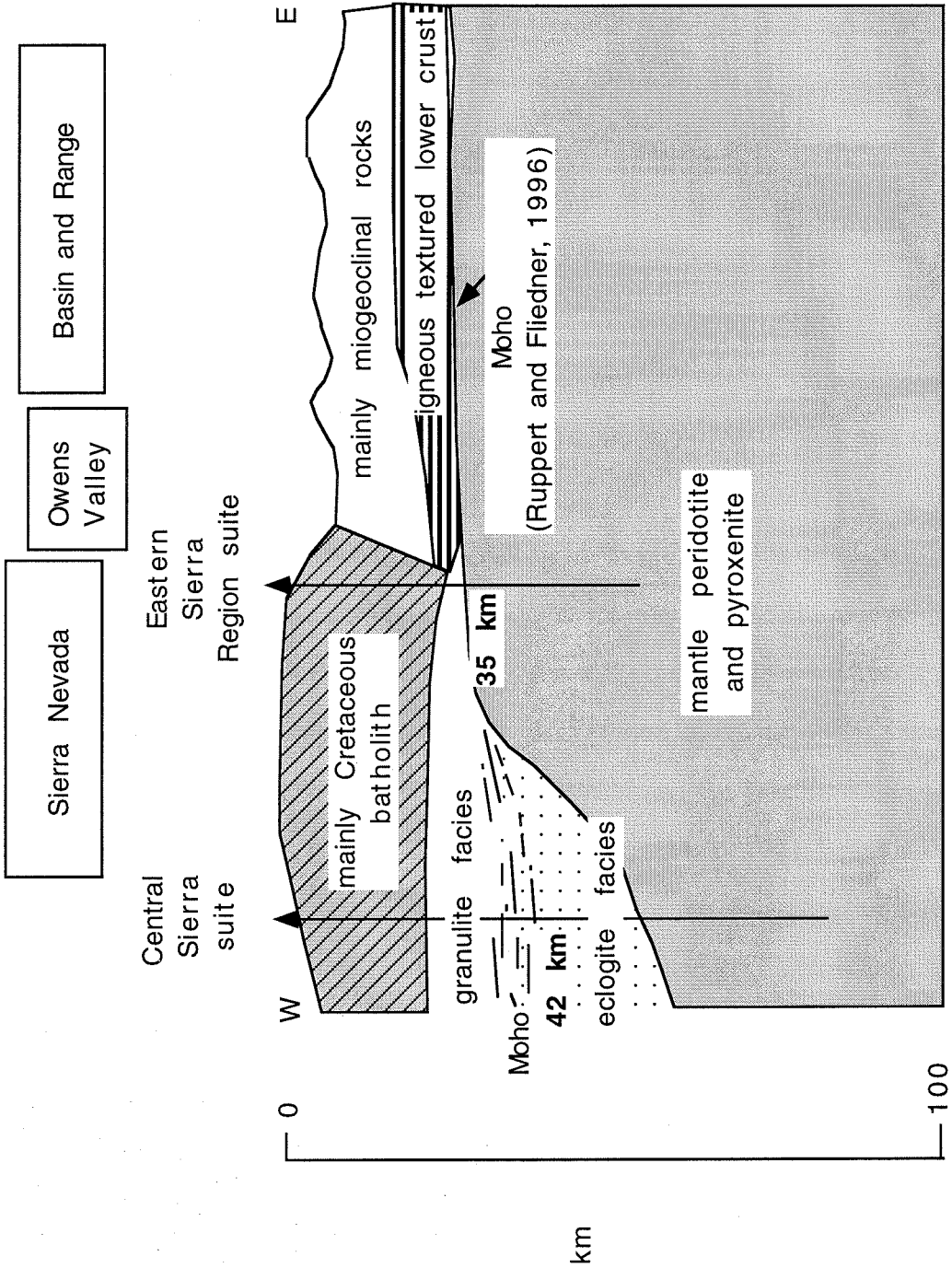
of the Eastern Sierra Region xenoliths investigated in this study confirms this hypothesis. Although the barometry on garnet-absent lithologies of Eastern Sierra Region is subject to large errors, there is a ~1 GPa range in the spinel lherzolites and all samples show remarkably similar temperatures (1180-1250 ^{0}C). A solid adiabatic geotherm can be defined below 35-37 km (~1 GPa) beneath the Owens Valley. The recrystallization textures observed in many of the Eastern Sierra Region xenoliths suggest a dynamic evolution of the Eastern Sierra Region upper mantle. These observations are consistent with having the convective upper mantle at the base of the crust beneath the eastern side of the Sierra Nevada and Owens Valley. The juxtaposition of hot asthenospheric mantle with the lower crust in the Owens Valley can be responsible for the significant fraction of crustal melts identified throughout the Owens Valley, including the Long Valley caldera.

The Central Sierra Nevada peridotites and garnet websterites also define an adiabat (Figure 2-5), but the temperatures are around 950-1000 ^{0}C, ~250 ^{0}C less than the Eastern Sierra Region adiabat.

One possible explanation for this adiabat is that the mantle beneath the Central Sierra Nevada behaved as a convective domain at the time of xenolith entrapment. This hypothesis is based on the magnitude of extension that occurred since Miocene in the area to the east. However, the chemical and isotopical signature of the ultramafic xenoliths and their host basalts from both the Central Sierra Nevada and the Eastern Sierra Region is characteristic of mantle lithosphere (Mukhopadhyay and Manton, 1994; Beard and Glazner, 1995). In particular, if we were to postulate the presence of the convective upper mantle as shallow as ~65 km in the Central Sierra Nevada and ~35 km in the Eastern Sierra Region, it should be pointed out that this asthenosphere-like behavior is a small-scale convection (Buck, 1985) of the old, thinned mantle lithosphere, in response to extension. However, an adiabatic gradient in a convective upper mantle is unlikely at ~ 950 ^{o}C, that is beneath the Central Sierra.

The adiabatic-like trend "B" could, alternatively, be an artifact produced by the side-heating from the Basin and Range. In order to test this possibility, we modeled the temperature distribution in the Sierra Nevada cold upper mantle and the changes associated with the juxtaposition of hot, asthenospheric mantle to the east. We solved the transient, two-dimensional heat conduction equation:

$$\frac{\partial^2 T}{\partial x^2} + \frac{\partial^2 T}{\partial y^2} - \frac{1}{\kappa}\frac{\partial T}{\partial t} + \frac{A_0}{K} = 0 \qquad (2)$$

for a rectangular slab representing a west-east cross section through the Sierra Nevada (Figure 2-8), down to 150 km, where T = temperature, t = time, x = horizontal distance, y = depth, and A_0 = heat production in the crust. As boundary conditions we used a temperature of 15 ^{0}C at surface (y=0), a mantle heat flux (q_m) of 16 mW/m^3 (Lachenbruch and Sass, 1977) and a constant, high thermal gradient at the eastern edge of the rectangle, such that temperatures of 1250 ºC are attained at a depth of 65 km, which is also set to be the lithosphere-asthenosphere boundary. The initial condition is represented in this problem by the low, conductive thermal gradient deduced from today's heat flow measurements in the western Sierra Nevada (Lachenbruch and Sass, 1977), applied throughout the Sierra Nevada block. The problem was solved by the finite difference method using a computer program by Slawomir Tulaczyk (Caltech). Results for the change in the temperature distribution after 4 and, respectively, 10 m.y. are shown in Figure 2-8. The eastern edge boundary condition is somewhat unrealistical because it is more likely that the edge high heat flows were attained gradually. The general trends shown in Figure 2-8 will, however be similar. The results show that it is very likely that heating during a reasonable time scale of 10 m.y. can produce an adiabatic-like temperature distribution in the Sierra Nevada lithosphere without any convection being involved in the top 150 km beneath the Sierra Nevada.

Figure 2-8. Changes in the Sierra Nevada thermal gradient due to the juxtaposition of hot, asthenospheric mantle to the east, in the westernmost Basin and Range. The figure shows the solution to the transient, two-dimensional heat conduction equation (2, see text). The horizontal length in the problem is 100 km (the label 100.0 corresponds to Owens Valley). The vertical dimension in the problem is 150 km (0 corresponds to the surface). The initial condition is a low thermal gradient (Dumitru, 1990), applied throughout the rectangular slab. A boundary kept at high and constant thermal gradient (1200 ^{0}C at 65 km) is imposed on the eastern margin. The changes in the thermal gradient in the slab (shown here for 4 and 10 m.y. after the juxtaposition of the hot boundary) can generate an adiabatic-like temperature gradient in the slab. This general trend holds true when this slab (which stands for cold Sierra Nevada lithosphere) is thinner.

Great Valley   Central Sierra   Eastern Sierra
and Owens Valley

4 Ma of heating

km

0.0

100

0.0   50.0   100.0
km

500.0   1000.0

Temperature

Great Valley   Central Sierra   Eastern Sierra
+Owens Valley

10 Ma of heating

km

0

50

100

0.0   50.0   100.0
km

500   1000

Temperature
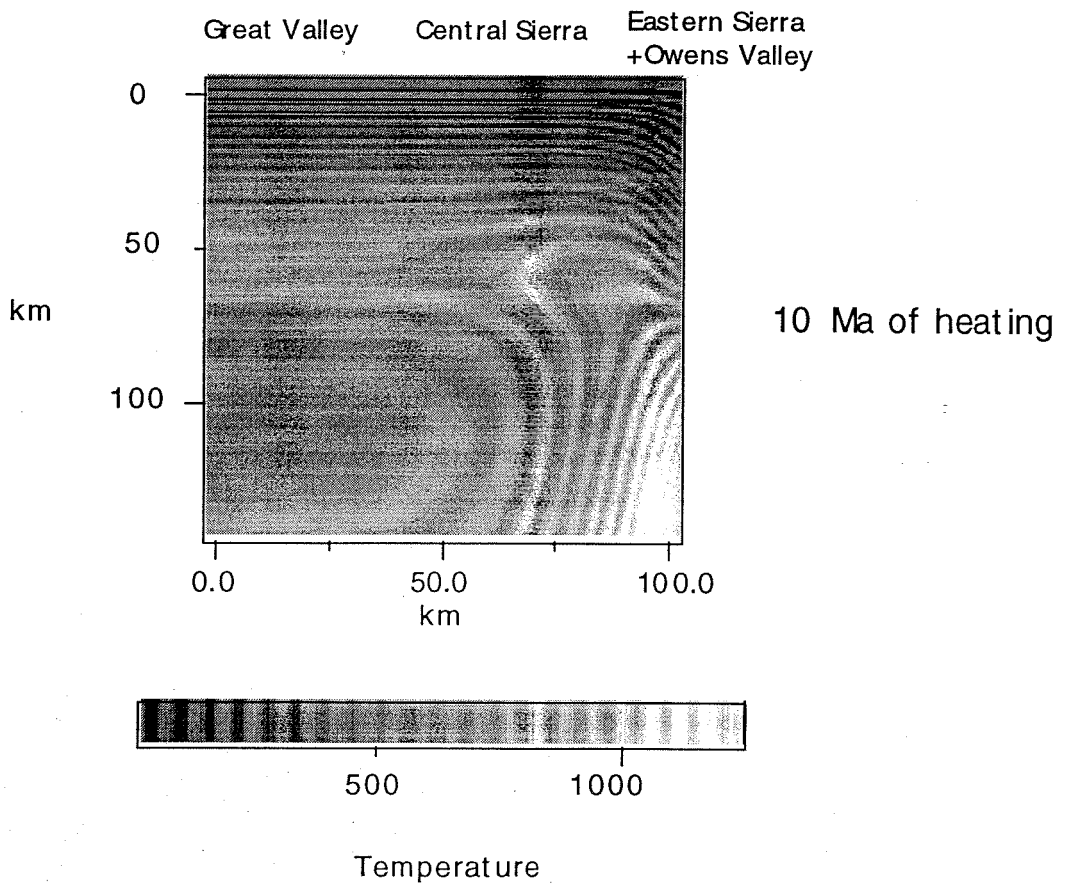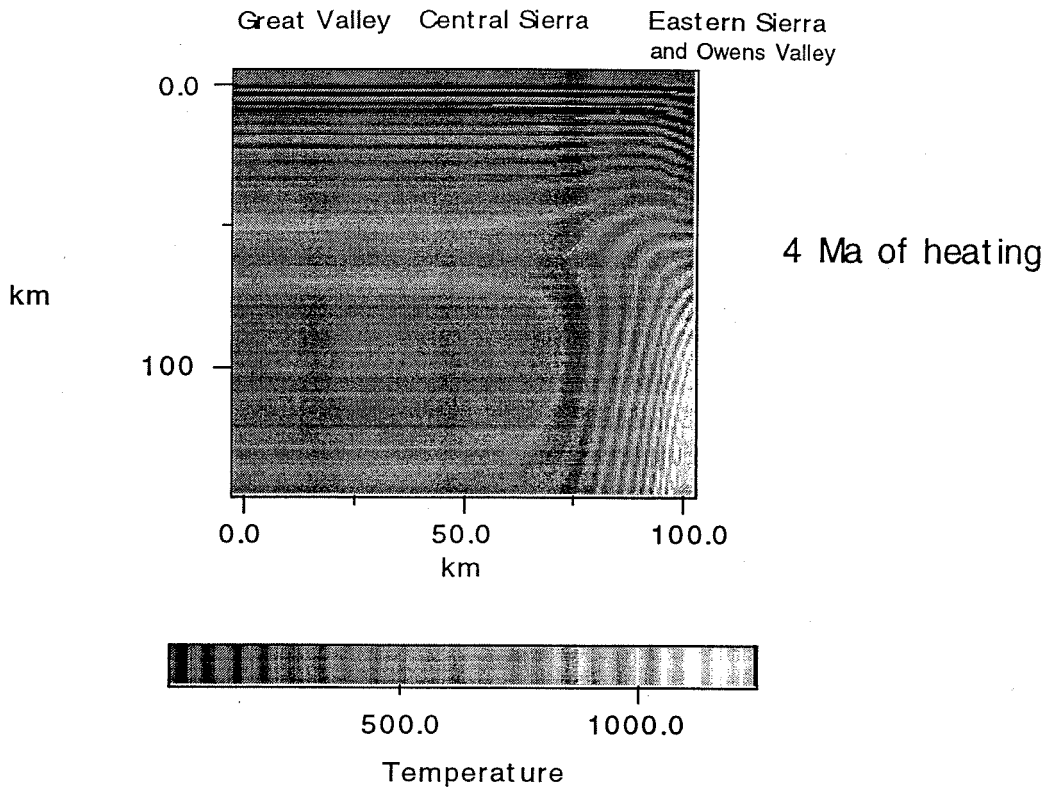
2.6. Buoyancy sources and lithospheric dynamics

As we showed above, the present day Sierra Nevada has a thin crust. The crustal thickness is insufficient to hold the mountain range's elevations. We will define below the "missing root problem" for the Sierra Nevada (see also Jones et al., 1994; Wernicke et al., 1996). Then our results from xenolith petrography and thermobarometry will be used to constrain the possible buoyancy sources for the "unrooted" Sierra Nevada. In order to asses the buoyancy of the Sierra Nevada, the effects of lithospheric thinning and melting, as well as crustal thinning, must be considered.

The missing root problem. The Sierra Nevada crustal root is defined here as the difference between Sierra Nevada and western Basin and Range crustal thickness. As previously mentioned, recent seismic refraction experiments show an average crustal root of ~5 km for the Southern Sierra (Wernicke et al., 1996). The xenolith data presented here is consistent with a shallow Moho underneath the Sierra Nevada. Regardless of the nature of the crust-mantle boundary beneath the Sierra Nevada and westernmost Basin and Range, the thin, low density (low seismic velocity) crustal material is insufficient to hold up the 2800 m average elevation mountain range, 1800 m higher than the neighboring western Basin and Range (Wernicke et al., 1996), assuming isostatic equilibrium (Airy equilibrium). If the average lower crust in the Sierra Nevada above 35 km is tonalitic ($\rho=$ 2800 kg/m^3) and the Basin and Range deep crust is basaltic ($\rho=$ 3000-3100 kg/m^3), only 15-20 km of thicker crust in the Sierra Nevada than in the Basin and Range would be required to support the mountain range's elevation (Figure 2-9a). A mafic lower crust in the Sierra Nevada would require 20-25 km of crustal root and the elevation must be explained mainly by localized mantle buoyancy beneath the Sierra Nevada. These figures are based on the assumption of a constant mantle density of 3300 kg/m^3.

Figure 2-9. Possible support mechanisms for the present-day Sierra Nevada topography (modified after Jones et al., 1994). (a) an Airy model would require c. 15-25 km of low density "root"; (b) a crustal Pratt model can not explain the topography (see text); (c) a mantle Pratt model, involving a lower density mantle beneath the eastern part of the range than the western part of the range is supported by xenolith data. The overall high topography of the Sierra Nevada + Basin and Range compared to the area to the west (Great Valley, see Figure A1-1) can be explained by lithopsheric mantle thinning.

Sierra Nevada

Basin and Range

ρ=2700-2800 kg/m^3

ρ=2800 kg/m^3

15-25 km

a. Airy

ρ=3300 kg/m^3

Sierra Nevada

Basin and Range

ρ=2850 kg/m^3 ρ=2700 kg/m^3

b. Crustal Pratt

ρ=3300 kg/m^3

Sierra Nevada

Basin and Range

ρ–high ρ–low
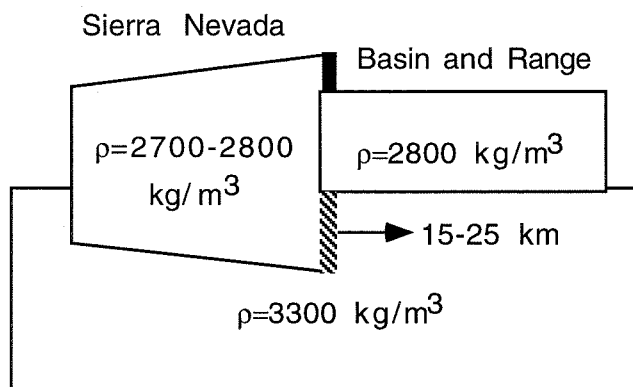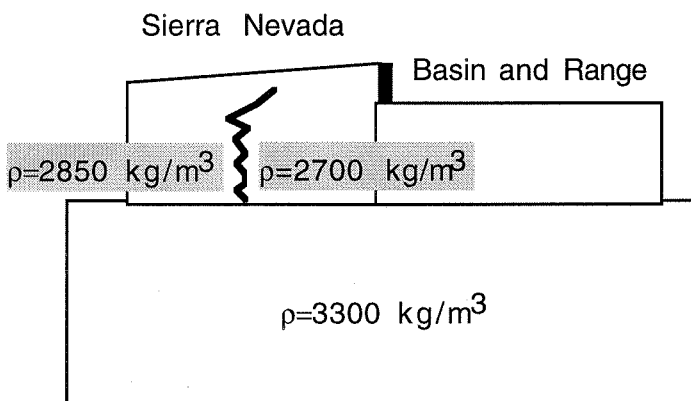
c. Mantle Pratt

?   ?   ?
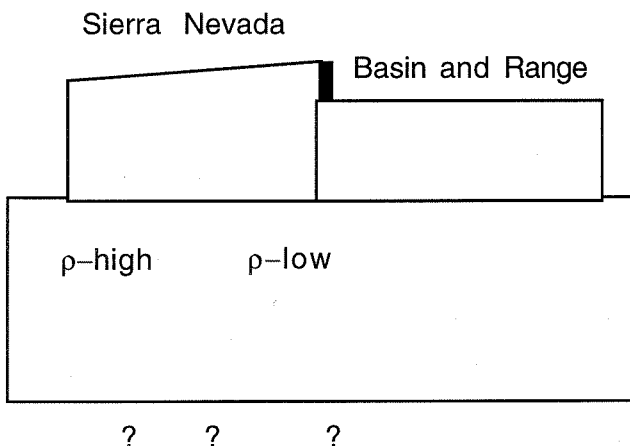
2000 m average elevation difference

Jones and others (1994) showed that lateral density variations within the Sierra Nevada crust (crustal Pratt equilibrium) are also insufficient to create the large elevation differences (Figure 2-9b).

None of these scenarios for crustal composition can explain the Sierra Nevada elevations. Ten to twenty kilometers of root are "missing" and a support mechanism within the seismologically defined upper mantle must be found (Figure 2-9c). The Sierra Nevada seems to be a typical rift shoulder, and an elevation support mechanism that incorporates extension-related processes must be found.

Lithospheric thinning and melting effects. Extensional processes tend to thin the lithosphere by replacing it with hotter, asthenospheric material. The decrease in density due to replacement of lithosphere with asthenosphere due to increased temperature is given by ϕ:

$$\phi = \rho_h / \rho_c = 1 / (1 + \alpha \, \Delta T) \qquad (3)$$

where ρ_h = asthenosphere density, ρ_c = lithosphere density, α = volumetric coefficient of thermal expansion and ΔT = the temperature difference between asthenosphere and lithosphere. For a 250 ^{0}C temperature difference (shown by xenoliths) and $\alpha = 3.4 \times 10^{-5}$ C $^{-1}$ (Cochran, 1982; White and McKenzie, 1989), replacement of only 33 km of cold with hot material can account for 3000 m difference in elevation. If the ΔT is smaller, say 150 ^{0}C, or even 100 ^{0}C, 60 km or 82 km of lithosphere, respectively, must be removed. If this is combined with the use of smaller α' s, as much as 150 km of lithosphere must be removed in order to support the average 2800-3000 m elevations.

Therefore, the dynamic lithosphere-asthenosphere replacement process would in general hold the Sierra Nevada approximately 3000 m higher than the neighboring Great

Valley to the west (sea level mean elevations) if ~35-150 km of lithosphere was removed from beneath the Sierra Nevada and further to the east.

Partial melting of the upper mantle beneath the eastern Sierra Nevada during asthenospheric upwelling is another potential source of buoyancy (McKenzie and Bickle, 1988).

The upper mantle beneath the Eastern Sierra has undergone partial melting with the generation of alkali-basalts and tholeiitic basalts in the Big Pine Volcanic Field (Ormerod et al., 1988), Coso Region, and the Long Valley Region (Luedke and Smith, 1981). There is also strong evidence for the presence of fluids, including melt inclusions not related to the host basalts in almost all Eastern Sierra Region xenoliths (Ducea and Saleeby, work in progress) and high electrical conductivity of the eastern Sierra Nevada upper mantle (Park et al., 1995b). However, melting may only be of second order importance for the Sierra Nevada support mechanism problem. For the recorded ΔT's, small stretching factors (compared to the oceanic lithosphere case) and initial lithospheric thickness of ≤ 200 km, such as in young orogenic regions, the melt "thickness" is negligible, and produces at most 0.3 km of uplift (White and McKenzie, 1989).

Crustal thinning effects. In general, crustal thinning produce subsidence. We will show that in the particular case of the Sierra Nevada this might not be true because thinning involves the removal of a very dense (eclogite facies) lowermost crust by lower density material. We want to estimate what is the net result of crustal thinning in this case. The magnitude of the subsidence generated by the thinning alone and the uplift generated by lowering the density of the lithospheric column will be estimated below.

The amount of crustal thinning is most easily quantified by the stretching factor (β). The β factor is based on the assumption of instantaneous extension of vertical columns of lithosphere and crust by equal amounts and of passive response of the asthenospheric

mantle which upwells to maintain isostatic equilibrium. When a vertical column of the lithosphere is stretched by a factor of β, it thins to $1/\beta$ times its original thickness (McKenzie, 1978). If the Sierra Nevada is viewed as a rigid block which did not experience crustal thinning ($\beta_{Sierra} \sim 1$), the uplift-generating effects of mantle lithosphere thinning described in the previous section can hold the mountain range at its current elevations. A 2000 m difference in elevation between the Sierra Nevada and the Basin and Range would be predicted by the White and McKenzie (1989) pure shear stretching model solely based on the increase of the β factor from 1 for the Sierra Nevada to ~ 2.5 for the Basin and Range. The type of lithospheric stretching is an important factor in determining the magnitude of the effect. A simple shear model would raise this number to $\sim 2300\text{-}2400$ m (Buck, 1985).

At the edge of the Sierra Nevada, in Owens Valley, mantle peridotites are found as shallow as 35 km, strongly favoring the hypothesis of complete lower batholithic crust removal. We think that this is strong evidence for significant crustal thinning, by a factor of at least two, beneath the highest part of the Sierra Nevada.

Mass conservation in the adjacent Basin and Range also requires the involvement of the Sierra Nevada in the significant thinning process (Wernicke 1992). Wernicke and others (1995) predict an average β of ~ 2 for the Sierra Nevada. If this is the case, and about 30 km of lower crustal Sierra was removed in the process, an unusually thick lithosphere ($\sim 250\text{-}300$ km) must have been replaced with asthenosphere if we are to explain the buoyancy by this process. Also, the small β_{Sierra}- $\beta_{Basin\ and\ Range}$ would not explain the difference between Sierra Nevada and Basin and Range elevations. Instead, a process involving some particular buoyancy source beneath the Sierra Nevada would be required.

The extension must have been "hidden," since there is no significant extensional feature observable at surface. Little is known about the extension mechanism. Wernicke

(1990) proposed as a stretching mechanism the removal of the mid-parts of the Sierran quartz-rich crust by laterally pumping it into the adjacent Basin and Range. The xenolith data suggests a more likely removal of the mafic lower crust.

We showed that the equilibration pressures of the Central Sierra Nevada suite lower crustal rocks exhibit a distinct change from feldspar-dominated granulites to bimineralic garnet clinopyroxenites at ~1.2 GPa. This is consistent with the garnet breakdown reaction (1) that we calculated for the garnet with average xenolith-like composition at the low temperatures of the Cenozoic Sierra Nevada forearc (Figures 2-5 and 2-6). The loss of the eclogite facies lowermost crust in the Eastern Sierra and possibly, more recently in the Central Sierra, too, could have taken place by (1) a static process of garnet breakdown as a result of side heating of the Sierra Nevada or (2) a dynamic process.

The first mechanism seems to be negated by the lack of xenoliths in the Eastern Sierra Region carrying the garnet breakdown mineral assemblages. The presence of mantle peridotites as shallow as 35 km strongly favors the hypothesis of complete lower crustal removal, if an initial Central Sierra Nevada-like, coherent batholithic section throughout the Sierra Nevada is assumed.

A dynamic process involving lower crustal removal is our preferred alternative. Lower crustal mafic rocks are less likely to flow than mid-crustal quartz-rich rocks (Wernicke, 1990). It is possible that the mafic root beneath the Eastern Sierra Region was transported *en masse* either laterally along a deep, crustal scale detachment surface (Wernicke, 1990), or was delaminated and sunk into the less dense peridotitic upper mantle (Kay and Kay, 1993). There is no data at present to support either mechanism.

The dynamic process of lower crustal removal would lead to the replacement of dense eclogitic assemblages (3400-3550 kg/m^3, based on the average modal composition of the garnet clinopyroxenites of the Central Sierra Nevada, 60% clinopyroxene and 40% garnet) with peridotitic upper mantle (3300 kg/m^3). The 100-250 kg/m^3 decrease in density is a significant buoyancy source. For a 30 km initial thickness of eclogitic lower crust, and

a 200 kg/m^3 change in density, 1800 m elevation can be supported using the isostatic equilibrium assumption.

Therefore, in the Sierra Nevada case, a ~ 2000-2400 m subsidence produced by a β factor of two (White and McKenzie, 1989) would be almost completely annihilated by the density decrease due to eclogite replacement by peridotite. The eclogite removal and peridotite replacement-related buoyancy effect discussed here is the only source we can deduce from the xenolith studies that can significantly enhance buoyancy beneath the high Sierra Nevada. The process could have removed the central Sierran lower crust since 8 My as well.

2.7. Conclusions

We defined two distinct xenolith suites, one from the Central Sierra Nevada (8-12 Ma volcanics) and one from the Eastern Sierra Nevada, Owens Valley and Inyo Mountains (0-1 Ma volcanics). Thermobarometric data cover the depth range between ~ 25 and 100 km and reveal several differences between the two xenolith suites, which are summarized in Table 2-3. The main results from xenolith petrography and thermobarometry are:

1) Central Sierra Nevada lower crustal and mantle xenoliths are commonly garnet-bearing, while the Eastern Sierra Nevada xenoliths have no garnet at all.

2) The Central Sierra Nevada lower crustal xenoliths consist of mafic lithologies down to ~ 65 km. The deeper 25-30 km of the mafic assemblages were sampled at ~ 8-12 Ma (host volcanic age) in the eclogite facies as garnet clinopyroxenites. The equilibration of the lowermost mafic crust as eclogite facies rocks is a consequence of the very low heat flows in the Sierra Nevada throughout the Cenozoic (Dumitru, 1990). It is unclear if there are any more eclogite facies rocks in the Central Sierra Nevada today.

2-55

Table 2-3. Summary of relevant differences between the Central Sierra Nevada and Eastern Sierra Region xenolith suites.

Central Sierra Nevada xenoliths	Eastern Sierra Region xenoliths
Age of host : 8-11 Ma	Age of host : 0-1 Ma
Garnet very common in lower crustal and upper mantle xenoliths	Garnet absent in all xenoliths
The deepest crustal rocks, equilibrated at ~2 GPa (~65 km)	Crustal rocks are not found below ~1 GPa (35 km)
Mainly metamorphosed lower crust (granulite and eclogite facies)	Igneous, non-metamorphosed lower crustal xenoliths
Adiabatic P-T slope below 65 km; temperatures of 950-1000 ^{0}C	Adiabatic P-T slope below 35 km: temperatures of 1200-1250 ^{o}C
Upper mantle most common lithologies: lherzolites and garnet websterites	Upper mantle most common lithologies: lherzolites and olivine clinopyroxenites

3) The mafic, batholith-related lower crust of the Central Sierra Nevada localities is absent in xenoliths from the Eastern Sierra Nevada region. Mantle peridotites are found in the Eastern Sierra Region below 35 km.

4) The mantle samples deeper than 65 km in the Central Sierra and ~ 35 km in the Eastern Sierra Region define adiabatic slopes in P-T space resembling convective upper mantle behavior. It is very likely that the lithosphere-asthenosphere boundary is very shallow, perhaps close to the base of the crust beneath Owens Valley and the eastern side of the Sierra. The adiabatic-like behavior of the Central Sierra mantle is either a result of small-scale convection in response to crustal thinning or an artifact of heating from the east.

5) There is general agreement between the shallow Moho observed by a recent seismic refraction experiment in the southern Sierra Nevada (Ruppert and Fliedner, 1995; Wernicke et al., 1996) and the xenolith thermobarometry, i.e., we systematically recorded lithologies that behave seismically as "mantle" at pressures higher than 1- 1.3 GPa (equivalent to 35-45 km).

It has been shown that the support mechanism for the Sierra Nevada can be constituted by the replacement of most of the lithosphere with asthenosphere if and only if the Sierra Nevada did not experience significant crustal thinning. The amount of thinning experienced by the Sierra Nevada is a parameter of great importance for our understanding of the behavior of rift shoulders and its determination is currently being addressed. Xenolith evidence from the Eastern Sierra Region suggest a significant thinning of the crust by a factor of two or more (~35 km of crust vs. ~65-75 km original crustal thickness). Therefore, an additional process must explain the buoyancy of the Sierra Nevada mantle. The replacement of dense, eclogite facies rocks of the pre-extension Sierra Nevada lowermost crust by peridotitic upper mantle can produce a ~100-250 kg/m^3 decrease in density, enough to annihilate the subsidence effect induced by the thinning itself. The presence of partial melt in the uppermost mantle of the eastern Sierra Nevada has, most likely, a second order effect in enhancing mantle buoyancy.

References

Ague, J. J. and G. H. Brimhall, Magmatic arc asymmetry and distribution of anomalous plutonic belts in the batholiths of California: effects of assimilation, crustal thickness and depth of crystallization, *Geol. Soc. Am. Bull., 100*, 912-927, 1988.

Atwater, T., and P. H. Molnar, Relative motion of the Pacific and North American plates deduced from sea-spreading in the Atlantic, Indian and South Pacific Oceans, *Proceedings of the Conference on Tectonic problems of the San Andreas fault System, Stanford, California, Stanford University Publications, Geological Sciences, 13,* 136-148, 1973.

Bateman, P. C., and J. P. Eaton, The Sierra Nevada batholith, *Science, 158,* 1407-1417, 1967.

Beard, B. L., and A. F. Glazner, Trace element and Sr and Nd isotopic composition of mantle xenoliths from the Big Pine Volcanic Field, California, *Jour. Geophys. Res., 100,* no. B3, 4169-4179, 1995.

Brey, G. P., and T. Kohler, Geothermobarometry in four-phase lherzolites: II. New thermobarometers and practical assessment of existing thermobarometers, *Jour. Petrol., 31,* 1353-1378, 1990.

Brey, G. P., K. G. Nickel, and L. Kogarko, Garnet-pyroxene equilibria in the system $CaO-MgO-Al_2O_3-SiO_2$: Prospects for simplified (T-independent) lherzolite barometry and an eclogite barometer, *Contrib. Mineral. Petrol. , 92,* 448-455, 1986.

Buck, W. R., Small-scale convection induced by passive rifting; the case for uplift of rift shoulders, *Earth Planet. Sci. Lett., 77,* 362-372, 1985.

Buck, W. R., F. Martinez, M. S. Steckler, and J. R. Cochran, Thermal consequences of lithospheric extension; Pure and simple, *Tectonics, 7,* 213-234, 1988.

BVSP, Basaltic Volcanism Study Project, Basaltic Volcanism in the Terrestrial Planets, *Pergamon Press, New York,* 1981.

Clemens Knott, D., Geologic and isotopic investigations of the early Cretaceous Sierra Nevada batholith, Tulare, CA, and the Ivrea zone, NW Italian Alps: Example of interaction between mantle-derived magma and continental crust, Ph.D. thesis, *California Institute of Technology,* 345 p., 1992.

Cochran, J. R., The magnetic quiet zone in the eastern Gulf of Aden: Implications for the early development of the continental margin, *Geophys. J. R. Astron. Soc., 68,* 171-201, 1982.

Coleman, R. G., D. E. Lee, J. B. Beatty, and W. W. Brannock, Eclogites and eclogites: Their differences and similarities, *Geol. Soc. Am. Bull., 76,* 483-508, 1965.

Crough, S. T., and G. A. Thompson, Upper mantle origin of the Sierra Nevada uplift, *Geology, 5*, 396-399, 1977.

Dalrymple, G. R., Potassium-argon dates of some Cenozoic volcanic rocks in the Sierra Nevada, California, *Geol. Soc. Am. Bull., 74*, 379-390, 1963.

Dewey, J. F., P. D. Ryan, and T. B. Andersen, Orogenic uplift and collapse, crustal thickness, fabrics and metamorphic phase changes: the role of eclogites, in *Magmatic Processes and Plate Tectonics,* Prichard, H. M. and others, eds., *Geological Society Special Publication, 76,* 325-343, 1993.

Dodge, F. C. W., L. C. Calk, and R. W. Kistler, Lower crustal xenoliths, Chinese Peak lava flow, Central Sierra Nevada, *Jour. Petrol., 27*, 1277-1304, 1986.

Dodge, F. C. W., J. P. Lockwood, and L. C. Calk, Fragments of the mantle and crust beneath the Sierra Nevada batholith: xenoliths in a volcanic pipe near Big Creek, California, *Geol. Soc. Am. Bull., 100*, 938- 947, 1988.

Dodge, F. C. W., and P. C. Bateman, Nature and origin of the root of the Sierra Nevada, *Am. Jour. Sci., 288A,* 341-357, 1988.

Domenick, M. A., R. W. Kistler, F. C. W. Dodge, and M. Tatsumoto, Nd and Sr isotopic study of crustal and mantle inclusions from the Sierra Nevada and implications for batholith petrogenesis, *Geol. Soc. Am. Bull., 94*, 713-719, 1983.

Ducea, M. N., and J. B. Saleeby, Thermobarometric constraints on the deep crustal-upper mantle composition of the Sierra Nevada, California, from mafic and ultramafic xenoliths, *Trans. Am. Geophys. Union, 75,* 583, 1994.

Ducea, M. N., R. W. Kistler, and J. B. Saleeby, Testing petrogenetic models for the Sierra Nevada lithosphere with REE data on crustal and mantle xenoliths, *Geol. Soc. Am. Abstracts with Programs, 27*, 15-16, 1995.

Dumitru, T. A., Subnormal Cenozoic geothermal gradients in the extinct Sierra Nevada magmatic arc: Consequences of Laramide and post-Laramide shallow angle subduction, *Jour. Geophys. Res., 95, no. B4,* 4925-4941, 1990.

Ellis, D. J., and E. H. Green, An experimental study of the effect of Ca upon garnet-clinopyroxene Fe-Mg exchange equilibria, *Contrib. Mineral. Petrol., 66,* 13-22, 1979.

Frost, R. B. and T. Chacko, The granulite uncertainty principle; limitations on thermobarometry in granulites, *Jour. Geol., 97,* 435-450, 1989.

Griffin W. L., and S. Y. O'Reilly, The lower crust in eastern Australia; Xenolith evidence, in *The nature of the Lower continental Crust,* Dawson, J. B., et al., eds., *Geol. Soc. Spec. Pub., 24,* 363-374, 1986.

Hanchar J. M., C. F. Miller, J. L. Wooden, V. C. Bennett, and J. M. Staude, Evidence from xenoliths for a dynamic lower crust: Eastern Mojave Desert, California, *Jour. Petrology., 35,* 1377-1415, 1994.

Harley, S. L., An experimental study of the partitioning of Fe and Mg between garnet and orthopyroxene, *Contrib. Mineral. Petrol., 86,* 359-373, 1984.

Harley, S. L. and D. H. Green, Garnet-orthopyroxene barometry for granulites and peridotites, *Nature, 300,* 697-701, 1982.

Henyey, T. L., and T. C. Lee, Heat flow in the Lake Tahoe, California-Nevada, and the Sierra Nevada-Basin and Range transition, *Geol. Soc. Am. Bull., 87,* 1179-1187, 1976.

Isacks, B. L., Uplift of the central Andean Plateau and bending of the Bolivian orocline, *Jour. Geophys. Res., 93, no. B4,* 3211-3231, 1988.

Ito, K., and G. C. Kennedy, The fine structure of the basalt-eclogite transition, *Mineral. Soc. Am. Spec. Pap., 2,* 179-191, 1970.

Jones, C. H., Is extension in Death Valley accommodated by thinning of the mantle lithosphere beneath the Sierra Nevada, California? *Tectonics, 6,* 449-473, 1987.

Jones, C. H., H. Kanamori, and S. W, Roecker, Missing roots and mantle "drips": Regional P_n and teleseismic arrival times in the southern Sierra Nevada and vicinity, California, *Jour, Geophys. Res., 99,* 4567-4601, 1994.

Kay R. W., and S. M. Kay, Petrology and geochemistry of the lower continental crust: an overview, in *The nature of the Lower continental Crust,* Dawson, J. B., et al., eds., *Geol. Soc. Spec. Pub., 24,* 147-159, 1986.

Kay R. W., and S. M. Kay, Delamination and delamination magmatism, *Tectonophysics, 219,* 177-189, 1993.

Kohler, T. and G. P. Brey, Calcium exchange between olivine and clinopyroxene calibrated as a geothermobarometer for natural peridotites from 2 to 60 kbar with applications, *Geochim. Cosmochim. Acta, 54,* 2375-2388, 1990.

Lachenbruch, A. H., and J. H. Sass, Heat flow in the United States and the thermal regime of the crust, in *Geophys. Monogr. Ser.,* vol. 20, *The Earth's Crust, Its Nature and Physical Properties,* J. G. Heacock, ed., pp. 626-675, AGU, Washington, D. C., 1977.

Luedke, R. G., and R. L. Smith, Map showing distribution, composition, and age of late Cenozoic volcanic centers in California and Nevada, *U. S. Geological Survey, Misc. Investigations Series,* Map 1091-C, 1981.

Mansfield, C. F., Upper Mesozoic subsea fan deposits in the southern Diablo Range, California, record of the Sierra Nevada magmatic arc, *Geol. Soc. Am. Bull., 90,* 1025-1046, 1979.

McKenzie, D., Some remarks on the development of the sedimentary basins, *Earth., Planet. Sci. Lett, 40,* 25-32, 1978.

McKenzie, D., and M. J. Bickle, The volume and composition of melt generated by extension of the lithosphere, *Jour. Petrol., 29,* 625-679, 1988.

Meissner, R., The continental crust, a geophysical approach, *Academic Press, London,* 1986.

Mooney, W. D., and C. S. Weaver, Regional crustal structure and tectonics of the Pacific Coastal States; California, Oregon and Washington, in *Geophysical Framework of*

the Continental United States, Pakiser, L. C. and W. D. Mooney, eds., Boulder, Colorado, *Geol. Soc. Am. Memoir, 172,* 129-159, 1989.

Moore, J. C. and T. W. Sisson, Geologic map of the Kern Peak Quadrangle, Tulare County, California, *U. S. Geological Survey, Geologic Quadrangle Map Series,* Map GQ-1584, 1985.

Mukhopadhyay, B., Petrology and geochemistry of mafic and ultramafic xenoliths from the Sierra Nevada batholith, Part 1, Ph.D. dissertation, *University of Texas at Dallas*, 215 p, 1989.

Mukhopadhyay, B., Garnet-clinopyroxene barometry; the problems, a prospect and approximate solution with some applications, *Am. Mineral., 76,* 512-529, 1991a.

Mukhopadhyay, B., Garnet breakdown in some deep seated garnetiferous xenoliths from the central Sierra Nevada: Petrologic and tectonic implications, *Lithos, 27,* 59-78, 1991b.

Mukhopadhyay, B. and W. I. Manton, Upper mantle fragments from beneath the Sierra Nevada batholith- partial fusion, fractional crystallization and metasomatism in a subduction-related ancient lithosphere, *Jour. Petrol., 35,* 1418-1450, 1994.

Newton, R. C., and D. Perkins, Thermodynamic calibration of geobarometers based on the assemblages garnet-plagioclase-orthopyroxene(clinopyroxene)-quartz, *Am. Mineral., 67,* 203-222, 1982

Oliver, H. W., Gravity and magnetic investigations of the Sierra Nevada batholith, California, *Geol. Soc. Am. Bull., 88,* 445-461, 1977.

Ormerod, D. S., C. J. Hawkesworth, N. K. Rogers, W. P. Leeman, and M. A. Menzies, Tectonic and magmatic transitions in the Western Great Basin, USA, *Nature, 333,* 349-353, 1988.

Papike, J. J., K. L. Cameroon, and K. Baldwin, Amphiboles and pyroxenes; Characterization of other than quadrilateral components and estimates of ferric iron

from microprobe data, *Geol. Soc. Am. Abstracts with Programs, 6*, 1053-1054, 1974.

Park, S., R. Clayton, M. Ducea, C. Jones, S. Ruppert, and B. Wernicke, The Southern Sierra Nevada Continental Dynamics Project: the Sierran root question, *EOS, 76,* 297-298, 1995.

Park, S. K., B. Hirasuma, G. Jiracek, and C. Kim, Magnetotelluric evidence of mantle thinning beneath the Sierra Nevada, *Jour. Geophys. Res.,* in press, 1995.

Perkins, D. III, and S. J. Chipera, Garnet-orthopyroxene-plagioclase-quartz barometry; refinement and application to the English River subprovince and the Minnesota River Valley, *Contrib. Mineral. Petrol., 89,* 69-80, 1985.

Perkins, D. III, and R. C. Newton, Charnockite geobarometers based on coexisting garnet-plagioclase-pyroxene- quartz, *Nature, 292,* 144-146, 1981.

Pickett, D. A., and J. B. Saleeby, Thermobarometric constraints on the depth of exposure and conditions of plutonism and metamorphism at deep levels of the Sierra Nevada batholith, Tehachapi Mountains, California, *Jour. Geophys. Res., 98, no. B1,* 609-629, 1993.

Powell, R. and T. J. B. Holland, An internally consistent thermodynamic dataset with uncertainties and correlations, 3. Applications to geobarometry, worked examples and a computer program, *Jour. Metamorphic Petrol., 6,* 173-204, 1988.

Renne, P. R., O. T. Tobish, and J. B. Saleeby, Thermochronologic record of pluton emplacement, deformation and exhumation at Courtright shear zone, central Sierra Nevada, California, *Geology, 21,* 331-334, 1993.

Rudnick, R. L., and S. R. Taylor, The composition and petrogenesis of the lower crust; a xenolith study, *Jour. Geophys. Res., 92, no. B13,* 13,981-14,005, 1987.

Rudnick, R. L., Xenoliths, samples of the lower continental crust, in *Lower continental crust,* D. M. Fountain, ed., 137-158, 1993.

Ruppert, S., and M. M. Fliedner, Crustal structure and thickness of the Southern Sierra Nevada from seismic refraction profiles, *Geophys. Res. Lett.,* submitted, 1995.

Sack, R. O., and M. S. Ghiorso, Chromian spinels as petrogenetic indicators; thermodynamics and petrological applications, *Am. Mineral., 76,* 827-847, 1991.

Saleeby, J. B. , Progress in tectonic and petrogenetic studies in an exposed cross section of young (C.100 Ma) continental crust, southern Sierra Nevada, California, in *Exposed Crustal Sections of the Continental Crust,* M. H. Salisbury and D. M. Fountain, eds., pp. 137-158, Kluwer Academic Publishers, Norwell, Mass, 1990.

Saleeby, J. B., and W. D. Sharp, Chronology of the structural and petrologic development of the southwest Sierra Nevada foothills, California: Summary, *Geol. Soc. Am. Bull., Part 1, 91,* 317-320, 1982.

Snow, J. K., and B. Wernicke, Mass balance of Tertiary tectonism in the central Basin and Range Province: Part 1, Magnitude, rate, partitioning, and distribution of upper crustal strain, *Jour. Geophys. Res.,* in review, 1995.

Taylor, S. R., and S. M. McLennan. The continental crust; its compositional evolution. *Boston, MA: Blackwell Scientific, 312 p, 1985.*

Van Kooten, G. K., Mineralogy, petrology, and geochemistry of an ultrapotassic basaltic suite, central Sierra Nevada, California, U.S.A., *Jour. Petrol., 21,* 651-684, 1980.

Wells, P. R. A., Pyroxene thermometry in simple and complex systems, *Contrib., Mineral. Petrol., 62,* 129-139, 1979.

Wernicke, B., The fluid crustal layer and its implications for continental dynamics, in *Exposed Cross-Sections of the Continental Crust, NATO Advanced Studies Institute, Series C, Mathematical and Physical Sciences, vol. 317,* M. H Salisbury and D. M. Fountain, eds., pp. 509-544, Kluwer Academic Publishers, Norwell, Mass, 1990.

Wernicke, B., Cenozoic extensional tectonics of the western U.S. Cordillera, in *The Cordilleran Orogen, Conterminous United States,* B. C. Burchfiel, ed., Geological Society of America, Geology of North America, Geological Society of America, Geology of North America, *G-3*, 111-116, 1992.

Wernicke, B., and 19 others, Origins of high mountains on continents: the Southern Sierra Nevada, *Science*, 283, 180-183, 1996.

White, R, and D. McKenzie, Magmatism at rift zones: The generation of volcanic continental margins and flood basalts, *Jour. Geophys. Res., 94,* no. B6, 7685-7729, 1989.

Wilshire, H. G., C. E Meyer, J. K. Nakata, L. C. Calk, J. W. Shervais, J. E. Nielson, and E. C. Schwarzman, Mafic and ultramafic xenoliths from volcanic rocks of the western United States, *U. S. Geol. Surv. Prof. Pap., 1443*, 179 p., 1988.

Wyllie, P. J., The nature of the Mohorovicic discontinuity, a compromise, *Jour. Geophys. Res., 68*, 4611-4619, 1963.

Zhang, Q., M. Enami, and K. Suawa, Aluminian orthopyroxene in a pyrometamorphosed garnet megacryst from Liaoning and Shandong provinces, northeast China, *Eur. Jour. Mineral., 5*, 153-164, 1993.

CHAPTER 3

The age and origin of a thick mafic-ultramafic root from beneath the Sierra Nevada batholith

Mihai N. Ducea and Jason B. Saleeby

Abstract

There are few direct observations constraining the vertical extent of large granitic batholiths and their composition at depths greater than 30 km. In this paper we present evidence for a thick (~ 100 km) sequence of cogenetic rocks which make up the roots of the Sierra Nevada batholith of California (SNB). The SNB magmatism produced tonalitic and granodioritic magmas which reside in the Sierra Nevada upper - to mid-crust, as well as deep eclogite facies crust/upper mantle mafic-ultramafic cumulates. Samples of the mafic-ultramafic sequence are preserved only as xenoliths in Miocene volcanics which erupted through the central part of the batholith. We have performed Rb-Sr and Sm-Nd mineral geochronologic analyses on seven fresh, cumulate textured, mafic-ultramafic xenoliths with large grainsize, and one high pressure metasediment. All of these samples equilibrated between ~35 and 100 km beneath the batholith and yield Sm-Nd mineral ages between 81 and 136 Ma, broadly coincident with the previously established period of most voluminous batholithic magmatism in the Sierra Nevada. The Rb-Sr ages are generally consistent with the Sm-Nd ages, but are more scattered. The whole rock initial $^{87}Sr/^{86}Sr$, $^{143}Nd/^{144}Nd$, $^{206}Pb/^{104}Pb$, $^{207}Pb/^{204}Pb$, $^{208}Pb/^{204}Pb$ ratios and the $\delta\ ^{18}O$ of the igneous xenoliths are similar to the ratios published for the outcrops of the central SNB. We interpret the mafic/ultramafic xenoliths to be magmatically related to the upper- and mid-crustal granitoids as cumulates and/or restites. This more complete view of the vertical dimension in a batholith demonstrates that there is a large mass of mafic-ultramafic rocks at depth

which complement the granitic batholiths, as predicted by mass balance calculations and experimental studies. The SNB magmatism was a large scale process responsible for segregating a column ~30 km thick granitoids from ~70 km of mainly mafic-ultramafic residues/cumulates. These rocks have resided under the batholith as eclogite facies rocks for at least 70 Ma after magmatism shutoff. If these dense residues are prone to delamination and recycling back into the mantle, at least in this case higher density itself has not been a sufficient condition for this process. The presence of this thick mafic-ultramafic keel also calls into question the existence of a "flat" (i.e., shallowly subducted) slab at Central California latitudes during Late Cretaceous-Early Cenozoic, in contrast to the southernmost Sierra Nevada and Mojave regions.

3.1. Introduction

Observations of magmatism in continental arcs and granitic batholiths come principally from upper- to mid-crustal levels exposed at the Earth's surface (e.g., Pitcher, 1993). These observations are complemented by experimimental studies of the plausible sources and liquid line of descent of arc magmas (Wyllie, 1984). A similar kind of scientific information has provided a successfull framework for understanding magmatism at mid ocean ridges (e.g., Klein and Langmuir, 1987). However, a number of first order questions regarding the origin of large granitic batholiths cannot be answered by these constraints, in particular the balance of contributions from the mantle wedge underlying the arc, continental crust, and/or the subducting slab. This uncertainty leaves unresolved the extent to which the continental crust is internally differentiated or is largely generated by extraction from the mantle during arc magmatism.

What escapes our observation and prevents us from unique interpretations are the access to the roots of batholiths, the deep crustal counterparts of the plutons that we can observe to levels ocassionally as deep as 30 km (Saleeby, 1990), but in many regions ~5-10 km exposure depth. The crustal thickness beneath modern magmatic continental arcs is more than 30 km. The Andes for example have a crustal thickness of 60-70 km in places (Isacks, 1988). Some lower crustal rocks tectonically emplaced as terranes into the upper crust and exposed at the surface, may have attained their peak metamorphic conditions beneath continental arcs and may be petrologically related to the generation of arc magmas (Clemens, 1988). However, since contemporaneous shallow level plutons or volcanic rocks are generally not preserved near these lower crustal exposures, the connection between lower and upper parts of continental arcs remains speculative. An exception could be the Kohistan arc of Pakistan (Coward et al., 1986) which exposes deep (40-50 km) as well as shallow levels of a Late Cretaceous-Eocene batholith.

Xenoliths brought to the surface by fast ascending mantle-derived magmas are another important source of information on the composition of the deep continental crust and underlying upper mantle (Rudnick, 1992). Xenoliths can carry key petrogenetic information recorded in their mineralogy, textures, trace element conentrations and isotopic compositions, and also preserve a record of lower crustal history that can be unraveled using geochronological methods. Thus, xenolith studies can be an important means of studying the deep crust and upper mantle beneath arcs.

The Sierra Nevada mountain range, California, exposes a large Mesozoic composite Cordilleran batholith, one of the best studied batholiths on Earth (Bateman, 1983). Several Miocene, extension-related mafic-intermediate volcanic centers (Moore and Dodge, 1980), erupted though the axis of the Sierra Nevada batholith (SNB), contain xenoliths of lower crustal and upper mantle origin (e.g., Dodge and Bateman, 1988). A number of mafic-ultramafic olivine-free xenoliths have equilibrated at depths of ~25 to 100 km (Mukhopadhyay, 1989; Mukhopadhyay and Manton, 1994; Dodge et al. 1986, 1988;

Ducea and Saleeby, 1996a). If proven to be cogenetic with the batholith, these samples represent a window into the lower crust of the type-Cordilleran batholith. Their trace element and isotopic compositions in particular could be important in distinguishing between various models of batholith generation. The first step to the succes of such an approach is to prove that these xenoliths are indeed cogenetic to the batholith. Based on their petrographic characteristics they could be also younger (Tertiary) cumulates in the lower crust, oceanic crustal fragments subducted under the Sierra Nevada, or posibly fragments of a lower crust totally unrrelated to the surface batholith. In order to distinguish between these hypotheses, we determined the Sm-Nd and Rb-Sr ages and bulk-rock Sr, Nd, Pb, and O isotope ratios of eight samples from a suite of lower crustal xenoliths in the central Sierra Nevada. The results indicate a direct connection to the SNB for these xenoliths, and provides with physical evidence of a ~100 km thick batholithic section.

3.2. The geology of the Sierra Nevada batholith- background information

Comprehensive information on the geology of the SNB can be found in recent reviews by Bateman (1983), Saleeby (1990) and references therein. We will briefly summarize the main petrologic and tectonic characteristics of the SNB. We will also provide an overview of the Tertiary xenolith-bearing volcanics which erupted in the central part of the SNB.

The Sierra Nevada magmatic arc formed as a product of the prolonged ocean floor subduction beneath the southern edge of the north-American continent (Dickinson, 1981). Magmatism took place in the Sierra Nevada between 220 Ma and 80 Ma (Everden and Kistler, 1970; Chen and Moore, 1982; Saleeby et al., 1987), although most of the exposed plutons yield ages between 125-85 Ma (Saleeby, 1990). It consists of numerous plutons

ranging in size from less than 1 km^2 to over 100 km^2, with compositions that are mainly tonalitic to granodioritic; intermediate rocks (e.g., monzonites) or mafic rocks (e.g., gabbros) are found, but are not common even in the exposures of the deeper intrusion levels of the batholith. The batholith has a clear petrographic, chemical and isotopic west to east zonation, which is almost perpendicular to the batholith's NNW-SSE long dimension (see Saleeby, 1990, for a review).

The batholith covers ~90% of the southern and central Sierra Nevada mountain range, and ~60-70% of the northern part of the range. Erosion, unroofing and tilting have taken place following magmatism. No metamorphic event has affected the Sierra Nevada batholith after its formation; igneous textures have been preserved almost without exception. The igneous crystallization depths of the rocks presently exposed, vary from 0 km represented by large ~100 Ma caldera deposits preserved in the high Sierra Nevada (Saleeby, 1990), to ~ 30 km in the southernmost Sierra Nevada (Pickett and Saleeby, 1993). Igneous barometry studies have shown that the igneous crystallization depths gradually increase from north to south, as well as from east to west (Ague and Brimhall, 1988). Overall, the Sierra Nevada has been preserved as a tilted, but coherent block providing almost continuous exposures of the upper 30 km of a gigantic Mesozoic batholith.

There is no direct information on the composition and vertical extent of the batholith at depths exceeding the equivalent of 1.0 GPa equilibration pressures. Hence, the extent and composition of the batholith at depths greater than ~30-35 km can be inferred either indirectly from petrologic constraints borne out of studies of the granitoid outcrops or from geophysical observations.

The origin of magmas for the SNB is the subject of numerous debates. Before the general acceptance of the plate tectonics theory, the batholith was thought to have formed by intracrustal melting at the deepest levels of an overthickened and strongly deformed "geosyncline" (Bateman and Eaton, 1967). Models that incorporate melting of the mantle

wedge above a subduction zone have been proposed for the batholith origin in more recent years (e.g., DePaolo, 1981). The limitation of simple mantle melting models is that typical olivine-rich upper mantle compositions (peridotites) can not produce granitoids by partial melting (e.g., Wyllie, 1984). Either mafic melts generated in the mantle have later incorporated a large amount of pre-existing continental crust (De Paolo, 1981), large scale fractional crystallization led to the distillation of uppermost crustal granitoids while leaving behind large volumes of mafic cumulates (Coleman et al., 1992), or both. In either model presented above, a significant mass of low silica residua/cumulates, as much as ten times more than the "surface" batholith (> 30 km thick), is predicted to exist at depth, depending on the composition of the source rocks in the crust and the proportion of "juvenile" material supplied from the mantle. The lower the silica concentration of the crustal source and the higher the mantle wedge contribution to the mass budget of the batholith, the larger the mass of the predicted residue will be. Based on experimental petrology (e.g., Green and Ringwood, 1967; Wolf and Wyllie, 1993), the material left behind as residues or cumulates will be rich in garnet, pyroxene, and possibly amphiboles, given the great depths at which most of it will be located.

However, there is no geophyisical evidence for such a garnet-rich counterpart of the SNB at depth. A recent seismic profile across the Sierra Nevada has demonstrated that the area has a thin, low velocity, granitic crust (35-42 km), which is underlain by upper mantle with properties of peridotite (Wernicke et al., 1996). Geophysical data do not support the existence of a garnet-rich layer beneath the seismologically-defined crust.

The contradiction between the data emerged from petrological and geophysical data is an important one for understanding the origin of batholiths, and applies to other Cordilleran batholiths as well (e.g., the Peninsular Ranges batholith, Gromet and Silver, 1987). Are some batholiths flat-bottomed and thin (Hamilton and Maers, 1966) or have their roots been removed (Kay and Kay, 1993)? A satisfactory answer may be obtained

only when the vertical dimension of SNB, and of batholiths in general, are compositionally "mapped" to depths much greater than allowed by surface exposures.

The Cenozoic collapse of the Cordillera at the latitude of the Sierra Nevada and the high magnitude extension to the east of the batholith in the Basin and Range province was accompanied by significant volcanism, which extended into the Sierra Nevada mountain range. As many as 150 small volume flows, pipes and dikes of mafic to intermediate compositions have erupted through the central and southern Sierra Nevada batholith during the Late Cenozoic (Moore and Dodge, 1980). The volcanism can be divided temporally in three stages: Miocene (8-12 Ma), Pliocene (3-4 Ma), and Quaternary (0-1 Ma). Nineteen of these volcanic occurences, representing all the three stages, contain upper mantle and/or lower crustal xenoliths (Ducea and Saleeby, 1996a and b). Five of the Miocene localities contain unusually rich populations of apparent lower crustal origin, including high pressure assemblages described as "garnet granulites" (some could be in reality garnet-bearing gabbroic cumulates), garnet websterites, eclogites, and garnet clinopyroxenites (Domenick et al., 1983; Dodge et al., 1986, 1988; Mukhopadhyay, 1989; Ducea and Saleeby, 1996a). In particular, the locality of Big Creek, a trachyandesite pipe located in the central Sierra (lat: $37^0 13'$ N, long: $119^0 16'$ W), along the axis of the batholith, contains xenoliths which equilibrated at pressures as great as 4.2 GPa (Ducea and Saleeby, 1996b). The feldspathic rocks (e.g., the "granulites") have been interpreted to be cumulates of the Sierra Nevada batholith (Dodge et al., 1986), whereas the olivine-free and garnet-rich ("eclogitic") ultramafic assemblages, typically showing higher equilibration pressures, have been interpreted as batholith cumulates (Mukhopadhyay, 1989), or fragments of subducted oeanic crust (Dodge et al., 1988); but they could also be Tertiary cumulates related to the magmas that carried the xenoliths, or old lower crustal fragments that are unrelated to any of the above.

Table 3-1. Mineral composition, texture and petrography of the analyzed samples

Sample	Primary minerals[1]		Secondary minerals[2]	Alteration products	Reactions with host	Textures, structures	Rock type
	Principal (>1 vol %)	Accesory (<1 vol %)					
G36	garB, cpx	ru (in garB), hb, opx	sp, kel	none	none	cumulate[3], subhedral, poikilitic	eclogite
BC218	cpx, garB	ru (in garB), hb, opx	sp, kel	none	hb-rich corona	cumulate, subhedral, 120° triple junctions, poikilitic	garnet clinopyroxenite
G39	cpx, garB	ru (in garB), opx, hb, qz, sp (?)	sp (?), kel	none	none	layering, poikilitic cpx in garB, anhedral	garnet clinopyroxenite
BC207	garC, cpx	sph, ap, qz, mgt, opx	kel, plg	none	none	poikilitic cpx in garC, subhedral	eclogite
F34	garA, cpx, opx	ap	kel	none	partial melting due to host heat	layering, anhedral,	garnet websterite
B75	plg, garB, cpx	ap, opx, qz, zr	kel, sp, op	turbid plg	hb corona	cumulate, layered, subhedral, 120° triple junctions, poikilitic	layered gabbro
BC35	plg, cpx, hb	ap, op, qz.	none	cpx turbid coronas	incipient melting of plg-hb contacts	cumulate, layering, 120° equilibrium textures, subhedral	layered gabbro
PBC	ol, opx, cpx, gar		kel, op	cc	none	porphyroclastic	peridotite
297	qz, cpx, garC	sph, ru, zr, ap	kel	none	partial melting	granoblastic	quartzite

[1] - Mineral abbreviations : garA, garB, and garC - garnet of type A, B, and C respectively from the classification scheme of Coleman et al. (1965); cpx - clinopyroxene; ru - rutile; hb - hornblende; ol - olivine; sp - spinel; kel - denotes a cryptocrystalline polymineralic breakdown product formed probably during the entrainment of the sample as xenoliths in the host melt, and consisting usually of plagioclase, spinel and an Al-rich orthopyroxene, opx - orthopyroxene; qz- quartz; sph - sphene; ap - apatite; mgt - magnetite; cc- calcite; plg- plagioclase; op - unidentified opaque minerals; zr- zircon.
[2] - These products appear to have formed after the inclusion of these samples in the host melt.
[3] - The term "cumulate" is used in this table. The term is strictly descriptive. These textures could be indicative of cumulate rocks formed during fractional crystallization in a magma chamber, but could also represent restites form a partial melting zone.

This paper reports geochronological results on lower crustal xenoliths from Big Creek. Data on equilibration temperatures and pressures were previously published (Ducea and Saleeby, 1996a).

3.3. Petrography

Eight samples from a larger set previously investigated for thermobarometry (Ducea and Saleeby, 1996a) were selected for geochronological analyses. They are four garnet clinopyroxenites (with accesory orthopyroxene), one garnet websterite, two mafic feldspathic rocks and one metasediment. A summary of the petrography of these samples is given in Table 3-1. These compostional types cover the spectrum of lower crustal lithologies found as xenoliths at Big Creek, that have resided at mid- to deep crustal levels (30 km or more) beneath the batholith, and equilibrated over a large pressure interval, between 0.85 and 3.3 GPa. These samples were also selected based on their large grainsizes, little if any alteration products, and minor interaction between the host trachyandesite and the xenoliths. We provide below a description of the analyzed samples. Figure 3-1 illustrates the textural appeerance of the main petrographic groups investigated in this study: garnet clinopyroxenites and eclogites (Figure 3-1a and 1b), garnet websterites (Figure 3-1c), and feldspathic mafic rocks (Figure 3-1d).

Four samples are composed mainly of garnet and clinopyroxenes (Table 3-1). In a more general sense, they are eclogite facies rocks with basic to ultrabasic chemistries. One sample (G36) has relatively high concentrations of Na_2O in clinopyroxene (2.5-3%) and a garnet with a almandine/pyrope ratio of 1.9 (Group C garnet, according to Coleman et al., 1965), and resembles a "true eclogite," commonly found in, but not restricted to subduction environments. Sample BC207 contains a grossular-rich garnet and an augitic clinopyroxene, as well as accessory minerals such as sphene and calcite. The other two

Figure 3-1. Photomicrographs of representative samples used in this study. Long dimension of photo is 5 mm in a-d, and 1 cm in e-f.

a. page 3-11, top, cumulate garnet clinopyroxenite; photograph is composed of a large dark (isotropic) crystal of garnet including poikilitic clinopyroxenes. Clinopyrroxene (white) is also present near the right edge of photo.

b. page 3-11, bottom, garnet clinopyroxenite cumulate. Detail of a pyroxene-rich layer showing static growth with 120° triple junctions. All crystals in photo are pyroxenes.

c. page 3-12, top, garnet websterite xenolith. Ga- garnet, opx- orthopyroxene, cpx- clinopyroxene. Note the kelyphitic rims on garnet and the lower garnet abundance compared to the garnet clinopyroxenites.

d. page 3-12, bottom, cumulate gabbro. Plagioclase crystals are white, showing some alterations, the grey crystals are clinopyroxenes, whereas the black crystal is magnetite. The cryptic layering observable in this sample including in this photograph is probably due to igneous accumulation rather than metamorphic banding.

e. page 3-13, top, pure garnet separate. Single crystal of translucid garnet (BC218) free of mineral inclusions or surface breakdown products.

f. page 3-13, bottom, impure garnet separate. Single crystal of impure, opaque garnet (BC218), due to the presence of a kelyphitic rim.
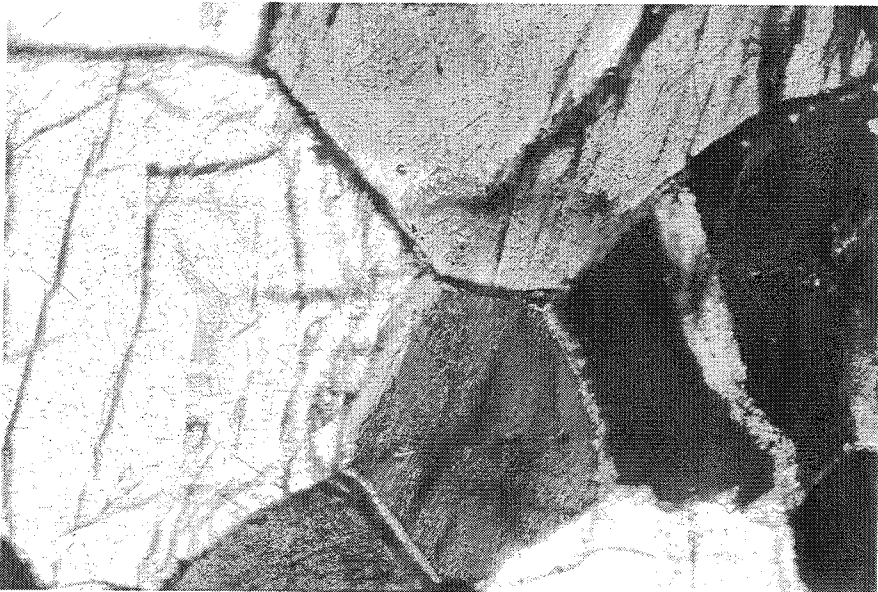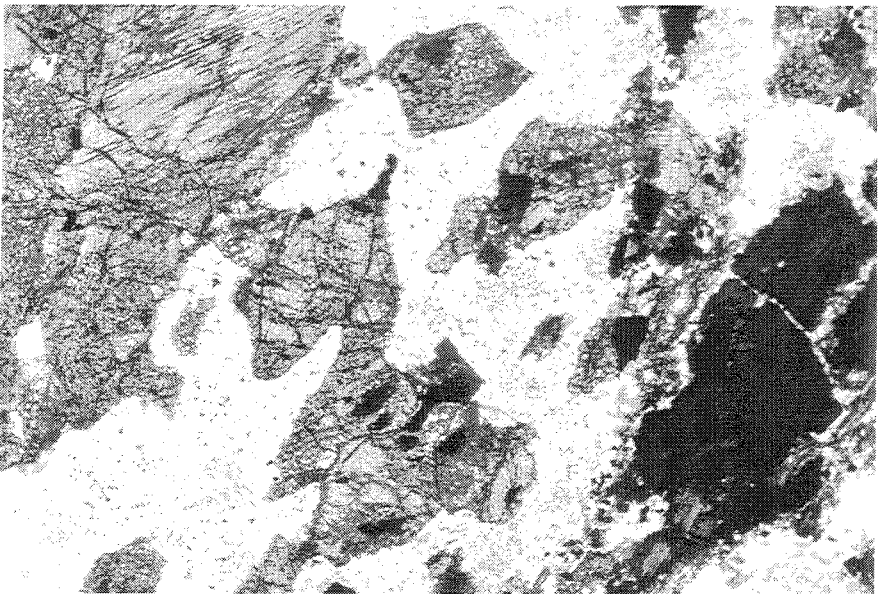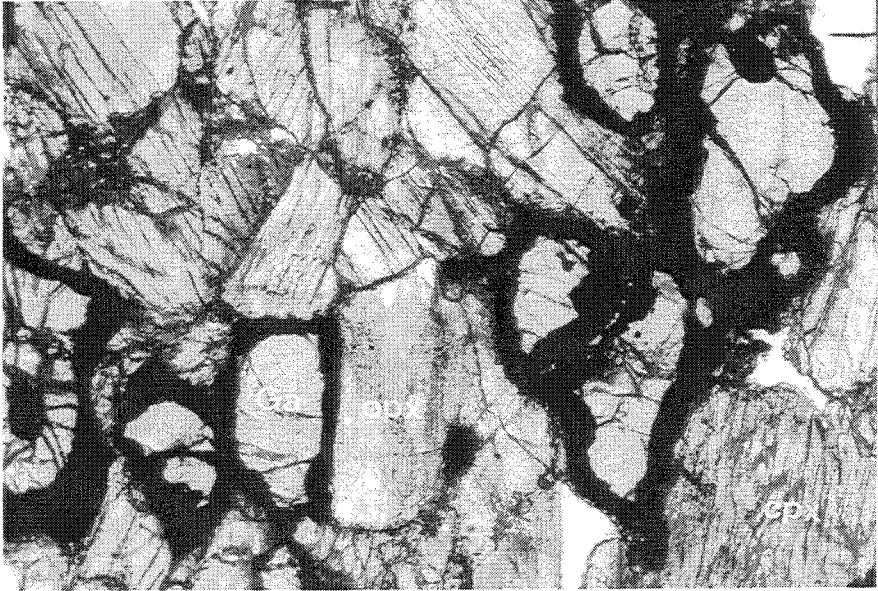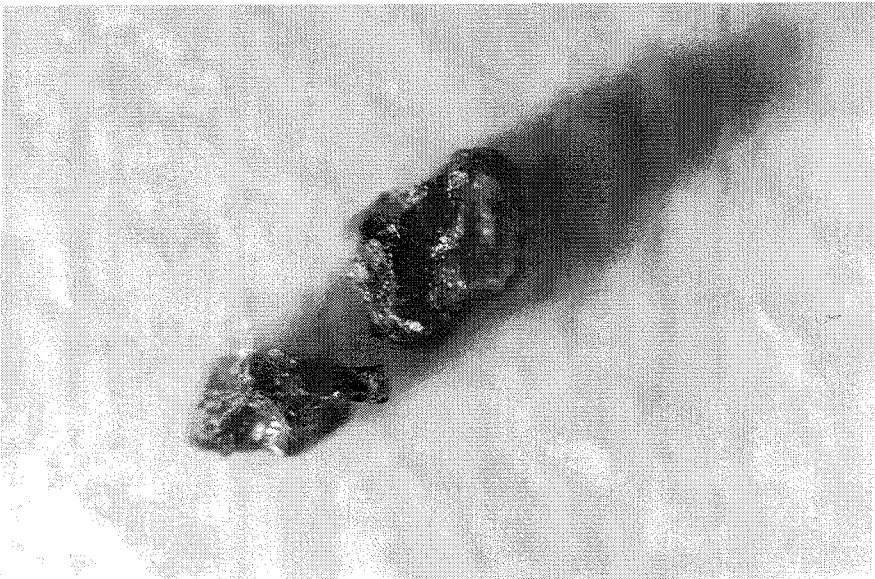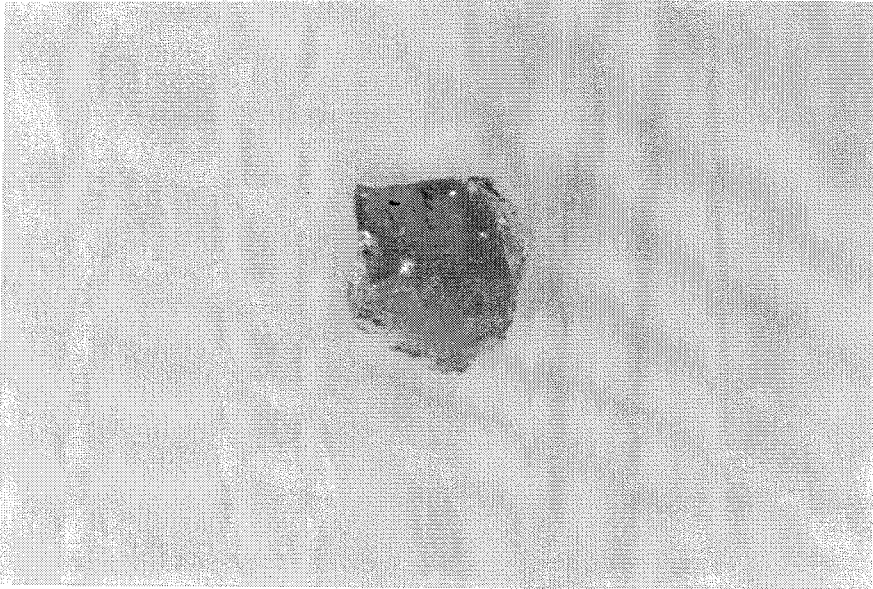
garnet-clinopyroxene rocks (BC218 and G39) contain Group B garnets (Coleman et al., 1965) and Na-poor diopsidic pyroxenes. Garnet-clinopyroxene rocks with such mineral compositions are commonly classified as "garnet clinopyroxenites," and are typically found in deep continental crustal environments (Carswell, 1990).

We believe, based on above mentioned thermobarometric results, as well as textural and whole rock isotopic arguments which will be presented below, that all four eclogites studied here are derived form the lower continental crust, and the bulk chemistry of the rocks produced the more unusual mineral compositions of garnets and pyroxenes in samples G36 and BC207. All four rocks contain accesory orthopyroxene and rutile (the last one mostly as inclusions in garnet). Other accessory minerals include hornblende, apatite, and quartz. All samples have uniform mineral compositions (Ducea and Saleeby, 1996a).

The textures of the four "eclogites" are very similar to the ones observed in igneous cumulates in stratified mafic magma chambers (Hunter, 1986). These rocks have attained textural equilibrium, and although the layering commonly faintly developed at xenolith scale (~ 5cm scale) may be suggestive of metamorphic banding, the ubiquitous poikilitic inclusions leave little doubt that these rocks are igneous cumulates (Figure 3-1a and b). The word "cumulate" is to be taken as a very broad term in that these rocks represent density-driven accumulations of crystals in a magma chamber, but they could also represent restites grown and compacted after the extraction of a large fraction of liquid (a "melanosome" in the migmatite terminology, Ashworth, 1985). The textural relations alone are not able to distinguish between these two scenarios.

Sample F34 is a garnet websterite (Figure 3-1c). This rock yielded the highest equlibration pressure in this suite (3.3 GPa), and is one of a number of high pressure garnet websterites (>2.5 GPa) found at Big Creek (Mukhopadhyay, 1989; Ducea and Saleeby, 1996a). There are a number of differences between garnet websterites and the eclogites: the abundance of orthopyroxene (20-30% in websterites compared to generally <1-3% in garnet clinopyroxenites and eclogites), the abundance of Cr in the clinopyroxene

(> 2% Cr_2O_3 in websterites, <1% Cr_2O_3 in eclogites), the nature of the garnet (pyrope-rich or Group A garnets of Coleman et al., 1965 in websterites, as opposed to Group B garnets in eclogites), the pressure of equilibration (2.5-3.3 GPa in websterites, compared to <2.6 GPa in eclogites). The differences could reflect simply the different depth range from which these samples were equlibrated, but they could also be genetically unrelated. The textural appearance of the websterite, including the sample analyzed for this study is however very similar to the eclogite textures. Sample F34 has typical cumulate textures.

Samples BC75 and B35 are feldspar-rich rocks (Figure 3-1d). Plagioclase constitutes about 50 vol percent of the rock. Other minerals present are garnet and clinopyroxenes in BC75, and clinopyroxenes, hornblende and garnet in BC35. Rocks similar to BC75 and BC35 previously found at Big Creek (Dodge et al., 1986) and at the neighboring xenolith locality of Chinese Peak (Dodge et al., 1988) were described as "granulites." Trace elements indicate a cumulate igneous origin for BC75 (Ducea et al., 1995). Perhaps the best petrographic name for BC75 is "cumulate gabbro." Sampe BC35, based on major and trace element characteristics, resembles the composition of a true mafic melt.

Sample 297 is a quartzite, which probably contained both carbonaceous and pelitic impurities. The rock contains ~90 vol% quartz, ~ 8 vol% diopside and grossular-rich garnet, and accesory sphene, rutile, zircon, and apatite. The rutile-sphene-grossular-kyanite barometer of Manning and Bohlen (1991) yields a minimum (no kyanite) equilibration pressure of 2.5 GPa assuming that rutile, sphene and grossular, which are usually not in contact but isolated within quartz-rich zones, were in equilibrium during their growth. The eclogite facies mineralogy of the alumosilicate phases, the high concentrations of Al in sphene and the optical identification of coesite mineral inclusions in garnet also suggest high depths of residence for this metasediment. This is the only sample from the suite analyzed in this study which does not display igneous, cumulate-like textures.

All the analyzed rocks preserve a simple geologic history, most likely crystallization at high temperature, and with the exception of the quartzite, in the presence of a magma that has since been extracted. There is strong chemical evidence that these rocks have crystallized in equilibrium with SNB-like silicic melts, although it is quite dificult to distinguish between a cumulate vs. a resiual origin. A geochemical study of these samples will be presented in Chapter 5 of this thesis.

A more recent, incipient metamorphic event has resulted in partial breakdown of garnets and clinopyroxenes from all the eight analyzed rocks. The products of this event are kelyphitic rims on garnet (a cryptocrystalline polymineralic product consisting of plagioclase, spinel, Al-rich orthopyroxene and anorthite) and the growth of a brown spinel at garnet-clinopyroxene contacts.

3.4. Analytical procedures

Whole-rock samples (typically 100-500 g) were carefully extracted from the host trachyandesite, broken down by hammer and crushed in a jaw crusher to about 1/3 of their average grainsize. Sample segments with visible alteration products were discarded. The samples were then homogenized and split, roughly two thirds for mineral separation, and a third for whole rock analysis. Both splits were initially washed in deionized water and then acid leached for 25-30 min in warm 1 N distilled HCl, while in an ultrasonic bath. The whole-rock samples were then ground in a fine powder using a WC shatterbox prior to their dissolution. The split for mineral analyses remained relatively coarse throughout the separation procedure, although for some samples rich in composite grains, a few additional grinding steps were necessary. Separation of minerals was accomplished by a Franz magnetic separator and handpicking in alcohol under a binocular microscope. The mineral separation procedure resulted in three fractions for each mineral: (1) ultrapure mineral separates, (2) lower purity separates, which contained occasional kelyphitic rims or very

rarely, inclusions of other minerals, and (3) impure fraction, with numerous composite grains. The third fraction was not used further for any analyses. We exemplify for garnet the difference between the first two fractions (Figure 3-1 e and f): the ultrapure fraction contained translucent grains with no stains or visible inclusions, whereas the lower purity fraction contained obvious black stains, the ubiquitous kelyphitic rims that accompany garnets. Although our aim was to analyze the purest grains for geochronology, we did analyze some separates of the lower purity "quality" to check whether their isotopic characteristics depart from the "pure" grains and if they carry any meaningful geochronometric information. The lower purity samples can be identified in Table 3-2 by the presence of the subscript "$_1$."

To eliminate any grainboundary alteration effects, the handpicked mineral separates were leached again in 2.5 N distilled HCl. The samples were then ultrasonically cleaned, rinsed multiple times with ultrapure water and dried in methanol.

The samples were spiked with ^{87}Rb, ^{84}Sr, and mixed ^{147}Sm-^{150}Nd tracers (Appendix 2). Dissolution of the spiked samples for isotopic analyses was performed in screw-cap Teflon beakers using HF-HNO$_3$ (on hot plates) and HF-HClO$_3$ mixtures (in open beakers at room temperature). The samples were taken in 1 N HCl and any undissolved residue was attacked in the same way. Separation of the Rb, Sr, and the bulk of the REE was achieved via HCl elution in cation columns. Separation of Sm and Nd was carried out using a LNSpec® resin. The highest procedural blanks measured during the course of this study were: 11 pg Rb, 180 pg Sr, 5 pg Sm, and 18 pg Nd.

Isotopic analyses for Sr and Nd, as well as isotope dilution analyses of Rb, Sr, Sm, and Nd, were performed at Caltech using a VG multiple collector mass spectrometer. The isotopic compositions of Sr and Nd were determined on the same spiked samples. The filament loading and mass spectrometric analysis procedures are given in Appendix 2 and represent an update of the ones previously described by Pickett and Saleeby (1994). The Sr

isotopic ratios were normalized to $^{86}Sr/^{88}Sr = 0.1194$, while the Nd isotopic ratios were normalized to $^{146}Nd/^{144}Nd = 0.7219$.

The grand means of isotopic ratios were corrected by an offline manipulation program, which adjusts for the spike contributions to both the fractionation correction and each ratio, and performs isotope dilution calculations. The analytical techniques for isotopic analyses of oxygen and lead are given in Chapters 4 and 5 of this thesis.

3.5. Results

The Rb-Sr and Sm-Nd mineral and whole rock analyses are given in Table 3-2. A whole rock Sr and Nd analysis of the Big Creek host trachyandesite is also given in Table 3-2. The calculated Rb-Sr and Sm-Nd ages for best-fit isochrons are given in Table 3-3. The isochrons, shown in Figure 3-2, are principally constrained by the garnet and clinopyroxene isotopic compositions. The whole rock values are potentially of interest because of the presence of accessory minerals such as apatite or sphene but are susceptible to exchange between xenolith and the host trachyandesite. For this reason we have calculated isochrons using the mineral pair garnet-clinopyroxene which gives the most robust slope for an isochron. In addition we have also calculated three or four point isochrons including the whole rock values and other phases if present. The advantage of the three- or more point isochrons is that they can better constrain the linear correlation between data points. If the correlation coeficient of the three- or four point linear best fit (listed in Table 3-3) was better than 0.99, we have used this fit for calculating the ages discussed further, although in such a situation the garnet-clinopyroxene pairs would yield a very similar age. If, however, this coefficient was lower than 0.99, we have used the garnet-clinopyroxene slope for calculating the age. The analtical uncertainty in calculating these ages is small, ~ 1% of the calculated ages. The uncertainty induced by poor correlations in three or four point isochrons, when observed, could be as high as 20% of

Table 3-2. Isotopic data for mineral and whole rock samples

Sample*	Rb (ppm)	Sr (ppm)	$^{87}Rb/^{86}Sr$	$^{87}Sr/^{86}Sr$	Sm (ppm)	Nd (ppm)	$^{147}Sm/^{144}Nd$	$^{143}Nd/^{144}Nd$	$\varepsilon_{nd}(0)$
Host-WR	78.51	348.2	0.334	0.705852	18.90	28.31	0.105	0.512532	-1.82
Eclogites									
G36-cpx	2.67	89.95	0.085	0.706290	1.79	3.62	0.299	0.512486	-2.96
G36-gar	1.83	3.24	1.626	0.708243	1.51	0.79	1.150	0.513008	7.21
G36-gar$_1$	2.47	10.45	0.679	0.706991	4.63	3.26	0.860	0.512850	6.04
G36-WR	8.66	113.68	0.219	0.706029	1.78	2.83	0.379	0.512547	-1.78
BC218-cpx	1.48	81.84	0.052	0.706239	0.77	0.78	0.594	0.512746	2.10
BC218-gar	3.05	5.87	1.493	0.707930	0.42	0.15	1.683	0.513352	8.92
BC218-WR	14.88	57.17	0.748	0.706452	0.92	0.92	0.605	0.512730	1.80
G39-cpx	2.01	76.94	0.075	0.706580	1.75	10.19	0.104	0.512387	-4.89
G39-gar	2.02	6.65	0.87	0.707085	12.51	29.00	0.261	0.512473	-3.21
G39-WR	1.98	70.32	0.081	0.706314	5.34	25.50	0.127	0.512392	-5.38
BC207-cpx	29.7	101.21	0.851	0.705895	0.17	0.80	0.129	0.512353	-6.54
BC207-hb	10.3	70.47	0.420	0.705353					
BC207-gar	5.8	8.37	1.981	0.706843	1.34	1.94	0.416	0.512558	-1.56
BC207-WR	15.1	53.55	0.810	0.705882	0.63	2.29	0.167	0.512403	-4.58
Websterite									
F34-cpx	0.19	208.07	0.003	0.705956	1.81	7.22	0.151	0.512468	-3.31
F34-cpx$_1$				0.705982				0.512581	
F34-opx	0.38	10.35	0.106	0.706383	0.17	0.54	0.194	0.512434	-3.99
F34-opx$_1$				0.706054				0.512579	
F34-gar	1.79	6.03	0.376	0.706616	1.07	0.92	0.700	0.512867	4.47
F34-gar$_1$				0.705940				0.512545	
F34-WR	1.93	158.30	0.035	0.705927	1.31	4.50	0.176	0.512462	-3.43
Mafic feldspathic rocks									
B75-cpx	0.66	80.33	0.023	0.705100	6.78	33.99	0.121	0.512669	0.60
B75-gar	0.27	0.93	0.838	0.707551	3.09	1.86	1.004	0.513125	9.49
B75-gar$_1$	2.68	30.36	0.254	0.706487	0.80	0.81	0.602	0.512866	4.46
B75-WR	6.10	190.44	0.091	0.705257	4.90	16.55	0.179	0.512689	0.61
BC35-cpx	0.197	48.10	0.012	0.707496	8.53	34.33	0.150	0.512321	-6.19
BC35-hb	1.03	27.86	0.037	0.708333	1.66	6.64	0.151	0.512346	-5.69
BC35-plg	10.23	1200.1	0.025	0.707348	12.50	9.89	0.764	0.512756	0.05
BC35-WR	5.73	659.01	0.025	0.707344	5.07	24.18	0.127	0.512344	-5.74
Garnet Peridotite									
PBC-cpx					7.00	31.67	0.134	0.512491	-2.87
PBC-gar					0.88	0.63	0.848	0.512528	-2.14
PBC-WR	1.22	21.45	0.164	0.705580	0.28	0.65	0.261	0.512496	-2.70
Metasediment									
297-cpx	0.82	109.72	0.022	0.709232	1.45	8.37	0.105	0.511871	-14.96
297-gar	3.39	22.89	0.427	0.711981	2.20	1.72	0.776	0.512247	-18.02
297-WR	2.88	29.90	0.277	0.710763	2.01	10.40	0.117	0.512059	-11.29

*- A petrographic description of the samples is given in the text. Host - Big Creek trachyandesite, WR - whole rock, cpx - clinopyroxene, opx - orthopyroxene, gar - garnet, hb - hornblende, plg - plagioclase. Mineral separates are super clean handpicked fractions except for the ones accompanied by the subscript "$_1$". The mineral samples with this subscript contained either small, but discernable inclusions of other minerals or kelyphitic rims.

3-20

Table 3-3. Grainsize, thermobarometric conditions, and Rb-Sr and Sm-Nd ages determined for the analyzed samples.

Sample	Grainsize (mm)[1]	Pressure[2] (GPa)	Temp.[3] (°C)	Rb-Sr age[4]	$^{87}Sr/^{86}Sr$ intercept	MSWD[5]	Sm-Nd age	$^{143}Nd/^{144}Nd$ intercept	MSWD[5]
G36	2.5	1.5 (Mk)	770 (EG)	89.4±0.90 (gar-cpx)	0.70618		93.7±0.8 (gar-cpx)	0.51230	
		1.4 (HG)		91.0±55 (gar-cpx-WR)	0.70596	2020	92.8±3.5 (gar-cpx-WR)	0.51231	1.32
BC218	4.5	1.6 (Mk)	725 (EG)	82.4±0.96 (gar-cpx)	0.70618		85.1±1.3 (gar-cpx)	0.51242	
				83.0±433 (gar-cpx-WR)	0.70597	4840	86.6±14.5 (gar-cpx-WR))	0.51240	3.67
G39	5	2.2 (HG)	675 (EG)	44.72±1.74 (gar-cpx)	0.70623		83.7±1.4 (gar-cpx)	0.51233	
		2.0 (Mk)		55.6±165 (gar-cpx-WR)	0.70638	735	86.7±11 (gar-cpx-WR)	0.51232	0.55
BC207	2.5	1.9 (HG)	650 (PN)	67.2±1.0 (gar-cpx)	0.70518		109.2±5.0 (gar-cpx)	0.51219	
		1.7 (Mk)		64.5±25 (gar-cpx-hb-WR)	0.70506	189	121.2±30 (gar-cpx-WR)	0.51223	5.52
F34	3.5	3.3 (HG)	860 (H)	124.6±3.69 (gar-cpx)	0.70595		111.1±5.2 (gar-cpx)	0.51236	
				126±80 (gar-cpx-opx-WR)	0.70599	610	120±30 (gar-cpx-opx-WR)	0.51232	7.20
B75	2.5	0.98 (NP)	920 (EG)	213.3±1.70 (gar-cpx)	0.70503		79.0±1.20 (gar-cpx)	0.51261	
				214±49 (gar-cpx-WR)	0.70501	24.6	80.0±3.12 (gar-cpx-WR)	0.51259	1.28
BC35	3	0.84 (NP)	872 (EG)	-	-	-	102.8±23.0 (cpx-hb-plg-WR)	0.51224	3.42
PBC	01.	4.2 (HG)	975 (EG)	-	0.70492	-	10±15 (gar-cpx)	0.51249	
297	0.3	2.5 (Mn)	645 (PN)	477.4±3.44 (gar-cpx)	0.70908		85.7±3.23 (gar-cpx)	0.51181	

[1] - rock average.
[2] - The following thermodynamic calibrations were used for pressure determinations (see also Ducea and Saleeby, 1996a): Mk - Mukhopadhyay (1991); HG - Harley and Green (1982); NP - Newton and Perkins (1982); M - Manning and Bohlen (1991).
[3] - The following calibrations were used for temperature determinations (see also Ducea and Saleeby, 1996a): EG - Ellis and Green (1979); H - Harley (1984); PN - Pattison and Newton (1989).
[4] - The isochrons are based exclusively on the mineral data of highest purity listed in Table 2. The uncertainties are 2σ values. Abbreviations are as in Table 2.
[5] - Mean Squared Weighted Deviation (York, 1969, Wendt and Carl, 1991), calculated for 3 or more points using the program provided by Ludwig (1991).

the calculated ages, but its cause needs to be elucidated individually for each of these "problem" samples.

The Sr and Nd ages for all samples but the quartzite 297 are Mesozoic, between 64.5 Ma and 214 Ma (Figure 3-2). Quartzite 297 has a Sr slope corresponding to an "age" of 471 Ma. No Sr mineral isochron could be calculated for sample BC35 using the available data in the absence of garnet from our dataset. The Nd mineral ages, including quartzite 297 fall within a much tighter interval, between 81.3 Ma and 118.7 Ma. These values and similarity of the Nd ages is indicative of a relationship between the surface batholith and these lower crustal rocks. Three Sr ages (samples G36, BC218, and F34) are similar with the Nd ages calculated on the same samples, reinforcing the previous statement. The spread of the other four Sr ages suggests a more complicated history and, to a first degree at least, these ages have to be considered suspicious. We noticed the high concentrations of Rb and Sr in some mineral separates compared to previously analyzed xenolith garnets and pyroxenes (e.g., Wendtland et al., 1996). We fear that part of the problem with the Rb-Sr system is the failure to obtain absolutely clean mineral separates with respect to Rb and Sr. For example, the concentrations of Rb in garnets and pyroxenes are expected to be low (~ 1 ppm) in eclogites and granulites, while some of our samples have higher Rb concentrations. The most outstanding is sample BC207, with ~30 ppm Rb in clinopyroxene, and 5.8 ppm Rb measured in garnet.

The Sr and Nd intercepts (Table 3-3) are very similar for all samples except for quartzite 297. The $^{87}Sr/^{86}Sr$ "initials" of the seven mafic rocks varied between 0.70501 and 0.70623, very much like the initial Sr ratios in the surface batholith rocks in the central Sierra Nevada (average central SNB $^{87}Sr/^{86}Sr_{100}$ = 0.7057, Kistler and Peterman, 1973, 1978). The $^{143}Nd/^{144}Nd$ ratios of the mafic rocks fall between 0.51232 and 0.51239, also very similar to the $^{143}Nd/^{144}Nd_{100}$ surface batholith average of 0.51234 in the central Sierra Nevada (DePaolo, 1981). The quartzite has somewhat larger $^{87}Sr/^{86}Sr$ and smaller $^{143}Nd/^{144}Nd$ ratios, 0.7095 and 0.51182 respectively (at 100 Ma).

Figure 3-2. Mineral isochrons for the (A) Sm-Nd and (B) Rb-Sr systems. The isochrons have been fitted through data points with or without taking into account the whole rock values, as explained in text. Estimated $\pm 2\sigma$ uncertainties: ^{87}Rb/^{86}Sr $= 0.15\%$, ^{87}Sr/^{86}Sr $= 0.0015\%$, ^{147}Sm/^{144}Nd $= 0.2\%$, and ^{143}Nd/^{144}Nd $= 0.002\%$. The size of the symbols is approximatively twice as large as the analytical uncertainties. We used the following decay constants: $\lambda_{Rb} = 1.42 \times 10^{-11}$ a^{-1}, and $\lambda_{Sm} = 6.54 \times 10^{-12}$ a^{-1}.

A. Nd mineral ages
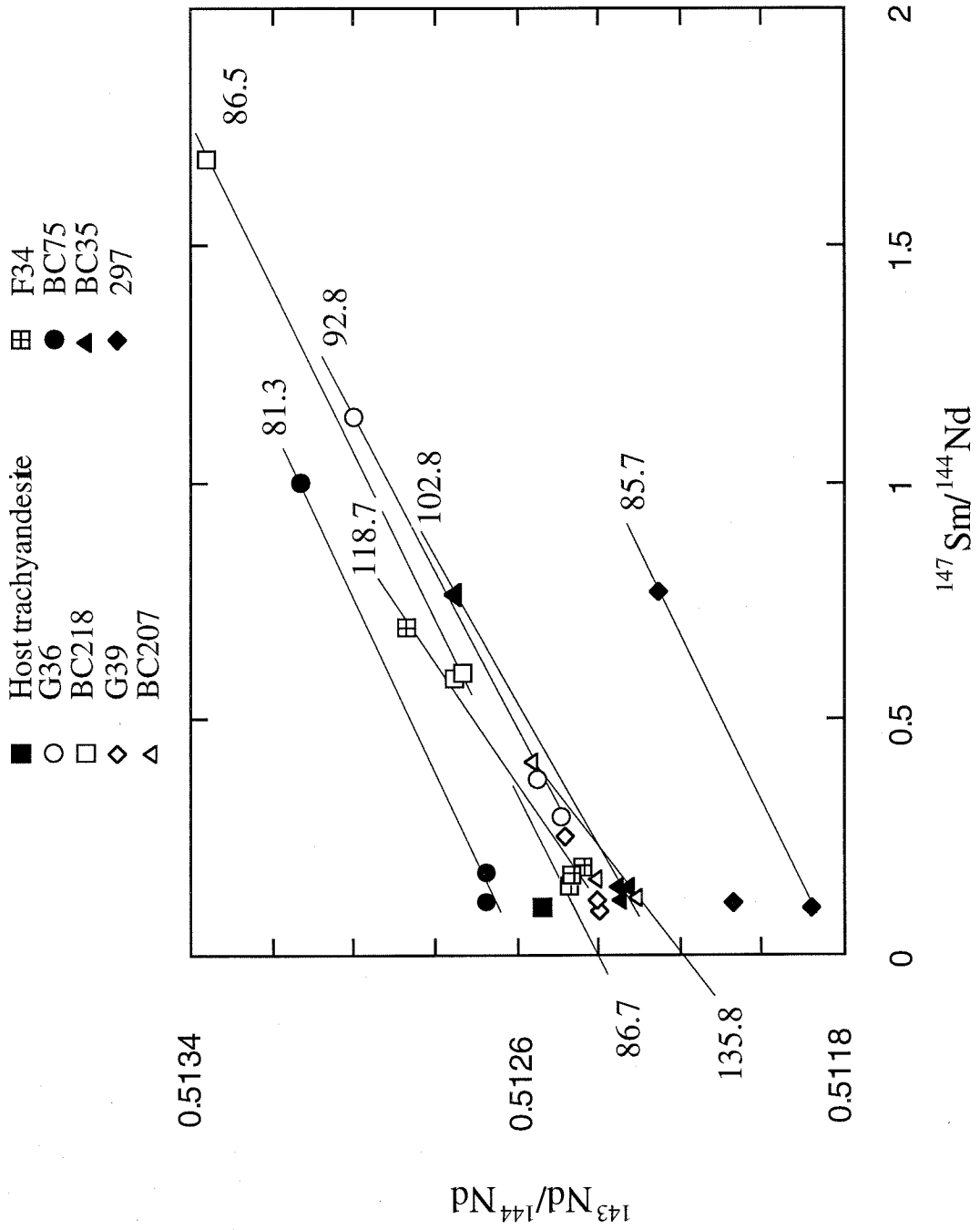
B. Sr mineral ages
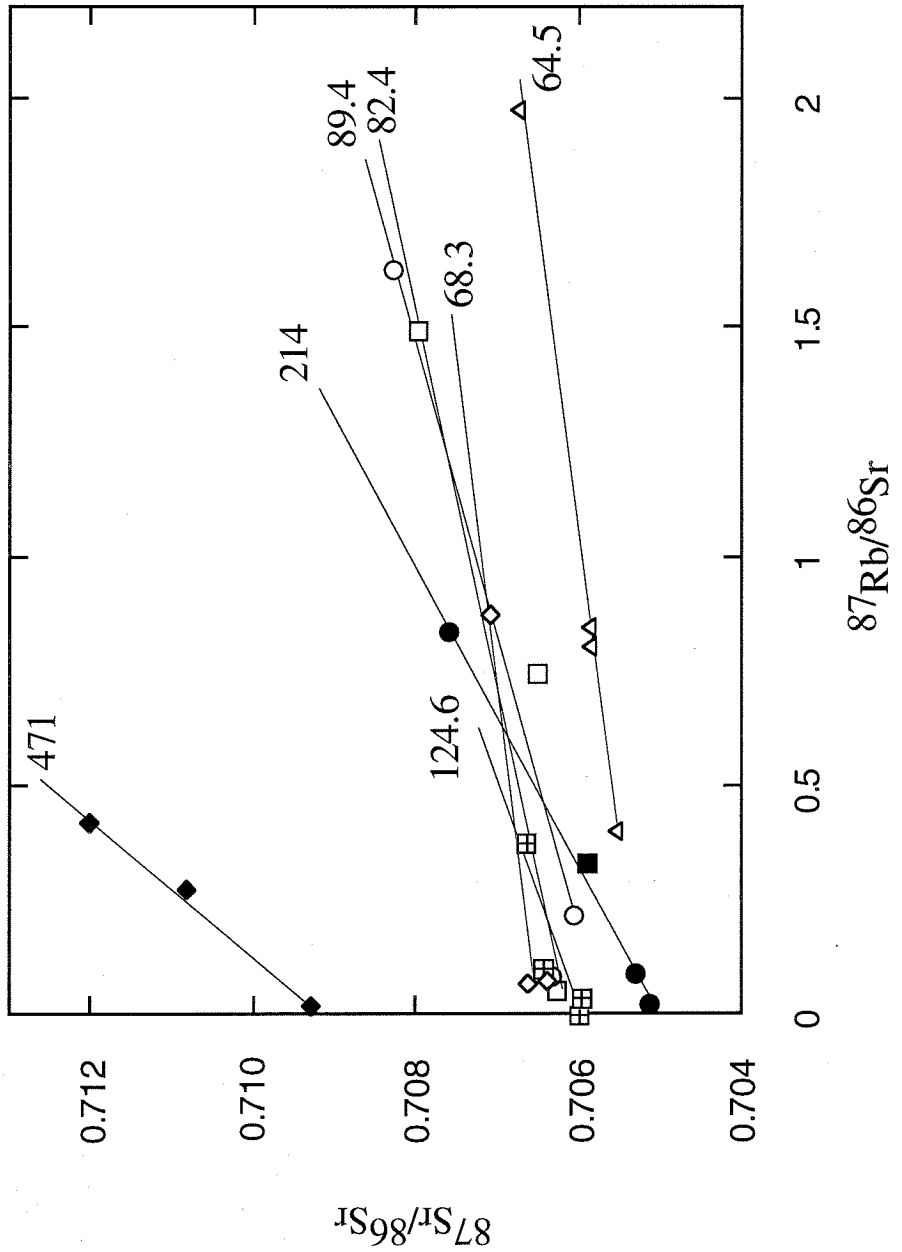
3.6. Data interpretation

The two geochronometric systems used in this study have: (1) an extremely favorable spread of Rb/Sr and particularly Sm/Nd ratios between pyroxenes and garnets, and (2) high closure temperatures in garnet-bearing lower crustal rocks (e.g., Coghlan, 1990; Metzger et al., 1992). The first characteristic helps constraining the isochrons while the second may be important for deciphering the thermal history of deep crustal fragments.

Interpretation of the mineral isochrons. Aware of all the limitation of establishing lower crustal ages on xenoliths, we have attempted to obtain useful geochronological information without necessarily expecting the high precisions and accuracies typical for the Rb-Sr or Sm-Nd results when applied to surface rocks. In our case, we searched for the bulk age of the lower crust: is it Paleozoic, Precambrian, is it batholith-related, are the ages scattered throughout the Mesozoic or cluster towards the end period of Mesozoic magmatism, or perhaps are they approaching the age of the Miocene volcanic host rock? Are these samples broadly cogentic, or do they exhibit a large spectrum of ages and initial ratios? Our results indicate that the samples equilibrated during the most prolific igneous period in the SNB (Chen and Moore, 1982). Furthermore, our data confirm the previous geochronological results on lower crustal xenoliths (Wendtland et al., 1996), indicating that the Sm-Nd system is quite a robust xenolith chronometer, while the Rb-Sr system is commonly not.

We interpret the Sm-Nd ages reported in Table 3-3 to record the time when these xenoliths have cooled below the blocking temperatures of this particular system. Most isochrons are defined by the clinopyroxene-garnet pairs, but the whole rock or additional minerals do not depart significantly from the two point isochrons. In some cases, for example samples 297 and BC75, the whole rock ratios have been modified by interaction with the host trachyandesite (Figure 3-3a). More specifically, we suspect that physically the split "xenolith whole rock" has been polluted by some small, undetected amounts of the

Figure 3-3. a. Nd isochron of sample 297, illustrating the contamination of the xenolith whole rock powder by the host trachyandesite; the whole rock $^{147}Sm/^{144}Nd$ and $^{143}Nd/^{144}Nd$ ratios of the analyzed "whole rock" are located along a mixing line (dashed line in the figure) between the host rock and the true location of the whole rock along the Nd isochron (solid line). b. Sr isochron of sample G36 illustrating, similarly to 3a, the contamination of the xenolith "whole rock" powder by the trachyandesite. c. Nd isochron of BC75 including the kelyphitic garnet (gar_1) separate; gar_1 lies close to the mineral isochron. d. Sr isochron of BC75, including kelyphitic garnet (gar_1); in contrast to 3c, the kelyphite lies off the mineral isochron indicating open system breakdown of garnet in the presence of the Sr-rich, Nd-poor phase, possibly an aqueous phase.
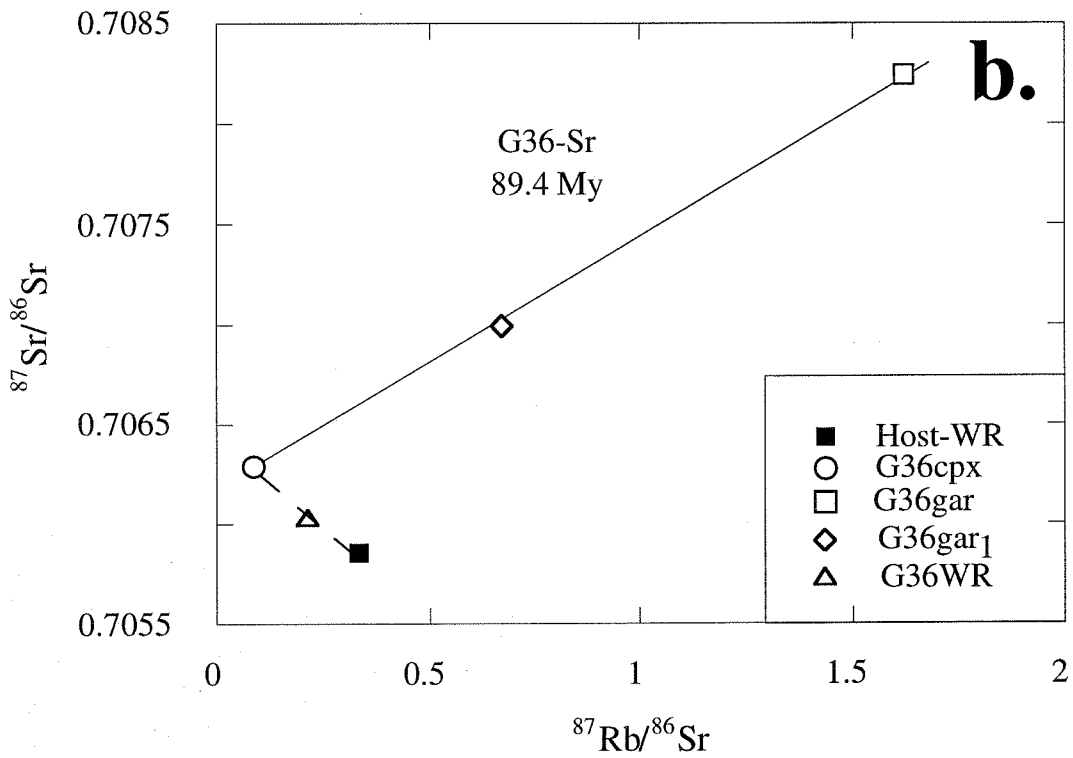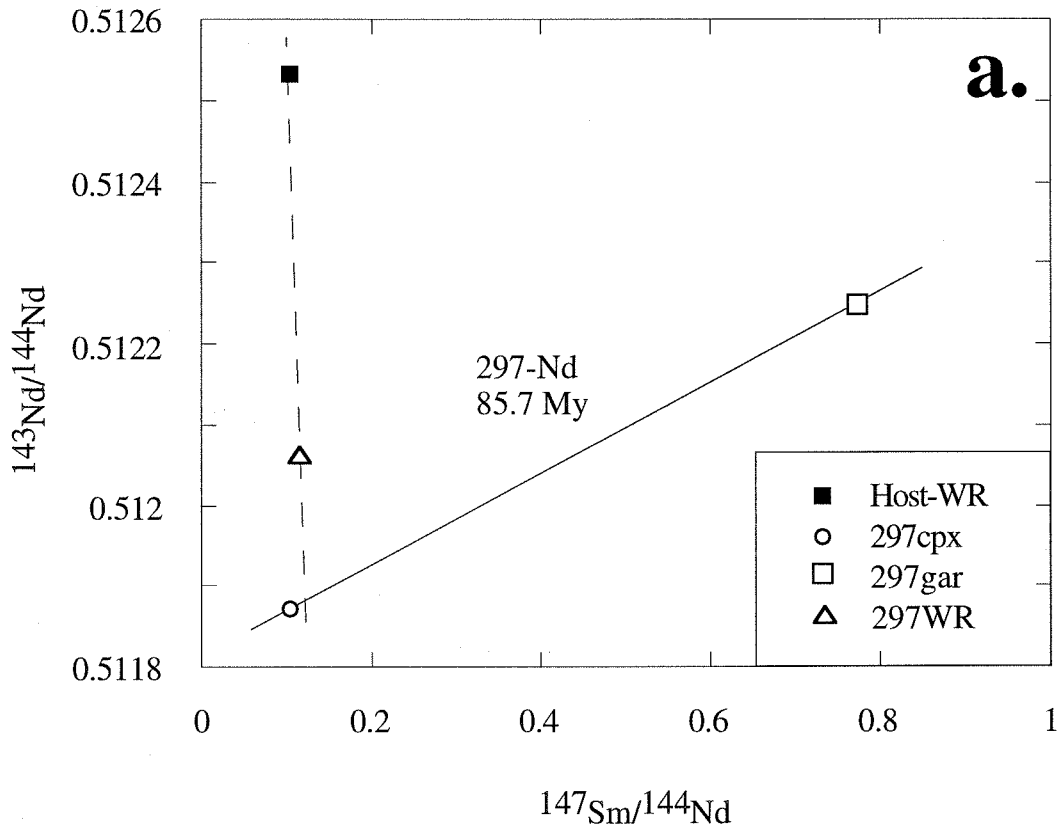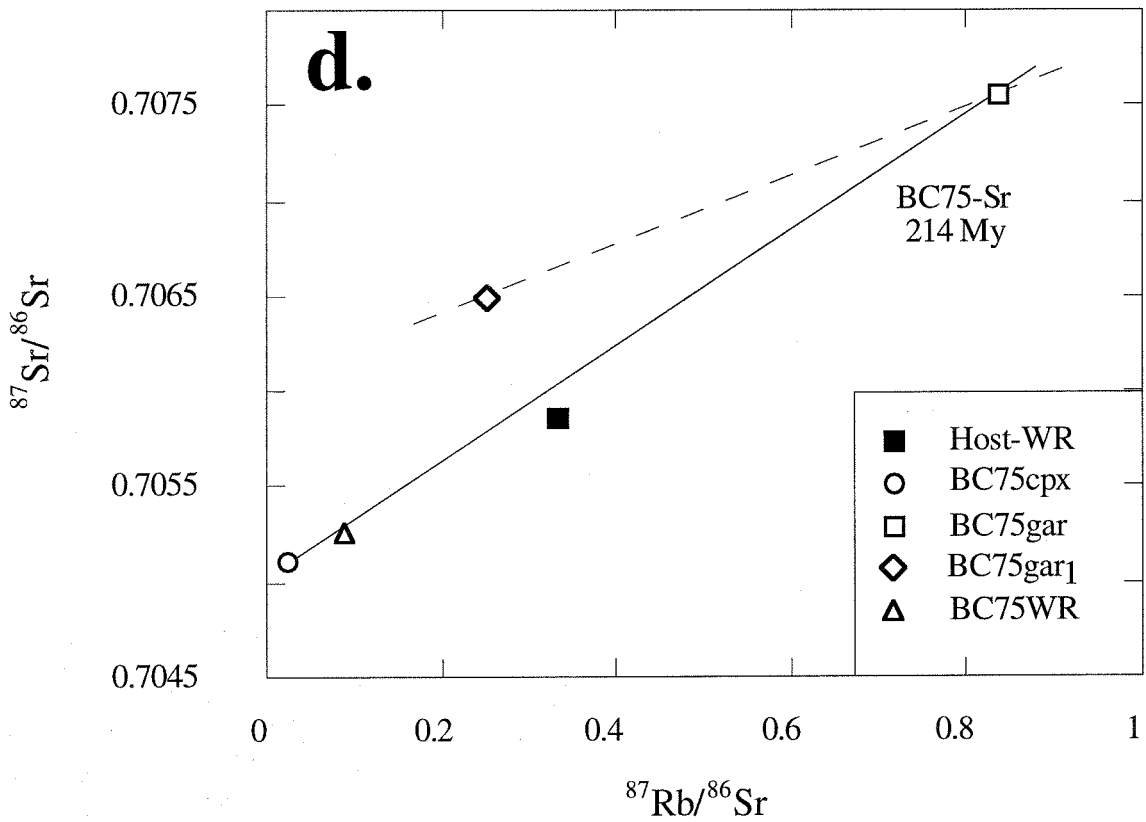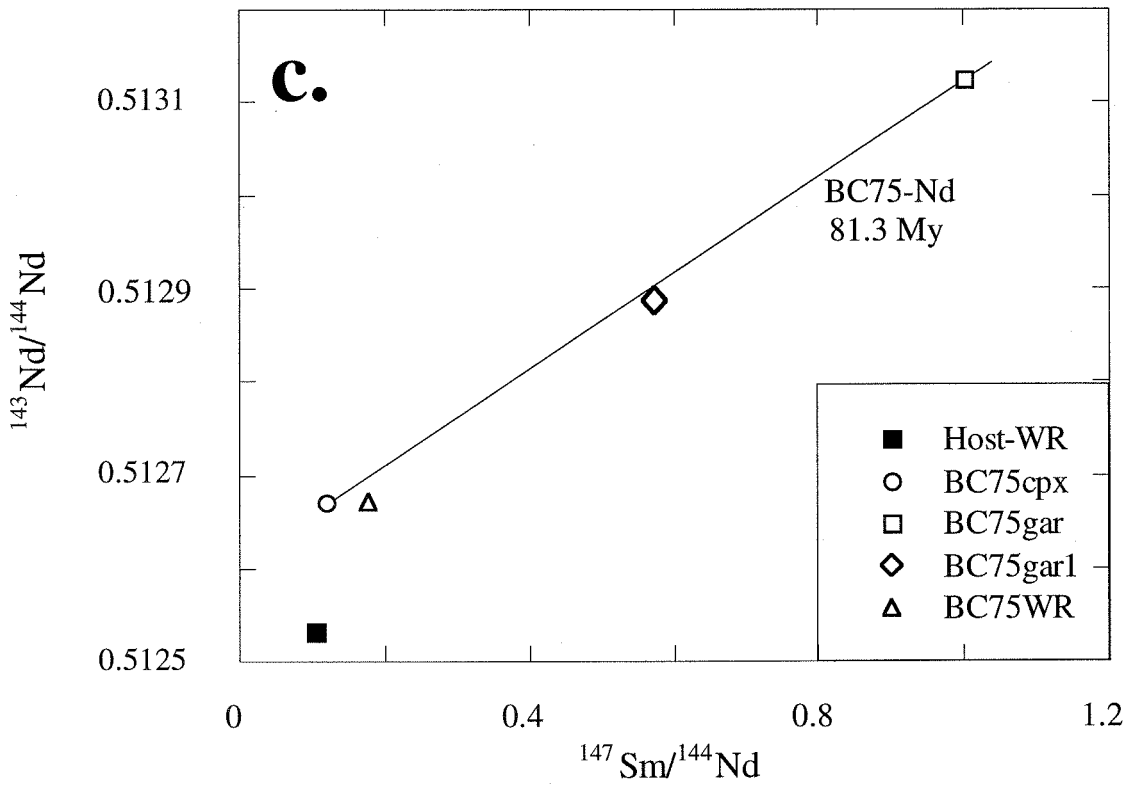
host trachyandesite. Such a behavior is not unexpected, particularly because we had less control over the purity of the whole rock spilts than over the mineral separates. The whole rocks have been crushed to powders, and despite the cautions that we have taken in sample preparation (see Analytical procedures), they could contain some intergranular material inherited from the host trachyandesite. The whole rock isotopic ratios of $^{143}Nd/^{144}Nd$ and $^{147}Sm/^{144}Nd$ are very similar to those of the clinopyroxenes, because clinopyroxene is the abundant mineral richest in Sm and Nd. From this perspective, the departure of some of the whole rock ratios toward the host trachyandesite is not very relevant; the clean, pure clinopyroxene fractions are better samples of the low Sm/Nd end of the isochrons.

The Rb-Sr ages have a larger range and are difficult to interpret. If we ignore potentially erroneous data points which are plausibly contaminated by the host lavas (Figure 3-3b), we can separate the Rb-Sr isochrons into three groups. Three samples, G36, BC218, and F34, yielded indistinguishable Sr and Nd ages (Group I), two samples, G39 and BC207 yield younger Sr ages (68.3, and 64.5, respectively) than their Nd ones (Group II), while BC75 and 297 yield anomalously high Rb-Sr ages, 214, and 477, respectively (Group III).

We interpret the Group I Sr ages as igneous or slightly post-igneous values for these cumulates, based on the coincidence with the Cretaceous magmatic peak of the SNB and the similarity with their corresponding Nd ages. Based on textural arguments and the lack of any product suggesting the presence of fluid phases in these rocks, it appears likely that the isotopic equilibration between garnet and pyroxenes in these rocks was entirely diffusional. The similarity between the Sr and Nd ages in these samples is what experimental data on Sr and Nd diffusion on garnet predicts (see next section) for the geologic scenario envisioned above.

Group II ages are consitent with the batholith derivation of these samples, but require some reseting of the Rb-Sr system at 64- 68 Ma, partial reseting at a time younger than 64-68 Ma, or disturbance in a geochronologically meaningless fashion, such as

exchange with a fluid phase. We have not observed petrographic evidence for alteration or metamorphic reactions in the presence of a fluid phase. However, the most vulnerable points on the Sr isochrons presented here are the garnets. The slope of a garnet-clinopyroxene Sr isochron can be perturbed by interaction with small fractions of a component which plots away from the isochron. The Sr "ages" will be either artificially decreased or increased, depending on whether the fluid plots below or above the isochron at the time of perturbation.

The Group III Sr ages are the most difficult to interpret. It is possible that interaction with the host trachyandesite has modified the original Rb/Sr and $^{87}Sr/^{86}Sr$ ratios of the clinopyroxene and the whole rock in sample 297. Such a process could also explain the low quality of the Nd whole rock isotope ratios for the same sample. However, it does not appear that the same explanation can hold for B75 (Figure 3-2) because the host rock isotopic ratios are nearly colinear to the B75 Sr isochron. It is also possible that the Group III Sr ages are geologically meaningful or at least have a "memory" of the prebatholithic history of this crustal section. Wendtland et al. (1996) consider the possibility that some lower crustal xenoliths from the Colorado Plateau display higher Sr ages than Nd ages because of failure of Sr to completely equilibrate, under the assumption that diffusion plays the primary role in isotopic equilibration. This interpretation is borne out of the experimental data of Coghlan (1990), which indicate that the equilibration time for diffusion of Sr in garnet is roughly three times longer than for Nd. In-situ SHRIMP analyses of zircons from Group III xenoliths (in progress) will hopefully help us better understand the prebatholithic history of these samples, if there is one preserved.

We have also analyzed the isotopic compositions of the kelyphitic rim-bearing garnets for a few samples (Table 3-2) in order to test if kelyphitization is a closed system effect (simple garnet breakdown, or breakdown reaction involving surrounding clinopyroxenes) or if it requires the presence of an additional component, foreign to the eclogite or gabbro. Neodymium isotopes on kelyphitic garnets for samples BC75

(exemplified in Figure 3-3c) and G36 indicate a closed system behavior. A similar result is indicated by the Sr isotopes in the kelyphitic garnets of sample G36. The Sr isotopes of the "garnet$_1$" fraction of sample BC75 depart from the reported Sr isochron for that sample (Figure 3-3d)suggesting an open system behavior of Sr during kelypthite formation in this sample.

Thermochronology. Two central questions will be addressed in this section. First, can we tell from thermochronology whether the samples analyzed here are pre-batholithic rocks which have been thermally reset at syn-batholith times or they are "batholithic" igneous rocks that crystallized shortly before their determined ages. Secondly, are the PT conditions determined on these samples locked in at the time "read" by the Sm-Nd chronometer?

Experimental data on closure temperatures for Sr and REE's in garnet and pyroxenes, although limited and subject to large errors (disscusion in Burton et al., 1995) may hold answers to the above questions. We will summarize the available experimental results in four graphs of closure temperature versus cooling rate (Figure 3-4), and point out some geologic implications for our results.

Figure 3-4a shows the effect of grainsize on closure temperature, calculated for spherical grains. The relevant diffusion parameters, i.e., the pre-exponential factor, D_0 (3 x 10^{-9} cm^2/s), and the activation energy, E (49 kcal /mole), were determined experimentally on an almandine-rich garnet by Coghlan (1990). The closure temperatures were calculated for a range of cooling rates between 1 and 1000 ^{0}C/Ma. We have chosen the range of grainsizes observed in xenoliths analyzed for this study (0.1-0.5 cm). There is a 150-250 ^{o}C difference between the closure temperatures of the 0.1 and 0.5 cm radius grains. Fast cooling rocks, such as igneous rocks, will record Nd ages close to their crystallization ages, regardless of their grainsize. However, a suite of crustal rocks which experience a metamorphic event (e.g., a batholith-related thermal pulse) followed by slow cooling, which leads to resetting, could be expected to display a positive correlation between

grainsize and age. There is no such correlation in our data, suggesting that these rocks experienced cooling from igneous to ambient crustal temperatures.

The experimental results of Coghlan (1990) indicate that the closure temperatures of Sr and Nd in garnet are similar (Figure 3-4b). Strontium may actually have a slightly higher closure temperature than Nd, but the difference shown in Figure 3-4b is within the error of the experimental results. The Sr and Nd garnet ages of a sample should therefore be similar, if diffusion was the only mechanism responsible for intermineral elemental mobility. Three of our samples (G36, BC218, and F34) yielded similar Sr and Nd ages (Figure 3-5), suggesting intermineral elemental mobility affected only by diffusion.

Figure 3-4c illustrates the large difference between the closure temperatures of different garnet end members (grossular, pyrope and almandine) calculated for spherical grains (radius = 0.3 cm) using data from Harrison and Wood (1980) and Coghlan (1990). In particular pyrope yields a closure temperature 300-400 ^{0}C lower than grossular or almandine. The proportion of the pyrope end member in Sierra Nevada xenoliths is the highest in the garnets which equilibrated at the deepest levels (Ducea and Saleeby, 1996a). It follows that, if two garnet-rich rocks from deep levels beneath the SNB have crystallized at the exact same time, but at different levels in the crust, they will yield different Nd garnet ages: the deeper sample will be expected to lock in a younger age. In contrast, our data contains deep samples (e.g., F34) which yielded higher ages than shallower samples (e.g., G36) suggesting asynchronous cooling at different depths. These ages appear to mark cooling of individual plutons to the ambient temperature and not cooling of the Sierran lithosphere as a block.

Taking into account the pyrope-rich compositions of the garnets analyzed in this study together with the dramatic effect of the presence of pyrope in lowering garnet REE closure temperature (Figure 3-4 c). We see that the temperatures locked in by the major cations in these xenoliths (Table 3-3) are broadly consitent with REE closure temperatures

Figure 3-4. Predicted closure temperatures (^{0}C) vs. cooling rates (^{0}C/Ma) for a. Nd in an almandine-rich garnet for various grain sizes, b. Nd and Sr in an almandine-rich garnet for spherical grains (r=0.3 cm), c. Nd for various garnet compositions (r=0.3 cm), and d. Sr and Nd in garnet compared to Sr and Sm in diopside (r=0.3 cm). These diagrams were constructed using experimental results from Harrison and Wood (1980), Sneeringer et al. (1984), and Coghlan (1990).

c. Nd in various garnets all r= 0.3 cm

almandine-rich

grossular

pyrope

T_c(ºC)

Cooling rate (ºC/my)

d.

r= 0.3 cm

Sr-diopside

Sm-diopside

Sr-almandine-rich garnet

Nd-almandine-rich garnet

T_c(ºC)
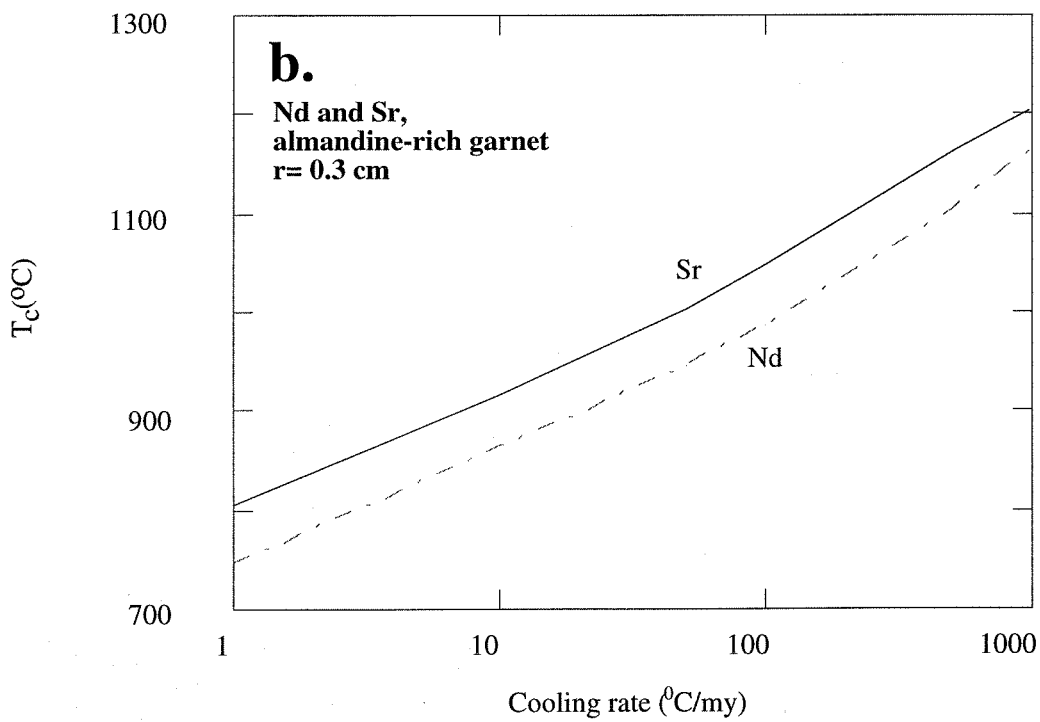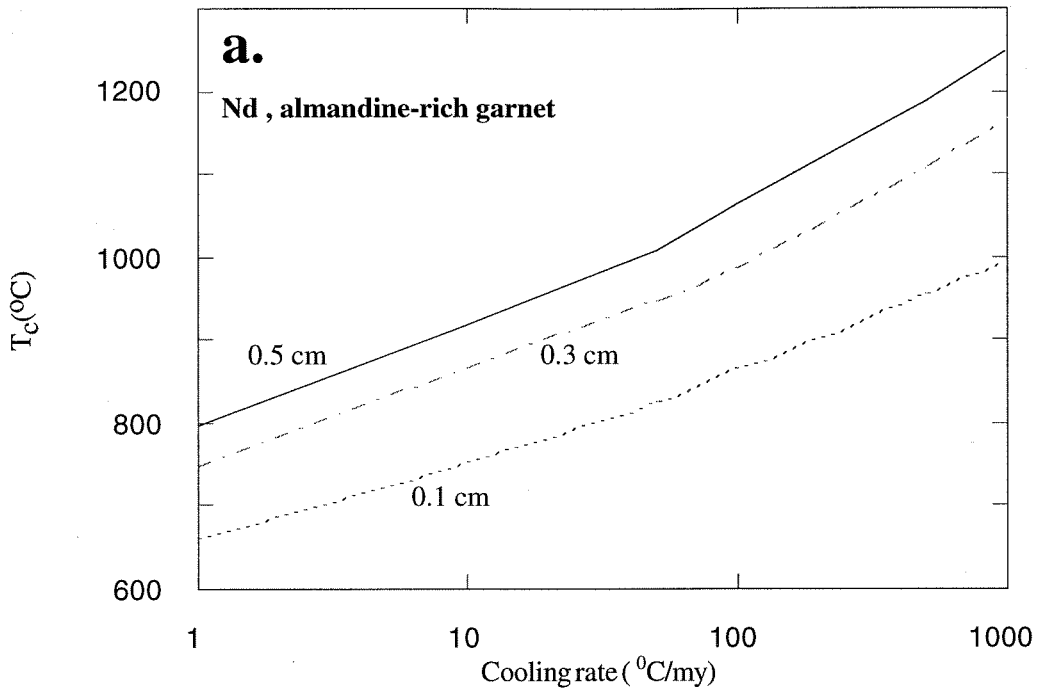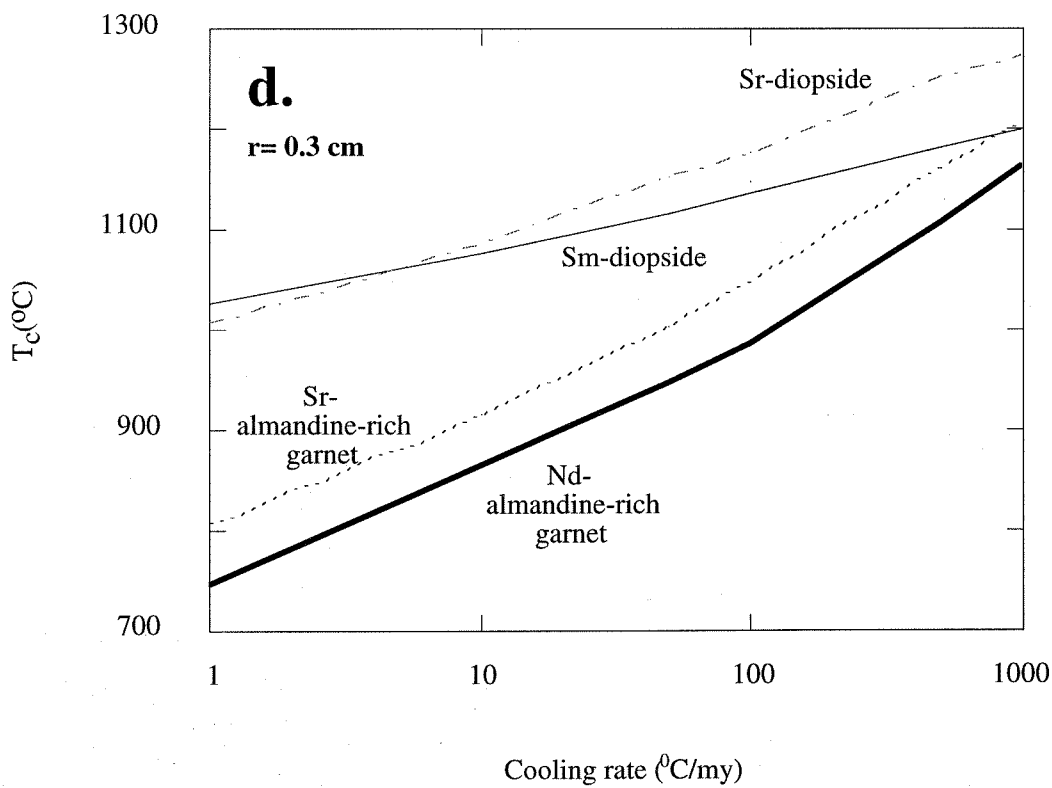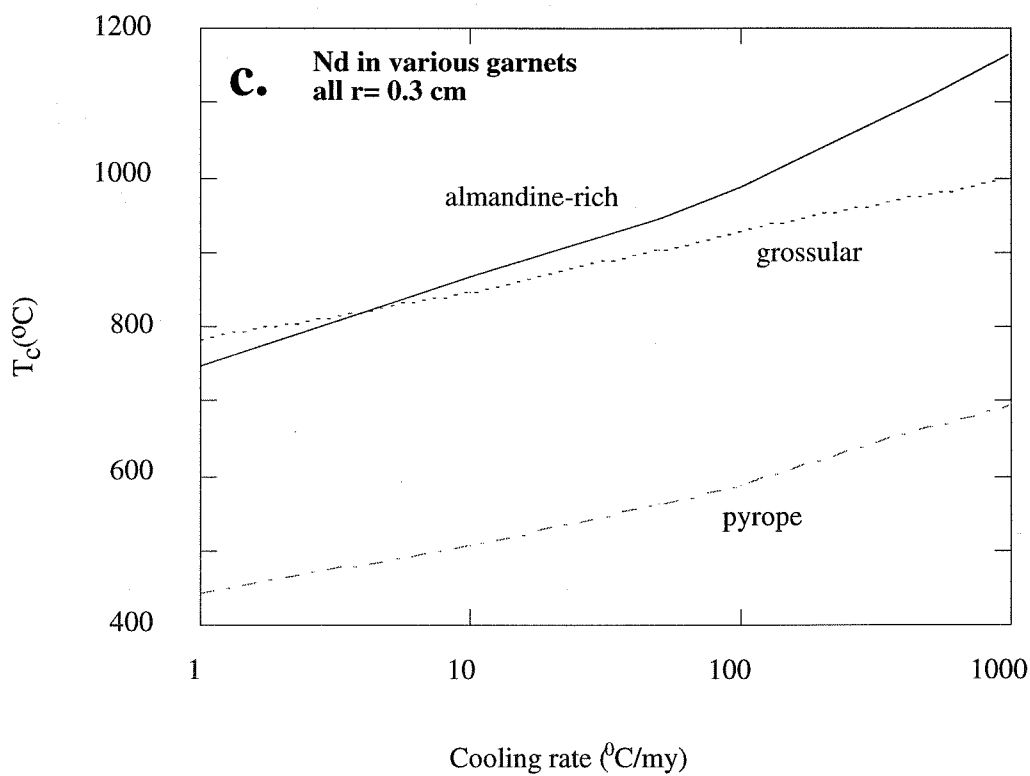
Cooling rate (ºC/my)

predicted by experimental results for fast cooling rates (hundreds of ^{0}C/Ma), assuming a linear correlation between the increase in the almandine component of a garnet and its closure temparature within the limits set by the end-members shown in Figure 3-4 c. These results suggest that the major elements used in thermobarometry (Ca, Mg, Fe) may have become immobile simultaneously with the REEs. Note that the "simultaneity" in this situation is easily achieved given fast cooling rates, and enhanced by artifacts such as large experimental uncertainties, errors in measuring PT conditions and isochrons, etc.

We have focused so far on the behavior of Sr and Nd in garnet. However, in eclogitic rocks including the ones from the present study, most garnets are adjacent to one other phase: clinopyroxene. If garnet is able to exchange with only one other phase, it may record time information that relates to the closure temperature of that mineral (Burton et al., 1995), clinopyroxene in this case. Strontium and Sm (as a proxy for Nd) diffusion data on diopside (Sneeringer et al., 1984) show the same similarity in closure temperatures between Sr and the REE (Figure 3-4d) as previously mentioned for garnets. The diospide closure temperatures are, however higher than those of garnets (Figure 3-4d) except at very high cooling rates where they are similar. This diagram indicates that the eclogite closure temperatures for Sr and Nd may be higher than predicted by the garnet data, particularly in slow cooling rocks, and be controlled by clinopyroxene rather than garnet, or perhaps by both phases in a complex way (Jagoutz, 1988; Burton et al., 1995). However, this complexity is likely to have a minimal effect on fast cooling igneous rocks, as the ones investigated in this study.

In conclusion: (1) there is evidence to support a post-igneous crystallization cooling path for the rocks analyzed here rather than some bulk thermal resseting of a pre-existing deep crust, and (2) it is proposed that our garnets record PTt points on the cooling trajectories of individual plutons from the deep Sierran lithosphere.

3.7. Petrologic and tectonic implications

The petrographic, thermobarometric and geochronologic results presented above refine our information on the composition of the central Sierra Nevada batholith at depth. We will relate the geology of the surface batholith with the lower crustal rocks and put constraints on the gross crustal structure of the batholith. The central Sierra Nevada Mesozoic crustal section, especially the lower half, appears to be radically different from the one observed in the southernmost Sierra; we will define the differences between the two sections and address their regional tectonic implications. Finally, we will speculate on the mechanisms that might have removed the batholithic lower crust from beneath the central Sierra Nevada during the Late Cenozoic.

Batholith residua/cumulate origin for the xenoliths

As mentioned above, the Sierra Nevada provides surface exposures of a composite Mesozoic batholith over a thickness of 30 km. Mafic and ultramafic xenoliths which equilibrated at depths of 35-100 km beneath the central batholihic exposures yield Sm-Nd ages which fall within the age range of 90% of the batholith plutons (125-85 Ma, e.g., Saleeby, 1990). These results establish a broad cogenetic relation between the surface batholith and its lower crust/uppermost mantle. The ages measured on the feldspathic and eclogitic xenoliths are igneous or near-igneous ages. Sample 297 may be a good example of a preexisting crustal rock which did not experience melting during the batholith formation. The Nd age of this sample was reset during the Late Cretaceous thermal pulse, while its Sr may have only partially been reset.

The mineral isochron intercepts for Sr and Nd (Table 3-3) as well as age-corrected whole rocks values obtained on similar xenoliths (Dodge et al., 1986, 1988; Mukhopadhyay, 1989; Ducea and Saleeby,1996b) have values similar to the initial Sr and

Figure 3-5. Sample Sr and Nd ages vs. equilibration pressures. Note there are three samples which yield almost identical Sr and Nd ages, while others do not. No correlation between ages and crustal depth is evident in our dataset.
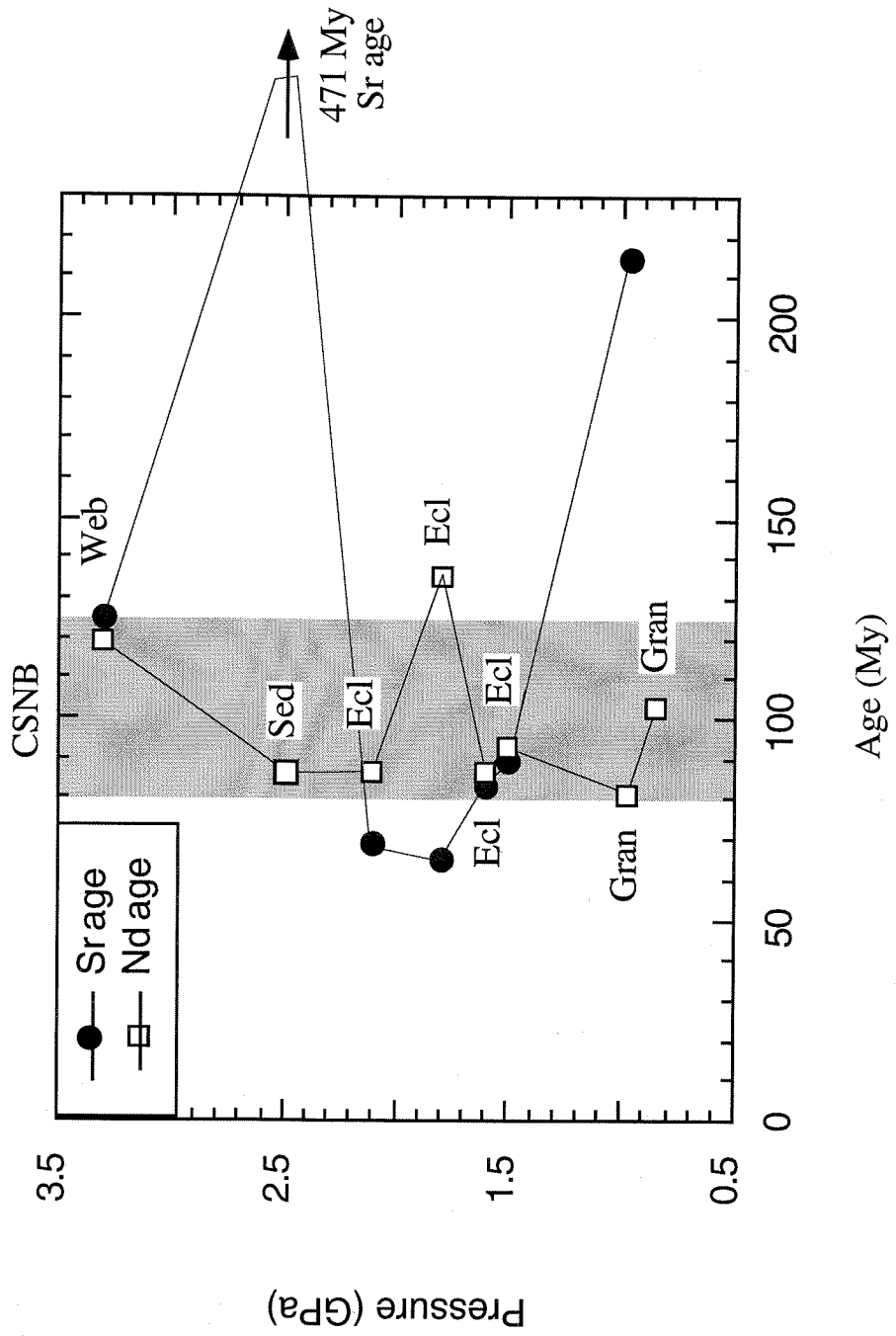
Nd isotopic ratios (Kistler and Peterman, 1978; DePaolo, 1981) of the surface batholith in the central Sierra Nevada (Figure 3-6a and 6b). The low, negative initial values of ε_{Nd} argue against derivation of all these eclogite facies rocks from oceanic crust. The Pb isotope ratios (Figure 3-6c) of the analyzed xenoliths also fall within the range defined by the central SNB (Chen and Tilton, 1991). These results are complemented by a few whole rock Pb isotopic data performed by Mukhopadhyay (1989) on garnet clinopyroxenites from Big Creek and a neighboring xenolith locality from the San Joachim Mines area. The Pb isotopic compositions of the feldspathic and "eclogitic" xenoliths (Mukhopadhyay, 1989) also fall within the range of the Pb isotopic ratio of the surface batholith in the same area (Chen and Tilton, 1991). The oxygen isotopic ratios ($\delta^{18}O$) of the eight samples reported in this study have been also been analyzed (Figure 3-6d) and will be presented in detail in Chapter 4. The whole rock $\delta^{18}O$ ratios of the seven mafic/ultramafic xenoliths fall within the range of $\delta^{18}O$ ratios of the surface batholith in the Central Sierra Nevada region (Masi et al., 1981). Note the relatively elevated $\delta^{18}O$ values (6.5 to 9 relative to SMOW) for most of these deep seated rocks. A supracrustal component at very deep levels is required by the relatively elevated $\delta^{18}O$ ratios (see Taylor, 1988, for a discussion on this issue and applications to the Peninsular Ranges batholith of Baja, California). This result points to a "crustal" derivation for rocks such as garnet clinopyroxenites, which otherwise could have been interpreted as "mantle rocks" based on their physical properties and their great depths of residence in the lithosphere.

Clearly, the mafic-ultramafic xenoliths analyzed here as well as the similar rocks analyzed only for whole rock isotopic compositions by Mukhopadhyay (1989), and Dodge et al. (1986, 1988) are directly related to the batholith: they could be either magma chamber mafic cumulates or restites from melt extraction. Mixing of mantle wedge-derived mafic melts with pre-existing lower crustal material in large magma chambers at the deepest

Figure 3-6. a. Initial $^{143}Nd/^{144}Nd$ vs. $^{87}Sr/^{86}Sr$ for the analyzed samples, compared to the field of central SNB (Kistler and Peterman, 1973, 1978, abbreviated in the figure as KP73, 78; and DePaolo, 1981, abbreviated as D81). b. Initial $^{87}Sr/^{86}Sr$ vs. $\delta^{18}O$ for the analyzed xenoliths compared to the field of central SNB (data from KP, 73, 78, Masi et al., 1981, abbreviated as M81) and the Peninsular Ranges Batholith (data from Taylor, 1988, abbreviated as T88). c. $^{207}Pb/^{204}Pb_i$ vs. $^{206}Pb/^{204}Pb_i$ for the analyzed xenoliths as well as similar xenoliths analyzed by Mukhopadhyay (1989) compared to the field of central SNB (from Chen and Tilton, 1991, abbreviated in figure as CT91). d. $^{208}Pb/^{204}Pb$ vs. $^{206}Pb/^{204}Pb_i$ similar to 6c.

- ◆ Garnet pyroxenites and feldspathic rocks - this study
- ◇ Metasediment (297)-this study

Central SNB - KP73, 78, D81

$^{143}Nd/^{144}Nd_i$

$^{87}Sr/^{86}Sr_i$

PRB-T88

Central SNB- M81, KP73, KP78

$\delta^{18}O$

$^{87}Sr/^{86}Sr_i$
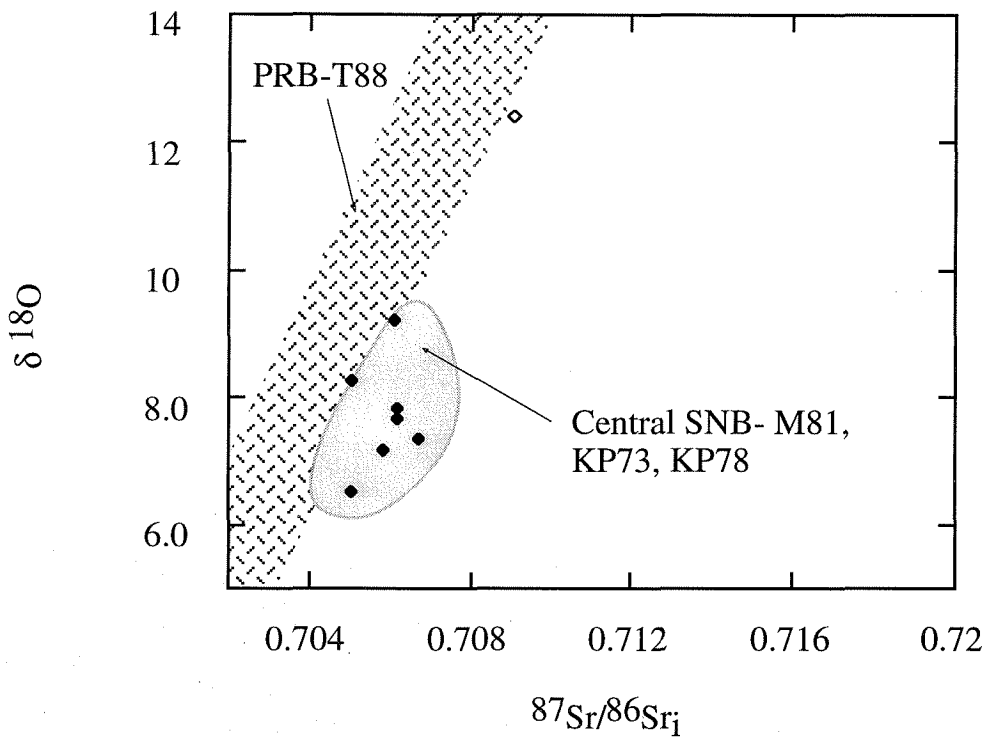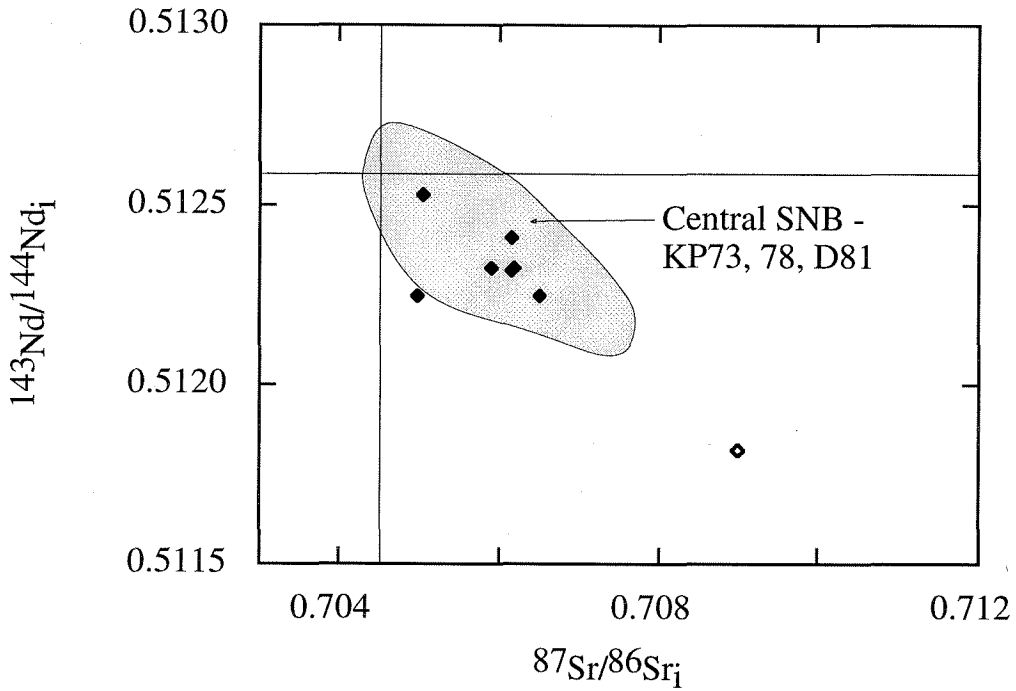
Garnet pyroxenite and feldspathic xenoliths

◆ This study

◉ Mukhopadhyay, 1989
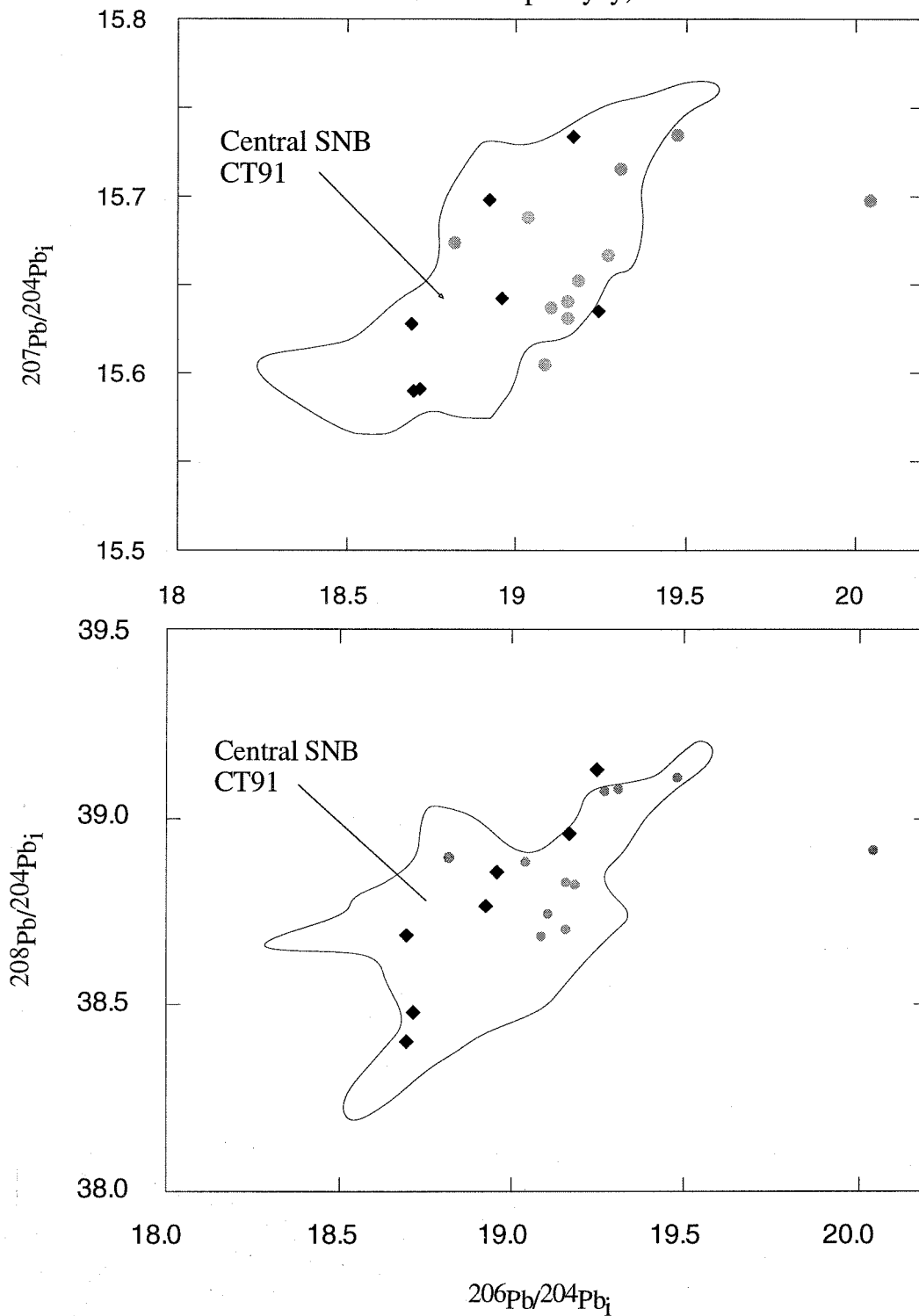
crustal levels could best explain the isotope data (the MASH hypothesis of Hildreth and Moorbath, 1988).

A proposed vertical section through the Sierra Nevada lithosphere

The composition of the SNB on a vertical dimension can be reasonably well constrained from surface exposures and geophysical data down to ~30 km (Saleeby, 1990). Assuming that the xenolith lithologies are representative for the depths they have equilibrated at, we will extend downwards the idealized vertical compositional column through the Sierra Nevada lithosphere.

The xenolith results show that a thick (70 km, possibly more) sequence of residual/cumulate mafic to ultramafic rocks complement at depth the upper- to mid-crustal rocks of the SNB. Our proposed lithopsheric column, based on surface rock and xenolith data is shown in Figure 3-7. Below we will outline some characteristics of the upper crust, the upper crustal to lower crustal transition, the lower crust, the crust-mantle boundary, and the upper mantle from beneath the Mesozoic SNB.

The upper 30 km of the Sierra Nevada crust consist almost entirely of tonalites, granodiorites, and granites of the SNB. This statement appears to hold even for the SNB exposures from the Tehachapi Mountains in the southernmost Sierra, at igneous exposure depths of 20-30 km (Pickett and Saleeby, 1993). Saleeby (1990) reports an average silica concentration of 60% for the Tehachapi exposures, slightly less siliceous than the bulk SNB exposures, ~65% SiO_2 (Bateman and Dodge, 1970). A recent seismic refraction experiment across the Sierra Nevada (Wernicke et al., 1996) shows that the seismic velocities remain fairly low (v_p = 6-6.4 km/sec) throughout the seismologically-defined crust, ~35 thick (Fliedner and Ruppert, 1996). Such low seismic velocities are charactreristic for quartz-rich, "granitic" rocks. The geophysical data is therefore consistent

Figure 3-7. Schematic lithospheric column for the region underlying the central SNB, based on outcrop and xenolith studies (see text).

Proposed lithospheric column for the central Sierra Nevada @ 100-10 Ma

60% tonalites,
30 %granodiorites (SNB)
& 10 % roof pendants

Granitoids to more
mafic compositions @
depth (SNB) + pendants

Feldspathic mafic
plutonic rocks &
cumulates

Eclogite facies cumulates
and residues of the SNB

Mixed zone of mantle
wedge peridotites and
eclogite SNB cumulates
and residues

Lithospheric mantle wedge,
including peridotite
cumulates & residues

Asthenosphere

with geological evidence indicating that the upper 30-35 km of the Sierran lithosphere consists mainly of granitoids.

The transition between the granitic upper crust and deeper, more mafic lithologies occurs between 30-40 km. If the xenolith data are representative for the crustal section they sampled, it appears that mafic rocks become progresively abundant in the 0.8 to 1.2 GPa interval. Feldspathic xenoliths with intermediate to mafic compositions generally display equilibration pressures lower than 1.2 GPa, while feldspar-free, mainly mafic rocks such as garnet clinopyroxenites and websterites equilibrated at pressures always higher than 1.0 GPa. A few xenoliths whose pressure of equilibration were calculated to be in the 1.0-1.4 GPa interval are cumulates with alternating felsdpar-rich and garnet-pyroxene rich layers.

Rocks that equilibrated at pressures higher than 1.5 GPa consist mainly of garnet, one or two pyroxenes, and amphibole. Garnet clinopyroxenites represent the most common deep xenolith rock type sampled at Big Creek. Rocks of broadly similar compositions are commonly found included as veins, pods or irregular bodies in larger volumes of garnet and spinel peridotites, for example in Alpine peridotites (Carswell, 1990). By analogy with the Alpine peridotites field relationships, one could interpret these rocks as mantle-derived. The composite feldpathic-garnet pyroxenitic cumulate xenoliths described above, the elevated, crustal $\delta^{18}O$ ratios measured in these rocks, as well as the scarcity of spinel peridotititc xenoliths (which equilibrated at pressures lower than ~2.5 GPa, Ducea and Saleeby, 1996a), all argue for the existence of a "eclogitic"-rich layer somewhere between 40-70 km beneath the Sierra Nevada. This layer corresponds in our view with the level at which large magma chambers have mixed mantle and crustal magmatic components during the Mesozoic, have distilled the SNB granitoids, and stored large volumes of garnet-rich cumulates/residues.

A lower crustal to upper mantle transition is hard to define beneath the Sierra Nevada, and perhaps under any batholith (Pitcher, 1993). Our deepest samples from Big Creek have equilibrated at pressures between 2.0-4.2 GPa (Ducea and Saleeby, 1996b),

and comprise of mainly garnet-bearing peridotites and garnet websterites. Presumably at greater depth peridotitic rocks predominate over pyroxenites. However, it is interesting to note that our garnet websterite sample F34, which equilibrated at ~100 km, has yielded synbatholithic Sm-Nd and Rb-Sr ages. The batholith-related magmatism in the Sierra Nevada has led to observable mass exghanges to at least 100 km depth. It is also worth noting that all samples recovered from Big Creek, including a garnet peridotite from 4.2 GPa, have isotopic characteristics of lithosphere. A Mesozoic age measured on F34 is consistent with the progressive development of a cold and thick lithosphere (130 km or more) beneath the Sierra Nevada during the vanishing stages and after the cessation of magmatism.

Two implications emerging from our interpreted lithospheric column may have important tectonic implications and will be outlined below: (a) the vertical scale at which batholith-related magmatism operates and (b) the efficiency of segregating light granitic crust form dense residues during batholithic magmatism.

(a) Our data and previously published work demonstrate that igneous products of the Late Cretaceous SNB are to be found from surface levels to at least ~ 100 km depth. There is evidence for two way exchange between the upper mantle and lower crust as well as between the lowermost crust and the upper crust. These results indicate that batholithic magmatism (at least in the Sierra Nevada) is a lithospheric scale process capable of isotopically homogenizing and thermochronologically resetting at least a 100 km thick lithosphere in a relatively short period of time (a few tens of millions of years). The crustal column is characterized by a coherent large scale major element chemical heterogeneity, typical for suites of consanguinous igneous rocks.

(b) It is remarkable how well the two entities, upper- to mid-crustal tonalites and granodiorites and the deep crustal/mantle mafic-ultramafic rocks appear to be spatially separated. Very often petrologists ask how much mass has been extracted out of the mantle during batholith formation, a question of relevance to the origin of continents. Data

presented here provide us with a different answer, potentially useful in understanding crustal growth: regardless of how much mass is recycled vs. juvenile, the SNB has efficiently "distilled" granitoids from a thick residual mafic-ultramafic mass.

No flat slab beneath the central Sierra Nevada

The data presented above show that a 100 or more km thick section, which can be related to the SNB, has resided at least between the Mesozoic and Mid-Miocene times under the Sierra Nevada. The low ε_{Nd} values of the lower crustal rocks (ε_{Nd} initial <1.8) argue strongly against an oceanic crustal origin for these rocks. Olivine-rich, garnet-bearing ultramafics underlay the crustal section described in this paper (Ducea and Saleeby, 1996a). Garnet peridotite inclusions from the pipes of Big Creek and the neighboring Pick and Shovel and Camp Sierra locations, all display continental lithospheric mantle isotopic signatures (Mukhopadhyay and Manton, 1994; our unpublished results). One garnet peridotite from Big Creek yielded an equilibration pressure of 4.2 GPa (Ducea and Saleeby, 1996b). We have no xenolith evidence for the existence of any rocks of oceanic derivation at any time between the Mesozoic and Mid-Miocene at least for ~130 km below the central Sierra Nevada surface. This result is at odds with the postulated "shallow subduction," or "flat slab" hypotheses, very often used to explain the sudden inland shift of magmatism in the western US during the Laramide orogeny, at the end of Cretaceous (Dickinson, 1981). These hypotheses predict a significant decrease of the subducting slab dip, and accordingly the depth to the slab top beneath the western US Cordillera starting at 65 Ma, and continuing for possibly as many as 40 Ma. More specifically, the slab top has been postulated to have passed as shallow as 35-60 km beneath the Sierra Nevada in Early Cenozoic times (Dumitru, 1990), refrigerating the Sierra Nevada throughout the Cenozoic. The data presented here require that the refrigeration mechanism could not have involved a

slab shallower than 130 km at any time since the Mesozoic. The 130 km depth constrained from our data raises serious questions regarding the viability of the "flat slab" mechanism under central California.

Contrasting post-batholith tectonics of the central and southern Sierra Nevada

The southernmost end of the SNB is exposed to igneous intrusion depths as high as 30 km, in the Tehachapi Mountains (Picket and Saleeby, 1993). Ensimatic metamorphic rocks of the Rand Schist tectonically underlie these deepest exposures of the SNB (Malin et al., 1995). The Rand Schist, as well as equivalent rocks found elsewhere in Southern California (Orocopia, Pelona Schists), have an oceanic derivation (Jacobsen et al., 1996). These relations show that the integrity of the Sierra Nevada batholith has not been maintained in its southernmost end. One can assume that the southernmost Sierra also had a similarly thick mafic-ultramafic "root," as the central Sierra Nevada did. Therefore, it is reasonable to infer that very shallow subduction has removed the batholith root at its southernmost end. The timing of the underthrusting of the Rand Schist is constrained by field relations and geochronologic data to be 80-86 Ma (Silver and Nourse, 1986). This period corresponds to a major cooling and uplift period throughout the entire Mojave area to the south and southeast of the Sierra Nevada (Henry and Dokka, 1992).

The observations presented above suggest a major difference between the post batholith tectonic behavior of the lithosphere in the central vs. the southern(most) Sierra Nevada. While the main part of the batholith has retained its crustal wealth throughout the Cenozoic (at least until Mid-Miocene) and maintained elevations above sea level, the southern end of the batholith, which is representative for the Mojave region, has been the site of shallow subduction, lost its lower crust and was submerged below sea level during the Miocene (Nilsen and Clarke, 1975). The southern vs. central Sierra post-batholithic tectonic difference may be analogous to the modern Andes, where the central segment of

the magmatic arc is underlain by a shallowly subducting slab, while the northern and southern Andes, by steeper segments of the slab (Isacks, 1988, and references therein).

The fate of batholithic mafic-ultramafic residues

We have shown that rocks that have Sierra Nevada batholith affinities and require some component of supracrustal rocks are to be found as deep as 100 km beneath the batholith. Rocks deeper than 35 km are eclogites in a broad sense, and they have cumulate textures, major and trace element chemistry (Ducea et al.,1995) as well as physical properties consistent with a cumulate origin. The elevated $\delta^{18}O$ ratios suggest that these lower crustal rocks might be also restites (melanosomes), implying a significant involvement of a preexisting continental crustal component in melting. Regardless of the actual mechanism that relates the eclogites to crust/mantle melting and various lower crustal igneous process, these rocks are the mafic-ultramafic counterparts of the composite SNB, they represent a ~70 km thick section of residual rocks beneath the Sierra Nevada batholith. These rocks have an average density of 3550-3600 kg/m³ (calculated using the program by Niu and Batiza, 1991), significantly higher than the typical upper mantle peridotites (3300 kg/m³), in which they appear to be rooted.

Such a dense mass would be expected to delaminate, i.e., sink in the peridotitic mantle (e.g., Kay and Kay, 1993). We know that the eclogites were present beneath the batholith between c. 100 Ma and 10 Ma, based on the geochronology presented in this paper and the age of the Big Creek trachyandesite. Since there are no substantial retrograde products to change the original syn-batholithic eclogite facies mineral assemblage, we also believe that these rocks have remained at great depths between ~100 and 10 Ma. However, there is evidence that these rocks might have disappeared from under the Sierra Nevada between 10 and 4 Ma. Late Miocene volcanics from the same area as the Mid-Miocene eclogite-bearing trachyandesites carry only spinel peridotites which probably equilibrated

between 35-70 km (Ducea and Saleeby, submitted). Younger, 0-1 Ma volcanics from the eastern Sierra Nevada also carry only spinel peridotites (Beard and Glazner, 1995; Ducea and Saleeby, 1996a). Not a single garnet-bearing rock has been recovered from the 3-4 and 0-1 Ma xenolith locations. Recent seismic studies have established that the Sierra Nevada has a thin, ~35-42 km thick crust (Wernicke et al., 1996). The seismologically-defined Moho could be suspected in this case to be a phase change (basalt-eclogite transition), but there is no evidence for anomalously high seismic velocities and/or low Poison ratios at sub-Moho depths, as expected from the presence of eclogites (Jones et al., 1994; Wernicke et al., 1996). It is likely that the eclogitic residues from underneath the Sierra Nevada have delaminated since the Mid-Miocene. Such a mechanism would provide buoyancy for the postulated late Miocene uplift of the Sierra Nevada (Ducea and Saleeby, 1996a), a process which can not be explained by the Late Cenozoic plate tectonic framework of California (e.g., Dickinson, 1981).

Data presented in this paper does not provide any particular evidence for the delamination process; arguments for a very young (late Miocene-Pliocene) delamination event have been presented elsewhere (Ducea and Saleeby, submitted). Here we address a different question which could have tectonic implications for the Sierra Nevada and its surrounding regions: why did this thick eclogitic root *not* delaminate for 70 Ma after the batholithic magmatism ceased? We believe that a key factor in the onset of crustal delamination is the mechanical weakness of the mid crust, the level where presumably the dense root splits. The simplest speculation is that an increase in the crustal heat flow could change a mid-crust with considerable strength into a weak domain (sometimes called "crustal asthenosphere"). A relatively siliceous and strong mid crust as in the SNB can become weak upon heating, while the lower crustal eclogite facies rocks would not suffer any significant mechanical changes. The root can then split at mid crustal levels. The region had a very low heat flow throughout most of the Cenozoic (Dumitru, 1990), but has been

heated in the recent past, perhaps by the extending Basin and Range province immediately to the east (Henyey and Lee, 1976).

The case for crustal delamination under the Sierra Nevada may be a strong one. However, little is known about the details of this process. The data presented here provide a potentially important constraint: if crustal delamination did occur beneath the Sierra Nevada magmatic arc, it happened with a "delay" of over 70 My after the cessation of magmatism, at a time coincident with a postulated significant uplift of the Sierra Nevada mountain range (Bateman and Eaton, 1967, and references therein).

3.8. Conclusions

The geochronologic results presented here confirm that the Sm-Nd mineral isochron method of dating garnet-rich lower crustal rocks can be succesfully applied to xenoliths to yield the timing of the peak thermal conditions. The Rb-Sr mineral isochron method applied on the same minerals is not nearly as reliable. Commonly, the Sr mineral ages are being reset, partially reset, or modified in a fashion which makes them hard to interpret.

The data presented in this paper provide a much more complete view of the vertical dimension of a large Cordilleran batholith. The SNB consists of at least a 2/1 ratio of mafic-ultramafic to granitic material. We have shown that the central SNB was underlain by a 70 km thick sequence of mafic-ultramafic cumulate rocks in granulite and eclogite facies, probably mixed with peridotites at great depths. These rocks have isotopically equlibrated between ~81-136 Ma, coincident with the most prolific period of magmatism in the SNB. The whole rock Sr, Nd, Pb and O isotopic ratios of the xenoliths are very similar to the isotopic ratios of the surface batholith in the vicinity of the xenolith-bearing Miocene pipe. The lower crustal xenoliths are clearly batholith-related rocks; they are either cumulates

from large lower crustal magma chambers, or restites of large scale crustal melting. We hypothesize that at least a 100 km thick lithospheric section beneath the SNB has been strongly affected by the Mesozoic magmatism, homogenized isotopically and reset thermochronologically. Large scale magmatism has efficiently segregated a high silica upper 30 km of the crust from residual/cumulate rocks in the deeper parts of the crust and mantle.

The thick batholithic section beneath the central Sierra Nevada raises serious questions to whether a flat slab has ever existed beneath central California. On the other hand it points out a major tectonic difference between the post batholith behavior of the central and southernmost Sierra Nevada: the southernmost Sierra and the Mojave regions were truncated at depth by an oceanic-like slab as shallow as 30 km at the end of the Cretaceous. Finally, if the thick ultramafic root of the central Sierra Nevada batholith has delaminated in the mantle, this process has been delayed for more than 70 My after the cessation of batholithic magmatism.

References

Ague J.J., and Brimhall G.H. (1988) magmatic arc asymetry and distribution of anomalous plutonic belts in the batholiths of California; Effects of assimilation, crustal thickness and depth of crystallization, Geol. Soc. Am. Bull., 100: 912-927.

Ashworth J.R. (1985) Migmatites, Blackie, Glasgow, 302 p.

Bateman P.C. (1983) A summary of critical relationships in the central part of the Sierra Nevada batholith, California, U.S.A., in Roddick J.A. (ed.) *Circum-Pacific plutonic terranes*, Geol. Soc. Amer. Memoir 159: 241-254.

Bateman P.C. and Dodge F.C.W. (1970) Variations of major chemical constituents across the central Sierra Nevada batholith, Geol. Soc. Am. Bull., 81:409-420.

Bateman P.C. and Eaton J.P. (1967) Sierra Nevada batholith, Science, 158:1407-1417.

Beard B.L. and Glazner A.F. (1995) Trace elements and Sr and Nd isotopic composition of mantle xenoliths from Big Pine Volcanic Field, California, J. Geophys. Res., 100:4169-4179.

Becker H. (1997) Sm-Nd garnet ages and cooling history of high temperature garnet peridotite massifs and high pressure granulites from lower Austria, Contrib. Mineral. Petrol., 127: 224-236.

Burton K.W., Kohn M.J., Cohen A.S., and O'Nions R.K. (1995) The relative diffusion of Pb, Nd, Sr, and O in garnet, Earth. Pl. Sci. Lett., 133:199-211.

Carswell D.A. (1990) Eclogite facies rocks, Chapman and Hall, New York, NY, 396 p.

Chen J.H. and Tilton G.R. (1991) Applications of lead and strontium isotopic relationships to the petrogenesis of granitoid rocks, central Sierra Nevada batholith, California, Geol. Soc. Am. Bull., 103: 439-447.

Chen J.H. and Moore J.G. (1982) Uranium-lead isotopic ages from the Sierra Nevada batholith, California: J. Geophys. Res., 87: 4761-4784.

Clemens, J.D. (1988) The granulite-granite connection, in Vielzeuf D. and Vidal P. (eds.) *Granulites and crustal evolution*, Kluwer Acad., Norwell, MA, ser. C, 311:25-37.

Coghlan. R. (1990) Studies in diffusional transport: Grain boundary transport of oxygen in feldspar, diffusion of O, Sr, and REE's in garnet and thermal histories of granitic intrusions in south-central Maine using oxygen isotopes, Ph.D thesis, Providence, Rhode Island, Brown University, 247p.

Coleman D., Frost T., and Glazner A. (1992) Evidence from the Lamarck Granodiorite for rapid Late Cretaceous crust formation in California, Science, 258:1924-1926.

Coleman D., Lee D., Beatty J., and Brannock W., Eclogites and eclogites; their differences and similarities, Geol. Soc. Am. Bull., 76: 483-508.

Coward M.P., and 7 others (1986) Collision tectonics in NW Himalayas, in Coward M.P and Ries A.C (eds.), *Collision tectonics*, Geol. Soc. Spec. Publ., 19: 203-219.

DePaolo D. (1981) A neodynium and strontium study of the Mesozoic calc-alkaline granitic batholiths of the Sierra Nevada and Peninsular Ranges, J. Geophys. Res., 86: 10470-10488.

Dickinson W. (1981) Plate tectonics and the continental margin of California, in Ernst W.G. (ed.) *The geotectonic development of California*, Prentice-Hall, Englewood Cliffs, N.J., 1-28.

Dodge F.C.W. and Bateman P.C. (1988) Nature and origin of the root of the Sierra Nevada, Am. J. Sci., 288A: 341-357.

Dodge F.C.W., Calk L.C., and Kistler R.W. (1986), Lower crustal xenoliths, Chinese Peak lava flow, Central Sierra Nevada, J. Petrol., 27: 1277-1304.

Dodge F.C.W., Lockwood J.P., and Calk L.C. (1988), Fragments of the mantle and crust beneath the Sierra Nevada batholith: Xenoliths in a volcanic pipe near Big Creek, California, Geol. Soc. Am. Bull., 100: 938-947.

Domenick M.A., Kistler R.W., Dodge F.C.W., and Tatsumoto M. (1983) Nd and Sr study of crustal and mantle inclusions from the Sierra Nevada and implications for batholith petrogenesis, Geol. Soc. Am. Bull., 94: 713-719.

Ducea M.N., and Saleeby J.B. (1996a) Buoyancy sources for a large unrooted mountain range, the Sierra Nevada, California: Evidence from xenolith thermobarometry, J. Geophys. Res., 101: 8229-8241.

Ducea M.N. and Saleeby J.B. (1996b), Rb-Sr and Sm-Nd mineral ages of some Sierra Nevada xenoliths; implications for crustal growth and thermal evolution, EOS, Trans. Amer. Geophys. Union, 77:780.

Ducea M.N., Kistler R.W. and Saleeby J.B. (1995) Testing petrogenetic models of the deep Sierra Nevada crust and upper mantle using REE data on xenolith assemblages, Geol. Soc. Am. Abstracts with Programs, 27:15.

Dumitru T.A. (1990) Subnormal Cenozoic geothermal gradients in the extinct Sierra Nevada magmatic arc: Consequences of Laramide and post-Laramide shallow subduction, J. Geophys. Res., 95:4925-4941.

Everden J.F., and Kistler R.W. (1970) Chronology of emplacement of Mesozoic batholithic complexes in California and western Nevada, U.S. Geol. Suv. Prof. Pap., 623: 1-42.

Fliedner M. and Ruppert S. (1996) 3-dimensional crustal structure of the Southern Sierra Nevada from seismic fan profiles and gravity modelling, Geology, 24: 367-370.

Green D.H. and Ringwood A.E. (1967) An experimental investigation of the gabbro to eclogite transformation and its petrological applications, Geochim. Cosmochim. Acta, 31:767-833.

Gromet P. and Silver L.T. (1987) REE variations across the Peninsular Ranges Batholith: Implications for batholithic petrogenesis and crustal growth in magmatic arcs, J. Petrol., 28: 75-125.

Hamilton W. and Maers W.B. (1966) The nature of batholiths, U.S. Geol. Surv. Prof. Pap., 554C; 30p.

Harrison T.M and Wood B.J. (1980) An experimental investigation of the partitioning of REE between garnet and liquid with reference to the role of defect equilibria, Contrib. Mineral. Petrol., 72:145-155.

Henry D.J. and Dokka R.K. (1992) Metamorphic evolution of exhumed middle to lower crustal rocks in the Mojave Extensional Belt, southern California, USA, J. Metamorphic. Geol., 10:347-364.

Henyey T.L. and Lee T.C. (1976) Heat flow in the lake Tahoe, California-Nevada, and the Sierra Nevada-Basin and Range transition, Geol. Soc. Am. Bull., 87, 1179-1187.

Hildreth W. and Moorbath S. (1988) Crustal contributions to arc magmatism in the Andes of central Chile, Contrib. Mineral. Petrol., 98:455-489.

Hunter R.H (1986) Textural equilibrium in layered igneous rocks, in Parsons I. (ed.) *Origin of igneous layering*, Kluwer Acad., NATO ASI Series C, 196: 473-505.

Isacks B.L. (1988) Uplift of the central Andean Plateau and bending of the Bolivian orocline, J. Geophys. Res., 93: 3211-3231.

Jacobsen C.E., Oyarzabal F.R., and Haxel G.B. (1996) Subduction and exhumation of the Pelona-Orocopia-Rand schists, southern California, Geology, 24: 547-550.

Jagoutz E. (1988) Nd and Sr systematics in an eclogite xenolith from Tanzania: Evidence for frozen mineral equilibria in the continental lithosphere, Geochim. Cosmochim. Acta, 52:1285-1293.

Jones C.H., Kanamori H., and Roecker S.W. (1994) Missing roots and mantle drips: Regional P_n and teleseismic arrival times in the Southern Sierra Nevada and vicinity, California, J. Geophys. Res., 99:4567-4601.

Kay R.W. and Kay S.M. (1993) Delamination and delamination magmatism, Tectonophys., 219:177-189.

Kistler R.W. and Peterman Z. (1973) Variations in Sr, Rb, K, Na and initial $^{87}Sr/^{86}Sr$ in Mesozoic granitic rocks and intruded wall rocks in central California, Geol. Soc. Am. Bull., 84:3489-3512.

Kistler R.W. and Peterman Z. (1978) Reconstruction of crustal blocks of California on the basis of initial Sr isotopic compositions of Mesozoic granitic rocks; U.S. Geol. Surv. Prof. Pap., 1071: 17 p.

Klein E.M. and Langmuir C.H. (1987) Global correlations of ocean ridge basalt chemistry with axial depth and crustal thickness, J. Geophys. Res., 92: 8089-8115.

Malin P.E., Goodman E.D., Henyey T.L., Li Y.G., Okaya D.A., and Saleeby J.B. (1995) Significance of seismic reflections beneath a titled exposure of deep continental crust, Tehachapi Mountains, California, J. Geophys. Res., 100:2069-2087.

Manning C.E. and Bohlen S.R. (1991) The reaction titanite+kyanite = rutile + anorthite and titanite-rutile barometry in eclogites, Contrib. Mineral. Petrol., 109:1-9.

Masi U., O'Neill J.R., and Kistler R.W. (1981) Stable isotope systematics in Mesozoic granites of central and northern California and soutwestern Oregon, Contrib. Mineral. Petrol., 76: 116-126.

Metzger K., Essene E.J., and Halliday A.N. (1992) Closure temperatures of the Sm-Nd system in metamorphic garnets, Earth. Planet. Sci. Lett., 113: 397-409.

Moore J.G. and Dodge F.C.W. (1980) Late Cenozoic volcanic rocks of the Southern Sierra Nevada, California; I. Geology and petrology: Summary, Geol. Soc. Am. Bull., 91: 515-518.

Mukhopadhyay B. (1991) Garnet breakdown in some deep seated garnetiferous xenoliths from the central Sierra Nevada:Peetrologic and tectonic implications, Lithos, 27:59-78.

Mukhopadhyay B. (1989) Petrology and geochemistry of mafic and ultramafic xenoliths from the Sierra Nevada batholith, Part 1, Ph.D. dissertation, Univ. Texas at Dallas, 215 p.

Mukhopadyay B., Manton W.I. (1994) Upper mantle fragments from beneath the Sierra Nevada batholith: Partial fusion, fractional crystallization and metasomatism in a subduction-enriched ancient lithosphere, J. Petrol., 35: 1418-1450.

Nilsen T.H. and Clarke S.H. (1975) Sedimentation and tectonics in the early Tertiary continental borderland of central California, U.S. Geol. Surv. Prof. Pap., 925:64p.

Niu Y. and Batiza R. (1991) DENSCAL: A program for calculating densities of silicate melts and mantle minerals as a function of pressure, temperature, and composition in melting range, Comp. Geosci., 17:679-687.

Pickett D.A. and Saleeby J.B. (1993) Thermobarometric constraints on the depth of exposure and conditions of plutonism and metamorphism at deep levels of the Sierra Nevada batholith, Tehachapi Mountains, California, J. Geophys. Res., 98: 609-629.

Pickett D.A. and Saleeby J.B. (1994) Nd, Sr, and Pb isotopic characteristics of Cretaceous intrusive rocks from deep levels of the Sierra Nevada batholith, Tehachapi Mountains, California, Contrib. Mineral. Petrol., 118:198-205.

Pitcher W.S. (1993) The nature and origin of granite, Blackdie Acad.& Prof., London, 321 p.

Rudnick, R.L. (1992) Xenoliths: samples of the lower continental crust, in Fountain D.M, Arculus R., and Kay R.W. (eds.) *Lower continental crust*, Developments in Geotectonics, 23: 269-317.

Saleeby J.B. (1990) Progress in tectonic and petrogenetic studies in an exposed cross-section of young (c. 100 Ma) continental crust, southern Sierra Nevada, California, in Salisbury M. H., and Fountain D. M. (eds.) *Exposed crustal sections of the continental crust*, Kluwer Acad., Norwell, Mass., 137-158.

Saleeby J. B., Sams D.B. and Kistler R.W. (1987) U/Pb zircon, strontium, and oxygen isotopic and geochronological study of the southernmost Sierra Nevada batholith, California, J. Geophys. Res., 92, 10443-10466.

Silver L.T. and Nourse J.A. (1986) The Rand Mountains thrust complex in comparison with the Vincent thrust-Pelona schist relationship, southern California, Geol. Soc. Am. Abstracts with Programs 18:185.

Sneeringer M., Hart S.R., and Shimizu N. (1984) Strontium and Samarium diffusion in diopside, Geochim. Cosmochim. Acta, 48: 1589-1608.

Taylor H.P (1988) Oxygen, hydrogen, and strontium isotope constraints on the origin of granites, Trans. R. Soc. Edinburgh Earth Sci., 79: 317-338.

Wendlandt E., DePaolo D.J., and Baldridge W.S. (1996) Thermal history of Colorado Plateau lithosphere from Sm-Nd mineral geochronology on xenoliths, Geol. Soc. Am. Bull., 108: 757-767.

Wernicke B., and 19 others (1996) Origin of high mountains on continents: The Southern Sierra Nevada, Science, 271: 190-193.

Wolf M.B. and Wyllie P.J. (1993) Garnet growth during amphibolite anatexis: Implications for a garnetiferous restite, J. Geol., 101:357-373.

Wyllie P.J. (1984) Constraints imposed by experimental petrology on possible and imposible magma sources and products, Phil. Trans. R. Soc. Lond., A310:439-456.

CHAPTER 4

Major and Trace-Element Concentrations and $^{18}O/^{16}O$ Ratios in Eclogitic Residues From Beneath the Sierra Nevada, California; Similarities Between Cordilleran Batholiths and Archean Granitoids

Mihai Ducea, Jason Saleeby, and Hugh P. Taylor, Jr.

Abstract. Garnet pyroxenites are the most common deep- crustal and upper- mantle xenolith assemblages found in Miocene volcanic rocks erupted through the central part of the Cretaceous Sierra Nevada batholith (SNB)[1,2]. We propose that the SNB granitoids and the pyroxenite xenoliths are respectively the melt and unmelted residue from partial melting of a "basaltic" protolith at depths exceeding 35-40 km. This protolith included ≥20-30% of material with a pre-existing near-surface hydrothermal and/or weathering history ($\delta^{18}O$ =6.5 to 9 ‰ in both xenoliths and SNB). There are many chemical similarities between the SNB granitoids and Archean granitoids, and between the Sierra pyroxenites and eclogitic xenoliths in kimberlites. We suggest that certain segments of the Cordilleran batholiths may have originated by petrologic processes similar to those which led to the extraction of the voluminous granitoids that make up the cratonic nucleii of the continents[3,4].

Arguably, at least 40% of the present day volume of the Earth's continental crust was extracted from the mantle during the Archean[5]. Granitoid plutons characterized by a distinct suite of tonalites, trondjemites and granodiorites (TTG) are the most abundant igneous rocks exposed at the surface in Archean cratons[6]. The TTG differentiation processes are critical in understanding the formation of the continental crust. Most models of Archean differentiation in the literature utilize actualistic plate tectonic concepts, yet the composition of new continental mass generated at modern plate margins appears to be predominantly basaltic[7]. An exception may be the Cordilleran regions of western North- and South-America, where large composite Phanerozoic granitic batholiths form and have

formed at convergent plate margins. Portions of these batholiths broadly resemble the composition of Archean TTGs[3,4], although some chemical differences between the two have also been established[5].

The Sierra Nevada batholith (SNB) is a rather typical Mesozoic Cordilleran batholith, composed primarily of tonalitic and granodioritic plutons, 90% of which were emplaced between 125-85 Ma[8]. Granitoid rocks are known from present day surface exposures to extend to a depth of at least 30 km in the Cretaceous crustal column[9]. Samples of deeper seated rocks are entrained as xenoliths in extension-related volcanic rocks of Miocene age from the central Sierra Nevada (2, and references therein). These provide a rare opportunity to constrain the composition of a Cordilleran batholith in the vertical dimension to levels that have not been exposed at the surface by tectonic processes (~100 km deep).

The most common petrographic types observed in these central Sierra Nevada xenoliths are cumulate-textured pyroxenites (clino-, and orthopyroxenites, as well as websterites), commonly garnet-, and amphibole-bearing and occasionally transitional to eclogites (i.e., rocks with high-Na clinopyroxene)[1,2]. We shall refer to all the above rock types as "Sierran pyroxenites." Other common lower crustal petrographic types in the xenolith populations are granulites and amphibolites. Barometric determinations[2] indicate that garnet-bearing Sierran pyroxenites equilibrated over a very large range of depths (between ~40 and 100 km, at least). This depth interval probably represents a complex petrologic sub-arc transition from "lower crust" to "upper mantle" environments, even though most of this material would be identified seismologically as "mantle" based on the high P-wave velocities of the eclogites. Peridotites are rare in the central Sierra Nevada Miocene xenolith populations; they contain either spinel + garnet or garnet and appear to have equilibrated at depths >70-80 km[2]. The lack of spinel peridotites and abundance of garnet pyroxenites, including some composite samples displaying transitions to feldspathic lithologies, suggests that during the Miocene, the depth interval between ~35 and at least 70

km beneath the SNB was comprised predominantly of olivine-free garnet-pyroxene (+ amphibole) assemblages. The garnet-bearing Sierran pyroxenites have Sm-Nd mineral ages identical to the range of ages calculated for the surface plutons in the central parts of the SNB[10, 11]. The Nd isochron intercepts as well as the age-corrected whole-rock Sr and Pb isotopic compositions of the pyroxenites fall within the fields of initial Sr, Nd, and Pb isotopic ratios measured on the surface rocks of the SNB in the same area where the xenolith-bearing volcanic rocks are located[10]. The geochronologic and whole-rock isotopic data clearly indicate that the garnet-pyroxenites are in some manner cogenetic with the overlying SNB, presumably as melts, cumulates, or residues after melt extraction.

In this paper we present new major- and trace-element, as well as $^{18}O/^{16}O$ data on 9 xenolith samples collected from the Big Creek pipe and Chinese Peak flow[2], central Sierra Nevada (Table 4-1). These samples, eight pyroxenites and one amphibolite, were selected from a larger set of 60 samples, picking those with the least amounts of alteration products in thin section. The selected samples all display negligible (0-2%) interactions with the host volcanic rocks[10]. Despite this lack of alteration, we mildly leached all samples before crushing them into powders, in order to eliminate any possible grain boundary effects. Major elements were determined on an automated, wavelength dispersive X-ray fluorescence spectrometer. Trace element determinations were performed on an Ar source quadrupole ICP-MS. USGS and NBS standards were used for calibrating the XRF and ICP-MS instruments. The oxygen was extracted using a laser fluorination line, followed by analysis of isotopic ratios of major minerals[12], expressed as $\delta^{18}O$ in per mil relative to SMOW. The whole rock $\delta^{18}O$ values were calculated by material balance using the modal proportions of major minerals in each sample.

Despite the postulated igneous consanguinity between the Sierran pyroxenites and the SNB granitoids, pyroxenites form trends highly oblique to the trends defined by SNB in major element diagrams (Figure 4-1). The weak correlations among the various major oxides in the pyroxenites can be explained in terms of the modal variations of the dominant

Table 1. Major, trace, and oxygen isotopic compositions of central Sierra Nevada xenoliths.

Sample	Bc216	Bc221	Bc218	B75	F34	Bc207	G39	G36	Bc117
*	c/g/h	o/c/g/h	g/c	g/c/p	c/o/g	g/c/h	g/c	c/g/h	p/h
SiO_2	45.75	43.15	41.67	43.14	49.77	45.5	45.2	46.08	48.39
TiO_2	0.27	1.09	0.34	2.87	1.17	0.53	3.46	0.58	1.63
Al_2O_3	17.6	12.95	20.56	13.64	7.15	12.58	9.41	12.68	19.19
FeO**	9.08	19.1	14.52	16.4	8.87	9.12	12.69	12.1	9.47
MnO	0.137	0.32	0.269	0.274	0.125	0.886	0.145	0.195	0.14
MgO	9.85	18.53	11.37	8.72	16.76	5.71	11.52	11.82	5.57
CaO	10.08	2.81	9.4	12.06	14.6	23.58	14.37	14.58	9.79
Na_2O	1.33	0.13	0.26	1.2	0.83	3.38	1.49	1.27	3.38
K_2O	0.37	0.25	0.09	0.21	0.13	0.35	0.22	0.23	1.22
P_2O_5	0.01	0.01	0.34	0.13	0.01	0.01	0.01	0.01	0.01
Rb	11.25	11.39	23.33	6.539	2.449	1.640	8.451	8.291	28.19
Sr	197.5	43.34	60.77	131.1	129.9	40.69	71.38	93.95	388.4
Y	4.597	37.64	17.63	57.29	10.47	22.69	14.49	66.16	24.38
Zr	9.346	31.24	16.48	69.49	20.42	16.17	130.4	14.44	32.18
Nb	0.405	3.225	0.534	7.516	0.570	1.174	29.06	0.228	6.536
Ba	152.8	163.3	335.2	181.1	54.11	55.72	66.68	205.7	373.1
La	1.160	1.429	0.37	8.383	2.404	2.950	8.068	1.056	11.54
Ce	2.849	2.682	0.673	20.29	6.856	4.479	26.26	1.278	20.96
Pr	0.575	0.493	0.151	3.743	1.546	0.691	5.731	0.676	3.388
Nd	2.783	2.119	1.177	17.31	7.548	2.359	24.91	4.777	12.64
Sm	0.646	0.808	1.036	5.222	2.249	0.612	5.170	2.783	2.994
Eu	0.295	0.437	0.497	1.579	0.596	0.193	1.168	1.124	0.929
Gd	0.677	2.249	2.521	7.353	2.278	1.062	4.309	5.312	3.611
Tb	0.101	0.448	0.437	1.109	0.281	0.184	0.454	0.889	0.490
Dy	0.623	4.347	3.753	8.606	1.635	1.862	2.416	8.016	3.412
Ho	0.100	1.132	0.876	1.971	0.290	0.507	0.426	1.636	0.693
Er	0.285	2.514	2.155	4.755	0.705	1.435	1.008	3.604	1.452
Tm	0.044	0.473	0.322	0.740	0.091	0.240	0.122	0.647	0.249
Yb	0.266	5.079	3.344	8.310	1.114	2.965	1.330	7.053	2.642
Lu	0.113	1.116	0.735	1.727	0.192	0.668	0.289	1.695	0.535
Hf	0.241	0.724	1.013	2.968	0.967	0.739	4.562	0.615	1.283
Ta	1.547	0.070	0.048	1.41	0.011	0.043	0.272	0.010	0.819
Th	0.201	0.212	0.004	0.191	0.017	0.189	0.113	0.069	0.784
U	0.120	0.108	0.051	0.184	0.035	0.124	0.221	0.103	0.551
$\delta^{18}O$ c	7.7	7.3	7.2	6.5	6.4	7.9	8.4	7.8	
$\delta^{18}O$ g	7.9	7.6	7.6	6.5	6.5	8.6	8.6	7.7	
$\delta^{18}O$ h		7.8				8.3			9.1
$\delta^{18}O$ o		7.7			6.4				
$\delta^{18}O$ p									9.2
$\delta^{18}O$ wr	7.80	7.62	7.51	6.50	6.42	8.24	8.55	7.8	9.14

* Major constituent mineral. Abbreviations: c- clinopyroxene, o- ortopyroxene, h- amphibole, g- garnet, p- plagioclase.

** Total $FeO+Fe_2O_3$

Figure 4-1. Silica variation diagrams for (**a**) CaO, (**b**) Al_2O_3, and (**c**) MgO for Sierran pyroxenite xenoliths (black triangles), amphibolite "A" (open triangle), and granitoid rocks from the surface outcrops of the central Sierra Nevada batholith (CSNB) in the vicinity of the xenolith-bearing volcanic rocks (dotted fields[13]). The average Sierran pyroxenite (ASP), calculated as explained in text, is represented by a star symbol.
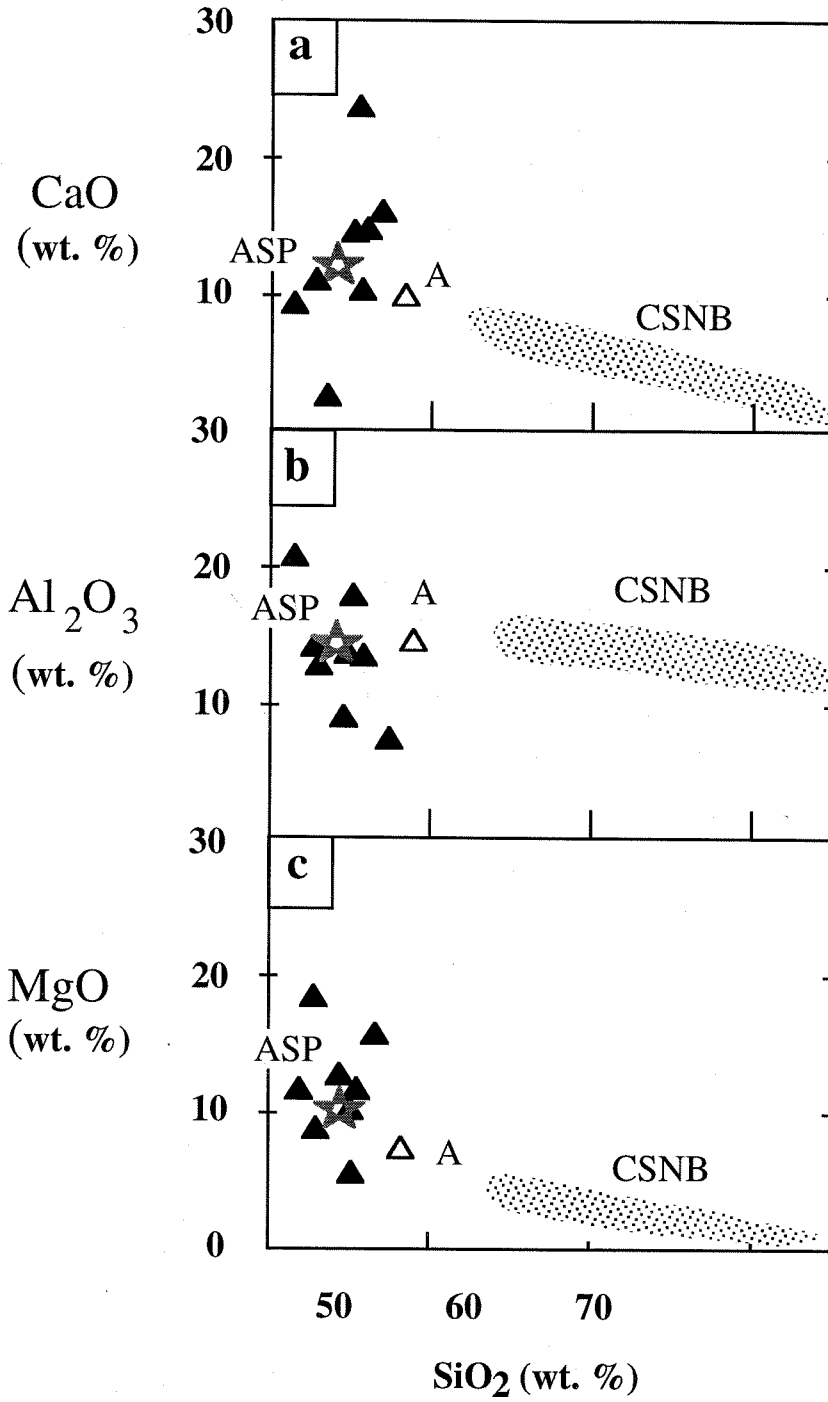
minerals (pyroxenes, garnet and amphibole); we interpret this as an artifact of the small sample size (2-5 cm radius) combined with the rather large grain size (~ 0.25-0.5 cm radius) of the analyzed xenoliths. Using the data presented in Table 4-1, we calculated the average major element concentrations of the Sierran pyroxenites (ASP). The major element concentrations of ASP are within 5% of the average pyroxenite major concentrations calculated using the average mineral chemistry of pyroxenes and garnet determined in 22 samples[2], and the average modal proportions of pyroxenes and garnet (pyroxene/garnet ~ 3/2) estimated in thin sections. This correspondence implies that the subset of 8 xenoliths whose chemical compositions were analyzed in this study covers and averages reasonably well the variability encountered in the entire pyroxenite xenolith population. For example, the average SiO_2 concentrations measured in xenoliths is 44.71%, whereas the average SiO_2 calculated from modes and mineral chemistry data is 45.01%.

The major element concentrations measured in the pyroxenites (e.g., SiO_2 as low as 41.7 wt.%) indicate that these rocks cannot be the high pressure equivalents of basaltic melts (e.g., modern MORB, or eclogites from subduction complexes); instead, these data, taken together with their textures and mineralogical features, are consistent with a residual/cumulate origin. Amphibolite Bc117, in contrast, has the chemical composition of a high-Al basalt. The ASP and the amphibolite lie on co-linear trends with the major-element trends defined by the nearby surface granitoids[13] on Harker diagrams (Figure 4-1). We modeled the REE compositions of liquids (c_l) in equilibrium with the ASP (c_S), a calculation which is dependent only on the modal proportions of solids in the residue and the partition coefficients (D) for any given element (i), and not on the percent of partial melt ($C_S=D_i*C_l$). We used intermediate melt (quartz-normative, 60% SiO_2) - solid (pyroxene/garnet/amphibole) partition coefficients[14], and obtained a close match between the model melts and the trace element concentrations observed in the SNB (Figure 4-2).

We interpret the pyroxenites to be an unmelted residue left behind at deep crustal levels after SNB-like, quartz-normative, relatively low-silica granitoid melts have been

Figure 4-2. Rare Earth Element (REE) concentrations (normalized to chondritic concentrations) of intermediate melts (circles) in equilibrium with a residue with ASP composition (filled triangles). The ASP (average Sierran pyroxenite) is assumed to contain 50% clinopyroxene, 40% garnet, and 10% amphibole in this model. The average REE compositions[20] of surface rocks of the central Sierra Nevada batholith (CSNB), i.e., granodiorites (open diamonds) and tonalites (open squares), are shown for comparison.
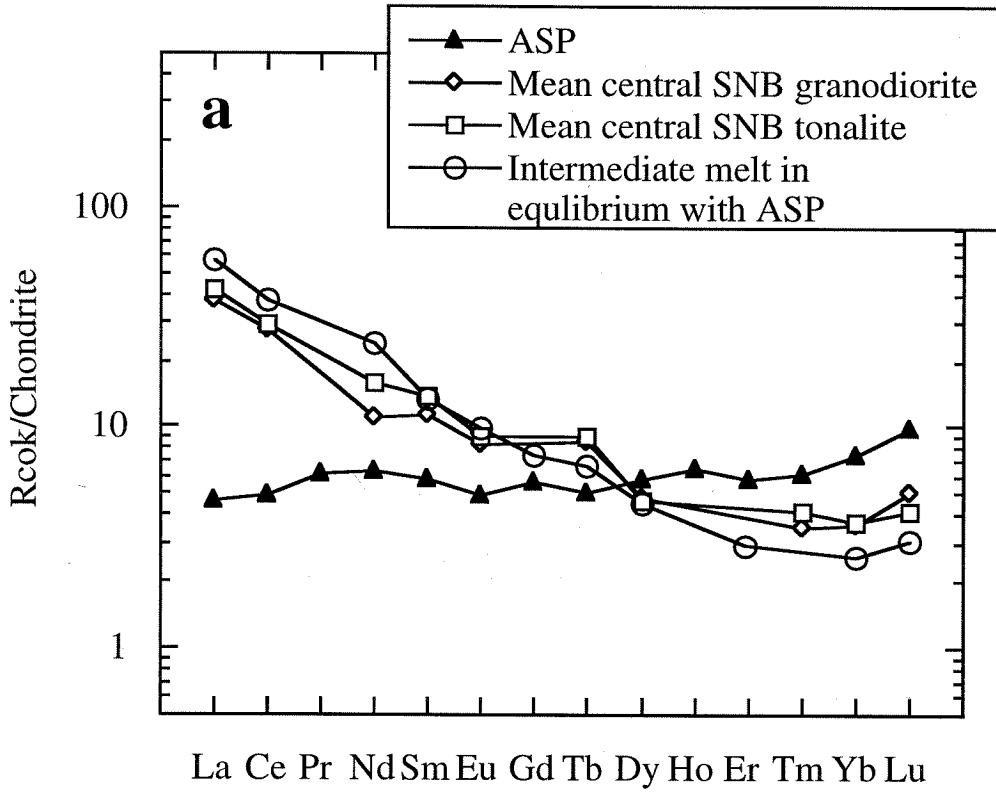
extracted out of an original "basaltic" protolith. The basaltic nature of the protolith is supported by a rough calculation on major element mass balance in the Sierra Nevada lithosphere. Here we detail the SiO_2 case, as an example. Based on published geological data[8,13], we estimate the average Sierra Nevada granitic crust (0-30 km crustal depths) to have ~63% SiO_2, while our data constrain the residue to have SiO_2 concentrations of ~45%. Thermobarometric estimates[2] constrain the ratio of residue to melts to be > 2/1 in the central Sierra Nevada, consistent with a basaltic protolith, possibly blended with some higher SiO_2 components. Amphibolite Bc117 may represent an unmelted example of what was undoubtedly a complex source material the deep lithosphere beneath the SNB during the Mesozoic. Available experimental data are consistent with this interpretation, in that experimental results[15, 16] demonstrate that tonalitic/granodioritic melts can be generated in equilibrium with an eclogitic (± amphibole) residue during 10-30% dehydration melting of amphibolites at pressures exceeding 10 kbar. There is an excellent agreement between: (1) the major element compositions of experimental residues[15,16] and the ASP; (2) the experimentally-produced tonalitic/granodioritic melts and the average central SNB granitoids; and (3) between the mineral chemistry of the residual phases (garnet, pyroxenes and amphiboles) in the experiments and the minerals in the Sierran pyroxenites[1,2].

A similar mechanism recently has been put forward to explain the differentiation of the large volumes of Archean TTGs[17,18]. The major- and trace-element compositions of the Sierran pyroxenites are remarkably similar to those of residual eclogites found within the deep lithosphere of Archean cratons (e.g., ref 19). The major-element compositions of ASP and the Archean residual eclogites in kimberlites from Sierra Leone[19] agree to within 5%, except for Na_2O. Figure 4-3 shows the strikingly similar composition of incompatible trace elements in two of the Sierran pyroxenites and a residual eclogite from the Udachnaya kimberlite pipe, in the Siberian craton[17]. We selected the Udachnaya and the Sierra Leone samples for comparison, because they were previously used to support the hypothesis of

Figure 4-3. Compositions of selected incompatible trace elements (normalized to chondritic concentrations) of two representative Sierran pyroxenites (Bc216, Bc218) are compared with the concentrations determined in an Archean residual eclogite (pyroxenite) from the Udachnaya pipe, in the Siberian craton[17].
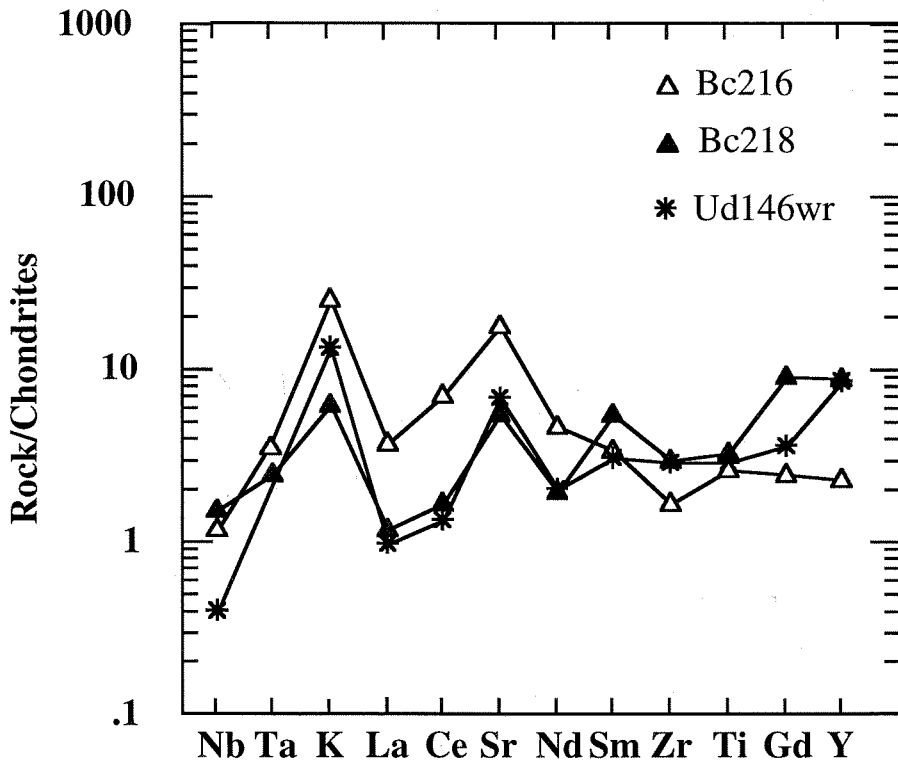
granitoid extraction from residual eclogites[17,18], and as pointed out in those references, because their chemistry was not subsequently modified during their long-term residence in the lithosphere. The chemistry of Sierran and Archean granitoids are also comparable. The two abundant rock types of the SNB are tonalites and granodiorites, with average major element concentrations within ± 7% of the average Archean granitoids[5], except for K_2O and Na_2O. Many trace-element concentrations in the central SNB are comparable to the TTGs, or transitional between estimates for Archean and Phanerozoic upper crustal masses. For example the central SNB granitoids have relatively high $LREE_n/HREE_n$ (La_n/Yb_n ~10), and Sr/Nd (>20) ratios, as well as minuscule to no negative Eu anomalies (exception: the high-silica granites)[20]. In addition, Saleeby[8] has documented comparable major-element chemistry between the southernmost SNB, presently exposed at intrusion levels of 20-30 km, and the Scourian granulites, which represent a similar exposure level of an Archean terrane. Based on these arguments, we hypothesize that the Sierra Nevada crustal mass (~90% of which consists of the SNB in the southern and central parts of the mountain range) has been differentiated from a basaltic reservoir at depths >35-40 km, similar to the mechanisms recently proposed for the formation of Archean TTGs.

The range of oxygen isotope analyses ($\delta^{18}O$ ~6.5-9, Table 4-1) from the Sierran pyroxenites is practically identical to the range of values measured in the central SNB granitoids[21]. The slightly, but consistently elevated $\delta^{18}O$ values indicate that at least a fraction of the source material has equilibrated with the hydrosphere in a near-surface environment prior to being transported to these great depths[22]. $\delta^{18}O$ values as high as ~13 ‰ were measured in lower crustal, high-Al granulitic (i.e., plagioclase-rich, pyroxene-, and garnet-bearing) xenoliths from the Chinese Peak locality[23]. Many Chinese Peak granulites are proven to also be residual rocks of the SNB[11, 23]. These rocks carry a larger proportion of the high ^{18}O component seen in most Sierran xenoliths. Assigning a $\delta^{18}O$ = +13, as a maximum value for the "near-surface" end-member component, this recycled end-member can be estimated to represent at least ~20-30% of the central SNB source

mass, assuming a $\delta^{18}O = 6$ for the mantle contributions. Many Archean residual eclogites are similarly characterized by departures of $\delta^{18}O$ from MORB-like values (e.g., ref. 24), and these are also interpreted as due to recycling (by subduction or subcretion) of near-surface, hydrothermally altered or weathered material in the Archean mantle, probably oceanic crust. We propose that some differences in the chemistry between the TTGs and the central SNB may reflect changes in the type of high-^{18}O ("near-surface") input to the source rocks of the granitoids. It is known that the K_2O concentrations and K/Na ratios are significantly higher in young batholiths than in Archean TTGs[5]. Deep lithospheric residues such as the Sierran pyroxenites may reflect to some extent the chemical characteristics of the original unmelted source rocks. Potassium is an abundant element in post-Archean surface environments, both continental[27] and marine[28]. The abundance of potassium in unaltered Sierran pyroxenites (this study) and granulites (ref. 23, results confirmed by our duplicates) is positively correlated with $\delta^{18}O$ (Figure 4-4), suggesting that the high $\delta^{18}O$ component present in the Sierran pyroxenites and inferred to have existed in the SNB source at depth may be relatively K-rich. The more K-rich nature of SNB (and other young batholiths) compared to TTGs conceivably could reflect "pollution" of the mainly basaltic source with some supracrustal (continental?) material, which would be expected to be significantly higher in both K_2O content and K/Na ratio in the Phanerozoic as compared to the Archean[27].

The tectonic mechanisms responsible for the introduction of basaltic material, including a high ^{18}O component into the source regions of modern arc magmas are not yet clearly resolved, and probably differ from region to region. The present-day oceanic slabs are probably too cold to undergo extensive melting during subduction, except when the oceanic lithosphere is very young, less than 25 My or so[3]. In the central Sierra Nevada, a plausible source for the Cretaceous SNB is represented by a mixture between various allochtonous oceanic masses accreted to the continent (a component carrying the high ^{18}O signature) and a Precambrian lower crustal (+ mantle lithospheric) basement autochtonous

Figure 4-4. Plot of K_2O (wt%) vs. $\delta^{18}O$ (relative to SMOW) for Sierran residual assemblages cogenetic with the SNB: pyroxenites analyzed in this study (black triangles) and granulites[23] (crosses).
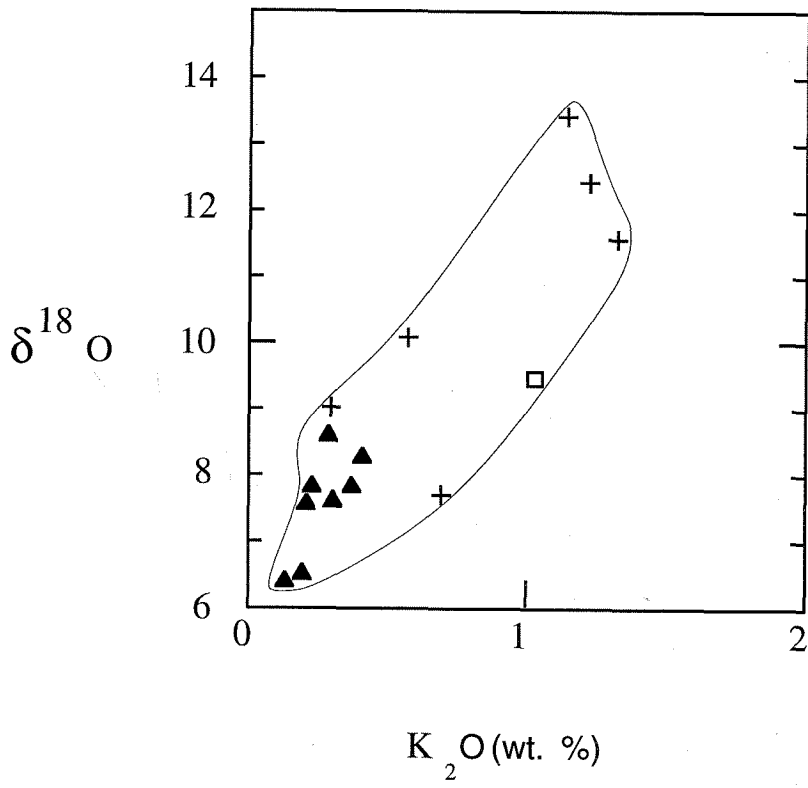
to western North-America[25]. Archean oceanic crust may have been hot and fusible during subduction[4], although the importance of subduction/collision of masses amalgamated by accretionary processes (e.g., oceanic plateaus) has also been recognized recently[26]. While the differentiation of central SNB (and possibly other Cordilleran batholiths) and Archean TTGs may be petrologically comparable, it remains an open question whether similar tectonic processes were responsible for locating a recylced basaltic source beneath both the Phanerozoic batholiths and Archean cratons.

References

1. Dodge, F.C.W., Lockwood, J.P., & Calk, L.C., Fragments of mantle and crust beneath the Sierra Nevada batholith: xenoliths in a volcanic pipe near Big Creek, California, *Geol. Soc. Am. Bull.*, **100**, 938-947 (1988).

2. Ducea, M. N. & Saleeby, J.B., Buoyancy sources for a large, unrooted mountain range, the Sierra Nevada, California; Evidence from xenolith thermobarometry, J. Geophys. Res., **101**, 1029-1041 (1996).

3. Drummond, M.S., & Defant, M.J., A model for trondhjemite-tonalite-dacite genesis and crustal growth via slab melting; Archean to modern comparisons, *J. Geophys. Res.*, **95**, 21503-21521 (1990).

4. Atherton, M.P., & Petford, N., Generation of sodium-rich magmas from newly underplated basaltic crust, *Nature*, **362**, 144-146 (1993).

5. Martin, H., The Archean gray gneisses and genesis of continental crust, in Condie, K. (ed.) *Archean crustal evolution*, 205-259, Elsevier, Amsterdam (1994).

6. Goodwin, A.M. (ed.) *Precambrian geology*, Academic Press, 666 p (1991).

7. Rudnick, R.L. (1995) Making continental crust, *Nature*, **378**, 571-578 (1995).

8. Saleeby, J.B., Progress in tectonic and petrogenetic studies in an exposed cross-section of young (c. 100 Ma) continental crust, southern Sierra Nevada, California, in Salisbury

M.H. & Fountain D.M. (eds.), *Exposed cross-sections of the continental crust*, Kluwer Acad., Norwell, Mass., 137-159 (1990).

9. Pickett D.A., & Saleeby, J.B., Thermobarometric constraints on the depth of the exposure and conditions of plutonism and metamorphism at deep levels of the Sierra Nevada batholith, Tehachapi Mountains, California, *J. Geophys. Res.*, **98**, 609-629 (1993).

10. Chen, J.H. & Moore J.G., Uranium-lead isotopic ages form the Sierra Nevada batholith, California, *J. Geophys. Res.*, **87**, 4761-4784 (1982).

11. Ducea, M.N., & Saleeby, J.B., The age and origin of a thickmafic-ultramafic root from beneath the Sierra Nevada batholith, *Contrib. Mineral. Petrol.*, (in review).

12. Sharp, Z.D., A laser-based microanalytical method for in-situ determination of oxygen isotope ratios of silicates and oxides, *Geochim. Cosmochim. Acta*, `**54**, 1353-1357 (1990).

13. Bateman, P.C., & Dodge, F.C.W., Variations of major element constituents acros the central Sierra Nevada batholith, *Geol. Soc. Am. Bull.*, **81**, 409-420 (1970).

14. Rollinson, H., *Using geochemical data: Evaluation, presentation, interpretation*, Longman, Essex, 108-111 (1993).

15. Wolf, M. & Wyllie, P.J., Garnet growth during amphibolite anatexis; Implications for a garnetiferous restite, *J. Geol.*, **101**, 357-373 (1993).

16. Rapp, R.P. & Watson, E.B., Dehydration melting of metabasaltsat 8-32 kbar; Implications for continental growth and crust-mantle recycling, *J. Petrol.*, **36**, 891-931 (1995).

17. Ireland, T.R., Rudnick, R.L., & Spetius, Z., Trace elements in diamond inclusions from eclogites reveal link to Archean granites, *Earth. Planet. Sci. Lett.,* **128**, 199-213 (1995).

18. Rollinson, H., Eclogite xenoliths in west African kimberlites as residues from Archean granitoid extraction, *Nature*, **389**, 173-176 (1997).

19. Taft, P.B., Hills D.V., & Haggerty, S.E., Crustal evolution and the granulite to eclogite transition in xenoliths from eclogites in the west African craton, *Tectonophysics*, **161**, 213-231 (1989).

20. Dodge, F.C.W., Millard Jr., H.T., & Elsheimer, H.N., Compositional variations and abundances of selected elements in granitoid rocks and constituent minerals, central Sierra Nevada batholith, California,*U.S. Geol. Surv. Prof. Pap.*, **1248**, 24 p (1982).

21. Masi, U., O'Neill, J.R., & Kistler R.W., Stable isotope systematics in Mesozoic granites of central and northern California and southwestern Oregon, *Contrib. Mineral. Petrol.*, **76**, 116-126 (1981).

22. Gregory R.T., and Taylor, Jr., H.P., 1986, Non-equilibrium metasomatic $^{18}O/^{16}O$ effects in upper mantle mineral assemblages, *Contrib. Mineral. Petrol.*, **193**, 124-135 (1986).

23. Dodge, F.C.W., Calk L.C., & Kistler, R.W., Lower crustal xenoliths, Chinese Peak lava flow, central Sierra Nevada, *J. Petrol.*, **27**, 1277-1304 (1986).

24. MacGregor, I.D. & Manton, W.J., Roberts Victor eclogites: Ancient oceanic crust, *J. Geophys. Res.*, **91**, 14063-14079 (1986).

25. Ducea, M.N., Clemens-Knott, D., Taylor, H.P., and Saleeby, J.B., Large magnitude isotopic heterogeneities in the source rocks of the Sierra Nevada batholith; Petrologic and tectonic implication, in prep.

26. DeWit, M.J., & 9 others, Formation of an Archean continent, *Nature*, **357**, 553-562 (1992).

27. Taylor, S.R., & McLennan, S.M., *The continental crust; Its composition and Evolution*, Blackwell Scientific, Oxford, 312 p (1985).

28. Thompson, G., Metamorphic and hydrothermal processes: Basalt-seawater interactions, in Floyd, P.A. (ed.), *Oceanic basalts*, Blackie, Glasgow, 148-174.

CHAPTER 5

Large Magnitude Isotopic Heterogeneties in The Source Rocks of the Central Sierra Nevada Batholith: Petrologic and Tectonic Implications

Mihai Ducea, Diane Clemens-Knott, Jason Saleeby, and Hugh P. Taylor, Jr.

to be submitted to *Geological Society of America Bulletin*

Abstract. Lower crustal and upper mantle xenoliths found in Late Cenozoic volcanic rocks from the central Sierra Nevada constrain the composition of the deep lithosphere beneath the Sierra Nevada batholith (SNB). The range of the whole rock $^{87}Sr/^{86}Sr$, $^{143}Nd/^{144}Nd$, $^{206}Pb/^{204}Pb$, $^{207}Pb/^{204}Pb$, $^{208}Pb/^{204}Pb$ age-corrected at 100 Ma and $\delta^{18}O$ ratios measured on xenoliths are comparable to, or larger than, the isotopic variations previously measured across the SNB surface rocks. The average isotopic ratios measured in xenoliths are strikingly similar to the local isotopic compositions of the batholithic rocks exposed at the surface in the area where the xenolith-bearing volcanic rocks were erupted. Our data indicate that the isotopic heterogeneities measured across the SNB are primarily inherited from a heterogeneous source, as originally proposed by Kistler and Peterman (1973), and not from assimilation processes in the upper crust. The isotopic compositions of the deep crustal batholith source rocks represent primarily a mixture between: (1) a Precambrian lower crustal ($\pm$ old lithospheric mantle) component ("C") and (2) a Phanerozoic (accreted?) arc component with a prior supracrustal history ("S"). A third, less important component, is represented by young additions from mantle beneath the arc ("M") and is discernible only in the Nd and O isotopes. Xenolith isotopic data in conjunction with thermobarometric constraints suggest that the "C" component has been located at deeper levels than the "S" component during the formation of the SNB, suggesting the existence of significant thrusting of accreted masses over the autochtonous units of western North America.

5.1. Introduction

The Late Mesozoic-Early Cenozoic batholiths of western North America (known as Cordilleran batholiths) are found along its convergent margin with the Pacific oceanic plate (Anderson, 1990). Two of the best studied Cordilleran batholiths are the Sierra Nevada (SNB; e.g.,, Bateman, 1983) and the Peninsular Ranges (PRB; e.g.,, Taylor and Silver, 1978) batholiths of California and Baja, California, respectively. Cordilleran batholiths are commonly characterized by systematic geographic variations of isotopic ratios of Sr, Nd, Pb, and O, as well as the abundances of many major and trace elements. Gradients of isopleths (contours of equal isotopic ratios) are typically found perpendicular to the long dimension of these batholiths (e.g.,, Kistler and Peterman, 1973). Remarkable longitudinal regularities are found in all plutons in a given geographic zone, are independent of pluton lithology, and have been interpreted by some to reflect mainly the nature of the deep crustal and/or upper mantle source materials from which the batholith were derived (e.g.,, Kistler and Peterman, 1973; Silver and Chappell, 1988). Alternatively, the isotopic heterogeneities of batholiths may be generated primarily by assimilation of heterogeneous upper crustal rocks in shallow- to mid-crustal magma chambers (DePaolo, 1981). The interpretations of isotopic compositions of batholiths remain ambiguous (Pitcher, 1993). The petrologic mechanisms responsible for large-scale melting in Cordilleran batholiths cannot be uniquely resolved through the study of upper crustal granitoids, the most abundant rocks exposed at the surface in continental arcs. A better understanding of the vertical composition of the lithosphere beneath continental magmatic arcs may hold clues to the origin of batholiths.

Volcanic rocks erupted through the Sierra Nevada during the Miocene (Moore and Dodge, 1980), probably in response to lithospheric extension in the region, contain occasionally xenoliths of deep crustal and mantle origin, many of which represent the deep counterparts of the SNB (Ducea and Saleeby, 1998a, 1998b). In this study, we

report new Sr, Nd, Pb, and O isotopic measurements of 30 deep seated rocks from beneath the central SNB, compare them with isotopic compositions of the adjacent SNB granitoids, and put constraints on the origin of the batholith source rocks.

5.2. San Joaquin Xenoliths and Surface Geology

The Sierra Nevada mountain range consists primarily of a large composite Mesozoic batholith (SNB), emplaced between 220 and 79 Ma (Everden and Kistler, 1970; Chen and Moore, 1983). About 90% of the surface exposures in the central Sierra Nevada range are SNB granitoids. The central SNB rocks are well characterized petrographically (e.g.,, Moore, 1959), chemically (Bateman and Dodge, 1970) and isotopically (Kistler and Peterman, 1973, 1978; DePaolo, 1981; Masi et al., 1981; Chen and Tilton, 1991). Small volume, Miocene (8-12 Ma) volcanic rocks have erupted through the central SNB, probably as a result of extensional collapse of the Cordillera at Sierra Nevada latitudes (Moore and Dodge, 1980). Six of the Miocene volcanic rocks located in the San Joaquin basin (Appendix 1) contain deep crustal and upper mantle xenoliths. Of them, Big Creek (Dodge et al., 1988), Camp Sierra, and Chinese Peak (Dodge et al., 1988) are of particular importance because of the abundance and petrographic variety of xenoliths. All three localities occur 10 miles from each other and contain similar xenoliths. Therefore, the San Joaquin volcanic field xenoliths can be used together to reconstruct one vertical "window" into the root of the SNB.

In this study we present isotopic data measured on xenoliths from these three locations. Many of the xenoliths contain garnet, and representative lithologies have been analyzed for thermobarometry and dated by Sm-Nd techniques (Ducea and Saleeby, 1996, 1998a). The most abundant xenoliths are olivine-free, mafic and ultramafic rocks: garnet pyroxenites, eclogites, granulites, and gabbros, all of which appear based on geochronology, trace element and whole rock isotopic compositions to be cogenetic with the SNB (Ducea and Saleeby, 1998a, 1998b; Ducea et al., 1998). These rocks

equilibrated at depths between ~25 and 100 km (Dodge et al., 1986, 1988; Ducea and Saleeby, 1996). Peridotitic assemblages, less common, become predominant at depths exceeding 70-80 km (Ducea and Saleeby, 1996, 1988a). All peridotites, including the deepest sample (which equilibrated at 42 kbar) have thermobarometric and isotopic characteristics of mantle lithosphere.

5.3. Sample Description and Analytical Methods

We selected a number of 30 samples for whole rock isotopic measurements, based on petrographic representativeness and lack of alteration in thin section observations. Some of the samples reported here were previously analyzed for Sm-Nd and Rb-Sr mineral geochronology (Ducea and Saleeby, 1998a), whole rock Sr, Nd and/or O isotopes (Domenick et al., 1983; Dodge et al., 1986; Clemens-Knott, 1996). For the purpose of this investigation, we define the following broad petrographic groups: (1) *granulites*, which are high-Al feldspathic rocks with lower crustal mineralogy (e.g.,, rich in pyroxenes, garnets) that equilibrated at depths <35 km; (2) *pyroxenites*, including all garnet-, and pyroxene-rich and feldspar-free rocks, including pyroxenites and some rocks transitional to eclogites, and equilibrated generally atdepths generally >35 km; (3) *metasediments*, with barometric record demonstrating residence in the deep crust (deeper than 20 km); and (4) *peridotites* (spinel-garnet, and garnet-bearing), which equilibrated at >70-80 km deep, and are thus samples from the deepest levels of the Sierran lithosphere. A key petrologic interpretation concerning granulites and pyroxenites is that they represent residues from granitoid partial melt extraction and therefore represent samples from a ~70 km thick "source" for the SNB magmas (Chapters 3 and 4). For more detailed petrographic descriptions of these samples and thermobarometric determinations, we refer to Chapter 2, and Dodge et al. (1986, 1988).

Whole-rock samples were cleaned for chemical separations and then dissolved as described in Pickett and Saleeby (1994). Samples were spiked with ^{87}Rb, ^{84}Sr and a

mixed ^{147}Sm-^{150}Nd tracer for isotopic dilution analyses of Rb, Sr, Sm, and Nd concentrations. The procedures for Rb, Sr, and REE elution are outlined in Pickett and Saleeby (1994). Lead was extracted following the technique of Chen and Wasserburg (1981). Isotopic analyses of Rb, Sr, Sm, Nd, and Pb were performed on a VG Sector multiple collector mass spectrometer following the procedures described in Pickett and Saleeby (1994). Strontium isotopic ratios were normalized to $^{86}Sr/^{88}Sr$= 0.1194 and $^{146}Nd/^{144}Nd$= 0.7219. Oxygen from mineral separates was extracted using a laser fluorination line (Sharp, 1990) and analyzed on a Finnigan M252 mass spectrometer. Whole rock $^{18}O/^{16}O$ ratios were calculated using the modal proportions of various minerals in each sample and presented in the conventional form of $\delta^{18}O$, relative to SMOW.

5.4. Results

The whole rock trace element concentrations of Rb, Sr, Sm, Nd, U, Pb and isotopic ratios of $^{87}Sr/^{86}Sr$, ε_{Nd}, $^{206}Pb/^{204}Pb$, $^{207}Pb/^{204}Pb$, $^{208}Pb/^{204}Pb$ and $\delta^{18}O$ are listed in Table 5-1. The radiogenic isotopes are age-corrected to 100 Ma, the age of peak magmatism in the SNB (Saleeby, 1990). Figure 5-1 consists of four histograms summarizing the whole rock isotopic ratios measured on lower crustal and mantle xenoliths from the San Joaquin area in this study as well as similar data reported in previous studies. The figure illustrates that the ranges of Sr, Nd, O, and Pb (only $^{206}Pb/^{204}Pb$ shown) isotopic ratios measured in lower crustal xenoliths in one vertical column are comparable to, or larger than, the ranges measured across the entire SNB (Kistler and Peterman, 1973, 1978; DePaolo, 1981; Masi et al., 1981; Chen and Tilton, 1991). The lower crust underlying the SNB is therefore isotopically as heterogeneous as the entire SNB. The mean xenolith ratios for all isotopes are, however, almost identical to

Table 5-1. Trace element and isotopic compositions of San Joaquin xenoliths.

Sample	Rock type*	Rb	Sr (ppm)	Nd (ppm)	Sm (ppm)	U (ppm)	Pb (ppm)	$^{87}Sr/^{86}Sr$ (100)	ε_{Nd} (100)	6/4 Pb (100)	7/4 Pb (100)	8/4 Pb (100)	$\delta^{18}O$
BC117	gran	28.19	388.45	12.64	2.99	0.551	2.68	.70542	-5.52	19.24	15.63	39.12	9.1
BC216	pyr	11.25	197.47	2.78	0.64	0.121	1.79	.70567	-3.51	18.92	15.69	38.76	7.8
BC221	pyr	11.39	43.34	2.12	0.81	0.108	1.08	.70522	-2.27	19.16	15.77	38.95	7.6
BC200	pyr	2.41	70.23	5.28	1.90	0.070	0.90	.70503	-3.02				
BC218	pyr	23.33	60.77	1.17	1.03	0.051	1.66	.70618	-9.16	18.89	15.33	38.10	7.6
B75$	pyr	6.53	131.10	17.32	5.22	0.184	1.59	.70501	-7.82	18.69	15.58	38.39	6.3
F34$	pyr	2.44	129.93	7.55	2.25	0.035	0.907	.70595	-6.23	18.95	15.64	38.85	6.4
BC207$	pyr	1.64	40.69	2.36	0.612	0.724	0.961	.70506	-5.15	18.42	15.60	38.52	8.2
G39$	pyr	8.45	71.38	24.91	5.18	0.221	0.954	.70623	-5.53	18.69	15.62	38.68	8.5
BC35$	gran	2.95	415.90	24.43	5.34	0.573	2.59	.70731	-7.18	18.71	15.591	38.48	9.8
G36$	pyr	8.29	93.95	4.77	2.78	0.102	7.17	.70618	-8.63	19.45	15.74	39.53	7.8
BC213	met	84.63	143.68	24.68	4.12	3.593	5.78	.71714	+4.00	22.02	15.82	38.74	6.9
297$	met	2.88	29.9	10.9	2.24	1.400	3.56	.70908	-15.46	21.16	15.96	38.79	13.3
F99&	pyr	0.84	54.7	8.50	2.81			.70626	-8.62				7.1
DB75&	gran	4.91	181.0	14.2	4.73			.70493	-1.84				6.7
KB126	gran	135.74	240.1	9.84	1.85	0.043	2.05	.71167	-3.04				12.8
CP230	pyr	6.95	118.1	5.95	1.66	0.038	0.22	.70536	-0.33				
CP164#	pyr	0.8	23.8	1.1	0.32			.70462	+1.49				
CP28#	pyr	0.75	12.5	0.63	0.16			.70455	+1.44				
CP67#	pyr	99.70	50.8	13.99	2.45			.70560	-9.72				

CP200[#] pyr 1.60 9.7 0.64 0.15   .70532 0.0

Table 5-1, continued

Sample	Rock type*	Rb	Sr (ppm)	Nd (ppm)	Sm (ppm)	U (ppm)	Pb (ppm)	$^{87}Sr/^{86}Sr$ (100)	ε_{Nd} (100)	6/4 Pb (100)	7/4 Pb (100)	8/4 Pb (100)	$\delta^{18}O$
CP73[#]	gran	60.40	188.4	21.91	5.58			.70715	-6.00				12.4
CP54[#]	gran	81.82	293.2	27.26	6.24	0.67	2.23	.70712	-4.95				11.8
CP211[#]	gran	11.01	400	16.59	4.13	0.176	3.03	.71023	-5.57				7.7
CP1[#]	gran	3.91	944	12.87	2.23	0.142	13.82	.70845	-6.01				9.0
CP12[#]	gran	29.70	541.6	19.67	4.71			.70949	-4.56				13.4
RM1	per	1.99	63.21	1.85	7.71			.70540	+0.50				
BCV	per	1.98	66.13	1.43	6.98			.70553	+1.23				6.4
P500	per	1.22	21.45	0.28	0.65			.70554	-5.15				6.0
P501	per	1.45	17.70	0.32	0.74			.70613	-5.81				6.2

* - Abbreviations: pyr - pyroxenites, gran - granulites, met - metasediments, per - peridotites (see text); [$] - Sm-Nd and Rb-Sr mineral geochronology also performed on these samples, Ducea and Saleeby (1998a); [&] - Sr and Nd isotopic analyses from Domenick et al. (1983); [#] - Sr and O isotopic analyses from Dodge et al. (1986).

Figure 5-1. Histograms of $^{87}Sr/^{86}Sr$ (a), $^{143}Nd/^{144}Nd$ (b), $^{206}Pb/^{204}Pb$ (c), and $\delta^{18}O$ (d), measured in lower crustal and upper mantle xenoliths from the San Joaquin volcanic field (data reported in this study, and previously published analyses on similar rocks from Mukhopadhyay, 1989; Mukhopadhyay and Manton, 1994; Domenick et al., 1983; Dodge et al., 1986). The ranges in isotopic compositions measured across the Sierra Nevada batholith are shown for comparison. The local (i.e., San Joaquin area) batholith isotopic ratios are marked with vertical arrows. Batholith data are from Kistler and Peterman (1973, 1978) for Sr isotopes, DePaolo (1981) for Nd isotopes, Masi et al. (1981) for O isotopes, and Chen and Tilton (1991) for Pb isotopes.

San Joaquin area, SNB
$^{87}Sr/^{86}Sr_i = 0.7057$

CSNB

a.

■ This study
■ Dodge et al. (1986)
□ Mukhopadhyay (1989)
□ Domenick et al. (1983)

analyses

$^{87}Sr/\ ^{86}Sr\ _{100}$

San Joaquin area, SNB
$\varepsilon Nd\ i = -4.3$

CSNB

b.

■ This study
■ Mukhopadhyay (1989)
□ Domenick et al. (1983)

analyses

$\varepsilon\ _{Nd}$
$_{100}$

San Joaquin area, SNB
$206Pb/204Pb_i = 18.9$

CSNB

c.

This study

Mukhopadhyay (1989)

$206Pb/204Pb_{100}$

San Joaquin area, SNB
batholith $\delta^{18}O = 7.8$

CSNB

d.

This study

Dodge et al. (1986)

$\delta^{18}O$

the mean local ratios in the SNB (Figure 5-1). This observation is in agreement with a previous conclusion that the mafic-ultramafic igneous-textured lower crustal rocks sampled as xenoliths represent the deep counterparts of the overlying SNB, and that no major lateral shift has taken place between the upper crust and the lower crust of the Sierra Nevada between the late Mesozoic and the Miocene (Dodge et al., 1986; Ducea and Saleeby, 1998a). The garnet pyroxenites in particular have isotopic ratios which fall within the ranges defined by the surface SNB, while the group of granulites tend to be the more isotopically "evolved" (higher $^{87}Sr/^{86}Sr_{100}$, and $\delta^{18}O$) than the SNB.

On a $^{87}Sr/^{86}Sr_{100}$ vs. $\delta^{18}O$ diagram (Figure 5-2), the xenolith data display a distribution broadly mimicking the fields defined by analyses of surface rocks in California batholiths. Most data points plot on an array parallel to the field defined by granitoids in the Peninsular Ranges Batholith (PRB; Taylor and Silver, 1978), slightly displaced to more radiogenic Sr isotopic ratios. The two end members defined by this broad positive correlation are identified as "C" (low $^{87}Sr/^{86}Sr_{100}$ and $\delta^{18}O$) and "S" (high $^{87}Sr/^{86}Sr_{100}$ and $\delta^{18}O$) and will be interpreted below. Two granulites may define a second trend resembling isotopic ratios measured in Cretaceous granitoids from the Mojave region and in the San Jacinto block, at the northern end of the PRB (Hill et al., 1986). However, we are not convinced that this San Jacinto-like second trend is representative of a distinctive component in the source of the SNB, but instead may be due to the high degree of petrographic alteration of these two samples reported in Dodge et al. (1986), which may have produced an increase in $^{87}Sr/^{86}Sr$. Therefore, we did not interpret this as a meaningful separate trend at this point. More data is required to test any significance of San Jacinto-like Sr and O isotopic ratios in the Sierra Nevada. The central SNB field (Masi et al., 1981; Kistler and Peterman, 1973, 1978) overlaps the garnet pyroxenite xenolith data.

Figure 5-2. Plot of $^{87}Sr/^{86}Sr$ (at 100 Ma) vs. $\delta^{18}O$ measured in lower crustal and upper mantle xenoliths from the San Joaquin volcanic field. The trend defined by xenolith data (except two potentially anomalous points, see text) is shown as a gray field. Legend: open squares - garnet peridotites, triangles - pyroxenites, crosses - granulites, stars - metasediments. End members "C," "M," and "S" are described in text. The field of the central Sierra Nevada batholith (CSNB) is based on data from Masi et al. (1981), while the field of isotopic compositions measured in the Peninsular Ranges batholith (PRB) was drawn using data from Taylor and Silver (1978) and Taylor (1988).

$\delta^{18}O$

15

10

5

0.70   0.71   0.72

S

PRB

M   C

CSNB

$^{87}Sr/^{86}Sr$ 100
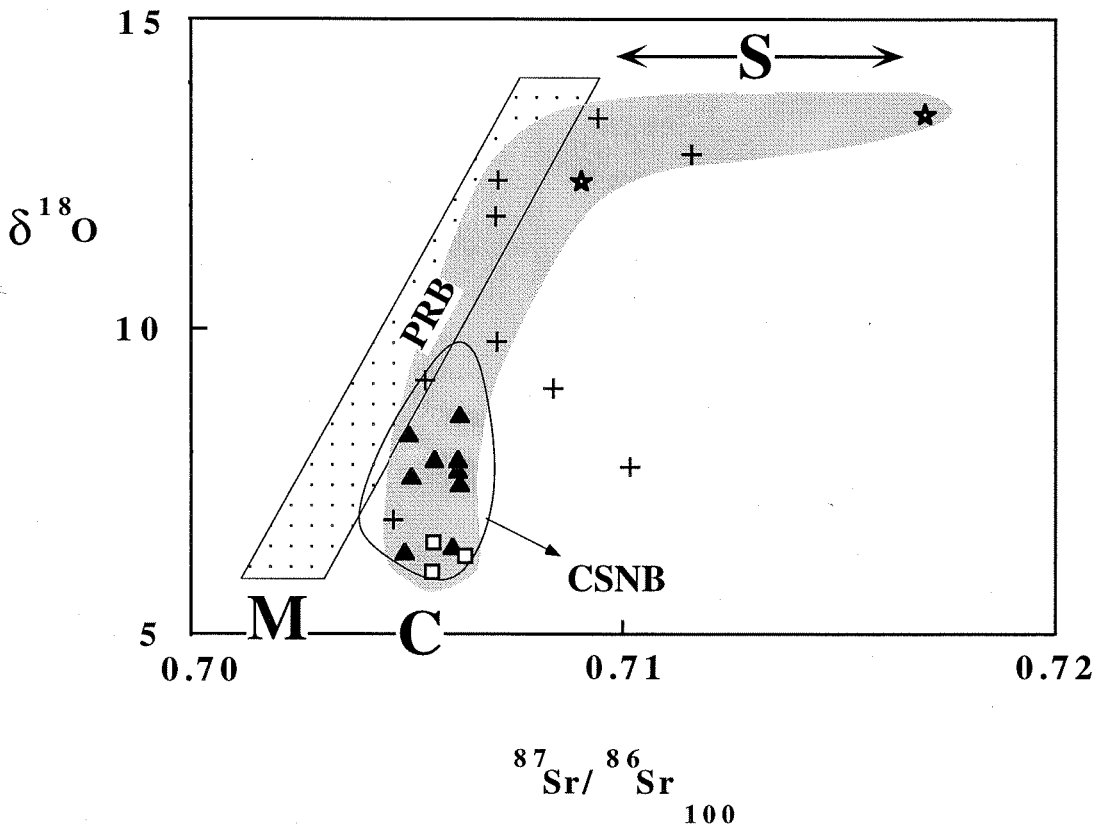
The presence of relatively elevated $\delta^{18}O$ in most olivine-free xenoliths indicate that a substantial component with a prior residence near the surface of the Earth was present at depth, in the source rocks of the batholith. Assigning a $\delta^{18}O = 13\%o$ to the supracrustal component, and $\delta^{18}O = 6 \%o$ for any contributions from the mantle, we calculate that rocks such as garnet pyroxenites contain about 20-30% of a supracrustal component by mass.

The Sr-Nd diagram (Figure 5-3) shows that most xenolith data cluster in a field defined by values similar to the central SNB, but with a tendency for some xenoliths to display more negative ε_{Nd}. A distinctive trend is represented by the granulites which display a positive correlation between $^{87}Sr/^{86}Sr_{100}$ and ε_{Nd}. This granulite trend points away from the field represented by bulk of the xenoliths to the previously identified component "S". The ε_{Nd} vs. $\delta^{18}O$ diagram (Figure 5-4) shows a broad positive correlation between these isotopes, which suggest that rocks with significant "supracrustal" component (high $\delta^{18}O$) have also younger crustal ages. A few data points deviate from the positive correlation between ε_{Nd} and $\delta^{18}O$, suggesting the presence of a more subtle, high ε_{Nd} -low $\delta^{18}O$ component in these rocks. We identified this component as "M" in Figures 2-4 and will discuss its significance below.

Xenolith model Nd ages (T_{CHUR}) fall commonly between 0.5-1.5 Ga, while some samples yield unrealistic model ages. These values may not be reliable measures of the actual crustal age of the xenoliths, given their potentially complicated geologic history. However, many of these rocks were most recently residues after granitoid melt extraction at depths where garnet is an important residual phase (Chapters 3-4), a process which

Figure 5-3. Plot of $^{87}Sr/^{86}Sr$ (at 100 Ma) vs. ε_{Nd} (at 100 Ma) measured in San Joaquin xenoliths. Symbols as in Figure 5-2. The horizontal line at $\varepsilon_{Nd} = 0$ and the vertical line at $^{87}Sr/^{86}Sr = 0.7046$ represent the isotopic composition of Nd and Sr, respectively, characteristic for the bulk silicate Earth (e.g.,, DePaolo, 1981).
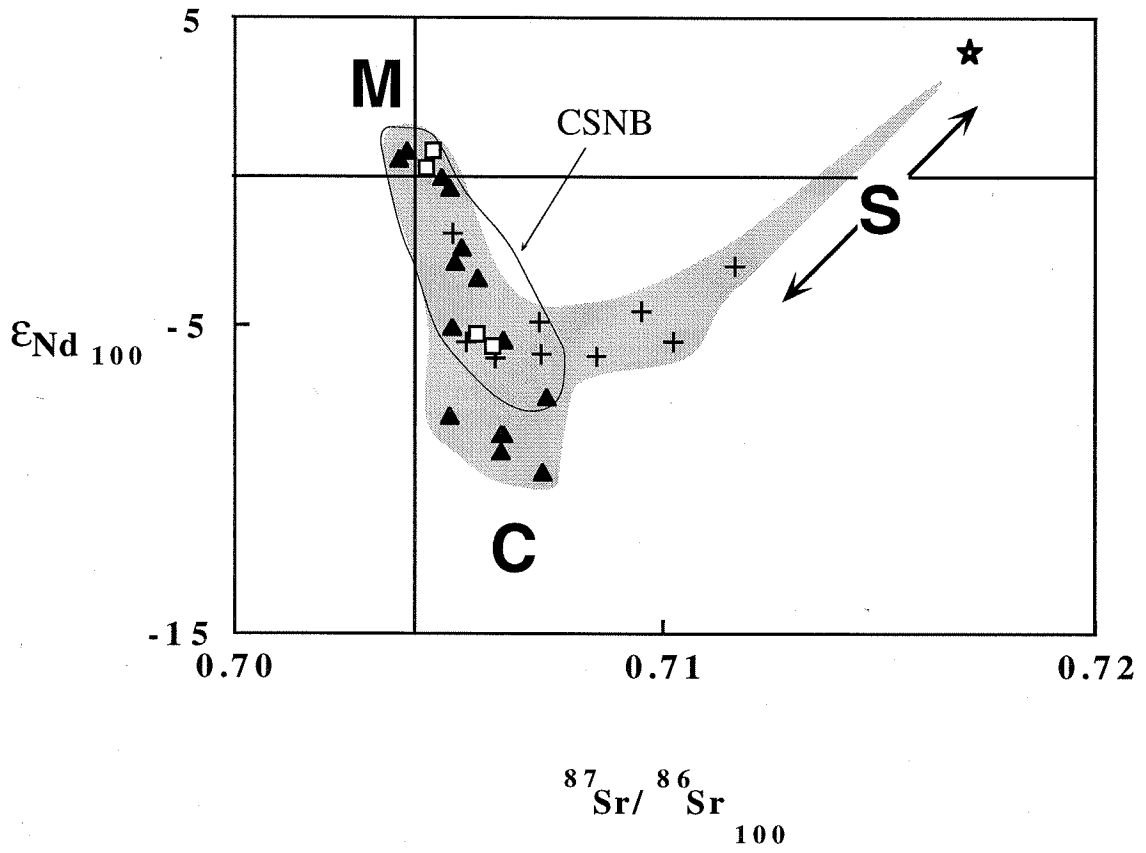
enriched these rocks in their Sm/Nd ratio compared to the original protolith and would lead to underestimated crustal ages. Even so, the ε_{Nd} ratios are quite low (between -10 and -2) indicating that at least the low ε_{Nd} component ("C") in the SNB source must be Precambrian.

5.5. Interpretation

The isotopic composition of the Sierra Nevada deep crust will be used to: (1) compare the isotopic heterogeneities in the SNB with the ones measured in its source rocks, (2) constrain the isotopic compositions and geologic significance of the end member components in the magmatic source reservoir, and (3) discuss the tectonic implications of the isotopic results.

Isotopic heterogeneities at depth. Data presented above indicate that vertical isotopic heterogeneities of the Sierra Nevada lithosphere are as prominent as the horizontal ones observed in the SNB. Previous studies have established that most of the lower crustal granulites and pyroxenites recovered as xenoliths are samples of a thick (60-70 km) residual zone from which the SNB magmas were extracted (Ducea and Saleeby, 1998a). The isotopic heterogeneities measured in residual xenoliths that resided at lower crustal depths, suggest that the range of isotopic ratios measured in the SNB is primarily inherited from the source rocks at depth (Kistler and Peterman, 1973), and not gained by assimilation processes in the upper crust (DePaolo, 1981). Upper crustal granitoids from the San Joaquin area appear to average out the range of isotopic ratios measured in their source rocks, as inferred from the comparison of mean isotopic ratios in xenoliths and SNB.

The origin of the SNB source rocks. Data presented in Figures 5-2 to 5-4 allow us to define two important end members which contribute to the isotopic heterogeneity of the SNB, and a third which appears to be of lesser importance. The first component,

Figure 5-4. Plot of ε_{Nd} (at 100 Ma) vs. $\delta^{18}O$ measured in San Joaquin xenoliths. Symbols as in Figure 5-2.
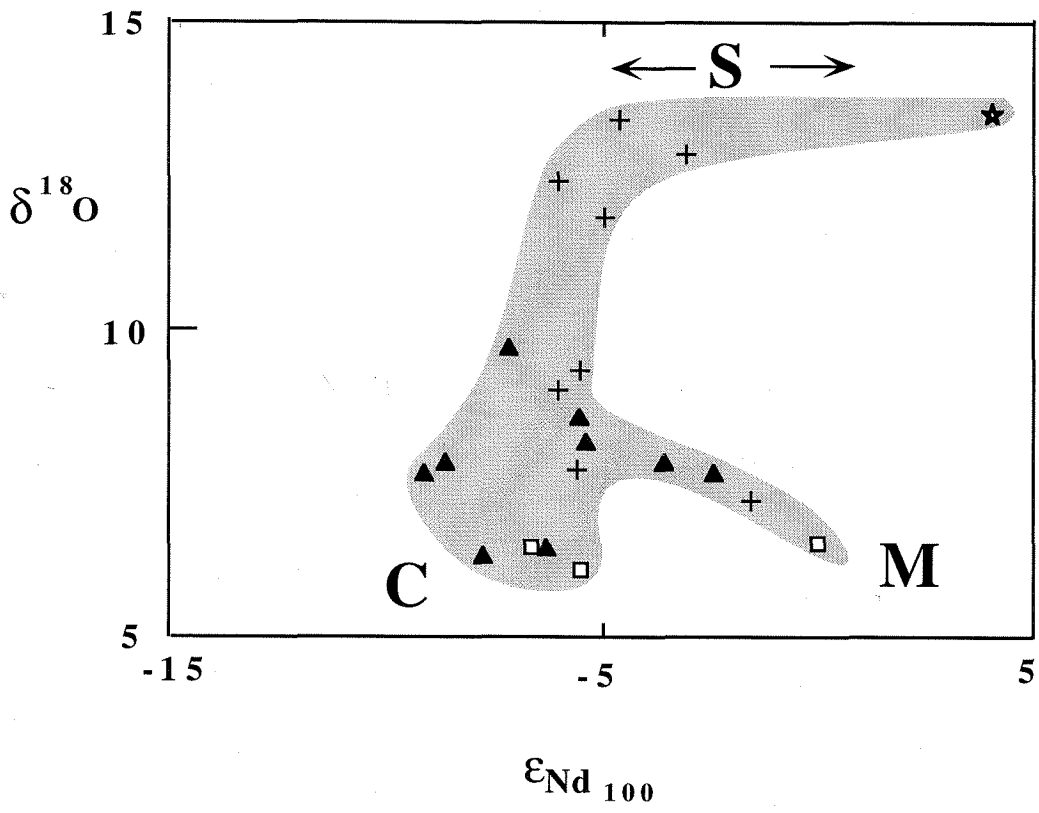
labeled "S" in Figures 5-2 to 5-4, is characterized by high $\delta^{18}O$, $^{87}Sr/^{86}Sr$, and relatively

elevated ε_{Nd}. The oxygen isotope data indicate that "S" is represented by rocks which

must have resided at or near the surface of the Earth prior to their transport to lower

crustal depths, and thus this end member is most likely sedimentary or volcanic in origin.

This end member is similar to the high $\delta^{18}O$ one identified by Taylor (1988, and

references therein) for the sources of California batholiths, based on extensive studies of

granitoids exposed at the surface. The second end member component, labeled "C" in

Figures 2-4, has $^{87}Sr/^{86}Sr$ (100), $\varepsilon_{Nd}(100)$, and $\delta^{18}O$ compatible with a Precambrian lower

crustal and/or lithospheric mantle material (see for example arguments in Taylor, 1988).

Both components were mafic in composition, based on the chemistry of the residual

xenoliths (Ducea and Saleeby, 1998a). The positive correlation between ε_{Nd} and $\delta^{18}O$

reflect a mixture between younger, probably Phanerozoic upper crustal rocks ("S") and

Proterozoic lower crustal rocks ("C"). The "S" resembles isotopically an island arc and

petrographically high-Al basalts, whereas "C" has the isotopic characteristics of the

western U.S. Precambrian basement (Wendtland et al., 1996) and petrography of mafic

lower crust. Mantle-derived melts, if they had any significant role in batholith

petrogenesis at this location, must have been primarily derived from old lithosphere (e.g.,

the two garnet peridotites analyzed for this study, Table 5-1, and Figures 2-4), based on

the low ε_{Nd} in the residues.

However, there is evidence that some material has been fluxed from young, more

depleted mantle. We identified a third end member, "M," which is apparent in the

$\varepsilon_{Nd}(100)$ vs. $\delta^{18}O$ plot (Figure 5-4). The $\delta^{18}O$ of the presumed "M" end member is low,

typical for mantle-derived materials, and the relatively elevated $\varepsilon_{Nd}(100)$ suggest that this

component may be derived from young accreted mantle beneath the arc. The mantle signature of "M" (transitional to a depleted mantle) is not distinguishable in the Sr isotopes. The limited knowledge of the composition of central SNB residues based on data available at present suggests that the "M" component was of limited significance at this location.

Kistler (1990) proposed the existence of two distinct types of lithosphere beneath the SNB: an accreted oceanic lithosphere ("Panthalassan") occupying the western parts of the SNB, and an eastern, autochtonous continental lithosphere ("North American"). We believe that end members "S" and "C" give the SNB "Panthalasan" (accreted) and "North-American" (autochtonous) lithospheric signatures, respectively, in the San Joaquin area. The "S" component can be viewed as a subducted/accreted supracrustal mass, while "C" as a lower crustal craton-like material.

The xenolith data suggest strongly that the central SNB granitoids (in the San Joaquin area) are chemically complementary and isotopically similar to the garnet pyroxenites which appear to be dominated by component "C" (Ducea and Saleeby, 1998a). End member "S" had a sizable role in batholith generation at this latitude, but becomes progressively more important in granulitic xenoliths (i.e., xenoliths derived from shallower levels than the garnet pyroxenites), which experienced only limited melting. The accreted (young) depleted- mantle end member component "M" is detectable only in the westernmost parts of the SNB where it takes over the "C" component, while "S" remains of significance (e.g.,, Kistler, 1990).

Lithosphere scale thrusting in the Sierra Nevada. The presence of both accreted and autochtonous lithosphere in the vertical column beneath the San Joaquin area suggests that accreted and autochtonous masses have been to some extent tectonically imbricated at the continental margin. Our data indicate that thickening of the arc crust took place, at least in part by thrusting accreted crust ("S") over a lower crustal continental mass of a probable Precambrian age ("C"). More specifically, we propose

Figure 5-5. Schematic interpretative cross section (vertical scale ~horizontal scale) through the Sierra Nevada lithosphere prior to the generation of the batholith. The approximate location of the future Sierra Nevada batholith (SNB) is indicated, as well as the Panthalassan (PT) and North American (NA) segments of the SNB, as defined by Kistler (1990). SJX marks the approximate location of the San Joaquin xenolith probe in the Sierra Nevada. We envision that these domains with rather sharp boundaries have been progressively blended by the long term and large scale magmatism which led to the formation of the SNB. Abbreviations of lithospheric domains: C - Precambrian lower crust, EM - Precambrian enriched mantle, S - accreted crustal rocks, M - accreted mantle, Mi - miogeoclinal rocks, PP - the subducting Pacific Plate.
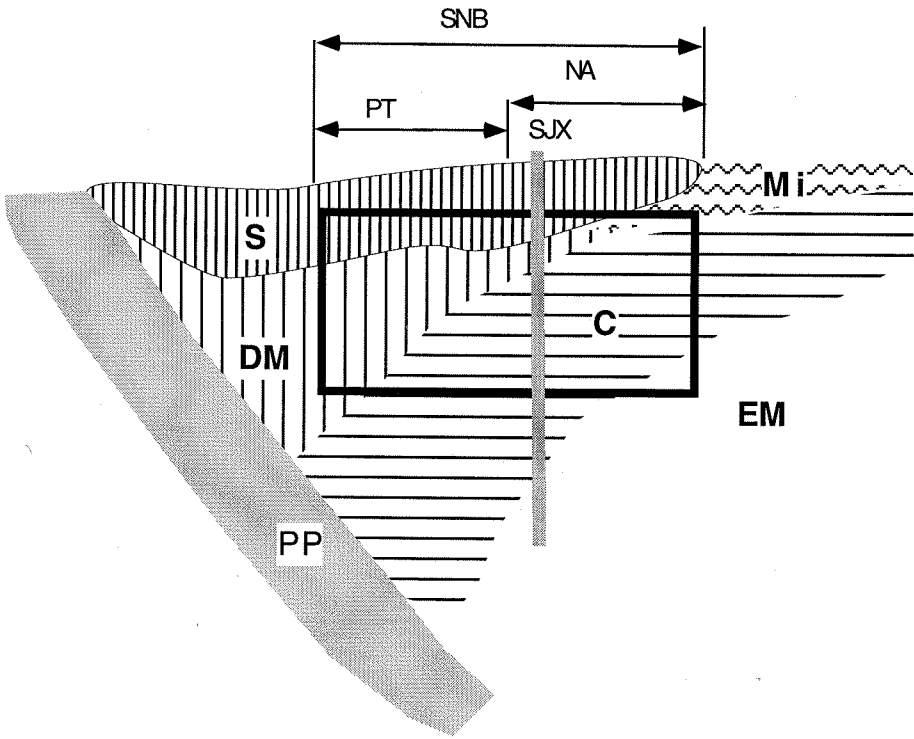
that Precambrian basement units of the western US miogeocline were underthrusted beneath Mesozoic arc rocks with oceanic or continental margin affinity, a process which led to significant lithospheric thickening in the Mesozoic Sierra Nevada and eventually triggered the large scale magmatism of the SNB (Figure 5-5). The presence of Precambrian basement beneath the central SNB is supported by geochronologic studies of zircon in SNB granitoids, which detected inherited zircon of Precambrian age (~1.8 Ga, Chen and Moore, 1983).

Significant crustal shortening of miogeoclinal and eugeoclinal sequences of the Cordillera has been documented to the east of the mainly Cretaceous SNB magmatic arc (e.g.,, Burchfiel and Davies, 1975). Thrust belts of early Paleozoic to Jurassic age correspond to distinctive Cordilleran orogenic events (Saleeby, 1983). The resulting fold and thrust belts located east of the present day central Sierra Nevada mountain range contain mainly supracrustal miogeoclinal rocks, while the whereabouts of the Precambrian basement of these thrust sheets are not known. Our data (this study and Ducea and Saleeby, 1998a) suggest that a thickness of at least 60-70 km of lower crustal/lithospheric mantle material with characteristics of North American craton was a significant end member in the source of the Mesozoic SNB, at least in its central and eastern parts.

The scenario envisioned in Figure 5-5 can explain the presence of the thick and old lithosphere underlying the batholith, and the isotopic patterns observed in the SNB. We have drawn schematically in Figure 5-5 a depth interval over which melting may have occurred and promoted the extraction of SNB-like melts. The western SNB plutons represent in this scenario mixtures between young accreted mantle ("M") and its corresponding supracrustal, probably arc-related rocks ("S"), while the central and eastern SNB isotopic signature is dominated by the Precambrian lower crust-lithospheric mantle ("C"), and overthrusted supracrustal arc-related rocks. The accreted mantle component played a comparatively minor role in batholith petrogenesis in the San

Joaquin area. This hypothesis based on deep crustal and mantle xenoliths is consistent with the isotopic compositions measured across the SNB (e.g., Kistler, 1990).

Overall, our data support the hypothesis that most of the isotopic heterogeneities measured in the SNB are derived primarily from their source rocks. The SNB source rocks were mainly crustal, a mixture of Precambrian lower crust and supracrustal arc basalts.

5.6. References

Anderson, J. L., 1990, The nature and origin of Cordilleran magmatism, Geol. Soc. Am. Mem., 174, 414 p.

Bateman, P.C., 1983, A summary of critical relationships in the central part of the Sierra Nevada batholith, California, U.S.A., in Roddick, J.A. (ed.) *Circum-Pacific plutonic terranes*, Geol. Soc. Am. Memoir, 159, 241-254.

Bateman, P.C., and Dodge, F.C.W., 1970, Variations of major chemical constituents across the central Sierra Nevada batholith, Geol. Soc. Am. Bull., 81, 409-420.

Burchfiel, B.C., and Davies, G.A., 1975, Nature and controls of Cordilleran orogenesis, western United States; Extension of an earlier synthesis, Am. J. Sci., 275A, 363-396.

Chen, J.H., and Tilton, G.R., 1991, Applications of lead and strontium isotopic relationships to the petrogenesis of granitoid rocks, central Sierra Nevada batholith, California, Geol. Soc. Am. Bull., 103, 439-447.

Chen, J.H., and Moore, J.G., 1983, Uranium-lead isotopic ages from the Sierra Nevada batholith, California, J. Geophys. Res., 87, 4761-4784.

Chen, J.H., and Wasserburg, G.J., 1981, Isotopic determination of uranium in picomole and subpicomole quantities, Anal. Chem., 53, 2060-2067.

DePaolo, D.J., 1981, A Neodymium and strontium study of the Mesozoic calc-alkaline granitic batholiths of the Sierra Nevada and Peninsular Ranges, J. Geophys. Res., 86, 10470-10488.

Dodge, F.C.W., Calk, L.C., and Kistler, R.W., 1986, Lower crustal xenoliths, Chinese peak lava flow, J. Petrol., 27, 1277-1304.

Dodge, F.C.W., Lockwood, J.P., and Calc, L.C., 1988, Fragments of the mantle and crust beneath the Sierra Nevada batholith; Xenoliths in a volcanic pipe near Big Creek, California, Geol. Soc. Am. Bull., 100, 938-947.

Domenick, M.A., Kistler, R.W., Dodge, F.C.W., and Tatsumoto, M., 1983, Nd and Sr isotopic study of crustal and mantle inclusions from beneath the Sierra Nevada and implications for batholith petrogenesis, Geol. Soc. Am. Bull., 94, 713-719.

Ducea, M., and Saleeby, J., 1996, Buoyancy sources for a large, unrooted mountain range, the Sierra Nevada; Evidence from xenolith thermobarometry, J. Geophys. Res., 101, 8029-8044.

Ducea, M., and Saleeby, J., 1998a, The age and origin of a thick mafic-ultramafic root from beneath the Sierra Nevada batholith, Contrib. Mineral. Petrol., in review.

Ducea, M., and Saleeby, J., 1998b, Residual eclogitic xenoliths from beneath the Sierra Nevada batholith, Science, submitted.

Everden, J.F., and Kistler, R.W., 1970, Chronology of emplacement of Mesozoic batholithic complexes in California and western Nevada, U.S. Geol. Surv. Prof. Pap., 623, 42 p.

Hill, R. L., Silver, L.T., and Taylor, H.P., 1986, Coupled Sr-O isotope variations as an indicator of source heterogeneity for the northern Peninsular Ranges batholith, Contrib. Mineral. Petrol., 92, 351-361.

Kistler, R.W., and Peterman, Z., 1973, Variations in Sr, Rb, K, Na, and initial $^{87}Sr/^{86}Sr$ in Mesozoic granitic rocks and intruded wall rocks in central California, Geol. Soc. Am. Bull., 84, 3489-3512.

Kistler, R.W., and Peterman, Z., 1978, reconstruction of crustal blocks of California on the basis of initial Sr isotopic compositions of Mesozoic granitic rocks, U.S. Geol. Surv. Prof. Pap., 1071, 17 p.

Kistler, R. W., 1990, Two different types of lithosphere in the Sierra Nevada, California, Geol. Soc. Am. Mem., 174, 271-282.

Masi, U., O'Neill, J.R., and Kistler, R.W., 1981, Stable isotope systematics in Mesozoic granites of central and northern California and Southwest Oregon, Contrib. Mineral. Petrol., 76, 116-126.

Moore, J.G., and Dodge, F.C.W., 1980, Late Cenozoic volcanic rocks of the Southern Sierra Nevada, California; I. Geology and petrology summary, Geol. Soc. Am. Bull., 91, 515-518.

Moore, J. G., 1959, The quartz diorite boundary in the western United States, J. Geol., 67, 198-210.

Pickett D.A., and Saleeby, J.B., 1994, Nd, Sr, and Pb isotopic characteristics of Cretaceus intrusive rocks from deep levels of the Sierra Nevada batholith, Tehachapi Mountains, California, Contrib. Mineral. Petrol., 118, 198-205.

Pitcher, W.S., 1993, The nature and origin of granite, Blackdie Acad.&Prof., London, 321 p.

Saleeby, J.B., 1983, Accretionary tectonics of the North American Cordillera, Ann. Rev. Earth. Planet. Sci., 15, 45-73.

Saleeby, J.B., 1990, Progress in tectonic and petrogenetic studies in an exposed cross-section of young (~100 Ma) continental crust, southern Sierra Nevada, California,

in Salisbury, M.H., and Fountain, D. M. (eds.) *Exposed crustal sections of the continental crust,* Kluwer Acad., Norwell, Mass., 137-158.

Sharp, Z., 1990, A laser-based microanalytical method for in-situ determination of oxygen isotope ratios of silicates and oxides, *Geochim. Cosmochim. Acta,* 54, 1353-1357.

Taylor, H. P., and Silver, L. T., 1978, Oxygen isotope relationships in plutonic igneous rocks of the Peninsular Ranges batholith, southern and Baja California, U.S. Geol. Surv. Open File Rep., 78-701, 423-426.

Taylor, H.P., 1988, Oxygen, hydrogen, and strontium isotopic constraints on the origin of granites, Trans. R. Soc. Edinburgh Earth Sci., 79, 317-338.

Wendlandt, E., DePaolo, D.J., and Baldridge, W.S., 1996, Thermal history of Colorado Plateau lithosphere from Sm-Nd mineral geochronology on xenolith, Geol. Soc. Am. Bull., 108, 757-767.

CHAPTER 6

Crustal Recycling Beneath Continental Arcs: Silica-Rich Glass Inclusions in Ultramafic Xenoliths from The Sierra Nevada, California

Mihai Ducea and Jason Saleeby

Abstract

We describe silica-rich (up to ~69.5% SiO_2) glass inclusions trapped as grain boundary films and within-grain pockets in ultramafic xenoliths hosted by Pliocene basalts from the Sierra Nevada, California. The ultramafic xenoliths are lherzolites which equilibrated in the Sierra Nevada upper mantle at 1150-1180 ^0C and ~ 1.4-1.8 GPa. The glass inclusions have trachytic compositions, similar to previously described silicic melts from mantle xenoliths [1-9]. We have determined the Sr and Nd isotope compositions of the grain boundary films using a leaching technique, and calculated the glass isotopic compositions. The glass $^{87}Sr/^{86}Sr$ (0.7077-0.7085) and $^{143}Nd/^{144}Nd$ (≈ 0.51244) ratios are higher than in the ultramafic xenoliths and distinct from the host basalt ratios. Glasses are characterized by Nb depletions (Nb_n/Nb_n* ~0.15), enrichment of light rare earth elements ($La_n/Yb_n \approx 50$), and the presence of negative Eu anomalies (Eu_n/Eu_n*$\approx$0.7-0.86), indicating a crustal origin for the melt source. The Nd isotope ratios ($\varepsilon_{Nd} \approx -4$) are inconsistent with an oceanic crust as the source for these former melts. The source rocks must have been continental materials recycled in the mantle, either foundered lower crust or subducted sediment. Low Rb/Sr (0.036-0.077) and high Sr/Nd (>35) ratios observed in the glasses are suggesting a lower crustal source. The Sierra Nevada lowermost crust (amphibole-bearing garnet pyroxenites and other dense Mesozoic cumulate mafic-ultramafic rocks), as defined by studies of older, Miocene xenolith-bearing volcanic rocks from the same area [10] has isotopic compositions similar to the glass inclusions. Geologic [10] and

geophysical [11] evidence indicate that the Sierra Nevada has lost its eclogitic arc root, probably by foundering in the mantle. We propose here that the silica-rich glasses were formed by low percent partial melting of the dense, cold Sierran batholithic lowermost crust during root delamination. Further tests need to be aimed at addressing the viability of the main alternative to our interpretation, i.e., derivation of glasses from melting subducted sediments.

6. 1. Introduction

Recent studies of ultramafic xenolith samples derived from both sub-continental and sub-oceanic environments have documented the common presence of silica-rich glass (SRG) inclusions [1-9]. These glasses are thought to represent trapped melts, which may [e.g., 8] or may not be exotic with respect to the peridotitic host xenoliths [e.g., 9]. The presence of these glass inclusions is direct evidence of mantle metasomatism, a process that enriches the mantle lithosphere in incompatible elements. The glasses commonly have high concentrations of large-ion lithophile elements, notably Na and K. Other chemical characteristics of these glass inclusions are high Al_2O_3 concentrations (15-25 wt.%), and low MgO and FeO concentrations (FeO < 4 wt.%, and MgO < 2 wt.%).

The source of the SRG is not clearly established, and perhaps is different from one environment to another. Possible candidates for the sources of these melts are hydrous phases in peridotites [9], hydrous eclogites (oceanic igneous crust) [1,8], and subducted oceanic sediments. Another candidate for the source of the SRG inclusions in peridotites, especially in continental lithospheric xenoliths, is melted lower continental crust that was recycled in the mantle. Lower crustal delamination (lower crustal "erosion," or "hidden subduction") is the splitting of crust, probably at quartz-rich, mechanically weak, mid-crustal levels [12], and sinking of the lower crust into the upper mantle [13]. There is

considerable debate as to whether the roots of the continental crust could delaminate under favorable conditions such as in orogenic regions with substantially thickened crust [13], although some process of recycling continental material into the mantle in addition to sediment subduction, is argued based on bulk Earth chemical mass balance calculations [14]. Testing the viability of crustal delamination is a very difficult task [15]. Geophysical methods may not have an adequate spatial resolution to track delaminated crust in the mantle, while possible melts delivered by a delaminating crust may not be distinguishable at the surface from crustal melts resulted by a simple increase in lithospheric heat flow. Several lines of evidence support crustal delamination, but all are equivocal [15].

In this study we describe SRG inclusions from the upper mantle beneath the Sierra Nevada, California, including some of the most silicic compositions ever reported in such environments. We present trace element as well as Sr and Nd isotopic evidence suggesting that these melts were derived from continental crustal materials which resided in the upper mantle. We propose foundering of the Sierra Nevada arc root as the mechanism responsible for crust-mantle interactions.

6. 2. Scepter Creek and Hill 8056 host basalts and peridotite xenoliths

Several mantle and lower crustal xenolith-bearing Miocene to Quaternary volcanic rocks are known in the Sierra Nevada [10, and references therein]. The Scepter Creek and Hill 8056 localities in the Sierra Nevada have not been studied before. The Scepter Creek locality was discovered by T. Sisson in 1983, and is located in the Tehipite Dome 15-minute quadrangle, California, $36^0 58'$ N, $118^0 48'$ W. The volcanic rock that carries xenoliths there is a trachyandesite flow that crops out along the Scepter Creek [16]. The Hill 8056 location (also known as Blue Knob, [17]) is a 500 x 300 m basaltic plug located along the Madera Creek in the Merced Peak 15-minute quadrangle, California, $37^0 33'$ N, $119^0 19'$ W.

The major element compositions and CIPW norms of the Scepter Creek and Hill 8056 volcanic rocks are given in Table 6-1. Both have high MgO concentrations, suggesting insignificant differentiation during ascent. Petrographically, the Scepter Creek trachyandesites are aphanitic, with a very finely crystallized groundmass rich in plagioclase, opaque minerals and ~ 0.2-0.5 mm phenocrysts of olivine and orthopyroxene. The Hill 8056 basalt is rich in large, up to 6 mm phenocrysts of olivine, orthopyroxenes, and plagioclase, some of which are probably xenocrysts, set in a groundmass that is mostly glassy.

The ages of both volcanic rocks are Pliocene (~3-4 Ma) [18, and T. Sisson, personal communication]. These volcanic rocks are part of a distinctive Pliocene group of mainly alkali basalts and trachybasalts erupted in the central Sierra Nevada, which differ from an older, Miocene group (8-12 Ma) of more silicic volcanic rocks. Volcanic rocks from both groups carry xenoliths; lower crustal garnet clinopyroxenites, amphibolites and granulites are common in the older group [10], while xenoliths of mainly ultramafic compositions predominate in the Pliocene group, including the Scepter Creek and Hill 8056 locations.

The most common ultramafic xenoliths from the Scepter Creek and Hill 8056 locations are spinel lherzolites and olivine clinopyroxenites, with mainly coarse, porphyroclastic textures. There is no textural anisotropy in the analyzed xenoliths, allowing the assumption to be made that surface modal abundances of glasses or various minerals measured in thin sections represent volume abundances. The spinel lherzolites represent typical upper mantle lithologies, have high Fo# in olivines (0.90-0.92) and contain 3-6% modal clinopyroxenes and 2-5% spinel (hereafter referred to as "common lherzolites"). The olivine clinopyroxenites are cumulates ponded in the mantle during a melting event, possibly related to the ~8-12 Ma volcanism [19]. An intermediate compositional xenolith type is represented by lherzolites rich in clinopyroxene, ~20-30% modal, hereafter referred

Table 6-1. Major element concentrations (in oxide wt.%) and CIPW norms of the Scepter Creek and Hill 8056 host volcanics.

	Scepter Creek	Hill 8056
Oxide concentration (wt%)[1]		
SiO_2	56.79	46.80
TiO_2	1.18	1.90
Al_2O_3	14.82	12.00
Cr_2O_3	0.06	0.08
FeO*	6.25	10.3
MnO	0.11	0.15
MgO	7.45	11.72
CaO	5.21	9.58
Na_2O	4.19	3.33
K_2O	3.57	1.62
P_2O_5	0.55	0.69
Total	99.70	98.09
CIPW norms[2]		
an	11.07	13.3
ab	35.42	21.9
or	21.07	9.8
en	8.98	11.3
wo	4.82	13.0
ol	10.47	13.9
ne	0.00	3.7
ru	0.00	1.9
mt+hm	0.00	10.5
ap	1.30	1.6

[1]- measured by X-ray fluorescence, using an automated Rigaku 3070 spectrometer (see Appendix 6-1 for procedures). SiO_2, TiO_2, Al_2O_3, and FeO are accurate to 1% of the amount present, MgO, CaO to 2%, Na_2O and K_2O to 3%, and P_2O_5 and MnO to 10%. Precision is better than 1% of the amount present except for Na_2O and K_2O for which precision is 2% of the amount present.
*- total Fe as FeO.
[2]- calculated using a computer program provided by D. Sykes.

Table 6-2. Mineral chemistry of the Scepter Creek and Hill 8056 lherzolites.

Oxide (wt%)	Olivine		Orthopyroxene		Clinopyroxene	
	SC9	H8-1	SC9	H8-1	SC9	H8-1
SiO_2	41.27	39.11	54.86	55.14	51.86	46.19
TiO_2	nd	0.05	0.12	0.11	0.44	2.05
Al_2O_3	nd	nd	0.87	1.55	2.85	7.74
Cr_2O_3	0.03	0.04	0.81	0.30	0.01	0.73
FeO	7.39	18.37	14.66	10.77	10.98	6.68
MnO	0.09	0.27	0.50	0.20	1.00	0.06
MgO	50.69	42.14	27.49	30.16	11.48	14.62
CaO	0.14	0.11	1.16	1.41	19.26	19.69
Na_2O	nd	nd	0.02	0.06	1.82	2.46
Total	99.61	100.01	100.49	99.77	99.70	100.12

Compositions were obtained using the Caltech JEOL 733 electron microprobe fitted with five wavelength spectrometers. The accelerating voltage was 15 keV, with a probe current of 25 nA (measured on brass), count times of 60-80 s, and probe diameter of 10 μm. Sodium was analyzed first in order to reduce alkali migration. The CaO in olivine has been analyzed with 0.01 wt.% absolute error (1σ) at the 0.1 wt.% level. The analyses presented here are averages of at least five grains of each mineral in thin sections.
H8-1- Hill 8056 lherzolite (see text); SC9- Scepter Creek lherzolite (see text); nd- not determined.

to as "enriched lherzolites." The enriched lherzolites have lower olivine Fo# (0.80-0.83) than the common lherzolites, and orthopyroxenes and clinopyroxenes are Al-enriched. In this study we have analyzed a common lherzolite from Scepter Creek (SC9) and an enriched lherzolite from Hill 8056 (H8-1), both rich in glass inclusions. The olivine clinopyroxenites from these locations have few inclusions of glass and, although they are a probable end-member of the enrichment process, they have not been considered further in this study.

Samples SC9 and H8-1 show no phase alterations or interactions with their host lavas. Their mineral compositions determined by electron microprobe are given in Table 6-2. We have determined the temperatures and pressures of equilibration for the two samples. We have used the lherzolite thermometers of Brey and Kohler [20] and determined temperatures of 1150 (±40) ^{0}C for SC9 and 1180 (±40) ^{0}C for H8-1. The pressures were determined using the Ca-in-olivine barometer [21]; SC9 equilibrated at 1.8 ±0.3 GPa, and H8-1 at 1.4 ± 0.3 GPa. Despite a large uncertainty associated with Ca-in-olivine barometer, the calculated pressures are in agreement with the depths at which spinel is stable in peridotites. The temperatures and pressures support the upper mantle origin of the lherzolites and are consistent with the late Cenozoic Sierra Nevada mantle geothermal gradient reported by Ducea and Saleeby [10] using xenoliths from the eastern Sierra Nevada.

6.3. Glass inclusions in lherzolites; petrography and major element chemistry

Both common and enriched lherzolites from Scepter Creek and Hill 8056 contain amorphous inclusions. These inclusions represent trapped remnants of melts. Most nodules contain ≤ 2-3 volume% glass in thin sections but occasionally the glass abundance is higher. The two lherzolites selected for analysis are unusually rich in these glasses, ~10-12

volume%. Morphologically, the glass inclusions can be divided in two groups: (1) interconnected films and (2) isolated pockets included in various crystals, with no preferences for any particular mineral. The interconnected films (veinlets) form networks and are present at grain boundaries as well as filling grain fractures. The pockets are subordinate in abundance. The composition of the melt pockets are very similar to the films, and we believe that in fact they represent cross sections of the glass films penetrating through various crystals.

The two morphological types are shown in two SEM backscattered electron images (Figure 6-1). Figure 6-1a shows typical glass films of 10-20 μm width, hosted within and along the grain boundaries of a large crystal of olivine, as well as a melt pocket. The width of the films can be as much as 50 μm, especially at grain boundaries. A detail of a melt inclusion in olivine is shown in Figure 6-1b.

The only matrix phase that shows a mineralogical reaction with these passing melts is spinel, which commonly breaks down upon interaction (Figure 6-1a). There is little evidence for interaction between the glasses and olivine or clinopyroxene (Figure 6-1b, and 1c). Although the BSE images show evidence for zoning of the glass inclusions, no crystallites are present. One should acknowledge that these glasses are inevitably reacting with the peridotite assemblage. However, in contrast to other studies [e.g., 9, 22] there is no evidence for preferential breakdown (e.g., by disequilibrium melting) of one or both pyroxenes.

We have analyzed the major element chemistry of these glasses using an electron microprobe (see Appendix 6-1 for analytical procedures). Representative glass analyses are given in Table 6-3 for both samples. The glasses show consistently high SiO_2 concentrations (58.5-69.5 wt.%), Al_2O_3 concentrations (15-24 wt%), are very rich in alkalis (up to 10 wt.% K_2O and 6 wt.% Na_2O), display low MgO (usually < 1 wt.%) and FeO (<3 wt.%) concentrations, and have highly variable CaO concentrations (0.3-5.6 wt.

Figure 6-1. SEM backscattered electron images of glass films in SC9. **a.** page 6-10, top, glass films within grains and along grain boundaries of olivine and spinel. A melt pocket is also present at the right of the spinel grain. Gl- glass, Ol- olivine, Sp- spinel. The spinel breaks down upon interaction with the melt. **b**. page 6-10, bottom, detail of two glass pockets located along the grain boundary between two olivine crystals. No phenocrysts are present in the SRG; the heterogeneity of the backscattered image indicates a chemical zonation (see text). **c**. page 6-11, glass pockets included in orthopyroxene (opx) showing some chemical heterogeneity but no crystallites formed in SRG inclusions (Gl) in contact with pyroxene.
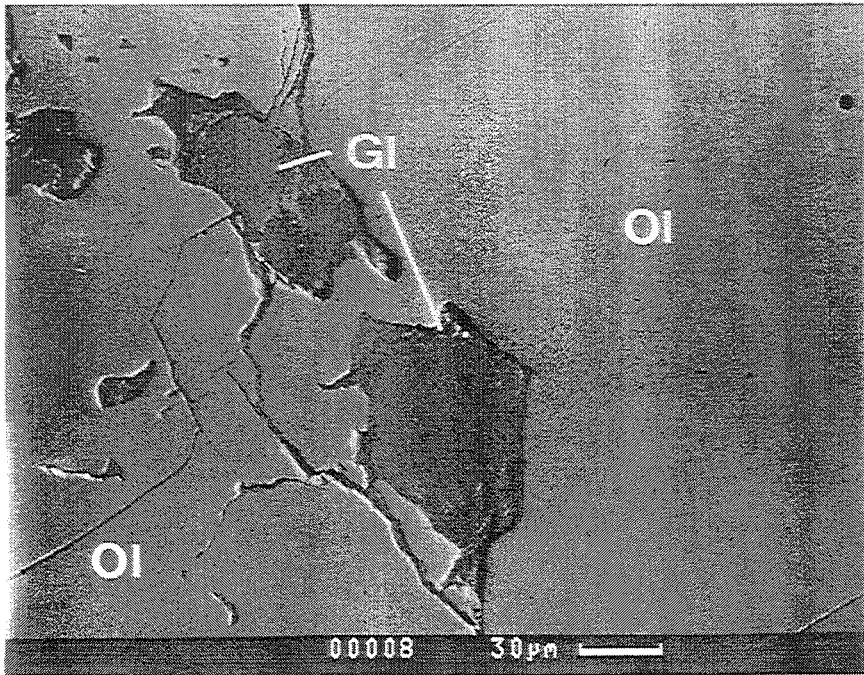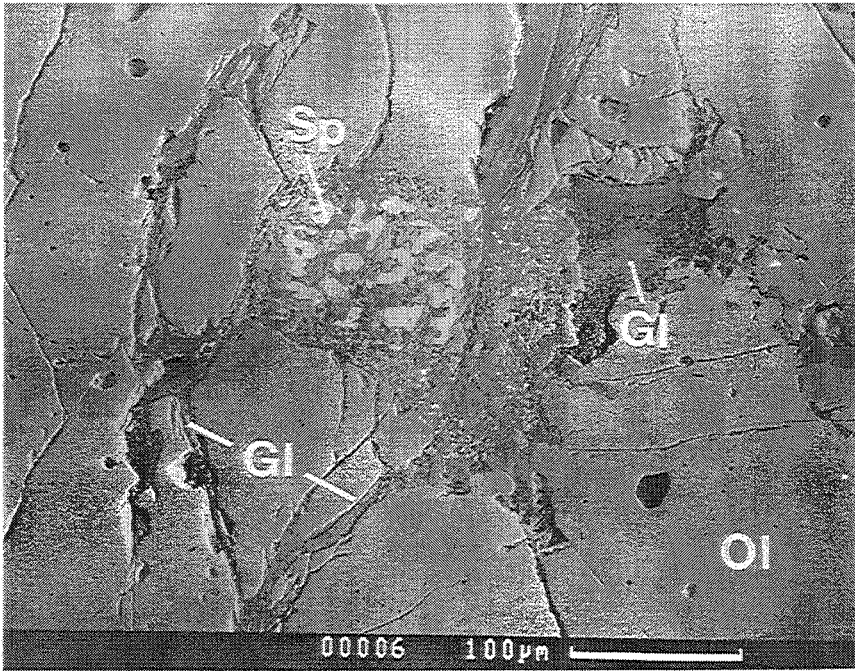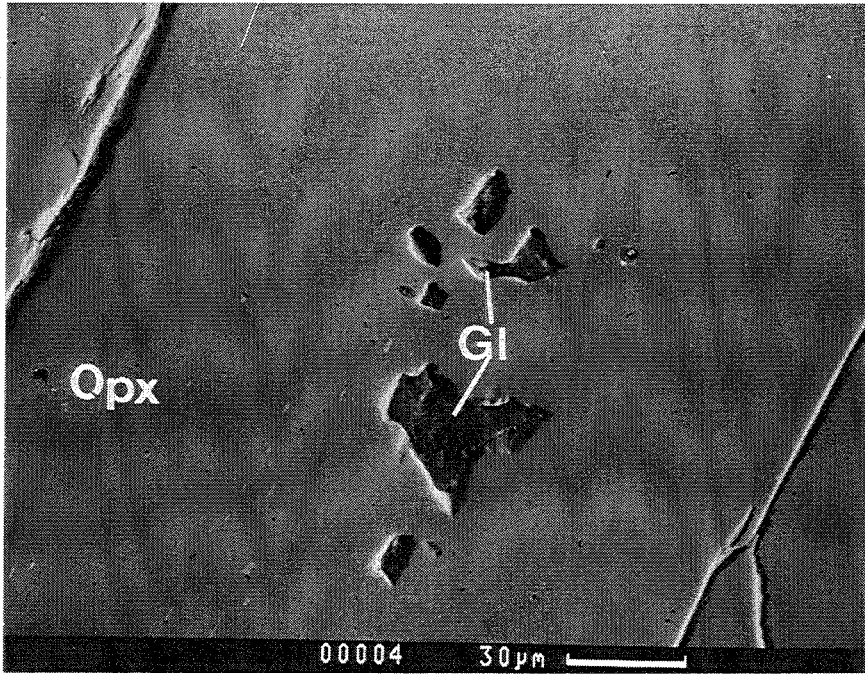
%).Various major elements oxides are plotted against SiO_2 in Figure 6-2. Na_2O, CaO, and Al_2O_3 show a negative correlation with silica, while K_2O displays a positive correlation with silica. These trends are similar to other SRG inclusions in continental mantle xenoliths [1-9]. The glasses are trachytic in composition [23], have alkaline character (based on the classification of Irvine and Baragar [24]), and are calc-alkaline to shoshonitic based on the K_2O-SiO_2 concentrations [23]. The shaded fields in Figure 6-2 represent only the high silica end of the fields of glass compositions from xenoliths reported in the literature. The fields of previously analyzed SRG in Figure 6-2 include the localities from West Eifel (Germany), Simcoe Mts (Washington, USA), Tariat Depression (Mongolia), Vitim (Russia) in continental ultramafic xenoliths and Society Islands, Comores, Kerguelen, and Canary Islands in oceanic xenoliths [1-9]. Overall, Figure 6-2 shows the remarkable similarity between the composition of glasses investigated in this study and SRG from xenoliths reported elsewhere. The glasses reported here also have silica concentrations at the highest silica end among all SRG inclusions ever reported. Only glasses in xenoliths from Mongolia reported by Ionov et al. [4] have comparable silica concentrations and trachytic compositions.

There is some chemical heterogeneity in the glass compositions, possibly due to interaction between glasses and the solid matrix. The BSE images of glass inclusions in Figure 6-1 illustrate the compositional heterogeneity of these glasses. Four microprobe traverses (two on each sample) consisting of 3-5 data points, display major element heterogeneities. These heterogeneities are within and much smaller than the compositional spectrum of analyzed glasses in each sample (Table 6-3). A decrease in SiO_2, Al_2O_3, and an increase in MgO, FeO from the glass cores to rims indicate that the SRG have interacted to various degrees with the peridotitic phases.

6.4. Trace element and Sr-Nd isotopic analyses on glasses

Figure 6-2. Major element compositions of the analyzed glass inclusions, plotted against silica (data reported in Table 6-3). The shaded fields represent data from similar glasses previously reported in [1-6], and [9]. Most of the data taken from the literature are very similar to the analyses presented in this study. However, Na_2O concentrations are significantly different in some data from [2] and [4], and they were plotted as separate dotted fields in the Na_2O-SiO_2 diagram. The line separating alkaline-subalkaline fields in the alkali vs. silica diagram is taken from [24].
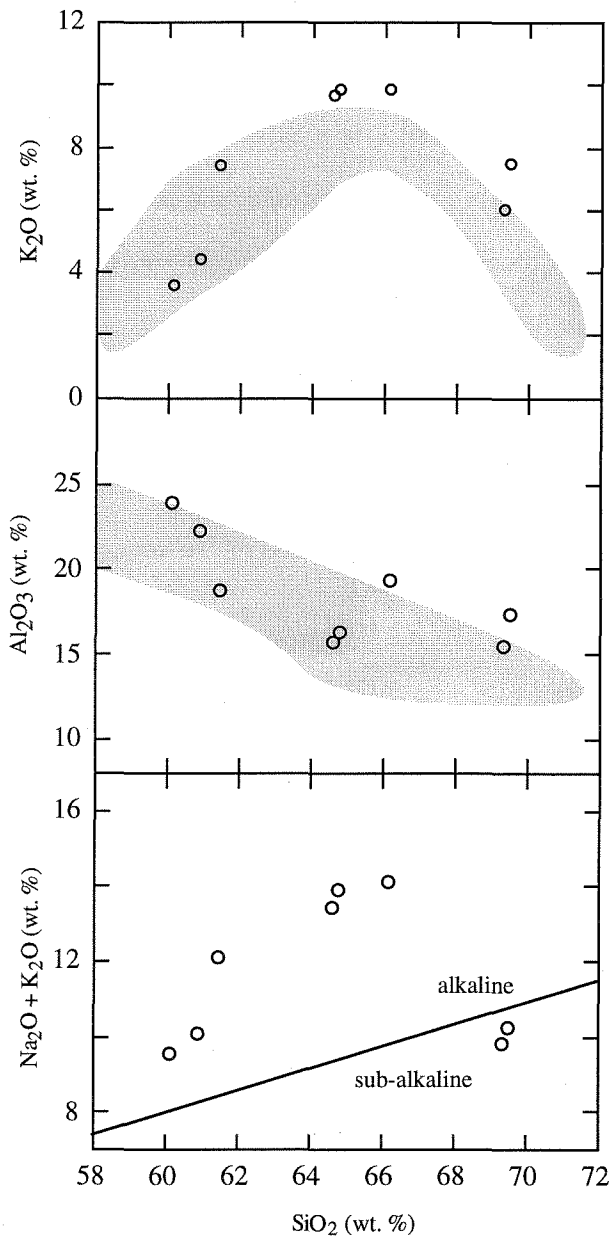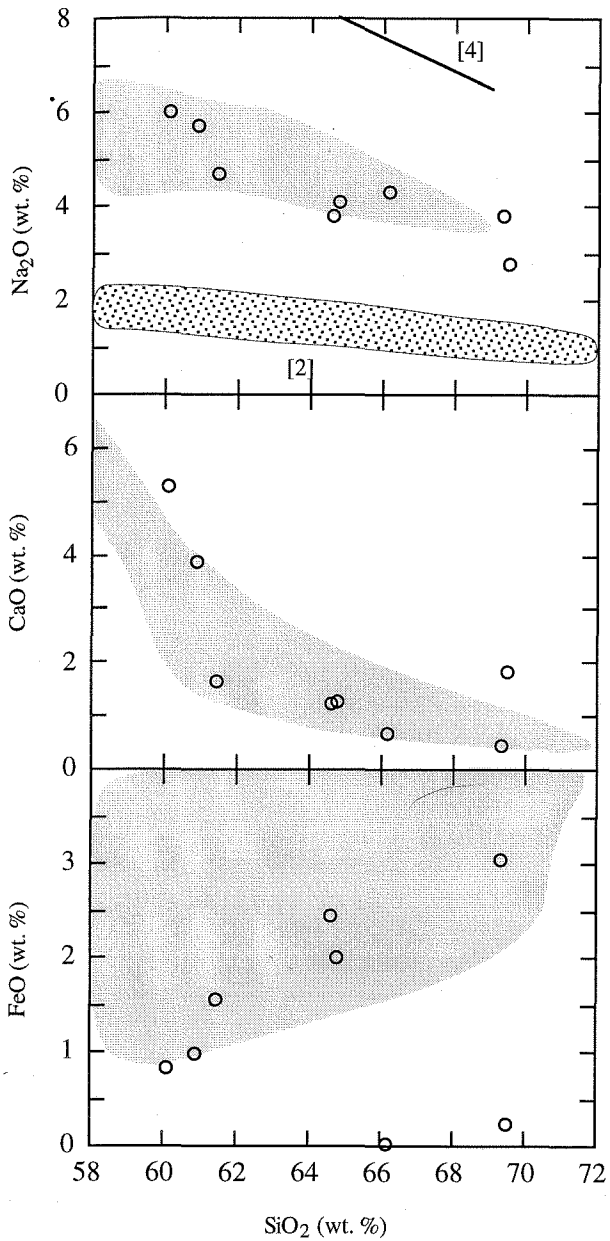
We have attempted to determine the Sr and Nd isotopic composition of the glasses described above in order to identify their source. Unfortunately, despite the large abundance of glass films in the two investigated xenoliths, the size and shape of the amorphous inclusions precludes their complete separation from the host xenolith. The glass inclusions were separated from the ultramafic xenoliths using a procedure that combined acid leaching and hand-picking (Appendix 6-1). The leachates, residue after leaching, and for SC9 an unleached fragment of the xenolith, were analyzed for Sr and Nd isotope ratios, Rb, Sr, Sm, and Nd concentrations by isotope dilution using a thermal ionization mass spectrometer. Two samples of the host basalts (SC3, and H8-103) leached in a similar fashion as the xenoliths were also analyzed for isotopic compositions. Selected trace element concentrations, including 14 rare earth elements, were measured by SIMS (see Appendix 6-1, for analytical procedures) on the SRG displaying the largest grain size. Table 6-3 lists the average trace element concentrations determined on glasses from the two samples. Individual SIMS analyses vary as much as $\pm 20\%$ of the average values reported in Table 6-3.

The REE patterns of the SRG in the two samples are quite similar (Figure 6-3a). Both SRG display significant LREE enrichment over HREE ($La_n \approx 100$, $La_n/Yb_n \approx 50$), consistent with the presence of garnet as a residual phase (Figure 6-3a). Europium displays negative anomalies in both samples. The Eu "depletion" is ≈ 0.7-0.86 relative to a Eu* on a smooth REE pattern. The HREEs display a relatively flat pattern ($Dy_n/Lu_n \approx 1.5$-2) in the two samples.

Figure 6-3b shows that all analyzed elements are enriched relative to primitive mantle values. The pattern contains a few characteristic features which will be discussed below: glasses display low Rb concentrations (5-35 ppm), relatively high Sr (220-500 ppm) and Ba (750-125 ppm) concentrations. In addition, there is a marked negative anomaly at Nb, whose normalized value is ~0.15 of the normalized compositions of the

Table 6-3. Major oxide and trace element compositions of representative glass inclusions in ultramafic xenoliths from Scepter Creek and Hill 8056, Sierra Nevada, California.

Oxide	Scepter Creek, glasses in SC-9				Hill 8056, glasses in H8-1			
	1	2	3	4	1	2	3	4
SiO_2	66.16	61.42	69.50	69.33	60.14	64.76	64.62	60.88
TiO_2	0.03	0.13	0.57	1.11	0.27	0.70	0.91	0.11
Al_2O_3	19.34	18.75	17.37	15.51	23.89	16.30	15.68	22.32
Cr_2O_3	0.03	0.01	nd	0.19	0.03	nd	0.04	0.15
FeO*	0.03	1.56	0.23	3.04	0.82	2.01	2.45	0.98
MnO	nd	0.01	nd	nd	0.01	0.02	0.01	nd
MgO	0.10	0.96	0.10	0.10	0.28	0.75	1.65	1.02
CaO	0.66	1.65	1.81	0.43	5.30	1.27	1.24	3.89
Na_2O	4.31	4.68	2.77	3.80	6.02	4.07	3.77	5.72
K_2O	9.82	7.41	7.49	6.03	3.56	9.87	9.67	4.39
Total	100.48	96.58	99.84	99.54	100.32	99.75	100.07	99.46
Ti				6800				7412
Rb				33.14				8.32
Sr				443				250
Y				11.3				14.47
Zr				189.1				140
Nb				8.6				10.6
Ba				1120				794
La				22.24				19.84
Ce				31.20				27.98
Pr				1.99				2.47
Nd				9.51				7.31
Sm				1.40				1.21
Eu				0.46				0.33
Gd				1.95				2.26
Tb				0.44				0.32
Dy				1.78				1.71
Ho				0.31				0.41
Er				1.00				1.36
Tm				0.08				0.11
Yb				0.80				1.00
Lu				0.14				0.19

Analytical procedures for major elements as in Table 6-2. Trace element analytical procedures are given in Appendix 1. *- total Fe expressed as FeO. nd- not determined. Each reported major element analysis represents an average of 5 analyzed spots on glasses. The labels 1, 2, 3, and 4 for each sample distinguish different glass inclusions size groups; "1" represents averages of glass inclusions with the small dimension ("width") < 20 μm, "2" represent glasses with the small dimension between 20-30 μm, "3" for glasses between 30-40 μm wide, and "4" for glasses with a width >40 μm. The trace element averages are based on 8-10 analyses performed on the largest glasses (>40 μm).

Table 6-4. Sr and Nd isotopic compositions of peridotites, leachates, and host basalts.

Sample	Rb (ppm)	Sr (ppm)	$^{87}Sr/^{86}Sr$	Sm (ppm)	Nd (ppm)	$^{143}Nd/^{144}Nd$
SC9(r)	1.50	32.3	0.70658	1.21	4.35	0.51231
SC9(l)	18.32	250.2	0.70834	1.02	7.03	0.51241
SC9(x)	4.05	68.3	0.70734	1.15	5.04	0.51233
H8-1(r)	0.75	67.8	0.70666	0.43	1.34	0.51230
H8-1(l)	1.55	90.0	0.70695	0.52	1.94	0.51234
SC3(b)	45.88	1541.1	0.70631	6.29	51.14	0.51234
H8-103(b)	49.31	6726.5	0.70396	8.91	62.15	0.51282

SC- Scepter Creek sample; H8- Hill 8056 sample. (x)- unleached xenolith, (l)-leachate, (r)- xenolith, residue after leaching, (b) - host basalt. See Appendix 1 for procedures. Standard errors (2σ) are < 0.002% for the $^{87}Sr/^{86}Sr$ ratios, and <0.003% for the $^{143}Nd/^{144}Nd$ ratios.

Figure 6-3. a. Rare earth element patterns of the Sierra Nevada SRG inclusions, normalized to chondritic values. **b.** Primitive mantle-normalized incompatible trace element compositions of the SRG.
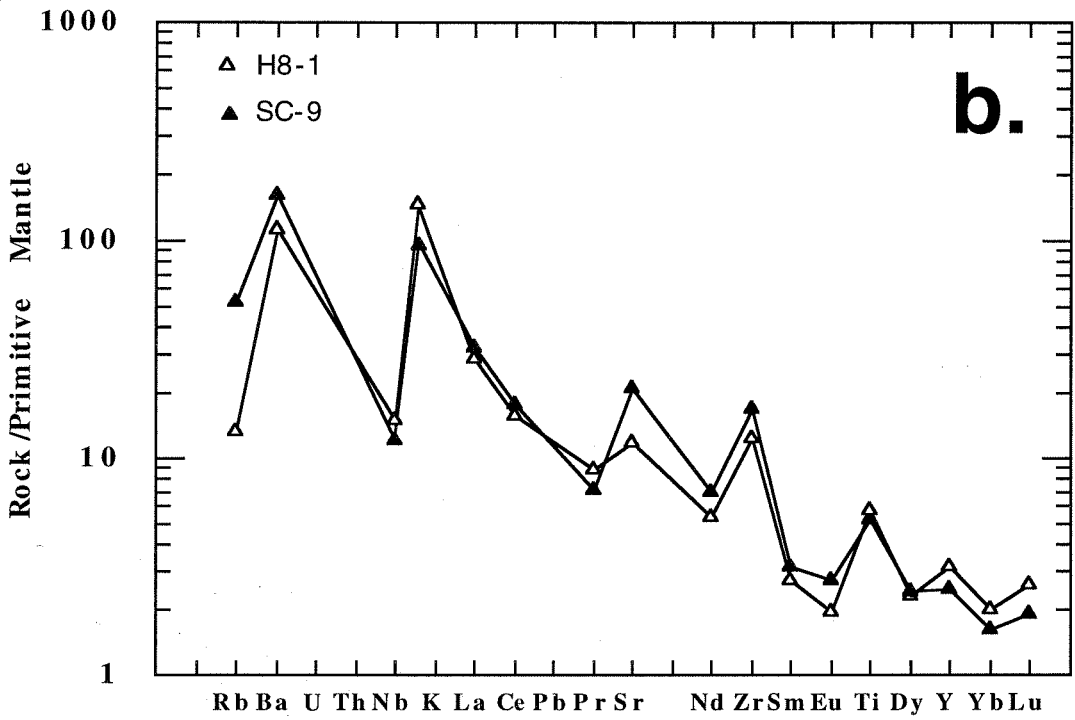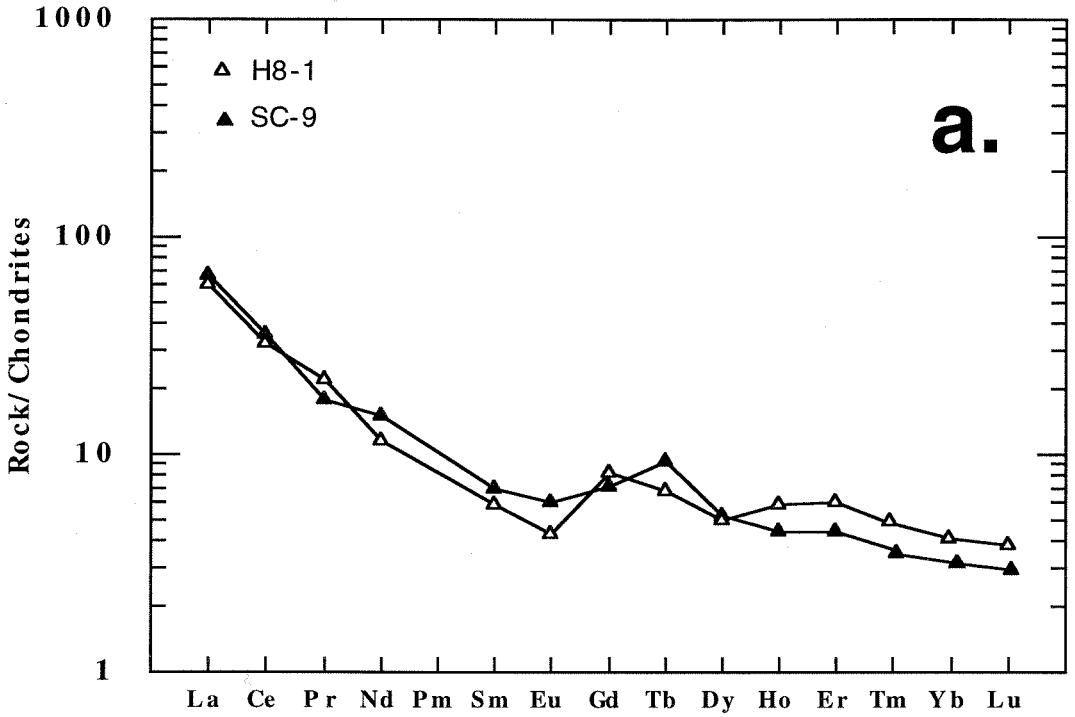
neighboring (i.e., similar incompatibility during melting) analyzed elements in this diagram: Ba and K.

The leachate trace element concentrations (Rb, Sr, Sm, and Nd) and isotopic ratios ($^{87}Sr/^{86}Sr$ and $^{143}Nd/^{144}Nd$) are shown in Table 6-4. The elemental concentrations and isotopic ratios for leachates ideally represent the glass compositions. However, even though we have succeeded in completely separating the glass from residues, the leachates are mixtures of glass films and the host lherzolites. Since the elemental concentrations of Rb, Sr, Sm, and Nd as well as the $^{87}Sr/^{86}Sr$ and $^{143}Nd/^{144}Nd$ ratios are all higher in leachates than in the residues, the leachate numbers are *minimum* values for the actual concentrations and isotopic ratios of the glasses.

The complete separation of the lherzolites as "residues" from the lherzolite-glass mixture allows the calculation of the elemental concentrations and isotopic ratios of the "glass" end member by solving a simple mass balance equation (Appendix 6-2). The glass Rb, Sr, Sm, and Nd concentrations as well as the Sr and Nd isotopic ratios calculated in this way are given in Table 6-5. It is possible that the lherzolite-glass system has undergone some exchange, so that the calculated glass isotopic ratios are still lower than the actual SRG source. The difference between the major element compositions in the lherzolite phases and the SRG in SC9, the lack of chemical zonation in the lherzolite phases, as well as textural evidence, argue against strong lherzolite-melt interaction in that sample. H8-1 glass, in contrast, might have undergone some diffusional exchange and equilibration with the lherzolite, as suggested by the "enriched" nature of the lherzolite and the average lower silica concentration in glasses.

6.5. Continental crustal origin for the glass films

The first concern in interpreting the leachates isotopic data was that the grain boundary isotopic signature was not produced by the glass but some surficial process (i.e.,

after the eruption of the host volcanic rocks). The lack of alteration products argues against this. The main potential contaminant in such a scenario would be the Sierran surface waters [30]. The $^{87}Sr/^{86}Sr$ isotopic ratios as well as the Sr elemental concentration of the Sierra Nevada streams and ices (SNSI) are fairly well known [31]. The isotopic ratios are roughly the average of the present day batholithic ratios, that is ~0.7078 in the area where Scepter Creek and Hill 8056 are located. The Sr concentrations (Figure 6-4a) as well as the unknown (but probably very low) Nd concentrations of the SNSI rule out this surficial process as a cause of the high Sr and Nd isotopic compositions of the grain boundary leachates. Microscope-undetectable grain boundary material, other than the glasses and not related to the surface waters, may have contributed to the elemental concentrations and isotopic ratios of the leachates. We have two tests which demonstrate that the leachates do not contain components other than the glasses and peridotitic material: (1) the K_2O concentration of xenolith SC9(x) is all glass-derived, and (2) in-situ SIMS abundances of selected trace element concentrations are similar to the ones calculated from the leachate data. In sample SC9(x) the concentration of K_2O determined by XRF (0.6%) can be accounted for entirely by the presence of ~8% glass with an average K_2O concentration of 7.68 wt.% determined by electron microprobe (Table 6-3). The 8% glass in sample SC9 used in the preceding calculation is a minimum value for SC9 glass abundance. This very rough calculation indicates that all potassium in this sample is glass-derived. The concentrations of Sr, Nd, and Sm in glasses from the two xenoliths were measured by SIMS on the largest size group defined in Table 6-3. These concentrations are within 10% or less of the concentrations of Sr, Nd, and Sm (Table 6-5) calculated using leachate data (Table 6-4) and the mass balance algorithm from Appendix 6-2. We conclude that the leachate measurements are indeed reliable measurements of glasses.

The host volcanic rocks have different isotopic and chemical composition from the glass compositions (Tables 1, 3, 4, and Figure 6-4a). They could not be related to the high silica glass inclusions.

Figure 6-4. a. $^{87}Sr/^{86}Sr$ versus Sr (ppm) diagram for the samples analyzed in this study. The square symbols denote the Hill 8056 samples, while the circles denote the Scepter Creek samples. Filled symbols are the host volcanics. The open symbols are analyses on xenolith samples: "b" - basalt, "r" - residue after leaching, "x" - unleached xenolith, "l" - leachate, "g" glass compositions calculated using the algorithm from Appendix 6-2. "SNSI" - Sierra Nevada streams and ices [31]. This figure shows that the leachate isotopic compositions are incompatible with the host volcanics or the main expected surficial contaminant, represented by stream waters.

b. $^{143}Nd/^{144}Nd$ vs. Sr/Nd diagram for the analyzed samples. Sample symbols are as in **4a**. The field labeled "OS" represents the possible compositions of oceanic sediments [29, 41, 42], whereas the field labeled "SNLCX" which stands for Sierra Nevada lower crustal xenoliths, is drawn based on data from [19, 32-35]. The two ratios plotted in this figure (one elemental and one isotopic) do not change during melting (explanation in text). The calculated glass inclusion compositions are compatible with a lower continental crustal origin.

c. $^{143}Nd/^{144}Nd$ vs. $^{87}Sr/^{86}Sr$ diagram for the analyzed rocks. Data reported in this study is also presented in an enlarged view of the box labeled "d" in **Figure 6-4d**. "SNLCX" and "OS" are as in **4b**, "MORB" represents a depleted isotopic endmember representative for unaltered mafic oceanic crust [e.g., 29], whereas the "AOC" field denotes the field of altered mafic oceanic crust [39]. This diagram shows that the source of the SRGs could not be the mafic oceanic crust, altered or not. However, based only on the two isotopic systems plotted in this diagram, both oceanic sediments or lower continental crustal rocks could represent source reservoirs for the SRG.

d. Enlarged view of box "d" in Figure 6-4c displaying the isotopic ratios of the samples analyzed for this study, as well as the calculated "end member" ratios for the glasses.

Figure 6-4. a. $^{87}Sr/^{86}Sr$ versus Sr (ppm) diagram for the samples analyzed in this study. The square symbols denote the Hill 8056 samples, while the circles denote the Scepter Creek samples. Filled symbols are the host volcanics. The open symbols are analyses on xenolith samples: "b" - basalt, "r" - residue after leaching, "x" - unleached xenolith, "l" - leachate, "g" glass compositions calculated using the algorithm from Appendix 6-2. "SNSI" - Sierra Nevada streams and ices [31]. This figure shows that the leachate isotopic compositions are incompatible with the host volcanics or the main expected surficial contaminant, represented by stream waters.

b. $^{143}Nd/^{144}Nd$ vs. Sr/Nd diagram for the analyzed samples. Sample symbols are as in **4a**. The field labeled "OS" represents the possible compositions of oceanic sediments [29, 41, 42], whereas the field labeled "SNLCX" which stands for Sierra Nevada lower crustal xenoliths, is drawn based on data from [19, 32-35]. The two ratios plotted in this figure (one elemental and one isotopic) do not change during melting (explanation in text). The calculated glass inclusion compositions are compatible with a lower continental crustal origin.

c. $^{143}Nd/^{144}Nd$ vs. $^{87}Sr/^{86}Sr$ diagram for the analyzed rocks. Data reported in this study is also presented in an enlarged view of the box labeled "d" in Figure 6-4**d**. "SNLCX" and "OS" are as in **4b**, "MORB" represents a depleted isotopic endmember representative for unaltered mafic oceanic crust [e.g., 29], whereas the "AOC" field denotes the field of altered mafic oceanic crust [39]. This diagram shows that the source of the SRGs could not be the mafic oceanic crust , altered or not. However, based only on the two isotopic systems plotted in this diagram, both oceanic sediments or lower continental crustal rocks could represent source reservoirs for the SRG.

d. Enlarged view of box "d" in Figure 6-4**c** displaying the isotopic ratios of the samples analyzed for this study, as well as the calculated "end member" ratios for the glasses.
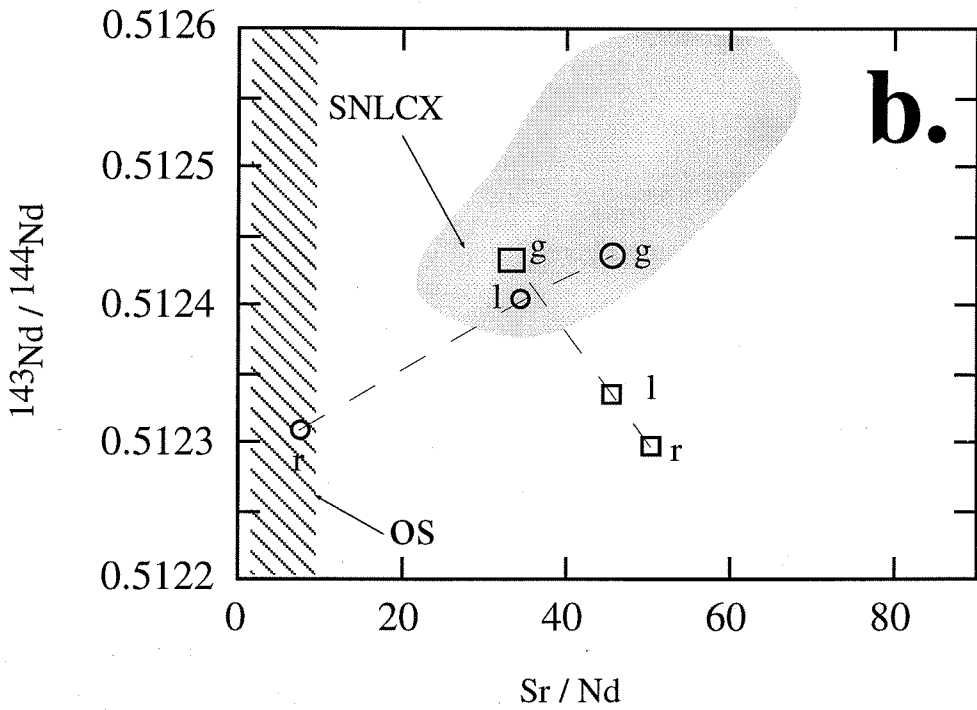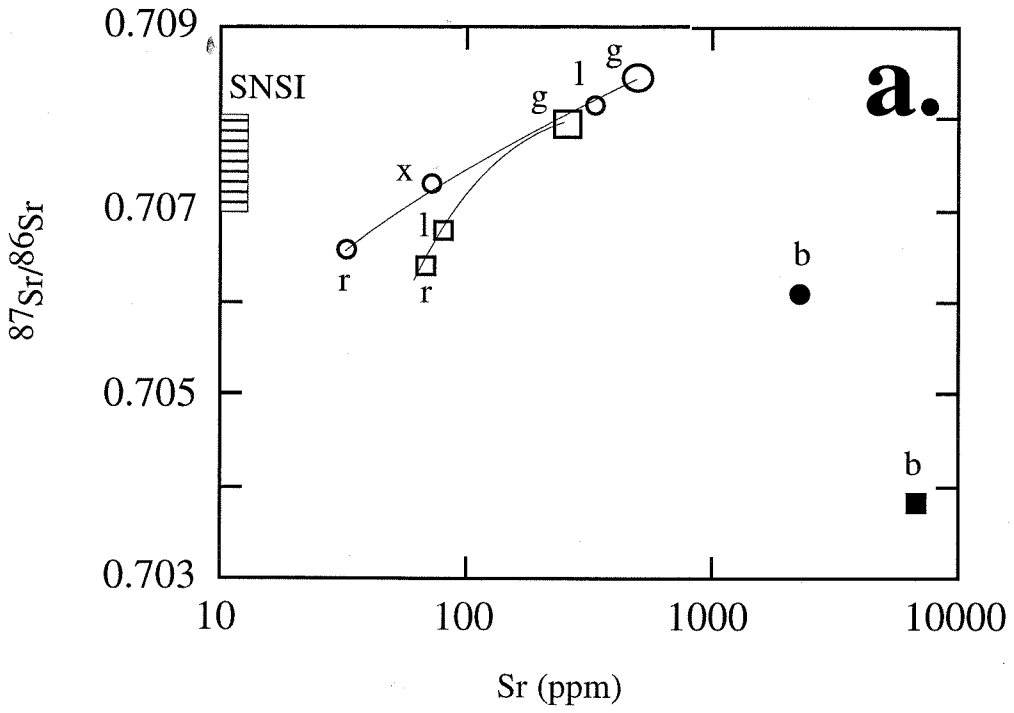
We consider the following potential melt sources for the SRG inclusions described in this study: (1) the Sierra Nevada upper mantle assemblages (peridotites or olivine clinopyroxenites), (2) subducted igneous oceanic crust, (3) subducted oceanic sediments, and (4) lower continental crustal rocks.

(1) The $^{87}Sr/^{86}Sr$ ratios of the SRG are more radiogenic than any ultramafic xenolith or individual mineral (including phlogopite from other Sierra Nevada xenolith localities) in ultramafic xenoliths determined from the Sierra Nevada upper mantle [19, 32-36], despite its isotopically enriched nature. Experimental results [37] show that by melting an anhydrous lherzolite, the composition of the partial melts will not be more silicic than an andesite, ~ 55% SiO_2, at 2% melt fractions. Melts as silicic as 65-69% SiO_2 can not be produced by partial fusion of anhydrous peridotites at 1.5-2 GPa, even if the liquid fractions would be extremely low [M. Baker, written comm.].

Recent results [7, 9, 22] have indicated that glasses similar, although typically less silicic than the ones presented here, were produced by melting hydrous phases in peridotites (phogopite, amphibole) and further reaction with primary pyroxenes in the peridotites. The Scepter Creek and Hill 8056 suites of ultramafic xenoliths from our collection do not contain phlogopite or amphibole. One can not rule out based on petrographic evidence that (i) such hydrous phases were originally present in our samples and subsequently melted completely contributing significantly to the SRG production, or perhaps (ii) the melts have migrated into our samples by being transported short distances (e.g., tens of centimeters) from an amphibole- or phlogopite-bearing volume of peridotite. However, even if hydrous phases were originally present in or nearby our Scepter Creek and Hill 8056 mantle samples, the involvement of such phases in melting would not be able to account for some of the trace element characteristics measured in the SRG if fully mantle-derived. First, the negative Eu anomalies ($Eu_n/Eu_n* \approx$ 0.7-0.86) measured in glasses (Figure 6-3a) are not characteristic for mantle (feldspar-free) rocks, but are commonly

Table 6-5. Rb, Sr, Sm, Nd elemental concentrations, and ^{87}Sr/^{86}Sr and ^{143}Nd/^{144}Nd ratios of the SC9 and H8-1 glasses, calculated using the algorithm outlined in Appendix 2, and average values for various possible melt sources.

	SC9	H8-1	Mafic oceanic crust*	Oceanic sediments**	Sierra lower crust***
Rb	33.14	8.51			
Sr	427.86	232.2			
Sm	1.61	1.12			
Nd	9.24	6.68			
Rb/Sr	0.077	0.036	0.06-0.1	0.5	0.01-0.1
Sr/Nd	46.63	35.00	10-20	1-10	20-70
^{87}Sr/^{86}Sr	0.708509	0.707772	0.702-0.710	>0.7075	0.706-0.712
^{143}Nd/^{144}Nd	0.512438	0.512436	0.5129-0.5132	0.5118-0.5126	0.51235-0.5126

*- references [29,39], **- references [41,42], ***- references [19,32-35]

found in crustal assemblages. Another indicator of a crustal source is represented by the low Nb concentrations (8.6-10.6 ppm) corresponding to a negative anomaly of $(Nb_n/Nb_n* \approx 0.15$, Figure 6-3b). Melts produced by a modally metasomatized peridotite are enriched in Nb [e.g., 7, 22]. The Nb depletions argue against a source dominated by the presence of hydrous mantle phases such as phlogopite or amphibole. In addition, the high concentrations of Ba (~800-1200 ppm) argue against an amphibole+phlogopite breakdown origin. We conclude that the SRG inclusions reported in this study could not have been produced by melting a typical mantle lithosphere assemblage. A crustal component is required in the source of the SRG inclusions described here.

(2) Melting of hydrous oceanic basalts (eclogites) has been proposed to explain chemical (not isotopic) characteristics of glass inclusions from the Philippines [8], broadly similar with the ones reported in this study. Adakites, volcanic rocks believed to have formed by melting a hot descending oceanic slab, [38] also have a composition similar to the glass inclusions described in this study, although they have significantly lower K_2O concentrations. However, the isotopic composition of the glass films rule out their oceanic slab origin. Young igneous oceanic crust has a depleted signature on an $^{87}Sr/^{86}Sr$ vs. $^{143}Nd/^{144}Nd$ diagram (MORB, Figure 6-4c). The oceanic crust can become enriched in the $^{87}Sr/^{86}Sr$ ratios due to interactions with seawater, but its $^{143}Nd/^{144}Nd$ ratios remain fairly close to the MORB values due to the extremely low Nd concentrations in seawater [39] (AOC component in Figure 6-4c). We conclude that the SRG can not be produced by melting of subducting mafic oceanic crust. The negative ε_{Nd} ratios indicate a continental origin for the SRG source.

(3) Ocean floor sediments have a wide range of chemical and isotopic compositions. They can undergo a low degree of partial melting if the slab is hot enough [40]. Oceanic sediments can be authigenic or allogenic. Authigenic sediments should have isotopic compositions identical to that of the seawater from which they precipitated. Biogenic calcareous sediments would produce Ca-rich melts, opposite from what SRG

show. The Sierran SRG $^{87}Sr/^{86}Sr$ ratios are consistent with Mesozoic/Cenozoic ocean water ratios [29, and references therein]. The SRG $^{143}Nd/^{144}Nd$ ratios (~0.51244) are slightly lower than Mesozoic/Cenozoic waters (~0.5125-5126, [29, and references therein]) although the difference is small and by itself can not negate an ocean authigenic sediment source for the SRG. In a more general sense, the Sr and Nd isotopic ratios in oceanic sediments, authigenic and allogenic (OS in Figure 6-4c), overlap the values calculated for SRG. The difficulty in accepting the sediment origin of the SRG source is based on the Rb/Sr and Sr/Nd ratios (Figure 6-4b). Figure 6-4b is a plot of two parameters, $^{143}Nd/$ ^{144}Nd and the Sr/Nd ratio which should not change during partial melting, the elemental ratio in particular because of the similarity of melt-residue partition coefficients between Sr and Nd assuming that feldspar is not a residual phase [14]. The analyzed glasses have high Sr/Nd ratios (>35), while the Sr/Nd in silicate-rich oceanic sediments is typically between 1 and 10 [41], and rarely > 15 (Figure 6-4b). The high Sr/Nd ratios calculated for SRGs (Table 6-5) contrast with typical ocean sediment values because, in a very general sense, allogenic ocean sediments are similar to (if not fully derived from) upper continental material, whereas the SRG seemed to have formed from a reservoir depleted in incompatible elements. For example, the average Rb/Sr ratio is ~0.5 in ocean sediments [41, 42], and 0.35-0.4 in upper continental crust [43], while in SC9 it is around 0.078 (based on either the measured or calculated values). If a typical ocean sediment undergoes partial melting during subduction, the Rb/Sr of the melt will be higher than ~0.5 because Rb is more incompatible than Sr during melting. Low Rb/Sr are characteristic for the lower continental crust, and not for an upper crustal sedimentary material. These results are generally inconsistent with a (subducted) sedimentary origin for the SRG source. A subducted sediment origin can not be fully rejected at this time, given the complex chemical and isotopic compositions characteristic for ocean floor sediments.

(4) The glasses analyzed in this study have chemical and isotopic compositions consistent with a continental crustal origin. First, the $K_2O/Na_2O > 1$ ratios are broadly

indicative of a continental source. The bulk composition of the lower continental crust in the Sierra Nevada is basaltic [10]. The presence of negative Eu and Nb anomalies in SRG spiderdiagrams (Figure 6-3) suggest a crustal protolith. The Sr-Nd isotopic compositions of the SRG component overlaps the field of Sierra Nevada lower crustal xenoliths (Figures 4b and 4c), amphibolites, granulites, and eclogites [19, 32-35]. The Sierra Nevada lower crust consists mainly of residues of the surface batholith [10, 19], and therefore has the low Rb/Sr and high Sr/Nd ratios required for the SRG source, as described before. In particular, the source rocks that upon melting would be likely to produce the major element composition as well as the trace elements and isotopic ratios measured in the SRG glasses would be amphibolites or hornblende garnet clinopyroxenites (Table 6-5).

Wolf and Wyllie [44] have demonstrated experimentally that silica-rich glasses similar in major element compositions to the ones presented here can form by partially melting an amphibolitic protolith. Yaxley and Green [45] have produced experimentally melts with major element chemistry similar to SRG by melting eclogites.

Based on the arguments presented above, we propose a lower continental crustal origin of the SRG inclusions described in this study.

6.6. Crust-mantle interactions: crustal delamination, mantle diapirism or sediment subduction?

The presence of continental crustal melts within upper mantle assemblages requires a mechanism to explain crustal recycling in the mantle. Two mechanisms have been proposed to produce continental crustal recycling: (i) lower crustal crustal delamination, and (ii) sediment subduction. Of the two, sediment subduction has been unambiguosly documented. Delamination, in contrast, is a rather speculative hypothesis. However, lower crustal foundering (delamination) may represent an important mechanism responsible for the differentiation of continental masses on Earth.

Foundering of the Sierra Nevada lower crust into the upper mantle would best explain the presence of the SRG in the Sierran mantle. Delamination of the Sierran crust is supported by a number of observations. First, the Sierra Nevada batholith had a thick mafic-ultramafic lowermost crust [10] and an unusually low heat flow during the Cenozoic [46], and accordingly its lowermost crust was very dense. The presence of a thick, ≥ 25 km eclogite facies lowermost crust [10] which is ~200 kg/m^3 denser than the underlying mantle makes the Sierra Nevada region an ideal site for lower crustal delamination. Second, a variety of geological and geophysical data demonstrate that the Sierra Nevada lost the lower half of its crust between mid-Miocene and present [47]. Third, barometric determinations on xenoliths [10, this study and Ducea and Saleeby, unpublished] indicate a 0.8 GPa overlap between the shallowest ultramafic xenolith recorded in the Pliocene volcanic rocks and the deepest crustal assemblages measured in the Miocene volcanic rocks. Finally, geophysical evidence suggests the presence of a fast, dense body at 150-190 km beneath the Sierra Nevada underlying a relatively low density mantle [11, 48]. Zandt and Ruppert [11] have recently proposed that the high velocity anomaly represents a delaminated lower crustal ("eclogitic") fragment.

Melting of the eclogitic keel from beneath the Sierra Nevada [10] would probably not be able to produce alkali-rich, SRG-like compositions, if only garnet and clinopyroxene were present. Moreover, a dry assemblage such as garnet + clinopyroxene would not melt upon being transported downwards adiabatically in the mantle, at least not at shallow depths in the mantle. Hornblende is a common accessory mineral in the dense assemblages of the Sierra Nevada root [10]. The presence of this (or other) hydrous mineral may trigger dehydration melting during root foundering. The pre-Pliocene Cenozoic temperatures of the Sierra Nevada lowermost crust were ~ 600-700 ^{0}C [10], while the Pliocene peridotitic mantle temperatures were ~1150-1200 ^{0}C [this study, and 10]. If the "eclogitic" root were to delaminate, the temperatures along the contacts between hot peridotitic mantle and the "root" material (850-900 ^{0}C) would be high enough to

Figure 6-5. Cartoon showing schematically the processes which may have led to the incorporation of SRG in peridotites. The diagrams are EW cross sections perpendicular to the axis of Sierra Nevada Mountain range (SN). The vertical scale in each cross section is ~150 km. **a.** During Miocene (8-12 My), the Sierra Nevada was underlain by a thick mafic-ultramafic lower crustal root, consisting mainly of eclogite facies rocks at depths greater than ~35-40 km. Melting of the root during the time interval 8-3.5 My may be the source of SRG investigated in this study. Two possible scenarios for lower crustal melting, not necessarily exclusive, are discussed in the text: **b.** intrusion of hot peridotite into the eclogitic root, and **c.** delamination (foundering) of the eclogitic root into the peridotitc mantle.
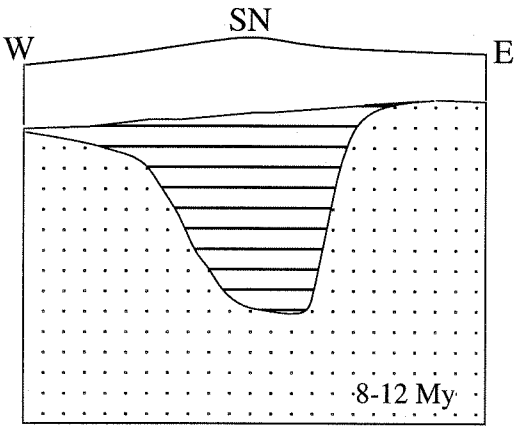
a.
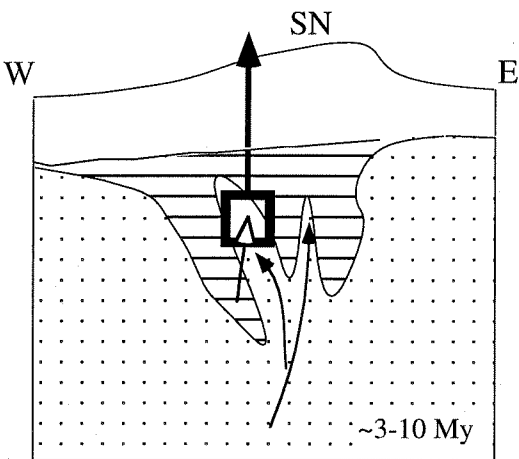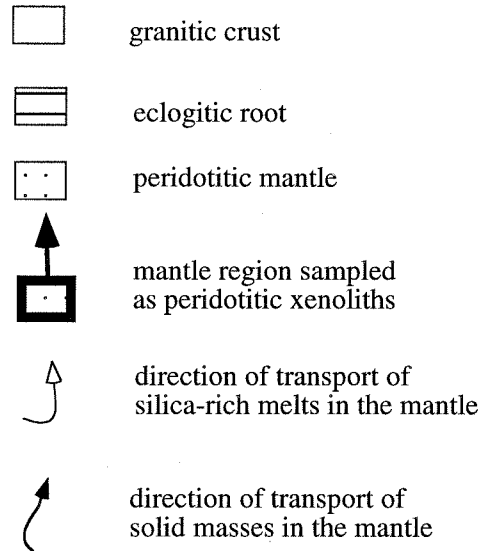
b.
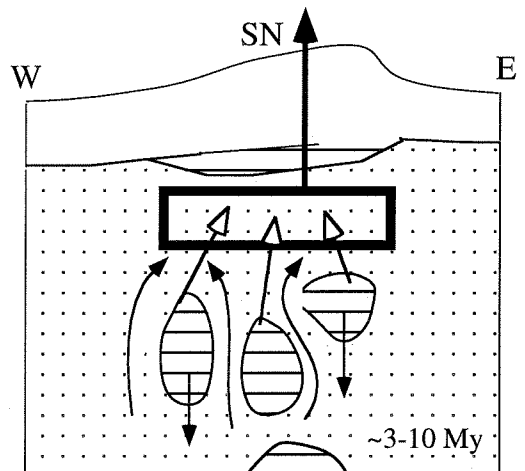
c.

produce dehydration-melting of hornblende-rich material (e.g., hornblende-garnet pyroxenites), at pressures up to ~ 3 GPa [49] . Therefore, we hypothesize that the glasses analyzed in this study are small volume melts of hornblende-bearing areas along the edges of lower crustal blocks foundering into the mantle (Figure 6-5a).

Alternatively, hot upwelling mantle may have intruded diapirically into the lower crust, causing melting of the crust and infiltration of these melts into peridotites (Figure 6-5b). The two scenarios (crustal foundering vs. mantle upwelling) are not necessarily exclusive. In fact, if the crust-mantle interactions were extensive beneath the Sierra Nevada during the Late Cenozoic, as indicated by the lower crustal (root) removal constraints, crustal foundering requires mantle upwelling and vice versa, assuming that the Sierra Nevada has not experienced Basin and Range-type lateral extension [47].

Sediment subduction is commonly viewed as the main mechanism of recycling continental crustal mass into the mantle [50]. There is no evidence for oceanic plate subduction beneath central California during Pliocene [51]. However, the Sierra Nevada region represented an active magmatic arc or forearc region for ~ 200 Ma at the convergent margin between the Pacific (oceanic) plate and the North American continent [51]. While some of the SRG trace elements investigated in this study are suggestive of lower crustal source rocks, and are therefore inconsistent with a sediment origin, further work is required to sort out the contribution from various possible crustal pollutants in the Sierra Nevada uppermost mantle and other continental mantle wedges.

References

[1] P. Schiano and R. Clocchiatti, Worldwide occurrence of silica-rich melts in sub-continental and sub-oceanic mantle minerals, Nature, 368, 621-624, 1994.

[2] E. Zinngrebe, S.F. Foley, Metasomatism in mantle xenoliths from Gees, West Eifel, Germany: evidence for the genesis of calc-alkaline glasses and metasomatic Ca-enrichment, Contrib. Mineral. Petrol., 122, 79-96, 1995.

[3] I.E., Ertan and W.P. Leeman, Metasomatism of Cascades subarc mantle: Evidence from a rare phlogopite orthopyroxenite xenolith, Geology, 24, 451-454, 1996.

[4] D.A. Ionov, A.W. Hofmann, and N. Shimizu, Metasomatism-induced melting in mantle xenoliths from Mongolia, J. Petrology, 35, 753-785, 1994.

[5] D.S. Draper, Spinel lherzolite xenoliths from Lorena Butte, Simcoe Mountains, Southern Washington (USA), J. Geology, 100, 766-776, 1992.

[6] A.D. Edgar, F.E. Lloyd, D.M. Forsyth, and R.L. Barnett, Origin of glass in upper mantle xenoliths from the Quaternary volcanic rocks of Gees, West Eifel, Germany, Contrib. Mineral. Petrol., 103, 277-286, 1989.

[7] S.M. Eggins, R.L. Rudnick, and W.F. McDonough, The composition of peridotites and their minerals: A laser ablation ICP-MS study, Earth. Planet. Sci. Lett., in press.

[8] G.M. Yaxley, V. Kamenetsky, D.H. Green, and T.J. Faloon, Glasses in mantle xenoliths from western Victoria, Australia, and their relevance to mantle processes; Earth. Planet. Sci. Lett., 148: 433-446.

[9] P. Schiano, R. Clocchiatti, N. Shimizu, R.C. Maury, K.P. Jochum, and A.W. Hofmann, Hydrous, silica-rich melts in the sub-arc mantle and their relationship with erupted arc lavas, Nature, 377, 595-600, 1995.

[10] M. N. Ducea, and J. Saleeby, Buoyancy sources for a large unrooted mountain range, the Sierra Nevada, California; Evidence from xenolith thermobarometry, J. Geophys. Res., 101, 8229-8244, 1996.

[11] G. Zandt, S. Ruppert, Lower crustal detachment and the evolution of the continental crust; Evidence from the Sierra Nevada (abstract), EOS, Trans. AGU, 77, 831, 1996.

[12] D.L Turcotte, J.Y. Liu, and F.H Kulhavy, The role of an intracrustal asthenosphere on the behavior of major strike-slip faults, J. Geophys. Res., 89, 5801-5816, 1984.

[13] R. W. Kay, and S. M. Kay, Creation and destruction of lower continental crust, Geol. Rundsch., 80, 259-270, 1991.

[14] R.L. Rudnick, Making continental crust, Nature, 378, 571-578, 1995.

[15] R. W. Kay, and S. M. Kay, Delamination and delamination magmatism, Tectonophysics, 219, 177-189, 1993.

[16] J.G. Moore, and W.J. Nokleberg, Geologic map of the Tehipite Dome Quadrangle, Fresno County, California, U.S. Geol. Surv., Map GQ-1676, 1991.

[17] H.G. Wilshire, et al., Mafic and ultramafic xenoliths from volcanic rocks of the western United States, U.S. Geol. Surv. Prof. Pap., 1443, 179 p, 1988.

[18] G.K. van Kooten, Mineralogy, geochemistry and petrology of an ultrapotassic basaltic suite, central Sierra Nevada, California, USA, J. Petrol., 21, 631-684, 1980.

[19] M. Ducea and J. Saleeby, Rb-Sr and Sm-Nd mineral ages of some Sierra Nevada xenoliths; Implications for crustal growth and thermal evolution (abstract), EOS, Trans. AGU, 77, 831, 1996.

[20] G. P. Brey and T. Köhler, Geothermometry in four phase lherzolites. II. New thermobarometers, and practical assessment of existing thermobarometers, J. Petrol., 31, 1353-1378, 1990.

[21] T. P. Köhler and G.P. Brey, Calcium exchange between olivine and clinopyroxene calibrated as a geothermometer for natural peridotites from 2 to 60 kbar with applications, Geochim. Cosmochim. Acta, 54, 2375-2388, 1990.

[22] G. Chazot, M.A. Menzies, and B. Harte, Determination of partition coefficients between apatite, clinopyroxene, amphibole and melt in natural spinel lherzolites from Yemen: Implications for wet melting of the lithospheric mantle, Geochim. Cosmochim. Acta, 60, 423-437, 1996.

[23] M.J. LeBas, R.W. LeMaitre, A. Streckeisen, and B. Zanettin, A chemical classification of volcanic rocks based on the total alkali-silica diagram, J. Petrol., 27, 745-750, 1986.

[24] T.N. Irvine and W.R.A. Baragar, a guide to the chemical classification of the common volcanic rocks, Canad. J. Earth. Sci., 8, 523-548, 1971.

[25] J. T. Armstrong, Quantitative analysis of silicates and oxide materials; Comparison of Monte Carlo, ZAF, and f (rz) procedures, in *Microbeam analyses*, 1988, edited by D.E. Newburry, 239-246, San Francisco Press, San Francisco, 1988.

[26] N. Shimizu and S.R.A. Hart, Applications of the ion microprobe techiques to geochemistry and cosmochemistry, Ann. Rev. Earth. Planet. Sci., 10, 483-526, 1982.

[27] G.J. Wasserburg, S.B. Jacobsen, D.J. DePaolo, M.T. McCulloch, and T. Wen, Precise determination of Sm/Nd ratios, Sm, and Nd isotopic abundances in standard solutions, Geochim. Cosmochim. Acta., 45, 792-805, 1981.

[28] Y. Niu and R. Batiza, DENSCAL: A program for calculating densities of silicate melts and mantle minerals as a function of pressure, temperature, and composition in melting range, Comp. Geosci., 17, 679-687, 1991.

[29] G. Faure, Principles of isotope geology, John Wiley and Sons, New York, 590 p., 1986.

[30] E. Jagoutz, R.W. Carlson, and G.W. Lugmair, Equilibrated Nd-unequilibrated Sr isotopes in mantle xenoliths, Nature, 286, 708-710, 1980.

[31] J.D. Blum, Y. Erel, and K. Brown, $^{87}Sr/^{86}Sr$ ratios of Sierra Nevada stream waters; Implications for relative mineral weathering rates, Geochim. Cosmochim. Acta, 58, 5019-5025, 1994.

[32] M.A. Domenick, R.W. Kistler, F.C.W. Dodge and M. Tatsumoto, Nd and Sr isotopic study of crustal and mantle inclusions from the Sierra Nevada and implications for batholith petrogenesis, Geol. Soc. Am. Bull., 94, 713-719, 1983.

[33] B. Mukhopadhyay, Petrology and geochemistry of mafic and ultramafic xenoliths from the Sierra Nevada batholith; Ph.D. dissertation, 215 p, Univ. of Texas at Dallas, 1989.

[34] F.C.W. Dodge, L.C. Calk, and R.W. Kistler, Lower crustal xenoliths, Chinese Peak lava flow, Central Sierra Nevada, J. Petrol., 27, 1277-1304, 1988.

[35] B. Mukhopadhyay, and W.I. Manton, Upper mantle fragments from beneath the Sierra Nevada batholith- partial fusion, fractional crystallization and metasomatism in a subduction-related ancient lithosphere, J. Petrol., 35, 1418-1450, 1994.

[36] B.L. Beard, and A.F. Glazner, Trace element and Sr and Nd isotopic composition of mantle xenoliths from the Big Pine Volcanic Field, California, J. Geophys. Res., 100, 4169-4179, 1995.

[37] M.B. Baker, M.M. Hirschmann, M.S. Ghiorso, and E.M. Stolper, Compositions of near-solidus peridotite melts from experiments and thermodynamic calculations, Nature, 375, 308-311, 1995.

[38] S.M. Peacock, T. Rushmer, and A.B. Thompson, Partial melting of subducting oceanic crust, Earth. Planet. Sci. Lett., 121, 227-244, 1994.

[39] M.T. McCulloch, R.T. Gregory, G.J. Wasserburg, and H.P. Taylor, A neodymium, strontium, and oxygen isotopic study of the Cretaceous Samail ophiolite and implications for the petrogenesis and seawater-hydrothermal alteration of the oceanic crust, Earth. Planet. Sci. Lett., 46, 201-211, 1980.

[40] G.T. Nichols, P.J. Wyllie, and J.R. Stern, Subduction-zone melting of pelagic sediments constrained by melting experiments, Nature, 371, 375-378, 1994.

[41] S.M. McLennan, S.R. Taylor, M.T. McCulloch, and J.B. Maynard, Geochemical and Nd-Sr isotopic composition of deep-sea turbidites; Crustal evolution and plate tectonic associations, Geochim. Cosmochim. Acta, 54, 2015-2050, 1990.

[42] J.P. Riley and R. Chester, Introduction to marine chemistry, Academic Press, London, 465 p., 1971.

[43] S.R. Taylor and S.M. Lennan, The continental crust; Its composition and evolution, 312 p., Blackwell Scientific, Cambridge, Mass., 1985.

[44] M. Wolf and P.J. Wyllie, Dehydration melting of solid amphibolite at 10 kbar-textural development, liquid interconnectivity, and applications to the segregation of magma, Miner. Petrol., 44, 151-179, 1991.

[45] G. M. Yaxley and D.H. Green, Reactions between eclogite and peridotite: Mantle refertilization by subduction of oceanic crust, submitted.

[46] T.A. Dumitru, Subnormal Cenozoic geothermal gradients in the extinct Sierra Nevada magmatic arc: Consequences of Laramide and post-Laramide shallow angle subduction, J. Geophys. Res., 95, 4925-4941, 1990.

[47] B. Wernicke, et al., Origin of high mountains on continents: The Southern Sierra Nevada, Science, 271, 190-193, 1996.

[48] C. Jones, H. Kanamori, and S.W. Roecker, Missing roots and mantle drips: Regional P_n and teleseismic arrival times in the southern Sierra Nevada and vicinity, California, J. Geophys. Res., 99, 4567-4601, 1994

[49] P.J. Wyllie and M.B. Wolf, Amphibolite-dehydration melting: Sorting out the

solidus, in *Magmatic processes and plate tectonics*, eds: H.M. Pritchard et al., Geol. Soc. Spec. Paper, 76, 405-416, 1993.

[50] T. Plank and C.H. Langmuir, Tracing trace element from sediment input to volcanic output at subduction zones, Nature, 362, 739-742, 1993.

[51] W. Dickinson, Plate tectonics and the continental margin of California, in W.G. Ernst (ed.) The geotectonic development of California, Prentice-Hall, Englewood Cliffs, N.J., 1-28, 1981.

Appendix 6-1- Analytical procedures

Whole rock compositions of the host rocks were determined on an automated, wavelength-dispersive, Rigaku 3070 X-ray fluorescence spectrometer. Samples were powdered in a tungsten carbide grinding mill and oven-dried for 24 hours before weighing. Aliquots weighing 0.8 grams were fused with lithium tetraborate-lithium carbonate flux containing La_2O_3 as a heavy absorber and cast into a glass disc. USGS, NBS, and SSC standards were used for calibration. The accuracy and precision of the analyses are given in Table 6-1.

The major element chemical composition of the xenolith minerals and glass inclusions were obtained using a JEOL 733 electron microprobe fitted with five wavelength spectrometers. Polished thin sections were initially carbon coated. The accelerating voltage on the microprobe was 15 keV, with a probe current of 25 nA (measured on brass), count times of 60-80 seconds, and a probe diameter of 10 μm. Sodium was analyzed first in order to reduce alkali migration. Element standards were well-characterized silicates and oxides, and the data were corrected using the CITZAF correction program [25].

Trace elements of the glass inclusions were analyzed by Secondary Ion Mass Spectrometry (SIMS) using a modified Cameca IMS-3F ion microprobe. The one-inch

diameter polished sections were those previously analyzed for major element concentrations. The primary beam was focused onto a 30 µm diameter glass spot. Samples were bombarded by a 14.5 KeV O⁻ primary beam with a 5 to 15 nA ion current. Positive secondary ions were then extracted and accelerated to ~4500 eV. The SIMS analytical procedures followed techniques previously described [26].

In order to perform trace element and isotopic analyses on the glass inclusions, we had to handpick and acid leach the samples. Two xenoliths (SC9 and H8-1) were crushed to about 1/3 of their average grainsize. A 1-2 minutes mild acid leaching in cold, 0.25N HCl was performed initially in order to clean any potential surficial grainboundary contaminants. The glass films were identified under a binocular microscope as translucid brownish stains, distinct from the green color of the lherzolite phases. The stained grains were separated and then leached in warm 6N HCl, followed by another inspection under binocular microscope. The grains that contained stains after HCl leaching were further separated and leached in a warm mixture 3N HNO_3 and 3N HF. The leachate concentrations were determined by weighing samples before and after each leaching step.

The residues after leaching, an unleached fragment of SC9, and the two host volcanics were dissolved in hot $HF-HNO_3$ and cold $HF-HClO_4$ mixtures in Teflon beakers. We used 100-200 mg of sample aliquoted from a larger homogenized sample mass, which varied from 5-10 grams (xenoliths) to 200 grams (host volcanics). The samples were then taken up in 1N HCl and any residue was dissolved in the same way. All samples, including the leachates, were then spiked with ^{87}Rb, ^{84}Sr, and mixed ^{147}Sm-^{150}Nd tracer solutions. The spikes were calibrated against NIMS-SRM materials for Rb and Sr, and against a mixed Sm-Nd standard described in [27].

The chemical separation procedures and filament loading are as in [27]. Mass spectrometric analyses were carried out on an automated VG Sector multicollector instrument fitted with adjusTable 6-10^{11} Ω Faraday collectors and a Daly photomultiplier.

Concentrations of Rb, Sr, Sm, and Nd were determined by isotope dilution, with isotopic compositions of Sr and Nd determined on the same spiked runs. Rb and Sm were run statically, Sr was analyzed multidynamically, using a four collector peak switch scheme, whereas Nd was analyzed multidynamically using a five collector scheme. An offline manipulation program was used for isotope dilution calculations.

Appendix 6-2. Mass balance calculations

The Sr and Nd elemental concentrations and isotopic ratios of the glass can be calculated using the residue and leach data combined with the determination of glass abundance in xenolith. The main assumptions in this calculation are (1) the residue has elemental concentrations and isotopic ratios of the lherzolite, and (2) the fraction of lherzolite that dissolves in the leach has the same concentrations and isotopic ratios as the residue. We will exemplify the calculation for the Sr elemental concentration case; obviously these equations can be applied to Nd, or any other element, as well as to determine isotopic ratios.

The validity of the first assumption is explained in the text. It can be written as:

$$Sr_{lherzolite} = Sr_{residue} \quad (1)$$

The second assumption requires that (a) isotopically the lherzolites are equilibrated, and (b) although the three main minerals present in lherzolites (olivine, orthopyroxene, and clinopyroxene) have different elemental concentrations (including Sr, and Nd), there is no noticeable difference in the rate of dissolution between them.

The mass balance equation for Sr concentration can be written as:

$$m_{residue}Sr_{residue} + m_{leach}Sr_{leach} = m_{lherzolite}Sr_{lherzolite} + m_{glass}Sr_{glass} \quad (2)$$

We also know the total mass of the xenolith used for analysis, m_{total}:

$$m_{total} = m_{residue} + m_{leach} \quad (3); \quad g = \frac{m_{residue}}{m_{total}} \quad (4)$$

The thin section investigation of the specimens yield information about the abundance of glass, namely the volume fractions F of lherzolite and glass. They can be converted into mass fractions (f) given the densities (ρ) of lherzolite and glass. We have calculated the 1 bar densities of the lherzolite and glass using a modified version of the program provided by Niu and Batiza [25], and assumed no porosity in the samples.

$$f_{lherzolite} = \frac{\rho_{lherzolite}F_{lherzolite}}{\rho_{lherzolite}F_{lherzolite} + \rho_{glass}F_{glass}} \quad ; f_{glass} = \frac{\rho_{glass}F_{glass}}{\rho_{lherzolite}F_{lherzolite} + \rho_{glass}F_{glass}} \quad (5)$$

Introducing (3), (4), and (5) into (2), we obtain:

$$gSr_{residue} + (1-g)Sr_{leach} = f_{lherzolite}Sr_{residue} + f_{glass}Sr_{glass}$$

which can be rearranged as:

$$Sr_{glass} = \frac{(g - f_{lherzolite})Sr_{residue} + (1-g)Sr_{leach}}{f_{glass}} \quad (6)$$

Equation (6) gives the elemental concentration Sr (in this case) of the glass end member. Similarly, elemental concentrations and isotopic ratios can be determined.

CHAPTER 7

A Case for Delamination of the Deep Batholithic Crust Beneath the Sierra Nevada, California

Mihai Ducea and Jason Saleeby

Abstract. Surface exposures as well as deep-crustal and upper-mantle xenoliths constrain the composition of the lithospheric column beneath the Sierra Nevada mountain range (California) as it resulted from the generation of the Mesozoic Sierra Nevada batholith (SNB). After the cessation of magmatism at ~80 Ma, the SNB consisted of a ~30 to 35 km thick granitic crust underlain by a batholithic "root," a ~70 km thick sequence of mafic-ultramafic, mainly eclogite-facies cumulate and residues. The deeper root assemblages consist largely of garnet and pyroxenes that precipitated as igneous cumulate phases during the SNB magmatism. The root assemblages were present beneath the SNB as recently as ~8 to 12 Ma, when they were sampled as xenoliths in fast-ascending magmas erupted through the batholith.

Several lines of evidence suggest that the eclogitic root may have disappeared from beneath the SNB since Miocene time, leading to a major change in the lithospheric column. There are no garnet-bearing xenoliths in the Pliocene and Quaternary volcanic rocks; instead, all xenolith lithologies found in the younger volcanic outcrops are peridotitic, have equilibrated at depths between 35 and 70 km, possess locked-in temperatures of ~1150 to 1200 ^{0}C, and display an asthenospheric-like adiabatic P-T trend. Some of the Pliocene uppermost-mantle peridotitic xenoliths contain exotic silica-rich glass inclusions that may have originated by partial melting of the eclogitic root. Geophysical evidence suggests that anomalously high seismic velocity may represent eclogitic bodies present at depths of 100 to 200 km beneath the SNB. All of these observations indicate that the ``eclogitic'' root may have detached and delaminated

(sunk) into the underlying mantle, a process compensated by diapiric rise of asthenospheric peridotitic material to the base of the shallow (~35 km) remnant crust. The delamination hypothesis is consistent with observations documenting the existence of a shallow Moho, a low-velocity, partially molten upper mantle observed today beneath the SNB, a gradual change in Miocene volcanism in the Sierra toward more primitive compositions, and significant late Miocene-Pliocene uplift in the area.

If the magmatic arc has indeed lost its root, delamination is an important mechanism in the differentiation of the continental crust at Cordilleran-type margins. The present-day crustal column in the Sierra (the SNB) is a mass extracted from the Earth's mantle predominantly during the Phanerozoic, although not necessarily only during batholithic magmatism. The ~35 km thick present-day crustal composition of the Sierra Nevada is similar to, or more evolved than, the average continental crust.

7.1. Introduction

Continental margins riding over subducting oceanic plates often are accompanied by large-scale granitic magmatism that leads to the formation of batholiths. Some of the largest batholiths on Earth are found in the American Cordillera, along the western margins of the American continents. The Sierra Nevada batholith (SNB) of California is the type-Cordilleran batholith (Bateman, 1983).

Deep segments of thick crustal sections in orogenic belts, including continental magmatic arcs, are prone to eclogite-facies metamorphism (e.g., Dewey et al., 1993), which leads to the formation of crustal roots denser than the underlying mantle. Most young and extinct continental arcs display a shallow Moho (30 to 40 km crustal thickness) (Christensen and Mooney, 1995) and are underlain by typical peridotitic mantle material. This observation contradicts the petrological prediction that thick, residual, garnet-rich and olivine-poor mafic-ultramafic masses should reside beneath granitic batholiths (e.g., Kay and Kay, 1991). Kay and Kay (e.g., 1991, 1993) have

proposed that eclogite-facies magmatic arc roots (e.g., in the Andes) become gravitationally unstable and founder into the underlying mantle.

The Sierra Nevada mountain range exemplifies this contradiction. The Sierra Nevada crustal thickness is ~35 to 42 km (e.g., Wernicke et al., 1996; Fliedner and Ruppert, 1996), and the crust is almost entirely ``granitic'' (compressional velocities of 6 to 6.3 km/sec). The sub-Moho material appears to be partially molten peridotite (Jones and Phinney, 1997). In contrast, deep-crustal and mantle xenoliths accidentally sampled by Miocene (8 to 12 Ma) volcanic rocks indicate the presence of a thick eclogitic root beneath the Sierra Nevada as late as Miocene time (Ducea and Saleeby, 1996a). In this paper, we present evidence that suggests that the eclogitic arc root has delaminated into the upper mantle since Miocene time. This process can explain the apparent contradiction between the predicted and observed lithospheric sections. If viable, arc-root delamination may be the most efficient process responsible for Phanerozoic granitic crustal addition.

7.2. Volcanic Rocks

Late Cenozoic volcanic rocks as well as lower-crustal and mantle xenoliths contain some of the most important information concerning the composition of the Sierra Nevada at depth. Many of the observations used in this study to argue for crustal delamination are based on studies of volcanic rocks and xenoliths from the Sierra Nevada. As background information, we provide below a brief description of the Late Cenozoic volcanism in the southern and central Sierra Nevada.

Late Cenozoic mafic to intermediate rocks erupted through the Mesozoic batholith in the southern and central Sierra Nevada (Moore and Dodge, 1980; van Kooten, 1980; Luedke and Smith, 1981; Ormerod et al., 1988), probably as a result of extensional collapse of the Cordillera at Sierra Nevada latitudes. The Late Cenozoic mafic to intermediate volcanic activity in the Sierra Nevada can be temporally divided

into three episodes (Moore and Dodge, 1980): late Miocene (8 to 12 Ma), Pliocene (3 to 4 Ma) and Quaternary (0 to 1 Ma).

Figure 7.1 is a map showing the distribution of mafic to intermediate Late Cenozoic volcanic rocks in the Sierra Nevada at latitudes south of 38^0 N. The hachured fields in Figure 7.1 cover the areas in which various mafic-intermediate volcanic exposures have been mapped. The volcanic rocks consist of dikes, plugs, and flows and occupy a small area (~1%) of the hachured areas in Figure 7.1. The Miocene volcanic rocks (MV) are mainly subvolcanic conduits, whereas most Pliocene volcanics (PV) and Quaternary volcanics (QV) are lava flows.

There are sufficient published radiometric data on these rocks to show that both MV and PV cluster in fields elongated in an ENE-WSW direction, as shown in Figure 7.1. These fields can be followed across the Owens Valley rift into the White-Inyo Mountains. The MV and PV fields alternate from north to south, except for a gap at the latitude of Mount Whitney. Volcanic rocks younger than 1 Ma (QV) erupted along the eastern margin of the Sierra Nevada, more or less following the NNW-SSE trend of the Owens Valley rift. At least 19 of the volcanic outcrops, representing all three age groups, contain xenoliths from the Sierra Nevada lower crust and upper mantle.

7.3. Cretaceous to Miocene Lithospheric Column

The Sierra Nevada mountain range consists primarily of a large composite batholith. We will refer to the exposed fragments of these plutons as the Sierra Nevada batholith. The SNB represents ~90% of the surface exposures in the southern and central Sierra. The magmatic arc formed as a product of prolonged ocean-floor subduction beneath the southwestern edge of the North American continent (Dickinson, 1981). Magmatism occurred in the Sierra Nevada between 220 and 80 Ma (Chen and Moore, 1982), although most of the plutons exposed at the surface yield ages between 125 and 85

Ma (Saleeby, 1990). Below we summarize the geologic information that constrains the composition of the Sierra Nevada lithosphere at the end of the batholithic magmatism. Apparently, the section remained intact in the central Sierra until at least 8 to 12 Ma, but subsequently changed, at least at depths greater than ~35 km.

An idealized lithospheric column based on observations made in the central Sierra Nevada is shown in Figure 3.7. This section was constructed on the basis of the geology of the surface batholith (see reviews in Bateman, 1983 and Saleeby, 1990), geophysical observations in the upper part of the column (Fliedner and Ruppert, 1996; Wernicke et al., 1996), and petrologic, thermobarometric, and geochronometric studies of deep-crustal and mantle xenoliths in the MV that have been reported by the authors elsewhere (Ducea and Saleeby, 1996a, 1996b). Most SNB plutons are tonalitic to granodioritic in composition. The igneous crystallization depths of the rocks presently exposed vary from 0 to ~30 km (Ague and Brimhall, 1988; Saleeby, 1990). The deepest exposures of the batholith are preserved in the southernmost Sierra Nevada, where igneous and meta-igneous rocks have crystallized at 20 to 30 km depth in the crust during the late stages of magmatism of the Cretaceous batholith (Pickett and Saleeby, 1993). The average chemistry of these deep exposures corresponds to that of a low-silica tonalite (Saleeby, 1990). Therefore, geological results indicate that throughout the upper 30 km of the Mesozoic Sierra Nevada lithosphere, the rocks are mainly "granitoids," suggesting that the SNB was at least 30 km thick. This conclusion is supported by recent geophysical results (Fliedner and Ruppert, 1996) that documented low compressional velocities (6 to 6.3 km/sec) throughout the seismologically defined crust, in a seismic refraction experiment undertaken across the southern part of the mountain range.

The composition of the Sierra Nevada lithosphere at depths greater than 30 to 35 km is constrained by xenoliths accidentally sampled by some of the Miocene volcanic plugs and dikes (Domenick et al., 1983; Dodge et al., 1986, 1988; Mukhopadhyay and Manton, 1994; Beard and Glazner, 1995; Ducea and Saleeby, 1996a). Only the MV carry

Figure 7.1. Schematic map of the distribution of Late Cenozoic volcanic rocks in the southern and central Sierra Nevada region, including the Owens Valley and White-Inyo mountains to the east. The volcanism is divided into three temporal groups-Miocene, Pliocene, and Quaternary-as in the text. Volcanic rocks cover only ~1% of the areas outlined as volcanic fields. Miocene and Pliocene volcanic groups alternate from north to south in the Sierra Nevada, with the exception of a volcanic "gap" between the Kings River and Kern River fields. Locations of the xenolith-bearing areas of Scepter Creek (SC) and Blue Knob (BK), mentioned in text, are indicated by black squares.
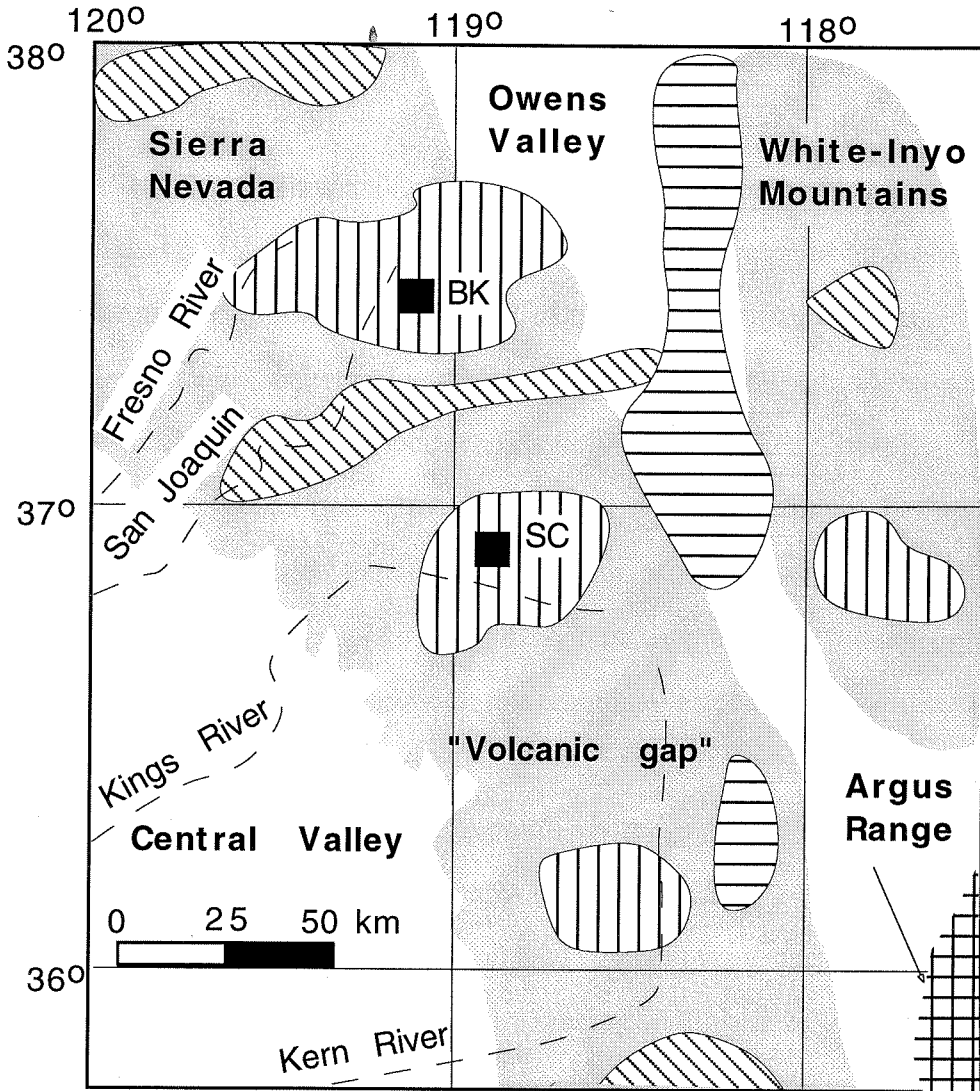
Areas covered mainly by pre-Cenozoic rocks

Areas covered mainly by Cenozoic rocks

Miocene volcanic field

Pliocene volcanic field   ■ SC- Scepter Creek, BK- Blue Knob

Quaternary volcanic field

deep samples proven to be related to the Mesozoic lithosphere beneath the SNB (Ducea and Saleeby, 1996a). A thermobarometric study conducted by Ducea and Saleeby (Ducea and Saleeby, 1996a) suggested that mafic rocks (diorites, gabbros) become progressively more abundant in the 30- to 40-km depth interval, although quantitative barometric determinations are not available for garnet-free diorites and gabbros. Many of the deep xenoliths in the MV contain garnet, and representative lithologies have been analyzed for thermobarometry and dated by Sm-Nd techniques (Ducea and Saleeby, 1996b). The results provide a link between the pressures of equilibration (and inferred depths) and the time at which pressures were locked in the mineral-chemistry equilibrium. All analyzed rocks yield Cretaceous (81 to 136 Ma) Sm-Nd ages as well as initial Sr-, Nd-, Pb-, and O-isotopic ratios similar to the SNB, suggesting batholith consanguinity. Most of the xenoliths have igneous cumulate textures. Textural, whole-rock isotopic, geochronologic, and trace-element arguments all point to a cumulate/residua origin for most of the garnet-rich xenoliths from the MV.

Garnet-bearing feldspathic xenoliths with intermediate to mafic compositions generally display equilibration pressures lower than 1.2 GPa (~40 km), while feldspar-free, mainly garnet pyroxenite and hornblende garnet pyroxenite xenoliths equilibrated at pressures exceeding 1.0 GPa (~35 km), reaching as high as 3.3 GPa (~100 km). A few xenoliths whose pressures of equilibration were calculated to be in the 1 to 1.4 GPa (~35 to 45 km) interval are cumulates with alternating feldspar-rich and garnet pyroxene-rich layers.

We interpret these observations as indicating a downward transition to gradually more mafic lithologies, and from feldspathic to feldspar-free ("eclogitic") assemblages. Our data suggest that such a transition may have occurred 35 to 45 km beneath the surface of the SNB.

Rocks that equilibrated at pressures higher than 1.5 GPa are mainly garnet pyroxenites and eclogites. The relatively elevated $\delta^{18}O$ ratios (6.5 to 9) in these xenoliths

(Ducea et al., 1997) require the presence of a supracrustal component ~45 to 100 km beneath the batholith, and argues for a crustal rather than a mantle origin for the pyroxenites. We interpret the garnet pyroxenitic xenoliths as being the predominant lithologies of a deep-crustal, eclogite-facies batholithic root (MASH zone of Hildreth and Moorbath, 1988), which extended to at least 100 km. We also have recovered peridotitic xenoliths (spinel-garnet and garnet) that equilibrated at pressures of 2.5 to 4.2 GPa (~75 to 130 km), indicating that a transition from eclogitic to peridotitic material may have existed at depths somewhere between 75 and 100 km. All analyzed xenoliths, including the deepest garnet peridotite, possess isotopic characteristics consistent with a lithospheric origin. The relatively low temperatures measured in all deep xenoliths, e.g., 975 ^{0}C at 4.2 GPa (130 km) in the deepest sample, also suggest a lithospheric origin. The Mesozoic to middle Miocene lithosphere therefore was at least 130 km thick.

In conclusion, the Sierra Nevada Late Mesozoic to Miocene lithosphere appears to have been composed of granitoids ~30 km in thickness, about twice as much residues and cumulates (mainly ultramafic rocks in eclogite facies), and deeper peridotites; in aggregate, these units constrain the minimum thickness of the post-batholith lithosphere to be at least 130 km.

7.4. Observations Supporting Root Delamination

Three geological and geophysical observations suggest that the eclogitic lower crust has delaminated, possibly together with its underlying mantle lithosphere, since the Miocene. They are: (1) contrasting xenolith populations in the MV and PV-QV; (2) the presence of crustal-derived silicic glass inclusions in peridotitic xenoliths from PV and QV; and (3) the existence of anomalously fast (high-compressional-velocity) bodies at great depth beneath the Sierra Nevada today.

Temporal change in xenolith lithology. Seventeen volcanic sequences of the three groups previously defined (MV, PV, and QV) contain lower-crustal and/or mantle

xenoliths. Xenoliths of the MV differ from the xenoliths in the PV and QV (Table 7.1.). Although the MV contains mainly garnet pyroxenites corresponding to equilibration depths of 40 to 100 km, the PV and QV contain only spinel peridotites and olivine-clinopyroxenites that equilibrated between ~35 and 65 km. In fact, no garnet-bearing xenolith has been recorded from any PV or QV rock. The MV xenoliths display a negative P-T slope, indicative of cooling from near-igneous temperatures to the low Cenozoic thermal gradients of the Sierra Nevada (Ducea and Saleeby, 1996a). More specifically, we interpreted this trend to be a "false" geotherm: deeper rocks cooled more slowly and locked in younger, lower temperatures (Ducea and Saleeby, 1996a). The PV peridotites from the same depth interval, in contrast, are high-temperature assemblages that define an adiabatic P-T slope and have tectonitic textures.

Based on these thermobarometric arguments, we believe that the aforementioned differences in xenolith lithology between the MV and PV represent a fundamental change in composition and thermal structure beneath the batholith. This change must have taken place between 8 to 12 and 3 to 4 Ma, at least in the central Sierra areas rich in xenolith-bearing MV and PV units. These observations suggest that the cold, mainly eclogitic root of the SNB was replaced during the late Miocene by hot, peridotitic, asthenospheric-like mantle.

Crustal-derived glass inclusions in mantle xenoliths. Some of the spinel lherzolites and olivine clinopyroxenites included in the PV lavas contain glass inclusions trapped as films along grain boundaries and as pockets, commonly included in olivine. We reported in Ducea and Saleeby, 1998, the major- and trace-element compositions as well as Sr- and Nd-isotopic ratios of glasses included in peridotites from two PV localities, Scepter Creek and Blue Knob (Figure 7.1.), which are 75 km apart. Representative glass major-element concentrations are plotted on Harker diagrams in Figure 6.2., while the trace elements and isotopic ratios analyzed on two glass-rich xenoliths are presented in Table 6.5. Glass inclusions in both Scepter Creek and Blue

Table 7.1. Summary of relevant differences between the MV and PV-QV xenolith suites in the Sierra Nevada.

MV (8-12 My) xenoliths	PV-QV (0-4 My) xenoliths
Mainly cumulate-textured olivine-free lower crust (granulite and eclogite facies) at depths greter than 35 km	Olivine-rich (peridotitic) ultramafic assemblages at depths greater than 35 km
Rocks in the 35-100 depth interval have Cretaceous (synbatholithic) Sm-Nd ages	Rocks which equilibrated deeper than 35 yield Late Cenozoic ages
Garnet very common in lower crustal and upper mantle xenoliths	Garnet absent in all xenoliths
Rocks with crustal $\delta^{18}O$ are found as deep as 100 km	Rocks with crustal $\delta^{18}O$ are not found below ~35 km
Lithospheric P-T slopes, and temperatures <1000 ^{0}C as deep as 130 km	Adiabatic, asthenospheric P-T slopes and temperatures of 1200-1250 ^{o}C below 35 km

Knob peridotites have unusually high SiO_2 concentrations, commonly between 65 and 69% SiO_2. These silica-rich glasses (SRG) also are characterized by high alkali and alumina concentrations as well as low Mg, Fe, and Ca abundances (Ducea and Saleeby, 1998). The SRG are, on average, trachytic in composition. Similar SRG inclusions in mantle xenoliths described previously (e.g., Ionov et al., 1994; Schiano and Clocchiatti, 1994; Schiano et al., 1995) have been interpreted as exotic melts with respect to the peridotitic host. The large difference between the glass and peridotite chemical compositions, and the preservation of glassy material at mantle depths, indicates near contemporaneity of the SRG melting with the eruption of the xenolith-bearing basalts.

The glass $^{87}Sr/^{86}Sr$ (0.7077 to 0.7085) and $^{143}Nd/^{144}Nd$ (~0.51244) are higher than those of the residual peridotitic xenoliths and quite different from those of the host basalts (Figure 6.4). Therefore, the glasses are exotic with respect to the surrounding peridotites and the basalt hosts. Melting of a hydrous phase in the mantle (e.g., phlogopite or amphibole)-which, although not present in the analyzed samples, may exist at deeper levels in the Sierra Nevada mantle-could explain the radiogenic Sr signature as well as the enrichment in K_2O but not the high silica concentrations and the unusually low Rb/Sr ratios. Young subducted oceanic crust and the product of its partial melting may have a wide range of $^{87}Sr/^{86}Sr$ isotopic ratios, as a result of interactions with seawater (McCulloch et al., 1980), but the $^{143}Nd/^{144}Nd$ should remain fairly close to depleted MORB-like ratios (>0.5130). The SRG $^{143}Nd/^{144}Nd$ ratios are much lower, therefore negating a mafic oceanic crustal origin.

Overall, the K_2O/Na_2O > unit value is indicative of a continental origin for the glasses. These glasses could have formed by melting subducted sediments, which are similar to (if not fully derived from) a continental source. However, the high Sr/Nd and low Rb/Sr SRG ratios are indicative of a lower-crustal origin, as opposed to an upper-crustal derivation typical for oceanic sediments. The Sierra Nevada eclogitic root has precisely the $^{143}Nd/^{144}Nd$, $^{87}Sr/^{86}Sr$, Sr/Nd, and Rb/Sr ratios required for the SRG

source. In particular, the source rocks that upon melting would be likely to produce the trace-element and isotopic ratios measured in the SRG glasses would be amphibolites or hornblende garnet pyroxenites (Figure 6.2). Wolf and Wyllie (1993) have demonstrated experimentally that silica-rich glasses similar to the ones presented here can form by partially melting a basalt+H_2O protolith.

In conclusion, the SRG appear to be the products of late Miocene-Pliocene partial melting of the batholith root. These melts were incorporated into hot peridotitic assemblages where they were trapped and froze. These observations are consistent with the foundering of the batholith root and diapiric ascent of mantle peridotite at the new base of the remnant light crust.

The presence of high-velocity and high-density anomalies at great depth beneath the batholith. Geophysical data grossly characterize the present-day vertical dimension of the Sierra Nevada. A recent seismic refraction experiment performed across the axis of the SNB has revealed that the Sierra Nevada mountain range is underlain by a relatively thin (35-42 km) crust (Fliedner and Ruppert, 1996; Wernicke et al., 1996). At least two independent teleseismic data sets collected from the Sierra Nevada at different latitudes (Jones et al., 1994; Zandt and Ruppert, 1996) contain information on the existence of one or more dense and fast bodies at 100 to 200 km, which may represent fragments of the delaminated eclogitic keel.

Zandt and Ruppert (1996) have combined the crustal model proposed for the Sierra Nevada by Fliedner and Ruppert (1996) with a tomogram of the upper mantle beneath the Sierra Nevada to generate an E-W P-velocity cross section to ~200 km depth. Their results indicate the presence of a high-velocity anomaly in the upper mantle. The anomaly is most clearly defined at depths between 100 and 180 km; it has a nearly vertical cylindrical form and a model density of 3500 g/cm^3, typical of eclogites. These results may indicate that the eclogitic lowermost crust from beneath the Sierra Nevada

detached and sank into the mantle, leaving behind a relatively thin, felsic remnant crust, according to Zandt and Ruppert (1996).

Jones et al. (1994) used teleseismic data to define a similar high-velocity anomaly in the upper mantle beneath the southern Sierra Nevada, northwest of Lake Isabella. The N-S extent of this anomaly (named the "Isabella anomaly") is ~40 to 60 km. The compressional velocities of the Isabella anomaly are ~4 to 5% higher than its surroundings at depths between 100 and 200 km. The Isabella anomaly could represent a fragment of delaminated mantle lithosphere or eclogitic lowermost crust.

7.5. Proposed Sierra Nevada Delamination Model

The xenolith data suggest that the post-Cretaceous lithosphere contained a 40 to 70 km thick eclogite-facies mafic-ultramafic root underlying the granitic batholith. The densities of Sierran eclogites are at least 0.2 g/cm^3 higher than those of peridotite, the material in which the eclogite probably was rooted (Appendix 1 and Figure 7.2). On the basis of the observations presented above, we hypothesize that gravitational instability of the eclogitic root caused the splitting of the lithosphere at a depth of 35 to 40 km and its eventual delamination into the mantle. The foundered root probably was replaced by hot peridotitic mantle, which rose to the new base of the crust (Figure 6.5).

The trigger for this process is not understood. Geochronological data on xenoliths demonstrate that eclogitic assemblages existed as batholith cumulates since at least the Late Cretaceous (Ducea et al., 1997). The presence of garnet pyroxenites in volcanics with an age of 8 to 12 Ma indicates that the eclogitic keel resided under the SNB for at least 70 m.y. before it foundered into the mantle. Density itself is not a sufficient condition for delamination, as discussed by Kay and Kay (1991). The heat from the Basin and Range-type extension may have been the cause for an increase in the Sierra Nevada heat flow in the Late Cenozoic (Saltus and Lachenbruch, 1990). Heating of the

Figure 7.2. Density of the Sierra Nevada lower-crustal and upper-mantle xenoliths as a function of pressure, calculated using the program of Niu and Batiza (1991). We used average xenolith mineral chemistry for garnet, orthopyroxene, and clinopyroxene. We calculated the densitites of orthopyroxene, clinopyroxene, and average garnet pyroxenite (average modal composition mixture of the three minerals) at 650 ^{0}C and 950 ^{0}C, i.e., the temperature interval measure by thermometry in the "eclogitic" samples analyzed by Ducea and Saleeby (1996a). The garnet pyroxenites are significantly more dense than are peridotites at any upper-mantle depth of interest.
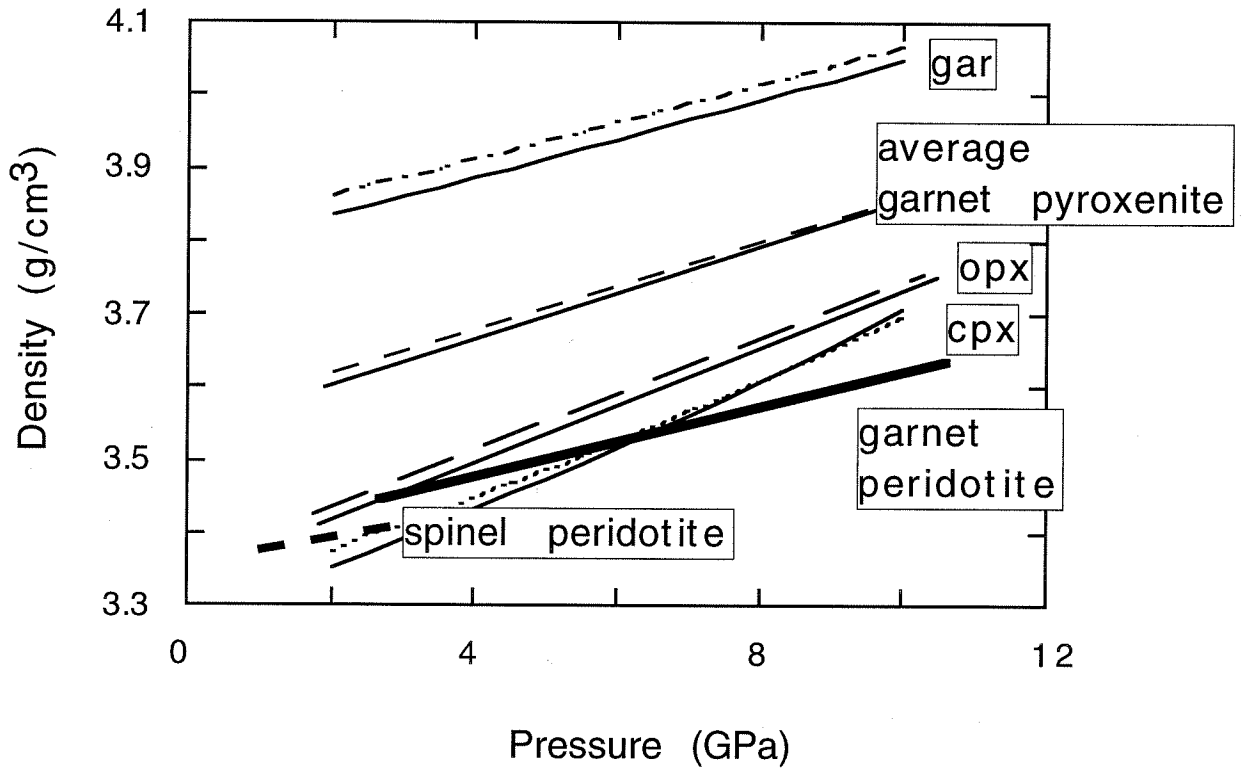
lithospheric column may significantly decrease the strength of the deepest levels rich in silica. Wernicke (1990) predicted lateral flow of a weak middle- to deep-crustal silica-rich layer in response to Basin and Range extension. The postulated mechanically weak layer at mid-crustal levels in the Sierra Nevada, perhaps near the transition from granitic to mafic lithologies, could enhance the splitting of the eclogitic root and result in its eventual delamination.

7.6. Predictions of the Delamination Hypothesis

Lower-crustal foundering must have a number of geological consequences (Kay and Kay, e.g., 1991, 1993), including (1) the upwelling of asthenospheric material at the base of the crust and an increase of the heat flow in the area; (2) a change in the regional style of volcanism toward more primitive, mantle-like magmas; and (3) regional uplift. Of course, none of the three processes mentioned above need to be generated by delamination, and therefore can not be used as a priori evidence for delamination. However, one would expect to see some evidence for all three in order to support the delamination hypothesis. In the Sierra Nevada, data exist that support the presence of shallow, partially molten asthenospheric mantle as well as the occurrence of a change in volcanism toward more primitive compositions. Evidence for late Miocene uplift also exists (e.g., Huber, 1981), although it has been questioned recently (Small and Anderson, 1996; Wernicke et al., 1996). Below we present the data that support delamination-model predictions for the Sierra Nevada.

Anomalously hot and slow sub-Moho mantle. The Jones et al. (1994) data set shows that the uppermost mantle (30 to 70 km) has relatively slow compressional velocities («7.6 km/s), indicating the presence of hot (asthenospheric?) material at the base of the crust. Upwelling of asthenosphere would be expected in response to the detachment of a dense crustal root. The presence of hot, buoyant asthenospheric mantle at

the base of the thin Sierra Nevada crust also has been suggested by the P-wave image of the upper mantle structure of the southern Sierra Nevada (Biasi and Humphreys, 1992), the teleseismic study of Benz et al. (1992) beneath the eastern part of the mountain range in northern California, and the larger-scale teleseismic study of Humphreys and Dueker (1994). At a regional scale, the uppermost (35 to 100 km) mantle beneath the western United States at the latitude of the Sierra Nevada alternates zones of high and low seismic velocities (Humphreys and Dueker, 1994), suggesting instability of a thick, pre-existing mantle lithosphere that in certain regions has been replaced by asthenosphere, possibly by diapiric ascent.

Humphreys and Dueker (1994) concluded that the low seismic velocities of the uppermost mantle beneath the Sierra Nevada are indicative of the presence of partial melt, expected from mantle volumes decompressing adiabatically as they rise to shallower levels in the mantle. Magnetotelluric data collected along a profile perpendicular to the Sierra Nevada axis show that the regions of slow, shallow-mantle seismic velocity also are characterized by extremely high electrical conductivity, most likely reflecting the presence of partial melt (Park et al., 1996). The presence of very young basaltic volcanic fields in the Sierra Nevada proper and along its eastern edge (e.g., Luedke and Smith, 1981) is consistent with these data.

Compositional change in regional volcanism. The MV appear to be distinct from the PV. The MV from the central Sierra Nevada on average are more silicic than the PV (Figure 7.3.). The MV and PV (trachyandesites, potassic and ultrapotassic basalts) are clearly distinct from the QV alkali basalts.

In order to avoid volcanic samples that may have been crustally contaminated, we have further analyzed only volcanic occurrences that carry lower-crustal and/or mantle xenoliths. Xenolith-bearing volcanic rocks are fast-ascending rocks that experienced a minimum of crustal interaction.

Figure 7.3. Histogram comparing the silica concentrations in MV (8 to 12 Ma) and PV (3 to 4 Ma) rocks from the central Sierra Nevada. Both data sets cover a wide range of SiO_2, but the younger volcanic rocks on average are more mafic. Data from Ducea and Saleeby (unpubl.) and Huber (1977).

Central Sierra Nevada

8-12 My
volcanic rocks

3-4 My
volcanic rocks

No. of analyses

SiO_2 (wt. %)
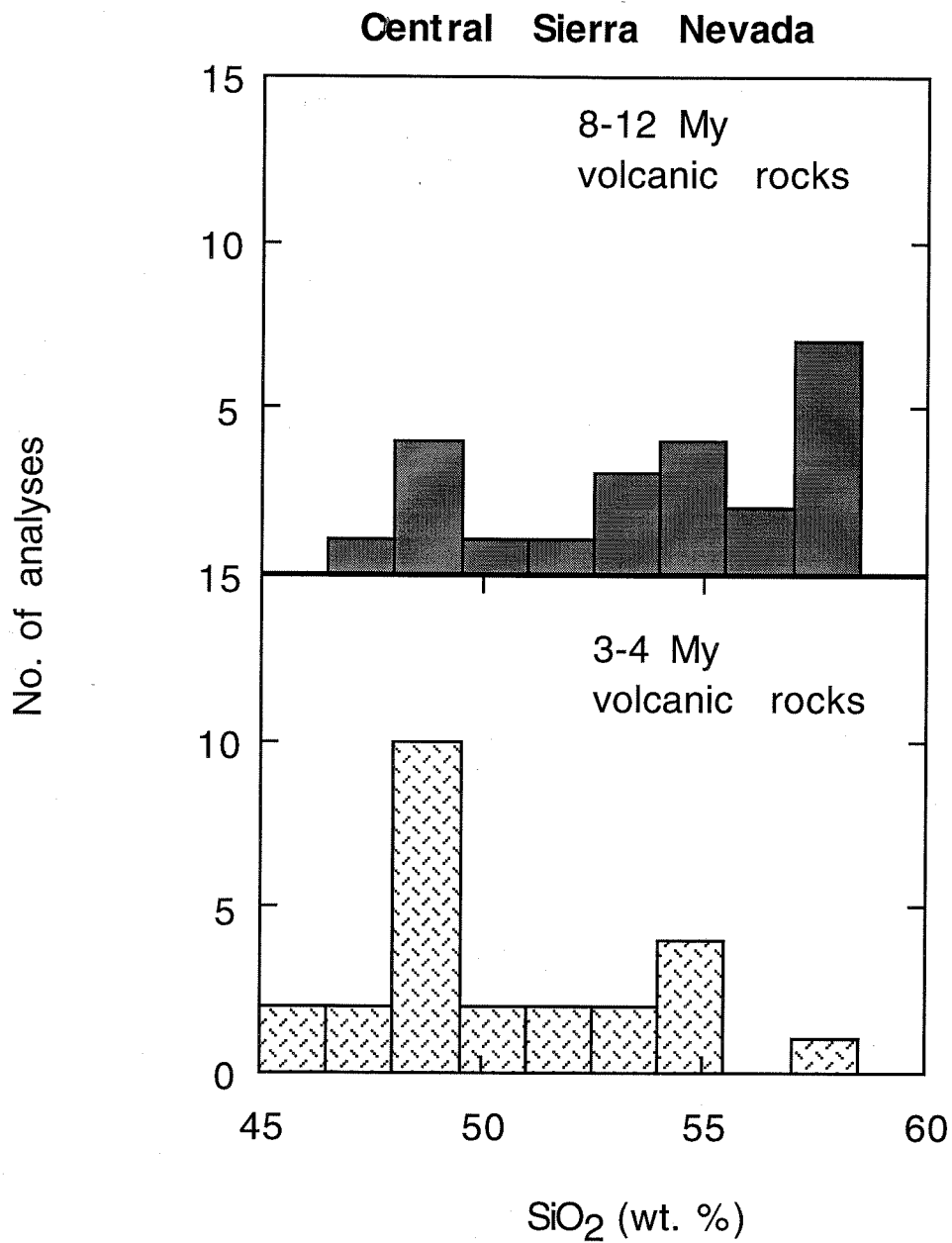
The equilibration pressures and stability fields of xenoliths present in the volcanic groups suggest that the MV originated at depths similar to or greater than those of the PV and QV. The presence of diamond and graphite pseudomorphs after diamond in pipes of the MV (Hausel, 1995; Ducea and Saleeby, 1977), as well as equilibration pressures as high as 4.2 GPa, indicate that the source of these trachyandesites is at least 120 to 140 km deep. In contrast, the equilibration pressures of mantle xenoliths of the PV and QV (Ducea and Saleeby, 1996a), as well as the absence of garnet in the peridotites, suggest that the xenolith-bearing PV and QV may have originated at shallower depths. Depths of as much as 120 km were established by van Kooten (1980) for the source of some PV from the Fresno River area. Therefore, the source depths for the PV were shallower than or similar to those of the MV; there is no indication that the PV and QV originated at greater depths than did the MV.

The oxygen-isotope ratios of fresh, xenolith-bearing PV and MV are shown in Figure 7.4. against MgO concentrations. Interestingly, the deeper MV magmas have crustal $\delta^{18}O$ ratios (7.1 to 8.2), whereas the PV and QV have mantle-like $\delta^{18}O$ (5.9 to 6.5) values. These results indicate that a crustal oxygen signature during Miocene time at ~120 km was replaced by a mantle signature at similar and/or shallower depths by the Pliocene.

In conclusion, Late Cenozoic volcanic rocks erupted through the Sierra Nevada record a progressive change at depth, from crustal-like (8 to 12 Ma) to mantle sources (0 to 4 Ma), as predicted by the delamination hypothesis.

Young uplift of the mountain range. Sierra Nevada geologists have long presented data suggesting that the mountain range experienced significant Late Cenozoic uplift accompanied by westward tilting, mainly because of tectonic forces (Lindgren, 1911; Christensen, 1966; Huber, 1981; Unruh, 1991). There is abundant evidence that most of the unroofing of the Mesozoic batholith to its present-day exposed levels took place shortly after batholith generation (Unruh, 1991; Renne et al., 1993). The region

Figure 7.4. $\delta^{18}O$ vs. MgO for xenolith-bearing volcanic rocks of the MV and PV groups. PV have more primitive (mantle-like) oxygen-isotope ratios.
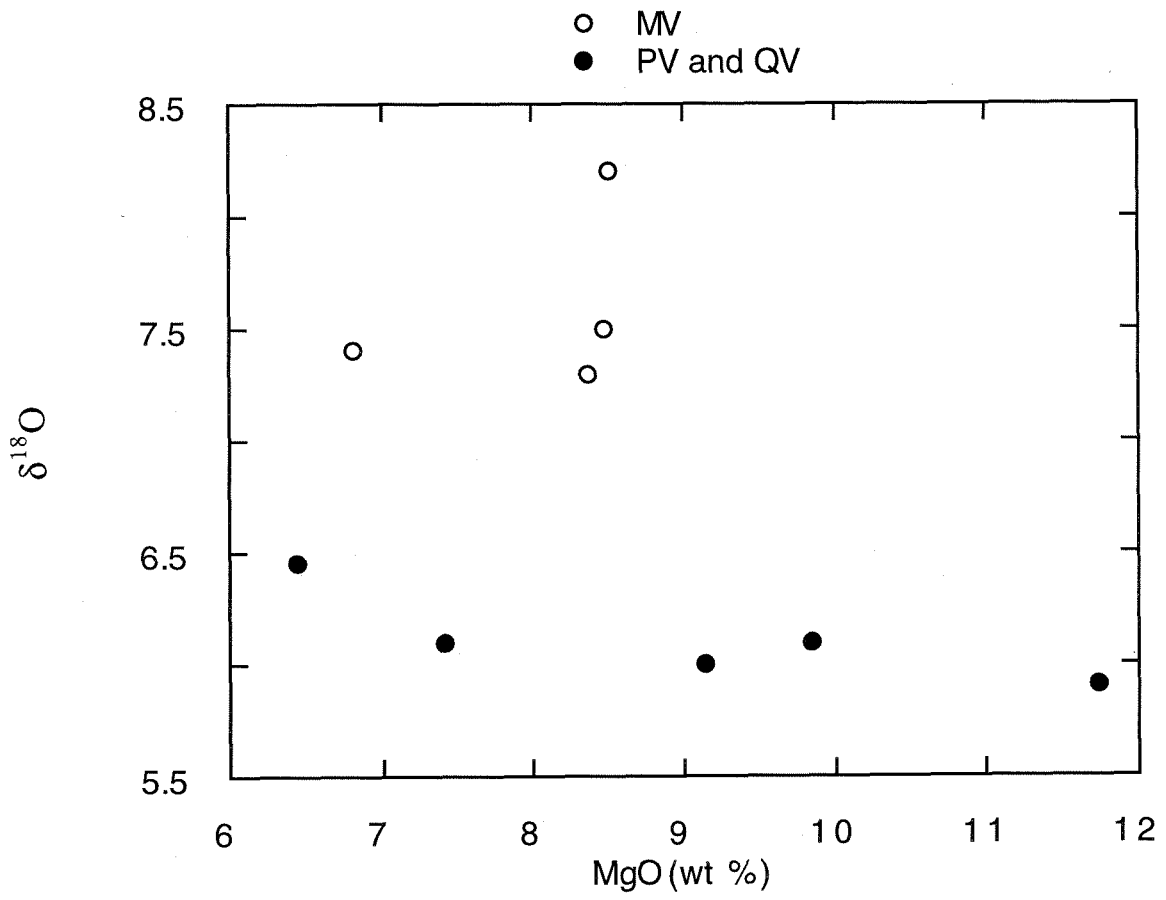
experienced little erosion during the first half of the Cenozoic, which led most researchers to believe that the Sierran topography was reduced from the presumed Mesozoic Andean-like relief to an unimpressive lowland during the Early Cenozoic (Huber, 1981). Christensen (1966) and Huber (1981) used paleofloral and geomorphological arguments to postulate that uplift was under way in the central Sierra Nevada during 50 to 25 Ma and continued subsequently, but has accelerated mainly over the past 10 m.y. and was demonstrably significant between 10 and 3 Ma.

However, this young uplift event in many ways is enigmatic, as it is not explained by tectonic thickening in an arc environment. The Sierra Nevada ceased to be an active magmatic arc at ~80 Ma (Chen and Moore, 1982). Furthermore, the region stopped being a convergent margin before the time of the fastest postulated uplift. A different cause for uplift must be found. Crough and Thompson (1977) were the first to propose that the late Miocene uplift of the Sierra Nevada must be related to the thinning of the mantle lithosphere beneath the Sierra Nevada, a hypothesis further developed by Eaton et al. (1978) and Jones (1987). Recently, some researchers have challenged all lines of evidence used to document Late Cenozoic uplift (Small and Anderson, 1996; Wernicke et al., 1996), claiming that although there is strong evidence for young westward tilting of the mountain range, it need not be accompanied by an increase in mean elevation. However, the large incision rates measured by Huber (1981) in the Sierran major drainages for the 10 to 3 Ma age range following a long period of erosional quiescence call upon some Late Cenozoic tectonic process to provide buoyancy in the area.

We believe that the cooling and development of the eclogitic root beneath the SNB during the late stages of magmatism and following its cessation inhibited erosion during the Early Cenozoic. The Late Cenozoic detachment of the eclogitic root (possibly a multi-step process) and its replacement by hot peridotite could have provided buoyancy and triggered renewed uplift of the mountain range.

7.7. Alternative Interpretations

Crustal foundering into the mantle is a mechanism capable of explaining the present-day relatively shallow crustal thickness and recent uplift of the Sierra Nevada mountain range. We presented above several geological and geophysical lines of evidence that are consistent with the delamination model. There are, however, alternative explanations for some of the observations presented above that support the concept of delamination.

Change in xenolith lithology. One could argue that the xenolith data are not representative of the composition of the deep lithosphere beneath the SNB. The Miocene pipes may have sampled preferentially garnet-rich lithologies, whereas the PV could have selectively sampled peridotitic material from similar depths. Therefore, the depth interval between 35 and 100 km may have been represented by a mixture of peridotites and eclogites at all times during the Late Cenozoic. However, the significant change in peridotite equilibration temperatures, from low values in MV units to near-solidus values in PV and QV units, argues against a sampling bias.

Crustal-derived glass inclusions in mantle peridotites. While crustal-derived glasses in mantle periodites clearly document interactions between deep-crustal and mantle materials, they may not necessarily require crustal delamination. It also is possible that hot diapirs of peridotitic material locally intruded the lowermost Sierra Nevada crust, resulting in the partial melting of the eclogitic assemblages and the incorporation of trapped SRG inclusions in peridotites (stage "B" in Figure 6.5). Pliocene and Quaternary volcanism in the Sierra Nevada, however, is not a local feature, shallow-level (35 to 70 km) spinel peridotite-bearing PV and QV being scattered throughout the region. Since the Sierra Nevada did not experience lateral extension comparable to the Basin and Range region to the east, we believe that regional peridotitic diapirism must have been accompanied by vertical removal of the lower crust.

High-velocity anomaly beneath the Sierra Nevada. The presence of partially molten material with low seismic compressional velocities measured below the base of the present-day seismologically defined crust could lead to the erroneous interpretation that dense eclogitic material is present at depth. The measured anomaly may instead simply represent a transition from partially molten to solid peridotite, rather than reflecting a chemical change.

7.8. Tectonic Implications

The data outlined above support the hypothesis that a thick, eclogite-facies mafic-ultramafic root that developed under the Sierra Nevada during and possibly after the formation of the composite Mesozoic batholith delaminated and foundered into the mantle. With the present data resolution, this interpretation is not unique, although it does satisfy all the important pertinent geologic and geophysical observations. If our favored interpretation is correct, it may have important tectonic implications for the post-arc evolution of the Sierran lithosphere and crustal growth at Cordilleran margins. These implications are discussed below.

Missing root. The Sierra Nevada arc resulted in the formation of an upper crustal structure characteristic of most Cordilleran-type magmatic arcs. The Andes, for example, represent a good equivalent in which magmatism is still active today. Despite the complex nature of the crust-mantle interface beneath batholiths (Hildreth and Moorbath, 1988; Pitcher, 1993), it is expected that a magmatic arc at a Cordilleran margin would contain large volumes of garnet-rich, non-peridotitic residues/cumulates beneath the granitic sections of the crust. Observations and mass balance calculations demonstrate that the ratio of arc cumulates to granitoids exceeds unity (Kay and Kay, 1991) and could

be as much as 10 to 20 if a large fraction of the magmatic input is mantle derived. Since Cordilleran granitoids can be as thick as ~30 km (e.g., Saleeby, 1990), one would expect to find cumulate/residue roots at least 30 km in thickness, but more likely 60 km or more.

The presence of eclogitic roots has not been recorded sesimically beneath extinct arcs, or even beneath the larger of the Cordilleran batholiths (e.g., Zandt and Ammon, 1995). The Sierra Nevada is one example of an extinct Mesozoic Cordilleran batholith whose crustal thickness today is ~35 km, and which is underlain by peridotitic mantle (Wernicke et al., 1996). Root delamination of defunct arcs is an appealing mechanism with the capacity for resolving this apparent contradiction between geophysical and petrological lines of evidence.

Crustal growth at Cordilleran margins. Although Andean margins have been considered to be prime sites for Phanerozoic crustal growth (e.g., Taylor and McLennan, 1985), geochemical studies show that the generation of typical Cordilleran granitoids requires a minimum two-step distillation from the mantle (e.g., Hildreth and Moorbath, 1988). Young accreted crustal masses, which commonly originated within island-arc settings, are found at Cordilleran margins in front of the magmatic arcs. These arc-related rocks are composed of water-rich volcanics intermixed with a variety of sediments that are melt-fertile in mid- to lower-crustal environments. Tectonic thickening can emplace young accreted arc sections and various other "non-subductable" units at considerable depths and lead to granitic magmatism via extensive melting in the lower parts of the crust (e.g., Pitcher, 1993). If the residue left after granitoid extraction remains in the crust, batholithic magmatism will lead primarily to the internal differentiation of the crust, whereas if the residue returns to the mantle, the addition of silica-rich material to the crust will be significant.

In the Sierra Nevada, there is evidence for widespread Jurassic submarine arc rocks along the western edge of the batholith and as wall-rock screens within the Cretaceous batholith (e.g., Saleeby, 1990, and references therein). Saleeby (1990)

presented strong evidence for downward flow of volcanic-arc rocks during the Cretaceous. Deep-crustal remelting of the Jurassic arc (blended with new mantle additions and possibly some other lower-crustal components) may represent the second event required for generating the silica-rich Cretaceous batholith in the Sierra Nevada (Ducea et al., 1997).

The post-Cretaceous upper 30 km of the Sierra Nevada crust, almost entirely occupied by SNB granitoids, therefore has a composition slightly more silicic than the average continental crust. Precambrian material no older than 1.8 Ga also may have been involved in the source of the SNB, but the ratio of Precambrian to Phanerozoic SNB source rocks based on Nd model ages is ~1. If delamination has recycled the ultramafic residues back into the mantle, the Sierra Nevada represents today a Mesozoic silica-rich crustal addition to the North American continent.

References

Ague J.J., and Brimhall G.H. (1988) Magmatic arc asymetry and distribution of anomalous plutonic belts in the batholiths of California; Effects of assimilation, crustal thickness and depth of crystallization, Geol. Soc. Am. Bull., 100: 912-927.

Bateman P.C. (1983) A summary of critical relationships in the central part of the Sierra Nevada batholith, California, U.S.A., in Roddick J.A. (ed.) *Circum-Pacific plutonic terranes*, Geol. Soc. Amer. Memoir 159: 241-254.

Beard B.L. and Glazner A.F. (1995) Trace elements and Sr and Nd isotopic composition of mantle xenoliths from Big Pine Volcanic Field, California, J. Geophys. Res., 100:4169-4179.

Benz H.M., Zandt G., and Oppenheimer D.H. (1992) Lithospheric structure of northern California from teleseismic images of the upper mantle, J. Geophys. Res., 97: 4791-4807.

Biasi G.P, and Humphreys E.D. (1992) P-wave image of the upper mantle structure of central California and southern Nevada, Geophys. Res. Lett., 19: 1161-1164.

Chen J.H. and Moore J.G. (1982) Uranium-lead isotopic ages from the Sierra Nevada batholith, California: J. Geophys. Res., 87: 4761-4784.

Christensen M.N. (1966) Late Cenozoic crustal movements in the Sierra Nevada of California, Geol. Soc. Am. Bull., 77:163-182.

Cristensen N. and Mooney W.D. (1995) Seismic structure and composition of the continental crust: A global view, J. Geophys. Res., 100: 9761-9788.

Crough S.T. and Thompson G.A. (1977) Upper mantle origin of the Sierra Nevada uplift, Geology, 5: 396-399.

Dewey, J.F., Ryan P.D., and Anderson T.B. (1993) Orogenic uplift and collapse, crustal thickness, fabrics and metamorphic phase changes: The role of eclogites, in *Magmatic processes and Plate Tectonics*, ed. Prochard H.M. et al., Sp. Pub. Geol. Soc. Am., 76: 325-343.

Dickinson W. (1981) Plate tectonics and the continental margin of California, in Ernst W.G. (ed.) *The geotectonic development of California*, Prentice-Hall, Englewood Cliffs, N.J., 1-28.

Dodge F.C.W., Calk L.C., and Kistler R.W. (1986), Lower crustal xenoliths, Chinese Peak lava flow, Central Sierra Nevada, J. Petrol., 27: 1277-1304.

Dodge F.C.W., Lockwood J.P., and Calk L.C. (1988), Fragments of the mantle and crust beneath the Sierra Nevada batholith: Xenoliths in a volcanic pipe near Big Creek, California, Geol. Soc. Am. Bull., 100: 938-947.

Domenick M.A., Kistler R.W., Dodge F.C.W., and Tatsumoto M. (1983) Nd and Sr study of crustal and mantle inclusions from the Sierra Nevada and implications for batholith petrogenesis, Geol. Soc. Am. Bull., 94: 713-719.

Ducea M.N. and Saleeby J.B. (1998) Silica-rich glass inclusions in ultramafic xenoliths from the Sierra Nevada, California, Earth Planet. Sci. Lett., 156, 101-116.

Ducea M.N., Taylor H.P., and Saleeby J.B. (1997) The age and origin of a thick mafic-ultramafic keel from beneath the Sierra Nevada batholith; Part II, Petrogenesis, abstract submitted to GSA Annual meeting, 1997.

Ducea M.N., and Saleeby J.B. (1996a) Buoyancy sources for a large unrooted mountain range, the Sierra Nevada, California: Evidence from xenolith thermobarometry, J. Geophys. Res., 101: 8229-8241.

Ducea M.N. and Saleeby J.B. (1996b), Rb-Sr and Sm-Nd mineral ages of some Sierra Nevada xenoliths; implications for crustal growth and thermal evolution, EOS, Trans. Amer. Geophys. Union, 77:780.

Eaton G.P., Wahl R.R., Prostka H.J., Mabey D.R., and Kleinkopf M.D. (1978) Regional gravity and tectonic patterns: Their relations to the late Cenozoic epeirogeny and lateral spreading in the western Cordillera, in Smith R.B. and Eaton G.P. (eds.) *Cenozoic tectonics and regional geophysics of the western Cordillera*; Geol. Soc. Am. Mem., 152: 51-91.

Faure G. (1985) Principles of isotope geology, John Wiley & Sons, New York, 590 p.

Fliedner M. and Ruppert S. (1996) 3-dimensional crustal structure of the Southern Sierra Nevada from seismic fan profiles and gravity modelling, Geology, 24: 367-370.

Hausel W. D. (1995) Diamonds and their host rocks in the United States, Mining Engineering, 47: 723-732.

Hildreth W. and Moorbath S. (1988) Crustal contributions to arc magmatism in the Andes of central Chile, Contrib. Mineral. Petrol., 98:455-489.

Huber N.K. (1981) Amount and timing of late Cenozoic uplift and tilt of the central Sierra Nevada, California - Evidence from the upper San Joaquin River basin, U.S. Geol. Surv. Prof. Pap., 1197; 28 p.

Huber N.K. (1977) Silica content of some late Cenozoic volcanic rocks from the southern Sierra Nevada, California - applications as a correlation tool, U.S. Geol. Surv. Open File Report 77-755: 40 p.

Humphreys E.D. and Dueker K.G. (1994) Western United States upper mantle structure, J. Geophys. Res., 99: 9615-9634.

Ionov D.A., Hofmann A.W., and Shimizu N. (1994) Metasomatism-induced melting in mantle xenoliths from Mongolia, J. Petrol., 35: 753-785.

Jones C.H. (1987) Is extension in Death Valley accommodated by thinning of the mantle lithosphere beneath the Sierra Nevada, California?, Tectonics, 6: 449-473.

Jones C.H., Kanamori H., and Roecker S.W. (1994) Missing roots and mantle drips: Regional P_n and teleseismic arrival times in the Southern Sierra Nevada and vicinity, California, J. Geophys. Res., 99:4567-4601.

Jones C.H. and Phinney R. (1997), Seismic structure of the lithosphere from teleseismic converted arrivals observed at small arrays in the Southern Sierra Nevada and vicinity, California, manuscript submitted to J. Geophys. Res.

Kay R.W. and Kay S.M. (1993) Delamination and delamination magmatism, Tectonophys., 219:177-189.

Kay R.W. and Kay S.M. (1991) Creation and destruction of the lower continental crust, Geol. Rundsch., 80: 259-270.

Lindgren W. (1911) The Tertiary gravels of the Sierra Nevada, California, U.S. Geol. Surv. Prof. pap., 73; 226 p.

Luedke R.G. and Smith R.L. (1981) Map showing the distribution, composition, and age of Late Cenozoic volcanic centers in California and Nevada, U.S. Geol. Surv. Misc. Invest. Ser. Map., 1091-C.

McCulloch M.T., Gregory R.T., Wasserburg G.J., and Taylor H.P. (198) A neodymium, strontium and oxygen isotopic study of the Cretaceous Samail ophiolite and implications for the petrogenesis and seawater-hydrothermal alteration of the oceanic crust, Earth. Planet. Sci. Lett., 46: 201-211.

Moore J.G. and Dodge F.C.W. (1980) Late Cenozoic volcanic rocks of the Southern Sierra Nevada, California; I. Geology and petrology: Summary, Geol. Soc. Am. Bull., 91: 515-518.

Mukhopadyay B., Manton W.I. (1994) Upper mantle fragments from beneath the Sierra Nevada batholith: Partial fusion, fractional crystallization and metasomatism in a subduction-enriched ancient lithosphere, J. Petrol., 35: 1418-1450.

Niu Y. and Batiza R. (1991) DENSCAL: A program for calculating densities of silicate melts and mantle minerals as a function of pressure, temperature, and composition in melting range, Comp. Geosci., 17:679-687.

Ormerod D.S., Hawkesworth C.H., Rogers N.K., Leeman W.P., and Menzies M. (1988) Tectonic and magmatic transitions in the western Great Basin, U.S.A., Nature, 333: 349-353.

Park S., Hirasuna B., Jiracek G., and Kinn C. (1996) Magnetotelluric evidence for lithospheric mantle thinning beneath the southern Sierra Nevada, J. Geophys. Res., 101: 16, 241- 16, 255.

Pickett D.A. and Saleeby J.B. (1993) Thermobarometric constraints on the depth of exposure and conditions of plutonism and metamorphism at deep levels of the

Sierra Nevada batholith, Tehachapi Mountains, California, J. Geophys. Res., 98: 609-629.

Pitcher W.S. (1993) The nature and origin of granite, Blackdie Acad.& Prof., London, 321 p.

Renne P.R., Tobish O.T., and Saleeby J.B. (1993) Thermochronologic record of pluton emplacement, deformation and exhumation at Courtright shear zone, central Sierra Nevada, California, Geology, 21: 331-334.

Saleeby J.B. (1990) Progress in tectonic and petrogenetic studies in an exposed cross-section of young (c. 100 Ma) continental crust, southern Sierra Nevada, California, in Salisbury M. H., and Fountain D. M. (eds.) *Exposed crustal sections of the continental crust*, Kluwer Acad., Norwell, Mass., 137-158.

Saltus R.W., and Lachenbruch A.H. (1990) Thermal evolution of the Sierra Nevada: Tectonic implications of new heat flow data, Tectonics, 10: 325-344.

Schiano P. and Clocchiatti R. (1994) Worldwide occurrence of silica-rich melts in sub-continental and sub-oceanic mantle minerals, Nature, 368: 621-624.

Schiano P., Clocchiatti R., Shimizu N., Maury R.C., Jochum K.P., and Hofmann A.W. (1995) Hydrous, silica-rich melts in the sub-arc mantle and their relationships with erupted arc lavas, Nature, 377: 595-600.

Small E.E. and Anderson R.S. (1996) Geomorphologically driven late Cenozoic rock uplift in the Sierra Nevada, California, Science, 270: 277-280.

Taylor S. R. and McLennan S.M. (1985) The continental crust; Its compositional evolution, Blackwell Sci., Cambridge, Mass, 312 p.

Unruh J.R. (1991) The uplift of the Sierra Nevada and implications for the late Cenozoic epeirogeny in the western Cordillera, Geol. Soc. Am. Bull., 103: 1395-1404.

van Kooten G.K (1980) Mineralogy, geochemistry and petrology of an ultrapotassic basaltic suite, central Sierra Nevada, California, U.S.A., J. Petrol., 21: 631-684.

Wernicke B., and 19 others (1996) Origin of high mountains on continents: The Southern Sierra Nevada, Science, 271: 190-193.

Wernicke B. (1990) The fluid crustal layer and its implications for continental dynamics, in *Exposed crustal sections of the continental crust*, NATO Adv. Study Ser. C., Math. Phys. Sci., v. 317, edited by M.H. Salisbury and D.M. Fountain, Kluwer Acad., Norwell, Mass., 509-544.

Wolf M.B. and Wyllie P.J. (1993) Garnet growth during amphibolite anatexis: Implications for a garnetiferous restite, J. Geol., 101:357-373.

Zandt G. and Ruppert S., (1996) Lower crustal detachment and the evolution of the continental crust; Evidence from the Sierra Nevada, (abstract), EOS, Trans. AGU, 77, 831.

Zandt G., and Ammon C.J. (1995) Continental crust composition constrained by measurements of crustal Poisson's ratio, Nature, 374: 152-154.

Appendix 1. The density of Sierra Nevada xenoliths

The density of the garnet pyroxenites as well as peridotite lithologies can be estimated from xenolith data. The density of average compositions of minerals from garnet pyroxenites recovered in MV are shown in Figure 7.2. More than 60 analyses were taken into account into averaging mineral densities. The mineral densities were calculated using the program provided by Niu and Batiza (1991) at two different temperatures: 650 $^{\circ}$C and 950 $^{\circ}$C as end values of a reasonable spectrum of temperatures in the lower crust. The average modal proportions of garnet, orthopyroxene and clinopyroxene in our collection was used to calculate an average garnet pyroxenite density as a function of pressure (depth), which is shown in Figure 6.4. The average densities for garnet peridotites from MV (using a mean temperature 1000 ^{0}C recorded in xenoliths) and spinel peridotites from PV and QV (using a mean temperature of 1200 ^{0}C) are also

shown in Figure 7.2 as a function of pressure. The peridotite densities are at least 0.2 g/cm^3 lower than those of pyroxenites at all pressures.

APPENDIX 1

Location and Field Description of Xenolith-Bearing Volcanic Rocks in the Central and Southern Sierra Nevada

Late Cenozoic volcanism is widespread throughout the central and southern Sierra Nevada (Moore and Dodge, 1980), although the volume of volcanic products is relatively small. In the southern Sierra, late Cenozoic volcanism can be temporaly divided into three episodes: Miocene (8-12 Ma), Pliocene (3-4 Ma), and Quaternary (0-1 Ma), based on published geochronological determinations (e.g., Luedke and Smith, 1981). The Miocene volcanic rocks are predominantly exposed as dikes, pipes, and necks, whereas younger exposures are mainly lava flows. I sampled nineteen volcanic suites representing all the three episodes which contain crustal and/or mantle xenoliths. The location of each of these sites is shown in Figure A1-1 and their geographic coordinates, age and morphology are listed in Table A1-1. Seven of these localities were previously undescribed. Some localities contain mainly altered xenoliths and/or fragments too small for complex chemical and isotopic analyses. Therefore, I investigated the petrography of xenoliths from all locations, while for chemistry and isotopic analyses I focused on the following volcanic outcrops which contain representative and fresh samples: Big Creek, Chinese Peak, Pick and Shovel, Camp Sierra, Red Mountain, Jackson Butte, Scepter Creek, Blue Knob, Oak Creek, Waucoba, Sawmill Canyon, and Aberdeen. Below I provide a brief description of the sampled localities listed in Table 1 and the types of xenoliths found at each.

Big Creek is a tracyandesitic pipe, elliptical (110 x 260 m) in plan, and is located at 1600 m elevation on a steep, east facing slope 1.5 km northwest of the town of Big Creek. The pipe has a 8.3 Ma age (based on a Rb-Sr biotite-whole rock isochron, Dodge et al., 1988). Fine grained euhedral mafic phenocrysts of orthopyroxene, clinopyroxene, hornblende, biotite, and plagioclase are commonly corroded; the groundmass is trachytic microcrystalline. The pipe is zoned, with a marginal facies characterized by blocky

Figure A1-1. Map showing the distribution of xenolith-bearing volcanic rocks from the Sierra Nevada, Owens Valley and Inyo Mountains investigated in this thesis. The grey-shaded areas delineate mountain ranges. CS - the xenolith localities representing the Central Sierra Nevada suites of Chapter 2, ES - the xenolith localities representing the Eastern Sierra region suites of Chapter 2.

○ Miocene volcanic rocks

◆ Pliocene volcanic rocks

● Quaternary volcanic rocks
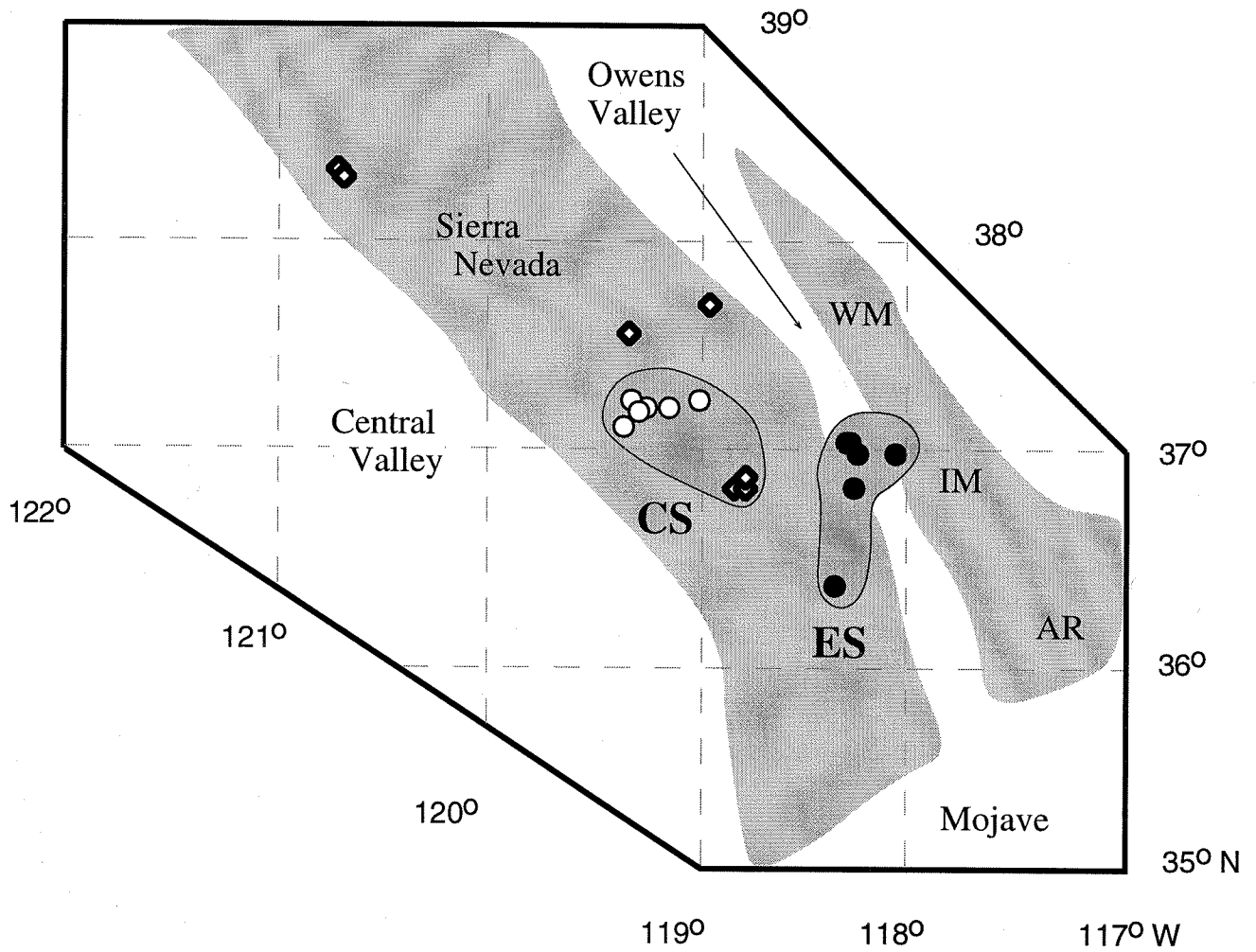
WM - White Mountains
I M - Inyo Mountains
AR - Argus Range

outcrops with columnar jointing and a central "soft" facies characterized by rubble-covered outcrops. Zoning of the pipe is reflected compositionally by the differences in relative abundances of phenocrysts. Zoning is also reflected in xenolith distribution: the marginal pipe is dominated by the presence of low density, crustal xenoliths, whereas the central facies contains mainly mafic-ultramafic xenoliths. The most common xenolith lithologies are: garnet clinopyroxenites, eclogites, websterites, garnet-free pyroxenites, garnet and garnet-spinel peridotites, feldspathic granulites, gabbros, granitoids and various metasediments. Some peridotites contain calcite of probable mantle origin.

Chinese Peak consist of a small trachybasaltic lava flow and its adjacent feeder neck (Dodge et al., 1986), and it is located near the summit of the Chinese Peak in the central Sierra Nevada. This trachybasalt yielded a whole rock K-Ar age of 10.2 Ma (Dodge et al., 1986). Petrographically, the rock is a reddish gray aphanitic and commonly vesicular rock, sparsely porphiritic. Augite, amphibole, phlogopite, olivine, sanidine, and plagioclase phenocrysts comprise up to ~ 50% of the volcanic rock volume, although some of these (phlogopite, olivine) may be xenocrysts. Xenoliths are abundant at Chinese Peak (in places, up to 15% of the rock volume). The typical size of the xenoliths is ~4-5 cm, although ocassionally samples as large as 20 cm in diameter are found. About three quarters of the xenoliths are monomineralic clinopyroxenites and orthopyroxenites. Feldspathic granulites and metasediments are common. Garnet pyroxenites, garnet peridotites and dunites are subordinate. Granitoid xenoliths are less abundant than in other localities.

Pick and Shovel Mine locality is a small trachybasaltic plug (?) located in the San Joaquin drainage (Mukhopadhyay, 1989). The age of this trachybasalt is Miocene (8-12 Ma), based on geomorphological constraints (no radiometric age has been performed on this rock). The volcanic rock is similar in composition with the Chinese Peak lava flow. The Pick and Shovel trachybasalt contains abundant xenoliths, and it is particularly rich in

Table A1-1. Locations, compositions and ages of the xenolith-bearing volcanic rocks.

Location	Latitude	Longitude	Composition	Age (Ma)[*]
Jackson Butte	$38^0 20$'N	$120^0 43$'W	dacite	2.4
Golden Gate Hill	$38^0 18$' N	$120^0 43$'W	dacite	2.5
Blue Knob	$37^0 34$'N	$119^0 20$'W	alkali-basalt	~3.5
Big Creek	$37^0 13$'N	$119^0 16$'W	trachyandesite	8.3
Pick & Shovel	$37^0 15$'N	$119^0 20$'W	basalt	8-12?
Chinese Peak	$37^0 13$'N	$119^0 09$'W	trachyandesite	10.2
Camp Sierra	$37^0 12$'N	$119^0 18$'W	basalt	11.1
Sugarloaf Hill	$37^0 08$'N	$119^0 22$'W	trachybasalt	9.0
Red Mountain	$37^0 15$N	$119^0 01$'W	trachybasalt	8-12
Hume Lake	$36^0 50$'N	$118^0 50$'W	alkali-basalt	3-4
Scepter Creek	$36^0 50$'N	$118^0 47$'W	trachyandesite	~3.6
Volcanic Knob	$36^0 52$'N	$118^0 47$'W	trachyandesite	3.6
Golden Trout	$36^0 22$'N	$118^0 22$'W	alkali-basalt	<0.01
Oak Creek	$36^0 50$'N	$118^0 17$'W	alkali-basalt	0.15
Sawmill Canyon	$37^0 00$'N	$118^0 16$'W	alkali-basalt	0.15
McGee Mountain	$37^0 40$'N	$118^0 55$'W	alkali-basalt	2.6
Goose Creek	$37^0 03$'N	$118^0 19$'W	alkali-basalt	<1
Aberdeen	$37^0 03$'N	$118^0 18$'W	alkali-basalt	0.09
Waucoba	$37^0 00$'N	$118^0 05$'W	alkali-basalt	0.8

[*] - references to ages of volcanic rocks are given in text.

garnet websterites, eclogites and garnet peridotites. Carbonated peridotites and pyroxenites are abundant granitoids and various metamorphic pendant-like rocks are rare.

Red Mountain, is a trachybasaltic volcanic plug of Miocene age (Hamilton and Neuerburg, 1956) located ~5 km southeast of the Chinese Peak plug and flow. The plug is ~500 m in diameter and is exposed for a vertical distance of ~200 m. The volcanic rocks form the topographic high (2800 m) contrasting to the surrounding granites (in this area the average granite relief is ~2200-2300 m). Columnar jointing are prominent especially in the marginal facies of the plug. The basalt is an aphanitic and vesicular rock whose groundmass is commonly glassy. Phenocrysts of augite, olivine, sanidine, biotite, and plagioclase were found in all samples. The plug contains xenoliths: peridotites, pyroxenites (without garnet), granulites, and granitoids were sampled. Xenoliths are not as common as at Chinese Peak or Big Creek, and are restricted to the central facies of the plug.

Camp Sierra is a near vertical dike, ~0.5 to 4 m wide, exposed over a length of ~300 m along the Big Creek drainage, ~ 1 km north of the town of Big Creek. It has a Miocene age (11.1 Ma, Dodge et al., 1988) and trachybasaltic composition. The host basalt is composed of a dark, glassy groundmass and microphenocrysts of phlogopite, clinopyroxene, and rare possibly xenocrystic olivine. Large blocks and slivers of granitic wallrocks are included in the dike, suggesting that the trachybasalt may have experienced some crustal contamination. Xenoliths are common and generally well preserved. Monomineralic ortho- and clinopyroxenites are the most frequent xenolith lithologies at Camp Sierra. Garnet clinopyroxenites, eclogites and websterites, including some of the deepest non-peridotitic lithologies found in the Sierra Nevada are also common. Spinel-garnet and garnet peridotites were also found. Similar to the Big Creek and Pick and Shovel localities, the Camp Sierra peridotites (and rarely pyroxenites) contain carbonates (i.e., calcite). Only two granulitic (feldspathic) lithologies were found at Camp Sierra.

Figure A1-2. a. View of the Camp Sierra dike (here about 0.3 to 2 m wide).

b. Photograph of the Miocene plug of Red Mountain, central Sierra Nevada, viewed from Chinese Peak. Red Mountain, as well as other exposures of Miocene volcanic rocks in the area, tend to form topographic high regions, relative to the surrounding granitoids.

c. View of the trachyandesite pipe of Big Creek. The photograph is taken from the "soft' center of the pipe (rich in eclogitic xenoliths) towards the marginal, "hard" facies, characterized by columnar jointing (rich in peridotites). Distance to the columnar joints in the background is ~100 m.

d. Xenolith-bearing, Quaternary basaltic lava filling the Sawmill Canyon, eastern Sierra Nevada. Outcrops of basalts are visible on both sides of the heavily vegetated area along the canyon bottom.
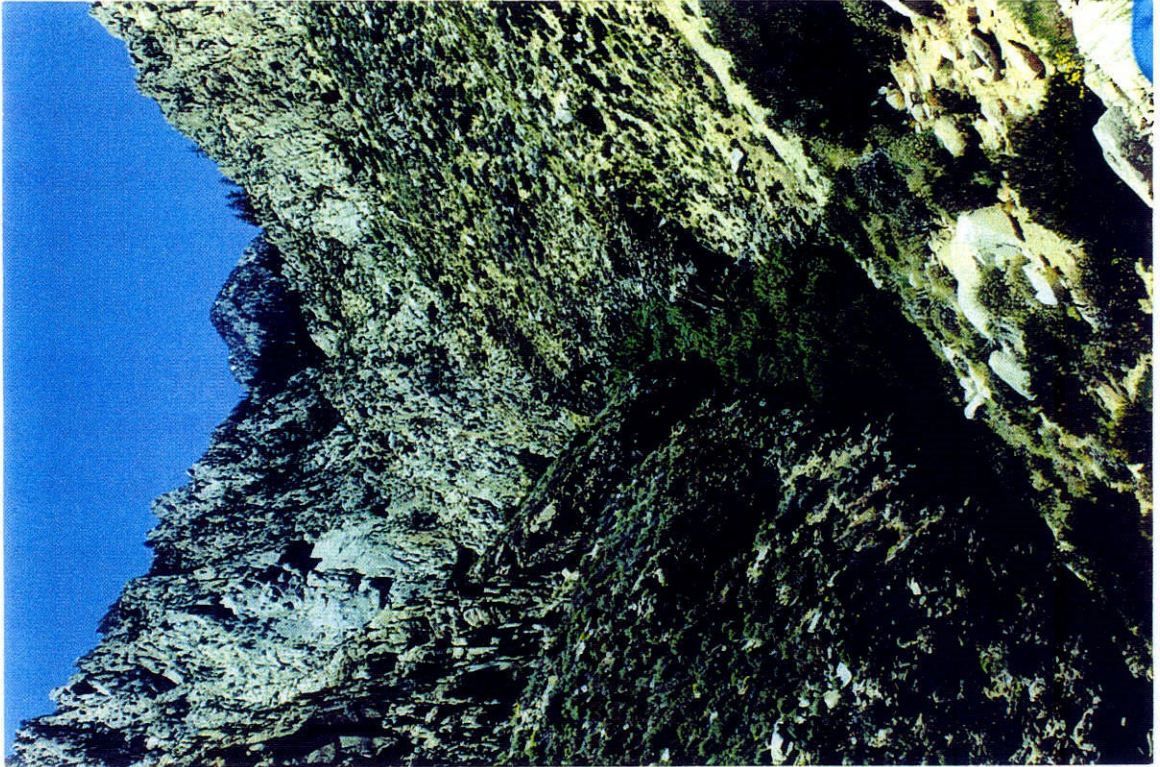
Jackson Butte is a volcanic plug located in the western Sierra Nevada foothills near the town of Jackson. It intrudes the Calaveras formation (Rose, 1959) at a steep angle (~70-80^0). The dome has a Pliocene age (~2.4 Ma, Rose, 1959). Jackson Butte is made up of banded hornblende-biotite dacite and its brecciated equivalent. Other phenocrysts present in the dacite are plagioclase, apatite and magnetite. The groundmass is gray, aphanitic, and consists mainly of microcrystals of plagioclase. The marginal, massive facies of the plug has a well defined, platy flow structure, which is partly due to the orientation of xenoliths, xenocrysts, and phenocrysts. The central facies is brecciated, and consists of a reddish-brown matrix and fragments varying in size from a few centimeters to ~5 meters. All exposures of the plug are significantly weathered.

Xenoliths constitute ~10-15% of the volume of the volcanic rock at Jackson Butte. However, most of xenoliths are either weathered out, resorbed in the magma, strongly deformed in the host magma environment, or very small (<2 cm). The better preserved assemblages are various hornblendites and gabbros, some with garnet. Peridotites (dunites, harzburgites, lherzolites) with spinel or without an aluminous phase, are also abundant, but are strongly resorbed in the dacitic magma. Other xenoliths found at Jackson Butte include: quartz-biotite-garnet schists, phyllites, quartzites, and various other quartzo-feldspathic rocks of unclear origin. Pyrope-rich garnet xenocrysts, unlike any garnet found in Jackson Butte xenoliths are abundant. Other xenocrysts include olivine and orthopyroxenes.

Blue Knob (also known as Hill 8056) is a volcanic plug located along the Madera Creek in the central Sierra Nevada. The plug has ~250 m in diameter and has a near vertical orientation. The margins of the plug display spectacular columnar jointing, indicating the proximity of the exposed volcanic rocks to the surface during magmatic emplacement (eruption?). The age of the plug is ~3.5 Ma (van Kooten, 1980). The Blue Knob volcanic rock is an alkali basalt, a fresh volcanic rock, rich in large, up to 6 mm phenocrysts of olivines, orthopyroxenes and plagioclase, some of which are probably xenocrysts, set in a groundmass that is mostly glassy.

Xenoliths are abundant and fresh at Blue Knob. Granitic and granitic gneiss inclusions are common, as well as banded cumulate gabbros and feldspathic granulites. Garnet-free pyroxenites (ortho-, clinopyroxenites and webseterites) are common but small, <3 cm. Porphyroblastic spinel peridotites and wehrlites of the Cr-diopsiode group are moderately abundant. Peridotites contain occasionally silica-rich glass inclusions, unrelated to the host basalt, and also exotic with respect to the xenoliths. Megacrysts of dark green clinopyroxenites are also present.

Scepter Creek is a Kings River tributary in the central Sierra Nevada. Several outcrops of a trachyandesitic flow are exposed in the creek. These outcrops are probably related to the Pliocene lava dome from Volcanic Knob (3.6 Ma, Dalrymple, 1963), ~2 km to the north. Petrographically, the Scepter Creek trachyandesites are aphanitic, with a finely crystallized groundmass rich in plagioclase, opaque minerals and ~0.2-0.5 mm phenocrysts of olivine and orthopyroxene. A few volcanic outcrops along Scepter Creek contain mantle and crustal xenoliths. Large and fresh peridotites and olivine clinopyroxenites are the most abundant xenoliths. Several peridotites contain exotic silica-rich glass inclusions, either as films along grain boundaries or as within-grain pockets. Granitic gneisses, granites, metasediments and granulites were also sampled. The crustal xenoliths are commonly altered or partially melted.

Hume Lake is a Pliocene (Dalrymple, 1963) basaltic flow in the Kings River area. Although the flow (or perhaps the series of flows) has a relatively large areal extent (~4 km^2), exposures are rare and small, generally restricted to the Converse Mountain area north of Hume Lake. The basalt has a red color and a massive structure. The groundmass is microcrystalline and dominated by the presence of plagioclase. The only phenocrysts are olivine and ortopyroxene. Granitic xenoliths are common. Sparse accidental fragments of peridotites and olivine clinopyroxenites are the only deep xenoliths found in the Hume Lake area. The xenoliths are altered and were not studied for whole-rock geochemistry, but were investigated for mineral chemistry by electron microprobe.

Oak Creek is the southernmost volcanic flow included in the Big Pine Volcanic Field of Owens Valley. Several outcrops of a ~0.15 Ma alkali basalt flow (Ormerod, 1988) are preserved near the mouth of Baxter Creek along the eastern edge of the Sierra Nevada. The basalt contains olivine, ortho- and clinopyroxene, as well as plagioclase phenocrysts in an aphanitic, microcrystalline to glassy groundmass. Mantle and crustal xenoliths were found in two outcrops which expose the basal part of the flow. The most common assemblages are spinel peridotites (lherzolites, harzburgites, dunites), while Cr-diopsode and Al-augite pyroxenites are less common. The only crustal lithologies are granitoids, which were probably derived from shallow depths given their similarity to the Cretaceous granitoids surrounding the basalts and the large size (commonly >10 cm) of these xenoliths.

Waucoba is a lava flow of 0.8 Ma age (Ormerod, 1988), located at the mouth of the Waucoba Canyon (Inyo Mountains). A cinder cone located up-canyon probably corresponds to the vent of the magma. The lava flow was directed toward the Owens Valley. The Waucoba canyon dissected the lava flow and exposed in places its entire thickness (up to 30 m). The base of the flow is xenolith-rich near the cinder cone feeder. The lava has an alkali-basaltic composition, a glassy groundmass and relatively large (2-3 mm) olivine phenocrysts. This locality is exceptionally rich in fresh, large xenoliths (up to 30 cm diamater). Most xenoliths are mantle-derived and are porphyroclastic lherzolites, abundant Cr-diopside and rare Al-augite clinopyroxenites, and orthopyroxenites. Granitic xenoliths are absent. Crustal xenoliths including metasedimentary rocks (schists, quartzites, marbles) are common.

Aberdeen is a small cinder cone in Owens Valley. The age of its eruption is unknown but based on its morphology must be very young, possibly younger than the last glaciation. It has alkali basaltic composition. Fragments vary in size from sub-centimeter to blocks larger than 5 m in diameter. The groundmass of the volcanic material is glassy, and the only phenocrysts visible in hand specimen are olivines. The cinder cone contains

abundant granitoid xenoliths, which are similar to the Jurassic granites exposed in the Owens Valley, just south of the Big Pine Volcanic Field. Large pyroxene-feldpsar gabbroic xenoliths (5-40 cm diamater), some with pegmatitic textures, are also common. Less abundant compositional types of xenoliths are peridotites and dunites. Xenocrysts of kaersutite are abundant; this locality is the only one in the eastern Sierra Nevada region which contains a hydrous mineral presumably derived from the mantle, although none of the peridotitic xenoliths contain this amphibole in their mineral assemblages.

Sawmill Canyon is a drainage which originates near the Sierra Nevada crest and empties into the Owens Valley. The deep canyon is carved mainly in Cretaceous granitoids. Outcrops of a 0.15 Ma lava flow (Gillsepie et al., 1984) are preserved along the canyon floor as well as occasionally as perched remnants on the canyon walls. The volcanic rocks are microcrystalline alkali basalts with phenocrysts of olivine and pyroxenes. Granitoid xenoliths and xenocrysts of olivine and pyroxene are common in the lava. Exceptionally fresh spinel lherzolites and harzburgites are preserved. The peridotites are preferentially concentrated near the base of the flow.

Other xenolith-bearing volcanic outcrops are: the Sugarloaf Hill trachybasaltic plugs in the San Joaquin River area (~9 Ma, Dalrymple, 1963), the Golden Trout alkali basalts in the southernmost Sierra (Quaternary, no geochronology information), the Goose Creek basalt of the Big Pine Volcanic Field (Quaternary, no quantitative geochronologic information), the McGee Mountain basaltic andesite in the Sierra Nevada crest region, ~15 km northwest of Bishop (2.6 Ma, Dalrymple, 1963), the Golden Gate Hill dacite in the western Sierran foothills (Rose, 1959), and the Wishon Reservoir/Volcanic Knob andesites in the Kings Canyon area (~3.6 Ma, Dalrymple, 1963) (Figure A-1). Samples collected from these locations are generally mineralogically altered.

The Sugarloaf Hill contains three trachybasaltic plugs whose textural appearence, phenocryst mineralogy, and xenolith population are similar to the Chinese Peak flow. The exposure of two of the three volcanic conduits is poor, and the rocks are altered. Small

pyroxenites, peridotites and clinopyroxene xenocrysts were sampled. The third volcanic plug does not contain xenoliths.

Petrographic observations performed in thin sections show that the Golden Trout and Goose Creek xenoliths are similar to fragments found in other Quaternary localities along the east side of the Sierra Nevada, while the xenoliths from the Wishon Reservoir/Volcanic Knob outcrops are similar to the better preserved fragments from Scepter Creek and Blue Knob. The Golden Trout xenoliths are important because they represent the only samples from the Sierra Nevada mantle south of Mt. Whitney latitudes. Peridotitic samples from the Golden Trout volcanic field have been investigated for mineral chemistry, but I did not attempt to determine whole rock chemical and isotopic analyses because of the large degree of mineralogic alteration in these xenoliths.

Beard and Glazner (1995) describe three additional distinct xenolith-bearing volcanic flows which they have sampled in the Big Pine Volcanic Field area. I have also noticed the occasional presence of xenoliths and xenocrysts in many of the Big Pine Volcanic Field lavas or cinder cones, other than the ones mentioned in detail above. However, all samples I collected from these locations are smaller than ~2 cm in diameter, and I did not analyze these for geochemistry.

Most McGee Mountain xenoliths appear to be shallowly derived from the Mount Morrison metamorphic pendant, the wallrocks in which the McGee Mountain magmas have intruded. No ultramafic or lower crustal xenoliths were found at this locality.

The Golden Gate Hill volcano (Rose, 1959) in the Sierra Nevada foothills is located on a private land with limited access. The Golden Gate Hill volcanic outcrops contain xenoliths of the same composition as the ones sampled from the neighboring Jackson Butte plug, based on the descriptions provided by Rose (1959).

References

Beard B.L., and Glazner A. F. (1995) Trace element and Sr and Nd isotopic composition of mantle xenoliths from the Big Pine Volcanic Field, California, J. Geophys. Res., 100: 4169-4179.

Dalrymple G.B. (1963) Potassium-argon dates of some Cenozoic volcanic rocks in the Sierra Nevada, California, Geol. Soc. Am. Bull., 74: 374-390.

Dodge F.C.F., Calk L.C., and Kistler R.W. (1986), Lower crustal xenoliths, Chinese Peak lava flow, Central Sierra Nevada, J. Petrol., 27: 1277-1304.

Dodge F.C.W., Lockwood J.P., and Calk L.C. (1988) Fragments of the mantle and crust beneath the Sierra Nevada batholith: Xenoliths in a volcanic pipe near Big Creek, California, Geol. Soc. Am. Bull., 100: 938-947.

Gillespie A.R., Huneke G.C., and Wasserburg G.J. (1982) Eruption age of an approximately 100,000 years old basalt from 40Ar-39Ar analysis of partially degassed xenoliths, J. Geophys. Res., 89; 1033-1048.

Hamilton W.B., and Neuerburg G.J. (1956) Olivine-sanidinetrachybasalts from the Sierra Nevada, California, Am. Mineral., 41: 851-873.

Luedke R.G., and Smith R.L. (1981) Map showing the distribution, composition, and age of Late Cenozoic volcanic centers in California and Nevada, U.S. Geol. Surv. Misc. Invest. Ser. Maps, 1091-C.

Moore J.G., and Dodge F.C.W. (1980) Late Cenozoic volcanic rocks of the Southern Sierra Nevada, California; I: Geology and petrology, Geol. Soc. Am. Bull., 91: 515-518.

Mukhopadhyay B. (1989) Petrology and geochemistry of mafic and ultramafic xenoliths from the Sierra Nevada batholith, Ph.D., dissertation, Univ. of Texas at Dallas, 215 p.

Ormerod D.S. (1988) Magmatic transitions in the western great basin, U.S.A., Ph.D. dissertation, Open University, Milton Keynes, U.K.

Rose R.L. (1959) Tertiary volcanic domes near Jackson, California, California Div. of
Mines and Geology, Spec. Rep., 60, 21 p.

Van Kooten G.K. (1980) Mineralogy, geochemistry, and petrology of an ultrapotassic
basaltic suite, central Sierra Nevada, California, U.S.A., J. Petrol., 21: 631-638.

APPENDIX 2

Analytical Techniques-TIMS

Late Cenozoic volcanic rocks and xenoliths were analyzed for major element chemistry of the constituent phases, whole rock and mineral separate major element, and trace element chemistry, as well as Sr, Nd, Pb, and O isotopic ratios. Various analytical procedures were outlined in the chapters of this dissertation. Here I present an overview of the analytical techniques employed in determination of radiogenic isotopic ratios by thermal ionization mass spectrometry (TIMS) methods. The procedures used in Dr. Saleeby's laboratory were previously described (Rubin, 1991; Pickett, 1991; Pickett and Saleeby, 1994; Gazis, 1995). This Appendix is intended to provide an update of these procedures, as they have changed somewhat, tabulate the isotopic analyses of Rb, Sr, Sm, Nd, and Pb standards and provide analyses of blanks performed in this laboratory during the course of this study (1994-1998). Most of the samples were spiked with ^{87}Rb, ^{84}Sr, and a mixed ^{147}Sm-^{150}Nd in order to determine the elemental concentrations of Rb, Sr, Sm, and Nd by isotope dilution. The spiking procedures and the spike concentrations are as in Pickett (doctoral thesis, 1991), Pickett and Saleeby (1994) and Gazis (doctoral thesis, 1995), and will not be detailed in the following discussion.

Mass spectrometric analyses were carried out on an automated VG Sector multicollector instrument fitted with adjustable 10^{11} Ω Faraday collectors and a Daly photomultiplier. Concentrations of Rb, Sr, Sm, and Nd were determined by isotope dilution, with isotopic compositions of Sr and Nd determined on the same spiked runs. Several offline manipulation programs were used for isotope dilution calculations.

A2.1. Sample dissolution procedures

Sample preparation for dissolution varied depending on the type of material analyzed. Crushing and leaching procedures, mineral separation techinques, are described

Table A2-1. Sr standard runs (Sr 987) analyzed during
the course of this study.

Isotopic ratios are normalized to $^{86}Sr/^{88}Sr = 0.1194$

Date	$^{87}Sr/^{86}Sr$	$^{84}Sr/^{86}Sr$
Prior to 1995*	0.710244±5	0.056514±10
6/13/95	0.7102745	0.0564873
6/25/95	0.7103127	0.0565316
9/11/95	0.7103226	0.0564816
3/2/96	0.7103125	0.0564810
6/5/96	0.7103011	0.0553887
11/14/96	0.7102048	0.0561602
1/15/97	0.7101144	0.0566930
1/22/97	0.7102132	0.0554731
10/14/97	0.7103531	0.0540836
10/14/97	0.7102285	0.0599350
12/8/97	0.7102874	0.0552327
12/8/97	0.7103615	0.0567211
Mean	0.7102738±7	0.0563057±12

*Averaged using data from Pickett (1991) and Gazis (1995)

in the chapters 3, 5, and 6 of this thesis. Between 20 and 200 mg of sample were weighed, put in Teflon beakers, moistened with 1N HCl and spiked prior to dissolution. After the spikes were added, the samples were dissolved. The usual procedure applied in this laboratory is to first dissolve in ~2 ml hot concentrated HF to which about 1 ml concentrated HNO_3 is added. This technique is efficient for most felsic rocks. However, most of the samples analyzed in this study were mafic or ultramafic, commonly quite resistant to dissolution in this mixture. A mixture of cold concentrated HF (or HNO_3) and $HClO_4$ proved to be more efficient in ultramafic rocks dissolution. After this dissolution step, the samples were dissolved in 1.5 N HCl, centrifuged and checked for solid residue. Any solid residue was taken up in the same way. The samples were then passed through the cation columns for Rb, Sr, and REE elution.

A2.2. Rubidium and Strontium isotopic analyses

Chemical separation. Separation of Rb and Sr, as well as the bulk of the Rare Earth Elements (REEs) was achived in cation columns containing AG50W-X4 resin, using 1N to 4N HCl (Pickett, 1991). A few felsic samples were separated in minicolumns, previously described in Gazis (1995). For better separation of Rb from Sr in the cation columns, Sr separates from samples presumed to have elevated Rb/Sr ratio were passed through the columns a second time.

Filament loading and mass spectrometric analysis. Rb was loaded onto single Re filaments, using silica gel and H_3PO_4. Sr was loaded onto single Ta filaments, with Ta_2O_5 powder. Rb was analyzed statically, while Sr multidynamically, using a four collector peak switch scheme, as described in Pickett (1991). Typical runs consisted of aquisition of 100 isotopic ratios.

Standards and blanks. Analyses of standard nRb AAA and Sr 987 are given in Tables A2-1 and A2-3, respectively. The mean values obtained on these standards during the course of this study are similar to values previously measured on the same batches of

Table A2-2. Nd standard runs (La Jolla Nd) analyzed during the course of this study. Isotopic ratios are normalized to ^{146}Nd/^{144}Nd = 0.7219.

Date	142/144	143/144	145/144	150/144
Prior to 1995*	1.14183±2	0.511853±3	0.348407±1	0.236448±13
Prior to 1995**	1.14182±3	0.511851±7	0.348404±2	0.236438±14
9/20/95	1.1417714	0.5118384	0.3483960	0.2363962
9/20/95	1.1418065	0.5118403	0.3484000	0.2364203
9/25/95	1.1418537	0.5118480	0.3483910	0.2364706
9/25/95	1.1418287	0.5118467	0.3483930	0.2364645
10/2/95	1.1419396	0.5118627	0.3483741	0.2364702
10/28/95	1.1418287	0.5118517	0.3483848	0.2365559
11/5/95	1.1418256	0.5118440	0.3483968	0.2364452
12/3/95	1.1418282	0.5118459	0.3483934	0.2365388
2/12/96	1.1418637	0.5118331	0.3483799	0.2366296
3/5/96	1.1418622	0.5118441	0.3483801	0.2364302
3/18/96	1.1419075	0.5118470	0.3483917	0.2364057
6/12/96	1.1419347	0.5118632	0.3483865	0.2364735
8/28/96	1.1418152	0.5118733	0.3483941	0.2354181
12/9/96	1.1416815	0.5118759	0.3483909	0.2359860
1/9/97	1.1418515	0.5118672	0.3484018	0.2362596
3/10/97	1.1418762	0.5118469	0.3483928	0.2365041
6/1/97	1.1417721	0.5118523	0.3483934	0.2364545
8/22/97	1.1418144	0.5118500	0.3483891	0.2364788
Mean	1.1418367±2	0.5118517±2	0.3483905±2	0.2363779±18

* Average of Pickett (1991), all loads
** Average of Pickett (1991), resin loads

standards (Pickett, 1991; Gazis, 1995). Procedural blanks averaged from 5 determinations were: Rb - 11 pg, Sr -150 pg.

A2.3. Samarium and Neodynium isotopic analyses

Chemical separation. The separation of Sm and Nd from the bulk of REEs, previously eluted in cation columns, was modified during the course of my labwork, compared to the procedures described in Pickett (1991). Separation of Sm and Nd was achived in 0.5 mm diameter columns with LN Spec resin, using 0.1N to 2.5N HCl (Pickett, 1991). The new procedures ensure a more efficient separation of the REEs, and is less time consuming (the new procedure is ~ twice as fast as the old one).

Filament loading and mass spectrometric analysis. Both Sm and Nd were loaded onto single Re filaments. Sm was loaded using platinized carbon, while Nd using resin beads. The resin for Nd loading was the same type as the one utilized for cation separations. Nd was analyzed multidynamically using a five collector scheme, whereas Sm was analyzed statically (Pickett, 1991). Typical runs consisted of aquisition of 100 isotopic ratios.

Standards and blanks. Analyses of standard LaJolla Nd and nSmβ are given in Tables A2-2 and A2-3, respectively. The mean values obtained on these standards during the course of this study are similar to values previously measured on the same batches of standards (Pickett, 1991). Procedural blanks averaged from 5 determinations were: Sm - 2.7 pg, Nd - 5.5 pg.

A2.4. Lead isotopic analyses

Chemical separation. The common isotopes of lead were analyzed on whole rocks samples, previously dissolved for Sr and REE separations. Separate batches of dissolved samples were saved for lead chemistry. Lead was extracted using an anion exchange

Table A2-3. Rb (nRb AAA) and Sm (nSmβ) standard runs analyzed during the course of this study.

Isotopic ratios of Sm are normalized to $^{149}Sm/^{152}Sm = 0.51686$.

Rubidium	nRb AAA	Samarium nSm β		
Date	85/87	Date	148/147	148/152
Prior to 1995*	2.6163±19	Prior to 1995*	0.74964±19	0.42049±5
9/18/95	2.6152360	11/17/95	0.7493134	0.4219955
1/31/96	2.6075525	12/2/95	0.7496552	0.4204821
1/31/96	2.6114049	3/7/96	0.7497871	0.4205120
4/1/96	2.6080942	7/20/96	0.7495636	0.4209689
7/30/96	2.6104561	12/11/96	0.7496211	0.4204061
8/2/96	2.6163434	1/28/97	0.7496367	0.4204477
2/3/97	2.6096520	5/18/97	0.7495994	0.4205526
8/4/97	2.6164556	9/10/97	0.7496348	0.4204551
Mean	2.6118993±20	Mean	0.7496014±21	0.4207275±6

* - Average ratios from Pickett (1991)

procedure modified after Chen and Wasserburg (1981). Lead separation is performed via elution in HBr. About 50 mg were passed through 0.5 ml resin (Biorad AG1x8, 100-200 mesh). The Pb elution procedure, including the type of reagents used and their volume are given in Table A2-4. The mass spectrometer signal increases up to 5-10 times for samples passed through a second, smaller column ("Cleanup column" in Table A2-4). Cleanup is performed in a smaller column using the same type of resin following the main extraction procedure, with the difference that Pb was eluted using HCl this time.

Filament loading. Lead was loaded with H_3PO_4 silica gel, onto a previously outgassed rhenium filament. The procedures for lead loading are similar to the ones described by Rubin (1991).

Mass spectrometric analysis. The lead isotopic analyses were perfomed using a static routine. All isotopes were measured in Faraday cups, with the exception of samples with low signal, whose ^{204}Pb was measured using a Daly photomultiplier. Filament temperatures were typically ~1350 °C and the current signal averaged ~10^{-11} Amps of ^{206}Pb and decreased during the course of the run. For most samples, 50 sets of isotopic ratios were measured.

Standards and blanks. The mean results of 4 analyses of lead standard NBS 981 are given below. These values are within the errors calculated for isotopic analyses of the same batch of NBS 981, performed in the Lunatic Asylum at Caltech.

NBS 981	206/204	207/204	208/204
This study (1997)-4 runs	16.945±22	15.492±20	36.698±25
Lunatic average (1980-1985)	16.948±16	15.503±20	36.676±20

The lead blanks measured during the course of this study were: Pb ~0.04±02 ng. The blank lead has an isotopic composition of: $^{206}Pb/^{204}Pb$ = 18.82±0.3, $^{207}Pb/^{204}Pb$= 15.66±0.3, and $^{208}Pb/^{204}Pb$=38.5±0.5. The amount of blank was determined by isotope

Table A2-4. Elution procedures for isotopic analyses of common lead isotopes.
Resin is Biorad AG1x8, 100-200 mesh, ~0.5 ml. Column works for up to 100 mg sample.
Cleanup column uses 0.1 ml of the same resin.

Steps	Reagents	Volume (ml)
1. Cleaning	Water	1.5
	6N HCl	2.5
	Water	1.5
	6N HCl	2.5
	Water	1.5
2. Equilibrating	1N HBr	1.5
3. Sample loading	in 1N HBr	up tp 3
4. Cleaning	1N HBr	2
	2N HCl	0.5
	6N HCl	0.25
5. Eluting Pb	6N HCl	2
6. Evaporation		
7. Re-dissolution	2N HCl	25 μl
CLEANUP		
8. Washing	6N HCl	0.5
	Water	0.5
9. Equilibrating	2N HCl	0.5
10. Sample loading	2N HCl	25 μl
11. Cleaning	2N HCl	0.3
12. Eluting Pb	6N HCl	0.2
13. Evaporation		

dilution analysis of a typical dissolution/separation procedure without any sample. The isotopic composition of the blank was determined on acids and dust particles in the laboratory.

References

Chen, J.H., and Wasserburg, G.J., 1981, Isotopic determination of uranium in picomole and subpicomole quantities, Anal. Chem., 53, 2060-2067.

Gazis, C.A., 1995, An isotopic study of the fluid flow and thermal history of the 2.8 Ma Chegem ash-flow caldera and related intrusive rocks (Caucasus Mountains, Russia), Ph.D. thesis, California Institute of Technology, 280 p.

Pickett, D.A., 1991, An isotopic and petrologic study of an exposure of the deep Sierra Nevada batholith, Ph.D. thesis, California Institute of Technology, 320 p.

Pickett, D.A., and Saleeby, J.B., 1994, Nd, Sr, and Pb isotopic characteristics of Cretaceus intrusive rocks from deep levels of the Sierra Nevada batholith, Tehachapi Mountains, California, Contrib. Mineral. Petrol., 118, 198-205.

Rubin, C. M., 1991, Structural, stratigraphic, and geochronologic analysis of the Alexander-Taku terrane boundary and the overlapping Upper Jurassic to Lower Cretaceous Gravina Sequence, Southeast Alaska, Ph.D. thesis, California Institute of Technology.

APPENDIX 3

Sulfur Variations in Glasses From Volcanic Rocks: Effect of Melt Composition on Sulfur Solubility

Mihai N. Ducea, Brent I. A. McInnes and Peter J. Wyllie

Abstract

A world-wide dataset of major element and sulfur analyses of undegassed lavas, pumices and melt inclusions from 14 volcanic locations was selected to investigate the compositional effects on sulfur solubility in magmas. We used analyses on calc-alkaline, alkaline, and tholeiitic rocks, with a range of 3400 ppm S variation. There is a strong correlation between chemical composition and the sulfur concentration: the less silicic and the more alkaline the rocks are, the more dissolved sulfur they can carry. Also, sulfur concentration is higher in rocks which represented less polymerized melts. Elemental correlations between FeO and S, well defined for tholeiites, do not hold for alkaline melts. The compositional effects are at least as important as the better-known pressure, temperature and fO_2 dependencies.

A3.1. Introduction

Sulfur is a common and petrologically important volatile constituent of magmas. The amount of sulfur carried by magmas depends on the initial concentration of sulfur in the source region, the solubility of sulfur in silicate melts, and various processes occurring between the magmatic source and magma consolidation.

Sulfur solubility in melts depends on temperature, pressure, oxygen fugacity, sulfur speciation and melt composition (Katsura and Nagashima, 1974; Carroll and Rutherford, 1985; 1987). Compositional dependencies are known for mafic tholeiitic melts (Haughton et al., 1974; Wallace and Carmichael, 1992; Dixon et al., 1990), but

insufficiently known for other magmas. Contents of dissolved volatile components have been observed to vary with melt composition in calc-alkaline volcanic rocks from Papua New Guinea oceanic island arcs. McInnes and Cameron (1994) reported 2.8% dissolved SO_3 in undegassed, alkaline melt inclusions trapped at high pressure and temperature in mantle xenocrysts from the high-K calc-alkaline volcanoes of the Tabar-Lihir-Tanga-Feni arc.

We have therefore explored the effect of melt composition on sulfur solubility in two ways: (1) compiling carefully selected analyses of volcanic glasses, and (2) experimental measurement of sulfur solubility in melts as a function of alkalinity. The analytical compilation and review is presented here, and preliminary experimental results given in Ducea et al. (1994) are being investigated further.

Sulfur solubility in silicate melts has been measured experimentally (Mysen and Popp, 1980; Carroll and Rutherford, 1985; 1987; Luhr, 1990), but these experiments focussed on melt composition effects only in that different compositions were used. A strong difference between sulfur solubility in synthetic Fe-free calc-alkaline and alkaline melt compositions under oxidized conditions was determined experimentally by Ducea et al. (1994), with as much as 6 times higher sulfur concentrations in alkaline melts. Other experimental investigations have concluded that melt alkalinity affects Cl (Metrich and Rutherford, 1992), H_2O (Dingwell et al., 1984) and CO_2 (Thibault and Holloway, 1994) solubility. Furthermore, it is almost axiomatic in petrology that alkaline magmas have higher volatile solubilities than their metaluminous equivalents (e.g., Sorensen, 1974), and the analyses presented below confirm this for sulfur.

For our interpretation of sulfur solubility in magmas, we selected published sulfur and major element analyses on worldwide young volcanic rocks and glass inclusions of different compositions. Our focus was on calc-alkaline and alkaline compositions which have been far less studied in this respect than tholeiitic mafic rocks. First, we compare sulfur contents in several volcanic products as a function of rock composition. Secondly

we examine whether compositional relations previously determined in tholeiitic basalts (Haughton et al., 1974, Dixon et al., 1990) hold through a larger range of melt compositions. The review establishes some very simple compositional dependencies on sulfur content: lower silica, more alkaline, and less polymerized magmas have higher sulfur concentrations.

## A3.2. Selection criteria of sulfur measurements in volcanic glasses

Sulfur concentration analyses are available for a variety of volcanic products such as lavas, pumices, and glass inclusions in phenocrysts. Most of the published analyses are from tholeiitic basalts obtained from submarine spreading centers. We searched the larger compositional spectrum with emphasis on glass-bearing calc-alkaline and alkaline rocks. The types of data and their sources are shown in Table A3-A3-1. The rocks are defined as "calc-alkaline" or "alkaline" on the basis of the total alkali-silica criterion (Le Bas et al., 1986). All "alkaline" compositions are represented in the figures as <u>filled symbols</u>, while the "calc-alkaline" ones are represented by <u>open symbols</u>.

The analyses cited in Table A3-1 were carefully selected using criteria to identify rocks which had best chance of being close to sulfur saturation. The most meaningful sulfur concentrations are those where the maximum sulfur content is attained in glasses which have crystallized a sulfur-bearing mineral, and degassing of the melt has not occurred. Melt inclusions in phenocrysts provide the best prospect for obtaining undegassed volatile compositions (Anderson, 1974) and many of the analyses used in this study were obtained from melt inclusion glasses. Submarine volcanic glasses are commonly undegassed, but the literature is skewed towards analyses of tholeiitic glasses, and calc-alkaline and alkaline compositions are relatively rare. If a set of chemical analyses representing a single pulse of magma (e.g., one eruption) shows variability in sulfur concentration (e.g., El Chichon, Luhr et al., 1984), we used only the highest sulfur concentration samples assuming that the

TABLE A3-1. List of sulfur-bearing magmatic products investigated.

Location	Material analyzed	Chemical composition	Method of S Analysis	Reference	Abbreviations in this paper's figures
El Chichon (Mexico)	phenocryst-free pumices	trachyandesites	wet chemistry and XRF	Luhr and Carmichael, 1984	El Chichon
Lascar Volcano (Chile)	lavas and glass inclusions	andesites and dacites	electron microprobe	Matthews et al., 1994	Lascar
Nevado del Ruiz (Colombia)	quenched glass	rhyolites	electron microprobe	Fournelle, 1990	Nevado del Ruiz
Mount Pinatubo (Philippines)	matrix glasses and glass inclusions	dacites and rhyolites	electron microprobe	Gerlach et al., in press	Pinatubo
Mariana arc and back-arc trough	glassy submarine lavas	basalts and andesites	wet chemistry methods	Alt et al., 1993	Mariana
Julcani Magmatic District (Peru)	pumices and lavas	high-K dacites and rhyolites	not described	Drexler and Munoz, 1980	Julcani
Edison Submarine Volcano, (Papua New Guinea)	matrix glasses	basaltic trachyandesites	electron microprobe	Herzig et al., 1994	Edison
Kavachi Volcano (Solomon Is.)	matrix glasses	andesites	electron microprobe	Johnson et al., 1987	Kavachi
Stromboli Volcano (Aeolian Islands)	melt inclusions	alkali-basalts	electron microprobe	Allard et al., 1994	Stromboli
Etna (Italy)	glass inclusions and matrix glasses	alkali-basalts	electron microprobe	Metrich et al., 1993	Etna
Vepe Caldera (Italy)	pumices and lavas	phonolites and tephri-phonolites	not described	Capaccioni et al., 1987	Vepe
Latera Volcano, Vulsinian District (Italy)	glassy pumices	latites and shoshonites	not described	Conticelli et al., 1987	Vulsini
Loihi Seamount, Hawaii	glassy rims of submarine basalts	alkali-basalts	mass spectrometry	Byers et al., 1985	Hawaii
Tavolato/Roman District	glassy lavas	leucite-phonolite	electron microprobe	Baldridge et al., 1981	Tavolato

Figure A3-1. Sulfur (ppm) vs. total FeO (%) concentrations (FeO+Fe$_2$O$_3$) for the analyzed rocks. Three FeO-S correlations (sulfur saturation lines) for basalts (Mathez, 1976; Poulson and Ohmoto, 1990; and Dixon et al., 1990) are shown. Most of the alkaline magmas considered in this study lie above the sulfur-saturation lines defined for basalts. Filled symbols represent alkaline rocks and all other symbols represent sub-alkaline rocks according to the classification of Le Bas et al. (1986). The sample locations abbreviated in the legend are listed in the last column of Table A3-1.
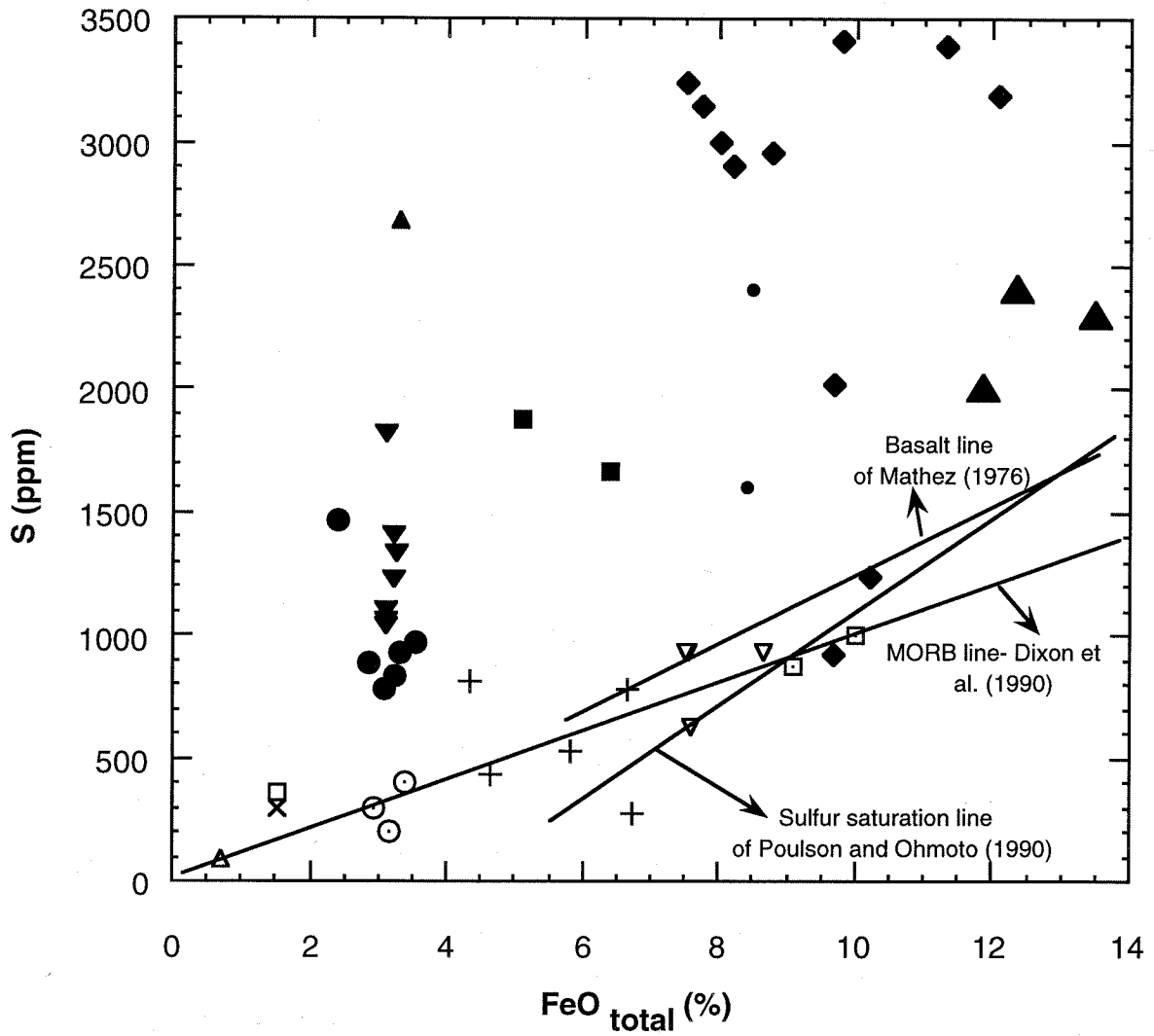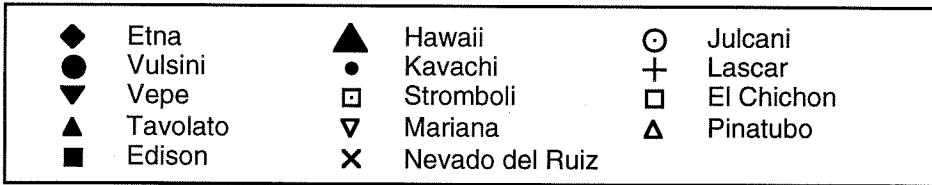
lower values were caused by degassing. For the pumices, it is not always possible to tell whether the analyzed samples contained anhydrite or sulfide (e.g., the 1991 Pinatubo pumices, Bernard et al., 1991,) and this is a potential source of overestimated solubilities in analyzed rocks. Therefore, we preferred not to include analyses of whole-rock pumices that might contain phenocrysts.

A3.3. Correlations between sulfur and other components in magmas

The analyses of the volcanic glasses presented in the literature cited in Table A3-1 were examined in some detail for possible correlations between sulfur concentration and other compositional parameters. Iron was taken into account as FeO_{total}. The following figures show variations in oxide concentrations and some CIPW normative values (computer program provided by D. Sykes) from the published major element chemistry of each sample. Correlations were found for sulfur with FeO, CaO, SiO_2, normative albite, wollastonite, and with alkalinity expressed as variation in normative quartz and nepheline.

Correlations between sulfur and FeO in silicate melts. Positive correlations have been observed or proposed between S and FeO in experiments at fO_2 < FMQ (Fincham and Richardson, 1954; Haughton et al., 1974, Carroll and Rutherford, 1985). This relationship has also been observed in natural tholeiitic basalts (Mathez, 1976; Dixon et al., 1990; Poulson and Ohmoto, 1990), who used the FeO-S correlations to construct "MORB-lines". These FeO-S correlations are reconstructed in Figure1 and compared to calc-alkaline and alkaline samples from Table A3-1. The samples range in composition from 43-75% SiO_2, and include both nepheline- and quartz-normative. Although the calc-alkaline samples conform fairly well with the MORB-lines, the alkaline glasses show much higher sulfur solubilities and no hint of a correlation between S and FeO.

The enrichment of sulfur above "MORB" values can not be attributed to the high oxygen fugacity in the silicate melts. Loihi volcanic lavas erupt under oxygen fugacity

Figure A3-2. Sulfur (ppm) vs. CaO (%) concentrations for the analyzed rocks. Filled symbols represent alkaline rocks and all other symbols, calc-alkaline rocks, as in Figure A3-1. Abbreviations are as in Table A3-1.

Figure A3-2. Sulfur (ppm) vs. CaO (%) concentrations for the analyzed rocks. Filled symbols represent alkaline rocks and all other symbols, calc-alkaline rocks, as in Figure A3-1. Abbreviations are as in Table A3-1.

conditions similar to MORB, and therefore it appears that bulk composition may have a control on S values. In addition, bulk composition appears to be important in S variations between both calc-alkaline and alkaline samples from volcanic arcs. These lavas erupted under relatively oxidizing conditions (QFM+1-2), and yet the sulfur content in calc-alkaline samples conform to the "MORB line". Results from Figure A3-1 imply that bulk composition of silicate melts, in addition to Fe content and/or oxidation state, is an important control on S solubility.

Correlations between sulfur and CaO in silicate melts. A positive correlation exists between S with CaO in Figure A3-2 for the calc-alkaline samples, an observation which has been previously noted by other workers (Katsura and Nagashima, 1974; Carroll and Rutherford, 1985; Luhr, 1990). For calc-alkaline magmas with oxygen fugacities above the NNO+1 buffer, sulfur dissolves as sulfate, and the correlation is attributed to the formation of calcium sulfate complexes in the melt. Carroll and Holloway (1994) pointed out that the correlation has not yet been established in experiments, because CaO has not been varied independently in the experimental melts.

For the alkaline samples in Figure A3-2, the highest sulfur contents occur in the samples with the highest CaO content, although there is no clear and systematic correlation between all the CaO and sulfur data for the alkaline samples.

Correlations between sulfur and SiO_2 in silicate melts. Figure A3-3 shows S content plotted against SiO_2, the major chemical variable in the volcanic samples. There is a broad negative correlation of decreasing S with increasing SiO_2, but two trends are discernible within the spread of points. The calc-alkaline analyses define a low-S trend, and the alkaline analyses occupy a high-S trend with steeper slope. A similar negative correlation between ppm S and SiO_2 was observed by Matthews et al. (1994) in the glass inclusions of Lascar Volcano (Chile).

Because basalts are the most abundant magmas erupted on the Earth, it would be useful to know whether a simple correlation exists between SiO_2 content and S. The

Figure A3-3. Sulfur (ppm) vs. SiO$_2$ (%) concentrations for the analyzed rocks. Filled symbols represent alkaline rocks, and all other symbols, calc-alkaline rocks, as in Figure A3-1. Abbreviations are as in Table A3-1.
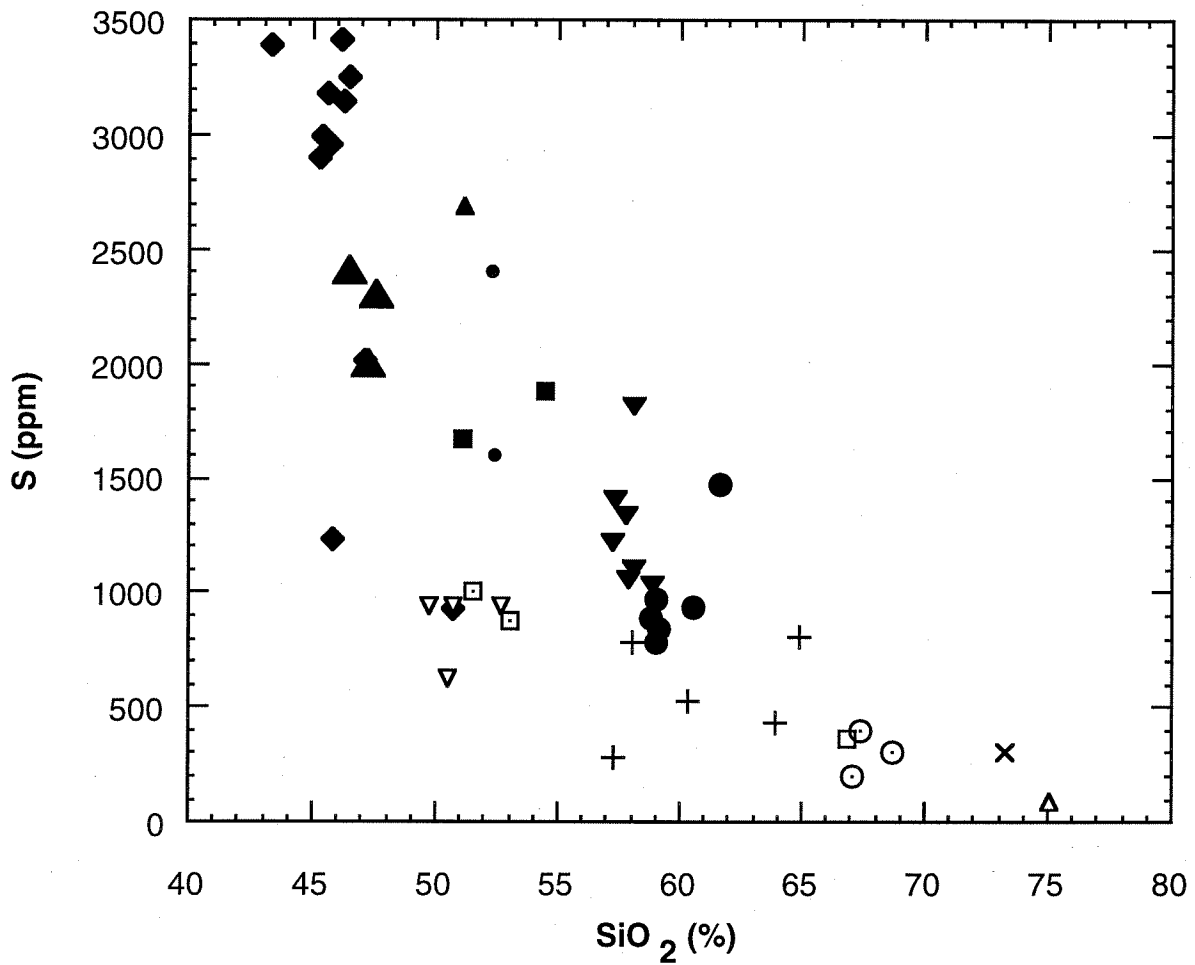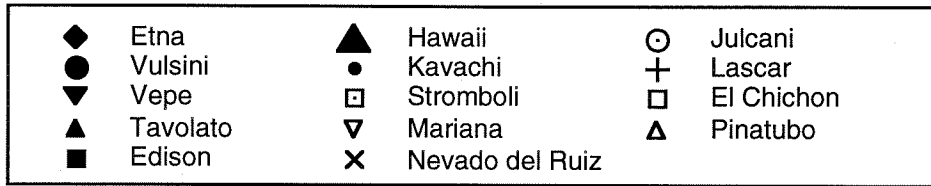
disparate trends in Figure A3-3 demonstrate the inadequacy of SiO$_2$-S plots in representing actual sulfur solubilities for basaltic melts, as S variation is quite significant (500-2700 ppm) over a limited range of SiO$_2$ (49-53%). We hypothesize that a relationship must exist between alkalinity and S content, rather than SiO$_2$ and S content, in silicate melts.

Sulfur, normative quartz, and normative nepheline. Figures 1-3 illustrate distinct differences in S contents of volcanic glasses defined by the present authors as alkaline or calc-alkaline. When single locations are compared, e.g., Etna or Hawaii, the more alkaline the lavas are, the more S they carry. In order to examine this aspect in quantitative detail, we used normative quartz (qz) or nepheline (ne) as a measure of magma alkalinity. Plotting all analyses against the normative parameters in Figure A3-4a shows that the petrographic names correspond closely to the chemical discriminant, with only minor overlap across the SiO$_2$-saturation line. The strong positive correlation between the sulfur concentrations and alkalinity is obvious, but in the ne-normative field the trend is wide. The smooth curve which bounds the field of plotted analyses in Figure A3-4a gives the maximum S content for each alkalinity. The equation which corresponds to this curve is:

$$S_{(ppm)} = 1668 \, e^{-0.054(Qz_{norm}-Ne_{norm})}$$

Figure A3-4b is the corresponding diagram for published experimental data on oxidized melts at temperatures between 775-900 ^{0}C. Sulfur solubilities in quartz-normative (> 10% qz) liquids from calc-alkaline rocks studied by Carroll and Rutherford (1987) and Luhr (1990) are less than 500 ppm. The preliminary results of Ducea et al. (1994) using Fe-free synthetic material give comparable results for a qz-normative composition, and markedly higher S values (900-1400 ppm) for a ne-normative composition. The experimental results thus reflect the observations for the natural samples.

Obviously, the S solubility is affected by many other parameters which will complicate this simple relation, but it is remarkable that regardless of the sulfur speciation,

Figure A3-4. (**a**). Sulfur (ppm) vs. normative quartz or normative nepheline for the analyzed rocks. Filled symbols represent alkaline rocks, and all other symbols, calc-alkaline rocks, as in Figure A3-1. Abbreviations are as in Table A3-1.

(**b**). Sulfur (ppm) vs. normative quartz or normative nepheline in different experimental runs of calc-alkaline and alkaline compositions. The experimental results plotted are selected in a temperature interval of 775 - 900 ^{0}C, pressures of 1.5-2 kbar and oxygen fugacities close to the NNO buffer.
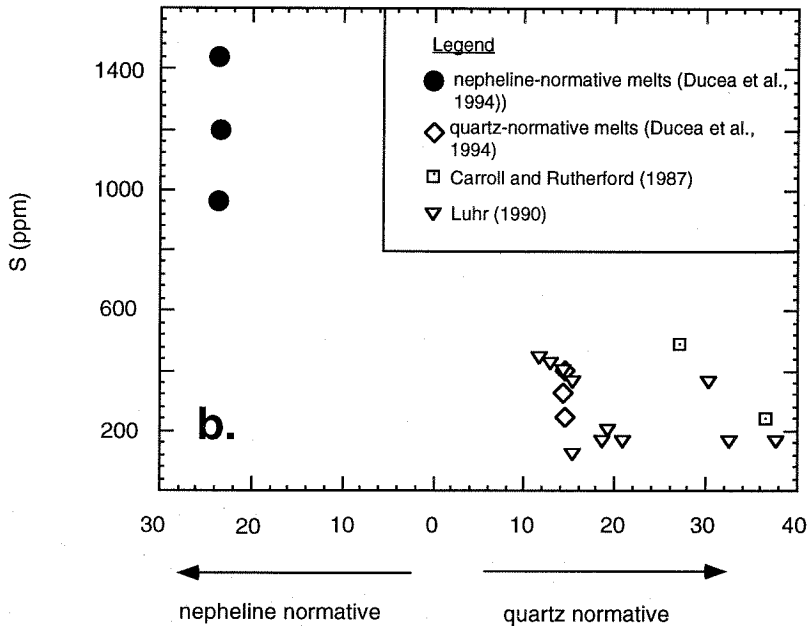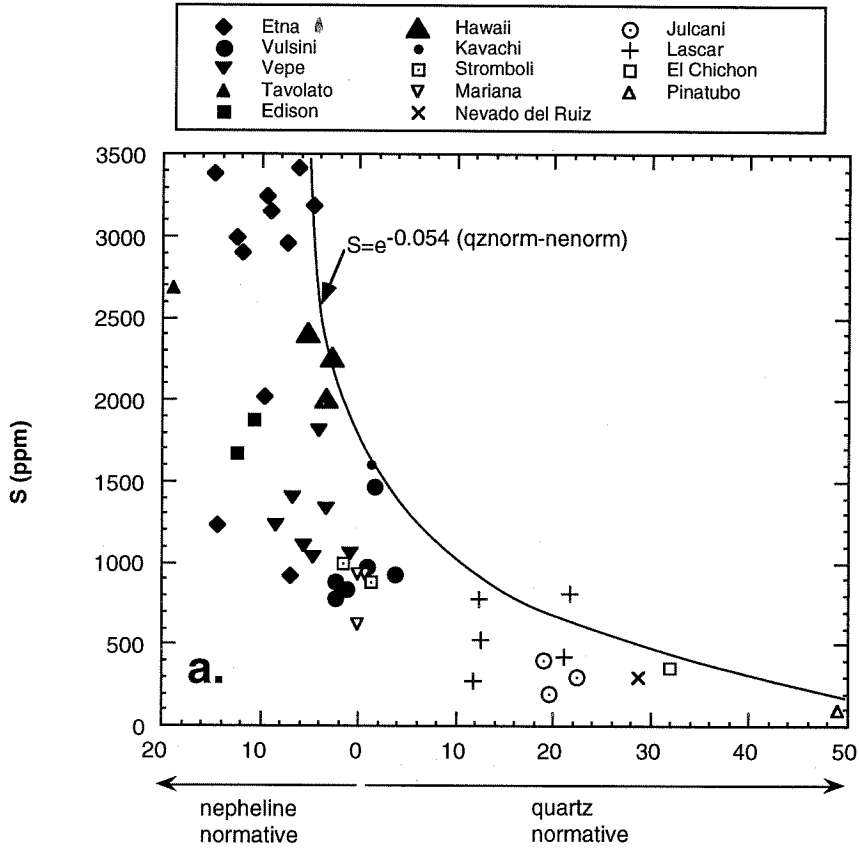
temperature, pressure or fO_2 of the magmas (which are not considered in this analysis), the negative correlation between S solubility and the degree of silica saturation in Figure A3-4 holds.

Sulfur, normative albite, and normative wollastonite. Figure A3-5 shows the relationship between sulfur concentrations in samples and their normative albite (ab) and wollastonite (wo) components. Figure A3-5a shows a negative correlation with ab, Figure A3-5b shows a scattered positive correlation with wo, and Figure A3-5c shows a more orderly positive correlation with the combined parameter wo minus ab (wo-ab). This parameter (wo-ab) is a measure of melt depolymerization, because in the analyzed glasses, albite and wollastonite are the dominant molecules of framework and chain silicates, respectively, and because a more polymerized melt has much higher normative framework silicates than chain and other less common, structural groups of silicates. A depolymerized melt dominated by chain silicates is, therefore, expected to carry more S, by analogy with arguments for the solubility of CO_3^{2-} in silicate melts (Fine and Stolper,1986).

Other correlations. No other major elements or normative components were found to correlate systematically with sulfur concentration. Chlorine measurements are available for most of the analyses considered here, in particular for alkaline melts. Chlorine shows correlations with melt compositions very similar to those of sulfur, the negative correlation with melt alkalinity being well defined (Figure A3-6).

A3.4. Conclusions

In Figures 1-6 we examined compositional dependencies between sulfur content and melt composition from carefully selected natural and experimental calc-alkaline and alkaline glasses formed under various temperature, pressure, and fO_2 conditions. The total range of S variation in calc-alkaline and alkaline magmas in this study is 3400 ppm. The following correlations were observed:

Figure A3-5.   **(a)**. Sulfur (ppm) vs. normative albite.

(b). Sulfur (ppm) vs. normative wollastonite.

(c). Sulfur (ppm) vs. wollaston minus albite (wo-ab), where wo-ab is a measure of melt depolymerization. Filled symbols represent alkaline rocks and all other symbols, calc-alkaline rocks. Abbreviations are as in Table A3-1.
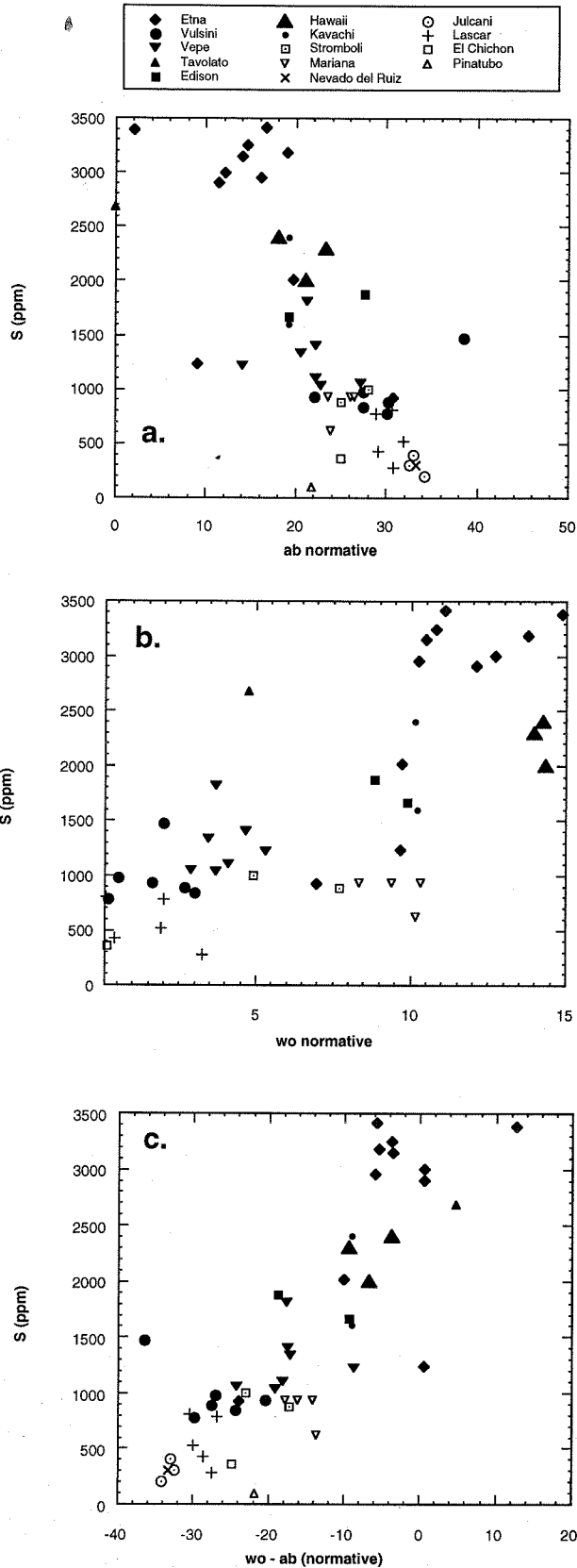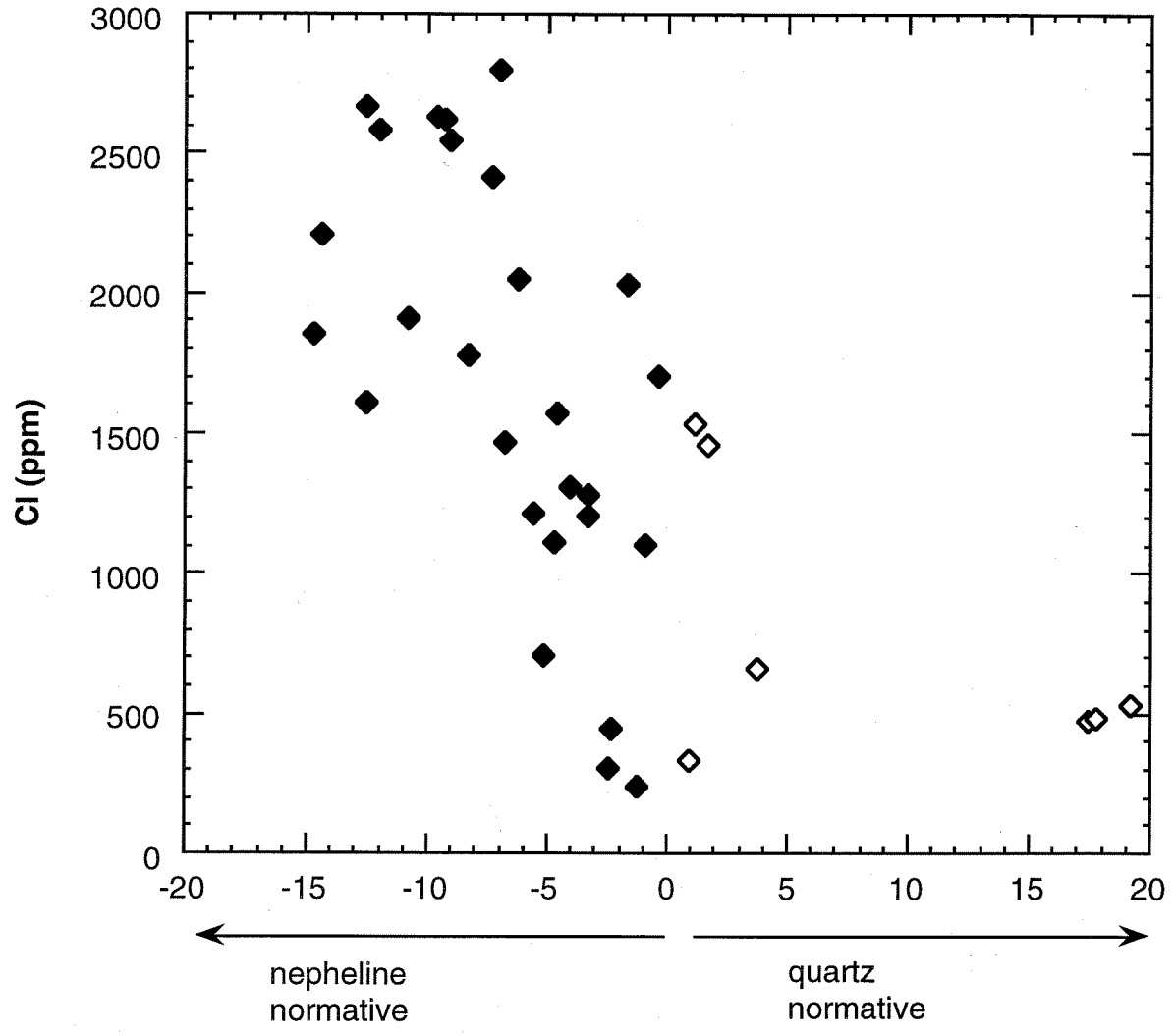
Figure A3-6. Chlorine (ppm) vs. normative quartz (normative) for the analyzed rocks from Table A3-1 in which Cl abundance was available.

(1) Calc-alkaline samples show a similar positive correlation between FeO and S content as tholeiitic basalts from mid-ocean ridge environments (Figure A3-1). For all FeO values, S is higher in alkaline than in calc-alkaline compositions. The alkaline samples exhibit no correlation between S and FeO.

(2) There is a positive correlation of increasing S with CaO in calc-alkaline compositions as previously noted (Figure A3-2). The alkaline samples show poor correlation between S and CaO.

(3) Two distinct trends of decreasing S with increasing SiO_2 occur (Figure A3-3) with calc-alkaline samples defining a low-S trend and the alkaline samples a high-S trend. A continuous variation of S with SiO_2 content in silicate melts is not evident.

(4) A continuous correlation between maximum sulfur content and alkalinity exists, indicating that bulk composition effects are significant. The empirical relationship which relates sulfur content as a function of melt alkalinity,

$$S_{(ppm)} = 1668\ e^{-0.054(Qz_{norm} - Ne_{norm})},$$

describes the maximum S content for tholeiitic compositions as well as calc-alkaline and alkaline compositions (Figure A3-4).

(5) The strong positive correlation between S and normative wollastonite minus albite (wo-ab), a measure of decreasing polymerization of the melt, supports the expectation that sulfur solubility increases with degree of depolymerization (Figure A3-5).

Because the sulfur content of alkaline melts can be several times that of calc-alkaline melts, we hypothesize that bulk compositional effects may be more important than P, T and fO_2 on sulfur solubility. The latter variables are probably the cause of the "noise" in Figures A3-1 to A3-6. Additional experimental studies involving nepheline-normative compositions are necessary to test this hypothesis, and to quantitatively assess the effects of melt composition on sulfur solubility.

References

Allard, P., Carbonnelle, J., Metrich, N., Loyer, H. and Zetwoog, P, 1994, Sulphur output and magma degassing budget at Stromboli volcano: Nature, v. 368, p. 326-329.

Alt, J. C., Shanks, W. C., and Jackson M. C., 1993, Cycling of sulfur in subduction zones: the geochemistry of sulfur in the Mariana island arc and back-arc trough: Earth Planet. Sci. Lett., v. 119, p. 477-494.

Anderson, A. T., 1974, Chlorine, sulfur and water in magmas and oceans: Geol. Soc. Am. Bull., v. 85, p. 1485-1492.

Baldridge, W. S., Carmichael, I. S. E., Albee A. L., 1981, Crystallization paths of leucite-bearing lavas: examples from Italy: Contrib. Mineral. Petrol. v. 76, p. 321-335.

Bernard, A., Demaiffe, D., Mattielli, N., and Punongbayan, R. S., 1991, Anhydrite-bearing pumices from Mount Pinatubo: further evidence for the existence of dulfur-rich silicic magmas: Nature, v. 354, p. 139-140.

Byers, C. D., Garcia, M. O., and Muenow, D.W., 1985, Volatiles in pillow rim glasses from Loihi and Kilauea volcanoes, Hawaii: Geochim. Cosmochim. Acta, v. 49, p. 1887-1896.

Capaccioni, B., Nappi, G., Renzulli, A., and Santi, P., 1987, The eruptive history of
Vepe Caldera (Latera Volcano): a model inferred from structural and geochemical
data: Periodico di Mineralogia, v. 56, no. 2/3, p. 269-284.

Carroll, M. R. and Holloway, J. R. (eds.), 1994, Volatiles in magmas: Mineralogical
Society of America, Reviews in Mineralogy, v. 30.

Carroll, M. R. and Rutherford, M. J., 1985, Sulfide and sulfate saturation in
hydrous silicate melts. Jour. Geophys. Res., v. 90, p. C601-C612.

Carroll, M. R. and Rutherford, M. J., 1987, The stability of igneous anhydrite;
experimental results and implications for sulfur behaviour in the 1982 El Chichon
trachyandesite and other evolved magmas: Jour. Petrol., v. 28, p. 781-801.

Conticelli, S., Francalanci, L., Manetti, P., and Peccerillo, A., 1987, Evolution of the
Latera Volcano, Vulsinian District (Central Italy): stratigraphical and petrological
data: Periodico di Mineralogia, v. 56, no. 2/3, p. 175-200.

Dingwell, D. B., Harris, D. M., and Scarfe, C. M., 1984, The solubility of H_2O in melts
in the system SiO_2-Al_2O_3-Na_2O-K_2O at 1 to 2 kbars: Jour. Geology, v. 92, p. 387-
395.

Dixon, J. E., Clague, D. A. and Stolper, E. M., 1990, Degassing history of water, sulfur,
and carbon in submarine lavas from Kilauea volcano, Hawaii: Jour. Geology, v.
99, p. 371-394.

Drexler, J. D. and Munoz, J. L., 1990, in "Recent advances in the geology of granite-
related mineral deposits", eds. Ishihara, S and Takenouchi. S. Mining Geology
Special issue, no. 8. p. 72-79.

Ducea, M. N., McInnes, B. I. A., and Wyllie, P. J., 1994, Experimental determination of
compositional dependence of hydrous silicate melts on sulfate solubility; application
to magma degassing: Trans. Am. Geophys. Union, v. 75., 44, p. 721
(abstract).

Fincham, C. J. B. and Richardson, F. D., 1954, The behaviour of sulphur in silicate and aluminate melts: Proc. R. Soc. London, Ser. A, v. 223, p. 40-62.

Fine, J. and Stolper, E. M., 1986, Dissolved carbon dioxide in basaltic glasses: concentration and speciation: Earth and Planetary Science Letters, v. 76, p. 105-121.

Fournelle, J., 1990, Anhydrite in Nevado del Ruiz November 1985 pumice: relevance to the sulfur problem: Jour. Volcan. Geotherm. Res., v. 42, p. 189-201.

Gerlach, T. M., Westrich, H. R., and Symonds, R. B., in press, Pre-eruption vapor in magma of the climactic Mount Pinatubo eruption: source of the giant stratospheric sulfur dioxide cloud.

Haughton, D. R., Roeder, P. L., and Skinner, B. J., 1974, Solubility of sulfur in mafic magmas: Econ. Geol., v. 69, p. 451-467.

Herzig, P., Hannington, M., McInnes, B., Stoffers, P., Vilinger, H., Seifert, R., Binns, R., and Liebe, T., 1994, Submarine volcanism and hydrothermal venting studied in Papua, New Guinea: EOS, Trans. Am. Geophys. Union, v. 75, 44, p. 513-516.

Johnson, R. W., and 8 others, 1987, Ridge subduction and forearc volcanism:petrology and geochemistry of rocks dredged from the western Solomonarc and Woodlark basin: in "Marine geology, geophysics, and geochemistry of the Woodlark Basin-Solomon Islands", eds. Taylor, B. and Exon, N., Circum Pacific Council for Energy and Mineral Resources Earth Science series, vol. 7., 155- 226.

Katsura, T. and Nagamashima, S., 1974, Solubility of sulfur in some magmas at 1 atmosphere: Geochim. Cosmochim. Acta, v. 38, p. 517-531.

Le Bas, M. J., Le Maitre, R. W., Streckeisen, A., and Zanettin, B., 1986, A chemical classification of volcanic rocks based on the total alkali- silica diagram: Jour. Petrol., v. 27, p. 745-750.

Luhr, J. F., Carmichael, I. S. E., and Varenkamp, J. C., 1984, The 1982 eruptions of El Chichon volcano, Chiapas, Mexico: mineralogy and petrology of the anhydrite-bearing pumices: Jour. Volcan. Geotherm. Res., v. 23, p. 69-108.

Luhr, J. F., 1990, Experimental phase relations of water- and sulfur- saturated arc magmas and the 1982 eruptions of El Chichon volcano: Jour. Petrol., v. 31, p. 1071-1114.

Mathez, E. A., 1976, Sulfur solubility and magmatic sulfides in submarine basalt glass: Jour. Geophys. Res., v. 81, p. 4269-4276.

Matthews, S. J., Jones, A. P., and Gardeweg, M. C., 1994, Lascar volcano, Northern Chile; evidence for steady-state disequilibrium: Jour. Petrol., v. 35, p. 401-432.

McInnes, B.I.A. and Cameron, E.M., 1994, Carbonated, alkaline metasomatic melts from a sub-arc environment: Mantle wedge samples from the Tabar-Lihir-Tanga-Feni arc, Papua New Guinea, Earth Planet. Sci. Letters, v. 122, p. 125-141.

Metrich, N. and Rutherford, M. J., 1992, Experimental study of chlorine behaviour in hydrous silici melts; Geochim. Cosmochim. Acta, v. 56, p. 607-616.

Metrich, N., Clocchiatti, R., Mosbah, M., and Chaussidon, M., 1993, The 1989-1990 activity of Etna magma mingling and ascent of a H_2O-Cl-S rich basaltic magma. Evidence from melt inclusions: Jour. Volcan. Geotherm. Res., v. 59, p. 131-144.

Mysen, B. O. and Popp, R. K., 1980, Solubility of sulfur in $CaMgSi_2O_6$ - and $NaAlSi_3O_8$ melts at high pressure and temperature with controlled fO_2 and fS_2: Am. Jour. Sci., v. 280, p. 78-92.

Poulson, S. R. and Ohmoto, H., 1990, An evaluation of the solubility of sulfide sulfur in silicate melts from experimental data and natural samples: Chem. Geology, v. 85, p. 57-75.

Sorensen, H., 1974, The alkaline igneous rocks: John Wiley & Sons, New York, New York, 622 pages.

Stormer, J. C. and Carmichael, I. S. E., 1971, The free energy of sodalite and the behaviour of chloride, fluoride and sulfate in silicate magmas: Amer. Mineral., v. 56, p. 292-306.

Thibault, Y. and Holloway, J. R., 1994, Solubility of CO_2 in a Ca-rich leucitite: effects of pressure, temperature and oxygen fugacity: Contrib. Mineral. Petrol., v. 116, p. 216-224.

Wallace, P. J. and Carmichael, I. S. E., 1992, Sulfur in basaltic magmas: Geochim. Cosmochim. Acta, v. 56, p. 1863-1874.

APPENDIX 4

Experimental Determination of Compositional Dependence of Hydrous Silicate Melts on Sulfate Solubility

Mihai N. Ducea, Brent I. A. McInnes, and Peter J. Wyllie

submitted to *European Journal of Mineralogy*

Abstract.

Magmas generated at convergent plate margins are often oxidized and accompanied by a sulfur-rich vapor phase. Under oxidizing conditions, sulfur dissolves in magmas as sulfate. Previous investigations have analyzed the sulfate solubility as a function of temperature, pressure and fO_2, but not as a function of melt alkalinity. We have measured the solubility of SO_3 in quartz-normative and nepheline-normative compositions in the system Na_2O-Al_2O_3-SiO_2-H_2O at temperatures from 800-825 °C and pressures between 1.5-1.7 kb (cold-seal vessels). We added 1.5, 3, 10 or 15% $CaSO_4$ to two H_2O-saturated synthetic compositions near the eutectics in quartz-albite-H_2O and nepheline-albite-H_2O. The low sulfate solubilities measured in the quartz-normative quenched glasses (0.06-0.12% SO_3) are similar to previous determinations on quartz-normative melts from natural rock compositions. The sulfate contents of quenched glasses in the nepheline-normative system are up to 6 times higher (0.17-0.36% SO_3). Precipitation of anhydrite in the quartz-normative melt requires addition of about 6% $CaSO_4$ at 800 °C, and 10% $CaSO_4$ at 820 °C. In contrast, < 1.5% $CaSO_4$ added to the nepheline-normative liquid is sufficient to cause precipitation of haüyne or an immiscible sulfate-rich liquid. We conclude that the sulfate solubility in hydrous magmas is significantly influenced by silica activity (melt alkalinity) and SiO_2 concentration in melts.

A4.1. Introduction

Understanding the solubility of sulfur in silicate melts from arc environments is a

subject of great interest because magmatic-volcanic processes are capable of: (1) producing economically important sulfide ore deposits (e.g., Barnes, 1979), (2) influencing global climate as a consequence of the volcanic emission of SO_2 gas (e.g., Devine et al., 1984), and (3) potentially predicting volcanic eruption using sulfur emissions (e.g., Stix et al., 1993). If sufficient data are available to parameterize the behavior of sulfur in silicate melts under all possible conditions, then first order problems such as global sulfur geodynamic cycles can also be constrained (Jambon, 1994). We have previously shown that naturally-occurring, undegassed glassy lavas and melt inclusions of alkaline composition have up to an order of magnitude higher sulfur concentration than do calc-alkaline samples (Ducea et al., 1994).

The effects of temperature, pressure and redox conditions on sulfur solubility have been addressed previously for melt compositions typical of arc environments (Carroll and Rutherford, 1985, 1987; Luhr, 1990). An important previous result is that in high $f(O_2)$ magmas sulfur dissolves as sulfate, $(SO_4)^{2-}$ (Nagashima and Katsura, 1973; Carroll and Rutherford, 1985). By analogy with the behavior of other volatile components in silicate melts (CO_2 - Thibault and Holloway, 1994; Cl - Metrich and Rutherford, 1992; H_2O - Dingwell et al., 1984), magma composition must influence sulfur solubility, but its dependence on magma composition has received less attention than the other influential parameters.

In this paper, we present results of experiments designed to measure how changes in melt composition affect sulfate solubility in hydrous, oxidized, iron-free, silicate melts. We investigated experimentally the systems quartz-albite-anhydrite-H_2O and nepheline-albite-anhydrite-H_2O, and measured the sulfate solubility in quenched glasses. We chose the starting mixtures and run conditions such that measured differences in sulfate solubility between the two simplified systems should be caused by melt composition differences, notably the melt alkalinity, while the other factors known to influence sulfate solubility were minimized.

A4.2. Previous experimental work

Sulfur solubility in silicate magmas depends mainly on temperature, pressure, oxygen fugacity, sulfur speciation, sulfur fugacity, water content, and melt composition (see Carroll and Webster, 1994, for a review). There is a strong interdependence between several of these parameters. Sulfur has variable oxidation states in nature, 2-, 0, 2+, 4+, and 6+, which has a significant role in melt sulfur solubility (Fincham and Richardson, 1954). Experiments with silicate melt compositions show that sulfur dissolves primarily as sulfide (S^{2-}, reduced), and sulfate (SO_4^{2-}, oxidized) species (e.g., Naghashima and Katsura, 1973; Carroll and Rutherford, 1985; Carroll and Rutherford, 1988). In general, dissolved sulfate only becomes significant at oxygen fugacities greater than ~1 log $f(O_2)$ unit above the FMQ buffer (e.g., Carroll and Rutherford, 1988). The precise response of melt sulfur content to the exact $f(S_2)$ is not known, but might be significant (Carroll and Webster, 1994).

Sulfur solubility is normally measured in sulfur-saturated or sulfur-oversaturated environments. Most experiments were sulfur-saturated, carried out in the presence of a sulfur-bearing vapor phase coexisting with the melt. In sulfur-oversaturated experiments a sulfur-rich condensed phase can form. This phase is usually an immiscible sulfide-rich liquid or pyrhottite in reduced magmas (e.g., Shima and Naldrett, 1975), and anhydrite in oxidized magmas (Carroll and Rutherford, 1985).

The fugacities of various gaseous species present in sulfur experiments can be controlled in 1 bar experiments (e.g., Haughton et al., 1974), but not at higher pressures (Carroll and Webster, 1994). Extrapolation of the gas fugacities measured in sulfur-saturated, 1 bar experiments (Katsura and Nagashima, 1974) to higher pressures indicates that the main sulfur species present in oxidized environments ($f(O_2) \geq$ NNO) should be SO_2.

Figure A4-1 summarizes the results of previous experimental work on sulfur

Figure A4-1. **a**. Schematic diagram showing sulfur solubility dependencies on temperature and fO_2, for intermediate calc-alkaline melts (trachyandesites, andesites, and dacites), under both reduced and oxidizing conditions, at pressures of 1-4 kbar (Carroll and Rutherford, 1985, 1987; and Luhr, 1990). The schematic contours on the shaded surface show a temperature minimum approximatively along the line for the NNO buffer. At lower oxygen fugacities, sulfur dissolves in melts as sulfide, whereas at higher oxygen fugacities, it dissolves as sulfate. **b**. Schematic cross section through the box in Figure A4-1a, along the A-A' line. The figure shows the solubility minimum corresponding to the sulfide-sulfate phase change, and how the solubility changes as a function of pressure (Wendlandt, 1982).

a.

S solubility

A — ~Ni-NiO — A'

Sulfide

Sulfate

log fO_2

T (°C)

b.

A — — — — — A'

S solubility

high P

low P

log fO_2
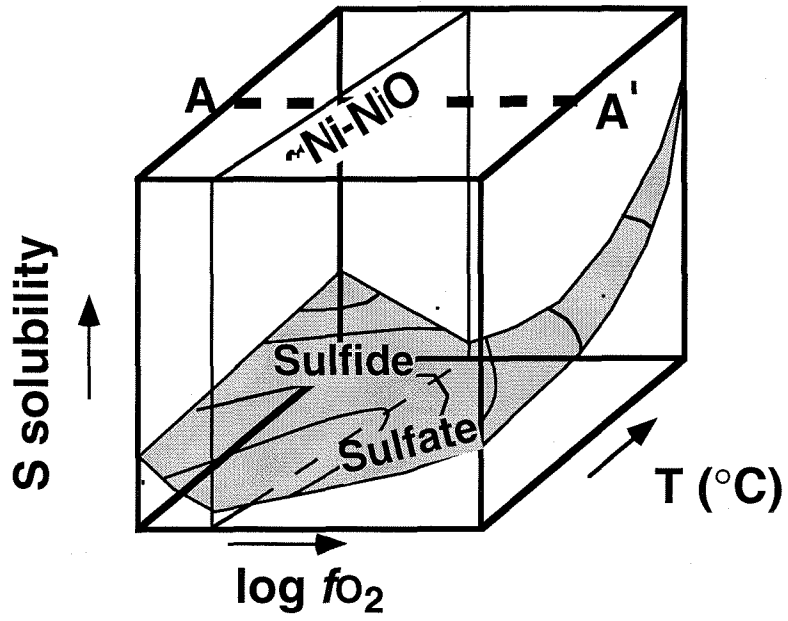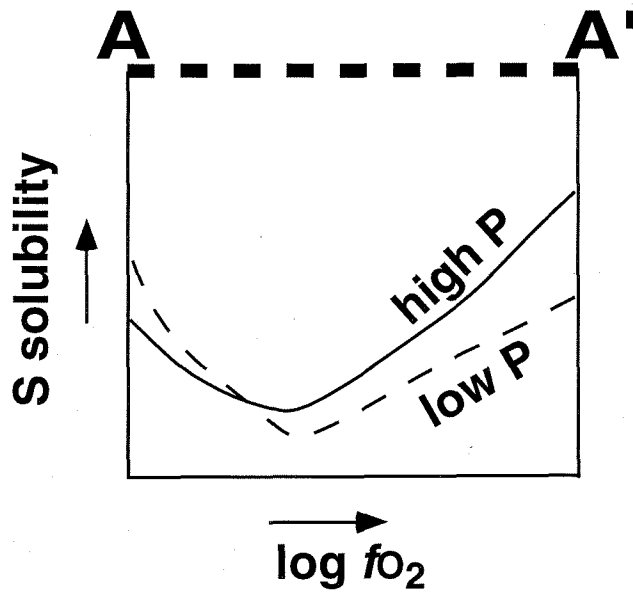
solubility, mainly in oxidized environments and at pressures ≤ 4 kbar (Wendlandt, 1982; Carroll and Rutherford, 1985, 1987; and Luhr, 1990). It shows schematically how sulfur solubility depends on the melt temperature, $f(O_2)$, and pressure. The shaded surface in Figure A4-1a illustrates the known variations of sulfur solubility in terms of temperature and $f(O_2)$ in silicate melts of intermediate to silicic compositions, such as andesites, trachyandesites and dacites, at 1-4 kbar. The schematic contours on the surface show a solubility minimum approximately along the line for the NNO buffer (Carroll and Rutherford, 1987). At lower oxygen fugacities the sulfur component is precipitated as sulfide, whereas at higher oxygen fugacities it is precipitated as sulfate. For the sulfide region, sulfur solubility remains low, increasing slightly with increasing temperature and decreasing $f(O_2)$. For the sulfate region, the solubility increases rapidly with increasing temperature and oxygen fugacity. The coupled effect of increasing T and $f(O_2)$ results in a significant, one order of magnitude enhancement of sulfur solubility in hot (> 1000 °C) magmas at $\log f(O_2)$ = MH, compared to magmas buffered at $\log f(O_2)$ = NNO (Luhr, 1990). The results shown in Figure A4-1a are similar to those obtained by Katsura and Nagashima (1974) on variable compositions (basalt to rhyolite) at 1 bar pressure.

The cross-section A-A' in Figure A4-1b shows the $f(O_2)$ minimum separating the two parts of the solubility surface. The two lines show how the solubility changes as a function of pressure based on the experimental results of Wendlandt (1982) and Luhr (1990). The S solubility is enhanced in oxidized melts at high pressures. In reduced melts, limited data suggest that sulfur solubility decreases with increasing pressure.

Very little is known about the influence of H_2O on sulfur solubility. However, the results of Luhr (1990) on anhydrous trachyandesitic melts, when compared with those in water-oversaturated trachyandesitic melts conducted at similar P-T-$f(O_2)$ conditions by Carroll and Rutherford (1987), would argue against a dramatic effect of H_2O on sulfur solubility.

A significant effect of melt composition on total sulfur solubility was determined in

1 bar experiments by Katsura and Nagashima (1974). SiO_2-rich melts (rhyodacites) have, generally, five to ten times lower S solubilities than low-SiO_2 melts (tholeiitic basalts). Under reducing conditions S solubility (as sulfide) is positively correlated with melt FeO content (see Poulsen and Ohmoto, 1990, for a review). The experiments of Carroll and Rutherford (1985, 1987) and Luhr (1990) cover a spectrum of compositions from trachyandesites to dacites but the effect of bulk composition on sulfur solubility was not investigated.

Experiments carried out in the Na_2O-SiO_2-Al_2O_3 system at 1 bar (Nagashima and Katsura, 1973; Kuznetzova and Krigman, 1978) showed higher sulfur contents correlating with more alkaline melts, under reducing conditions where sulfide is the dissolved sulfur ion. Solubilities increased from 140 ppm S in compositions corresponding to granites, to 300 ppm S in nepheline syenite compositions, to 7500 ppm S in agpaitic nepheline syenite composition. Kuznetzova and Krigman (1978) attributed the enhanced solubility to a different melt structure, with the less alkaline melts being more polymerized. Little is known about melt alkalinity effects in oxidized melts. Papadopoulos (1973) noted a strong positive correlation between sulfate solubility and the concentration of alkali metal components in 1 bar experiments. There are no sulfate solubility determinations in alkaline melts at pressures other than 1 bar.

In this paper we investigate the effects on melt alkalinity on sulfate solubility. We use two synthetic, hydrous, oxidized systems, one representing calc-alkaline magmas (quartz-albite-H_2O), and the other alkaline magmas (nepheline-albite-H_2O). We added anhydrite and determined the sulfur solubility at a constant pressure (~1.6 kbar). These mixtures melt at low enough temperatures (~760 °C) that differences in sulfate solubility between the two systems, if any, must be attributed primarily to melt composition.

A4.3. Experimental method

Experiments were conducted in cold-seal pressure vessels with oxygen fugacity buffered above the nickel-nickel oxide buffer by the reaction vessel (Eugster and Wones, 1962). Calibrated temperatures measured using external chromel-alumel thermocouples are accurate to 5 ^{0}C. Pressures are estimated to be accurate to 5%. Vessels were quenched in compressed air to 350 ^{0}C and then immersed in cold water; typically, a run was cooled down below the solidus in less than a minute.

The two silicate mixtures used were made from gels of albite$_{70}$-nepheline$_{30}$ and mixtures of gels of silica and albite with composition of albite$_{68}$-quartz$_{32}$, all dehydrated at 800 ^{o}C. The chemical compositions and CIPW norms of the two mixtures given in Table A4-1 reveal small amounts of CaO and K_2O. These compositions were selected to approximate the eutectic liquids M_1 (nepheline-normative) and M_2 (quartz-normative) shown in the H_2O-saturated system nepheline-quartz at 1 kb (Figure A4-2, after Tuttle and Bowen, 1958). The gel mixtures were ground to < 200 mesh under acetone in an agate mortar for 30 minutes and dried at 110 ^{0}C in a vacuum oven. Reagent grade anhydrite was ground to <200 mesh under acetone for 30 minutes, and then dried at 80 ^{o}C. Anhydrite was added to the silicate starting composition as follows: 1.5%, 3% and 10% to the quartz-normative mixture; and 1.5%, 3%, and 15% to the nepheline-normative mixture.

The solubility of H_2O in these silicate liquids at 1.5 kb is about 6% (Macmillan and Holloway, 1987). H_2O was added to all experiments in amounts sufficient to ensure the presence of a vapor phase. The targeted value of 10% H_2O was not always closely achieved, perhaps because of partial loss during capsule sealing. Table A4-2 lists H_2O ranging from 5% to 15% in runs containing $CaSO_4$. This must cause some variation in H_2O/SO_2 in vapor and liquid, but the amount of vapor is low enough that we conclude that this has little effect on the total sulfur dissolved in the liquid.

Approximately 100-200 mg of silicate-sulfate powder was packed into a 4 mm long gold capsule with a 2 mm internal diameter. Water was added to each capsule by microsyringe immediately before sealing using a graphite arc welder. A successful weld

Figure A4-2. Representation of the starting silicate mixtures compositions, viewed on the quartz-nepheline join in the residua system. The mixtures used in this study are labeled in the figure as M_1-nepheline normative mixture, and M_2-quartz normative mixture. Both M_1 and M_2 lie close to the albite-quartz and albite-nepheline eutectics at 1 kbar, as determined by Tuttle and Bowen (1958). Symbols: Ne-nepheline, Qz-quartz, Ab-albite, L-silicate liquid, V-vapor.

Ne-Qz-H$_2$O
P$_{total}$= P$_{H2O}$= 1kbar
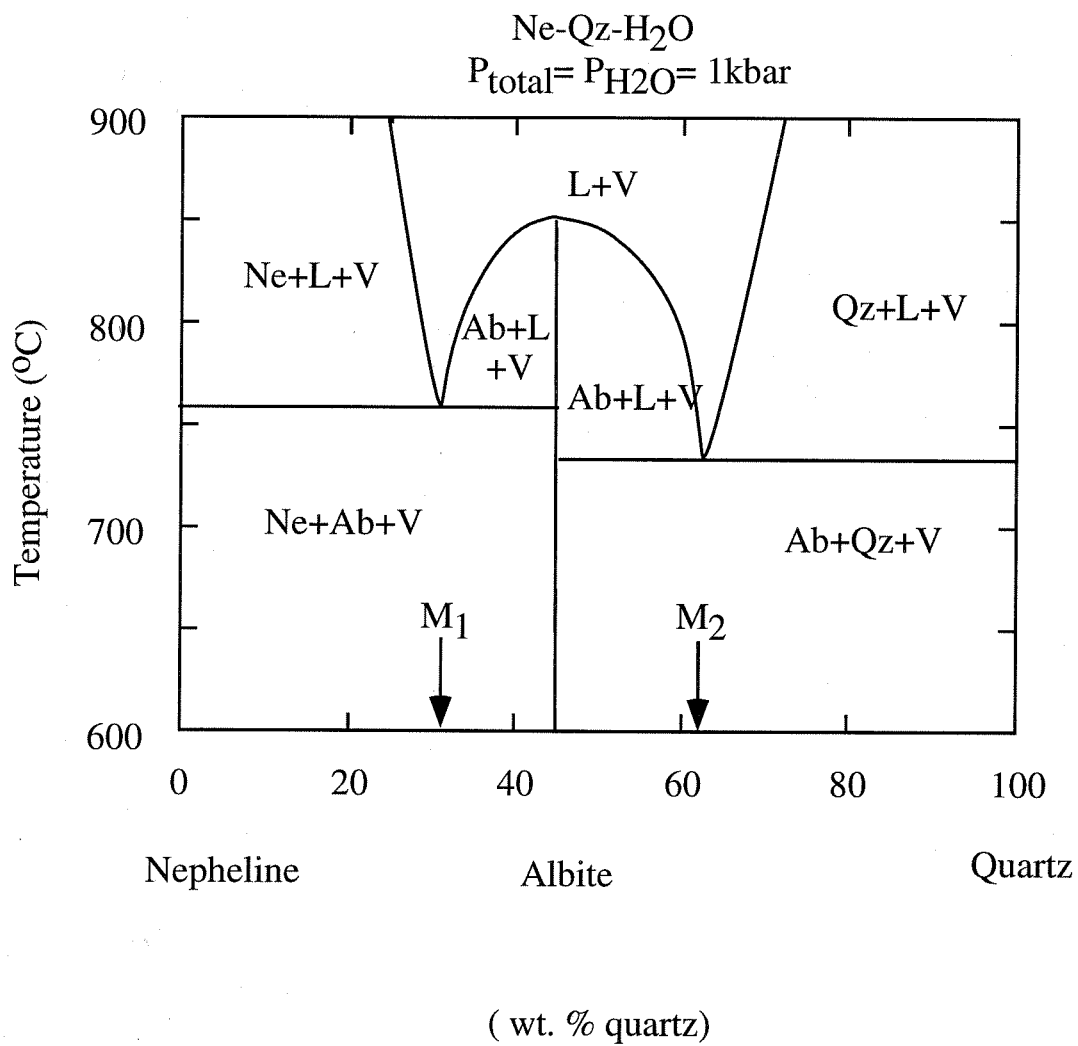
Table A4-1. Starting materials and CIPW norms.

	Nepheline-normative mixture (M_1)	Quartz-normative mixture (M_2)
Oxide wt.% *		
SiO_2	62.65	76.87
Al_2O_3	23.33	14.68
CaO	0.03	0.08
Na_2O	13.82	7.92
K_2O	0.17	0.45
CIPW norms		
Q	0.0	26.8
C	0.3	0.8
or	1.0	2.7
ab	76.6	69.3
an	0.1	0.4
ne	21.9	0.0

* - determined by electron microprobe

Table A4-2a. Experimental results in the system Ab_{70}-Ne_{30}-$CaSO_4$-H_2O.

Run #	% $CaSO_4$	T (°C)	P (bar)	% H_2O	t (hrs)	Run products
53	0	750	1476	5	40	Ab, Ne, V
52	0	775	1698	12	28	L, V
51	0	800	1669	13	28	L, V
50	0	825	1663	8	40	L, V
56	1.5	750	1476	6.5	40	Ab, Ne, Anh, V
55	1.5	800	1717	11	28	Ha, L, V
57	1.5	825	1627	12	40	L_1, L_2, V
63	3	800	1689	13	42	Ha, L, V
64	3	825	1517	15	38	L_1, L_2, V
60	15	800	1689	10	42	Ha, L, V
[58]*	15	825	1682	8	30	L, V

Ab = albite, Ne = nepheline, Anh = anhydrite, Ha = haüyne, L= glass, V = vapor;
*- ~ half sample loss during polishing.

Table A4-2b. Experimental results in the system Ab_{68}-Qz_{32}-$CaSO_4$-H_2O.

Run #	% $CaSO_4$	T (°C)	P (bar)	% H_2O	t (hrs)	Run products
1	0	750	1579	10	24	Ab, Qz, V
8	0	775	1698	7	37	Ab, Qz, L, V
9	0	800	1545	7	25	L, V
21	0	825	1600	10	27	L, V
4	1.5	750	1614	9	28	Ab, Qz, V
11	1.5	800	1717	13	35	L, V
10	1.5	825	1556	6	35	L,V
3	3	750	1614	12	28	Ab, Qz, Anh, L, V
22	3	800	1530	9	30	L, V
2	10	750	1579	7.5	24	Ab, Qz, Anh, V
6	10	775	1627	5	37	Anh, L, V
5	10	800	1717	9.6	35	trace Ab, Anh, L, V
7	10	825	1557	11	35	L, V

Ab = albite, Qz = quartz, Anh = anhydrite, L= glass, V = vapor.

was confirmed by the absence of bubbles when the capsule was placed in acetone. Typical run durations varied from several hours to two days (Table A4-2). After quenching, the samples were sectioned along their lengths, polished under oil and set into probe mounts. The polished charges were examined using a scanning electron microscope (SEM) operated in back-scattered electron (BSE) mode. Crystal-free glass areas were then selected for sulfur and major element analysis using an electron microprobe.

Mineral and glass compositions were preliminary determined using a Camscan scanning electron microscope (SEM) equipped with an energy dispersive spectrometer (EDS). The electron beam was unfocused to a 10 μm^2 area during mineral analyses in order to reduce alkali mobility. The accelerating voltage was 10 keV, with normal count times of 50-60 s. Glasses were analyzed on 20-30 μm^2 surfaces. Several glass analyses were performed on each capsule. The amounts of SO_3 dissolved in glasses is very small, commonly below the detection limit of the EDS.

Selected runs, previously analyzed by SEM, were analyzed by JEOL 733 electron microprobe (EMP) equipped with five wavelength dispersive spectrometers. Glass areas of 15 x 15 μm were used. The accelerating voltage was 15 keV with a low beam current of 7 nA. Raw data were reduced using a Bence and Albee (1968) procedure. We used anhydrite as a standard for S determinations. The SO_3 concentrations obtained from EMP are consistent with the few obtained on EDS.

The detection limit for sulfur on EMP is ~ 35 ppm which is consistent with values reported by Carroll and Webster (1994). The quartz-normative melts had very low sulfur solubility, close to the detection limit. Therefore, we used count times of 200-300 s.

We have also used the electron microprobe to determine the magnitude of the shift in the position of Skα peak from pure S^{2-} (Carroll and Rutherford, 1988), an effect which reflects the relative proportions of S^{2-} and S^{6+} in glasses. In all runs, sulfur dissolved in

melts as sulfate.

A4.4. Experimental results

The experimental design was to add $CaSO_4$ to H_2O-saturated, relatively low-temperature, near-eutectic silicate liquids M_1 and M_2 (Figure A4-2), and to measure the sulfur dissolved in the quenched glasses. This is similar to the approach used by Carroll and Rutherford (1985, 1987) with natural rocks, although they had the added complication in many experiments of being below the liquidus, with the assemblage minerals+liquid+vapor. With excess H_2O present, sulfur would be partitioned into the vapor phase, and SO_2/H_2O in vapor would be expected to increase as $CaSO_4$ content increased. SO_2/H_2O would also vary somewhat for different H_2O contents. With increasing $CaSO_4$ content, another measure of sulfur saturation was provided by the appearance of anhydrite (in quartz-normative compositions) or haüyne (in nepheline-normative compositions). One set of runs was made at lower temperatures, near the solidus.

Twenty four experiments were carried out between 750-825 ^{0}C and 1.5-1.7 kbar. Results are summarized in Table A4-2 and Figures 4-5. Examples of run products are shown in Figure A4-5. No interaction between the silicate melts and the gold capsules was observed.

All run products had vapor bubbles. The sulfur should be present mainly as SO_2 at the oxygen fugacities of these experiments (Nielssen and Peach, 1994). Anhydrite crystals accumulated at the bottom of some capsules (Figure A4-5a), while hauyne crystals did not separate from the melts. This textural observation can be explained by the difference in density between anhydrite or hauyne and the investigated melts. Anhydrite has a density of ~ 3g/cm^3 (Deer et al., 1992), significantly higher than the density of the melts investigated here, 2.5 g/cm^3 (calculated by the algorithm of Niu and Batiza, 1991, using the measured chemical composition, a temperature of 800 ^{o}C, and a pressure of 1.6 kbar). The density of

Figure A4-3. Phase relationships in the system albite$_{70}$-quartz$_{30}$-H$_2$O at 1.5 kbar, constructed from our sulfate-free runs and data from Whitney (1975), and McMillan and Holloway (1987). Runs #1, 8, 9 and 21 (see Table A4-2b, and Figure A4-5) all contain excess H$_2$O (> ~6% H$_2$O).
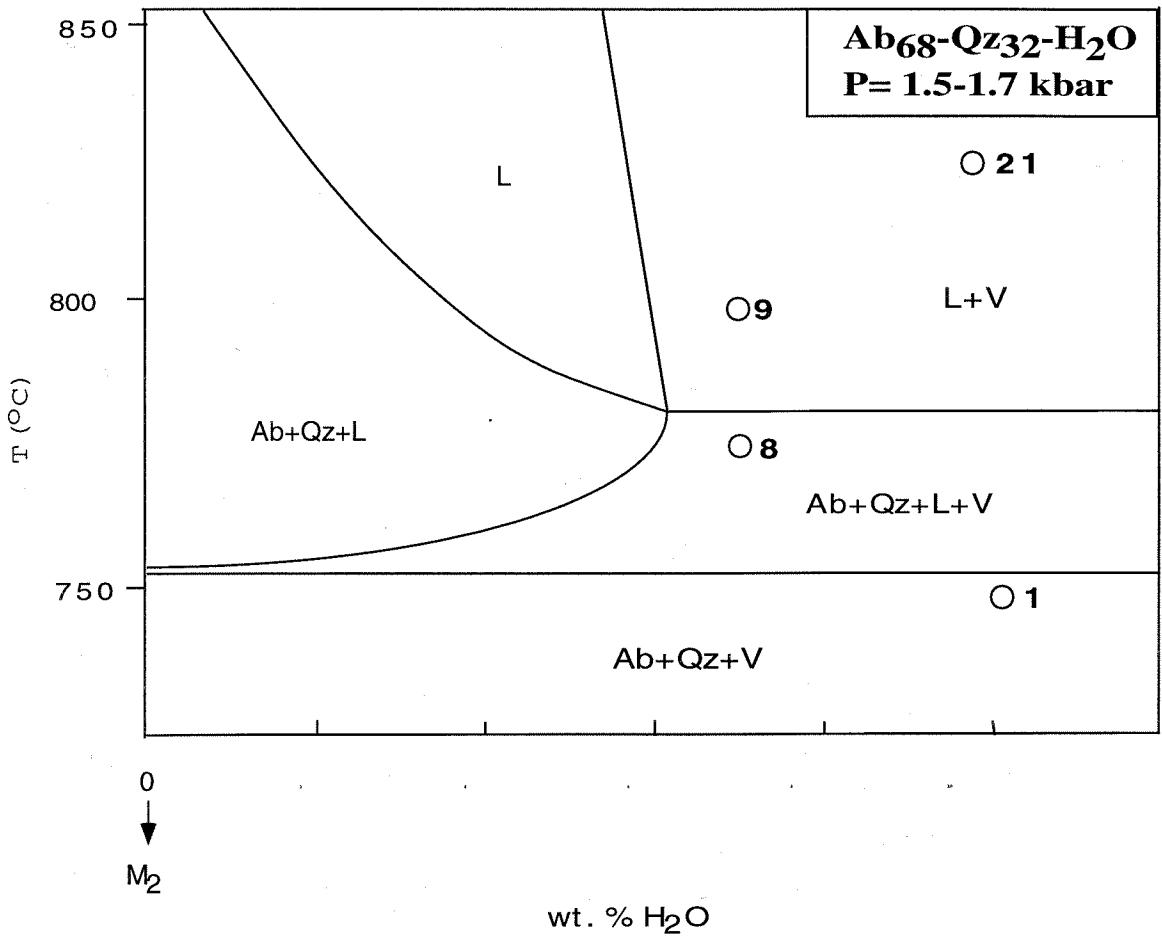
Figure A4-4. Phase relationships in the two investigated systems, quartz-normative, and nepheline-normative, at ~1.5-1.7 kbar, in the presence of excess H_2O .**a**) the nepheline-normative system, (albite$_{70}$-nepheline$_{30}$)-H_2O-$CaSO_4$. **b**). the quartz-normative system, (albite$_{68}$-quartz$_{32}$)-H_2O-$CaSO_4$. Abbreviations as in Figure A4-2. Additional abbreviations: Si= solid silicate mixture (Si$_1$= Ab+Ne, Si$_2$= Ab+Qz), Anh = anhydrite, Ha= haüyne. The amount "x"% of H_2O, added to both nepheline-normative and quartz-normative silicate mixtures, varies between 5-15% (see Tables 2a and 2b).

a. Albite$_{70}$-Nepheline$_{30}$-Anhydrite-H$_2$O
P= 1.5 -1.7 kbar

Legend:
- Si_1+Anh+V (filled square)
- Si_1+V (filled down-triangle)
- L+V (filled circle)
- Ha+L+V (filled diamond)
- L1+L2+V (filled up-triangle)
- L+V (striped square)

L+V

L$_1$+L$_2$+V

L+V ?

Ha+L+V

Anh+Ha+L+V

Si$_1$+Anh+L+V

Si$_1$+Anh+V

Temperature (^{0}C)

900
850
800
750

0   5   10   15

M$_1$ + x % H$_2$O

wt. % CaSO$_4$(Anh)

b. Albite$_{68}$-Quartz$_{32}$-Anhydrite-H$_2$O
P = 1.5-1.7 kbar

Legend:
◇ Si$_2$+Anh+V
◈ Si$_2$+V
○ L+V
□ Anh+L+V
▨ Si$_2$+Anh+L+V
⊖ Si$_2$+L+V

Temperature (^{0}C)

900
850
800
750

L+V

Si$_2$+L+V

Anh+L+V

Si$_2$+Anh+V

0   5   10   15

M$_2$+ x %H$_2$O   wt. % CaSO$_4$(Anh)

hauyne is ~ 2.35 g/cm^3 (Deer et al., 1992), a value that is comparable to the calculated 2.5 g/cm^3 melt density.

Crystallites of acicular albite, quartz and anhydrite formed during the quench are generally not longer than 10 μm (Figure A4-5b). They differ from the primary crystals of anhydrite (Figure A4-5c) which tend to have prismatic aspect, although their size is similar.

The sulfate and major oxide concentrations in representative glasses are given in Table A4-3 and plotted in Figure A4-6 against the normative quartz or nepheline in the two starting samples. Table A4-3 lists the averages of 8-15 analyses. The H$_2$O concentration listed is the difference between 100% and the total oxide wt.% of the analysis. The analytical uncertainties for sulfate measurements are high at the low sulfate concentrations associated with the experimental conditions selected, close to the minimum shown in Figure A4-1, at low temperatures (Luhr, 1990). These new results in the synthetic system are compared with results reported for natural hydrous, siliceous rock compositions by Carroll and Rutherford (1987) and Luhr (1990). Figure A4-6 presents all available experimental data on sulfate solubility in hydrous melts below 900 ^{0}C. The experimental conditions of the most oxidized experiments of Carroll and Rutherford (1987) and Luhr (1990) were similar to those of our experiments. Their compositions were Fe-bearing dacites and trachyandesites, which required more careful consideration of oxygen fugacity. Their results occupy the range of 10% to 19% normative quartz, with SO$_3$ contents between 0.025% and 0.124%.

A4.5. Interpretations

A4.5.1. Phase relationships at ~1.6 kbar

A few experiments were conducted with the silicate-H$_2$O mixtures to test the proximity of the mixtures to the estimated eutectics, M$_1$ and M$_2$. Results for the quartz-normative composition M$_2$ are shown in Figure A4-3. The solidus for NaAlSi$_3$O$_8$-SiO$_2$-H$_2$O at 1.6 kb is drawn according to Macmillan and Holloway (1987), and the H$_2$O

Figure A4-5. Backscattered electron SEM photomicrographs of experimental products. (**a**). Anhydrite accumulation at capsule bottom due to its higher density. (**b**). Acicular, quenched crystal of anhydrite. (**c**). Primary crystal of anhydrite. (**d**). Second, immiscible liquid (L_2) interlayered with a thin vapor film and separated from the main liquid (L_1).
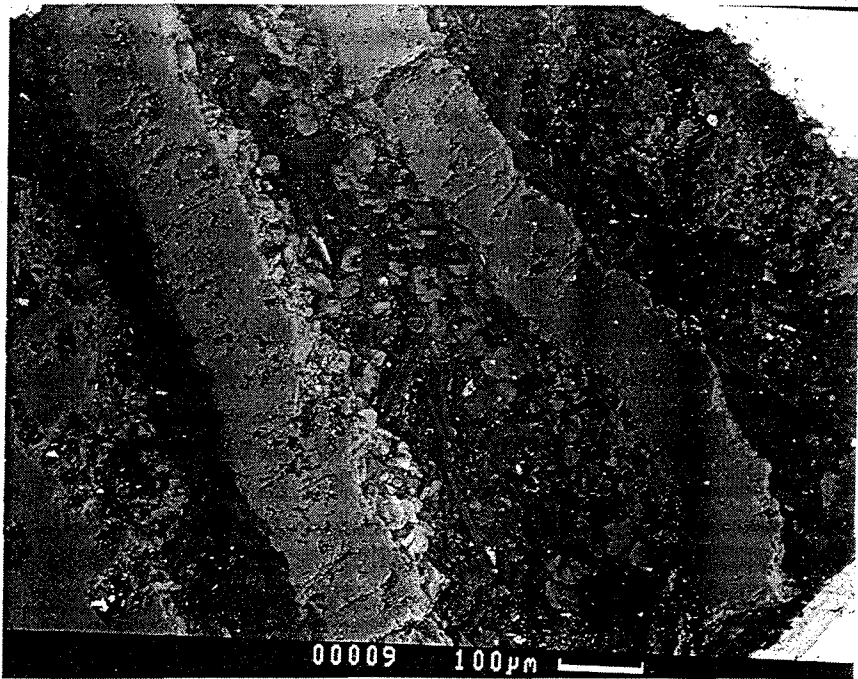
00006   100μm

00005   10μm
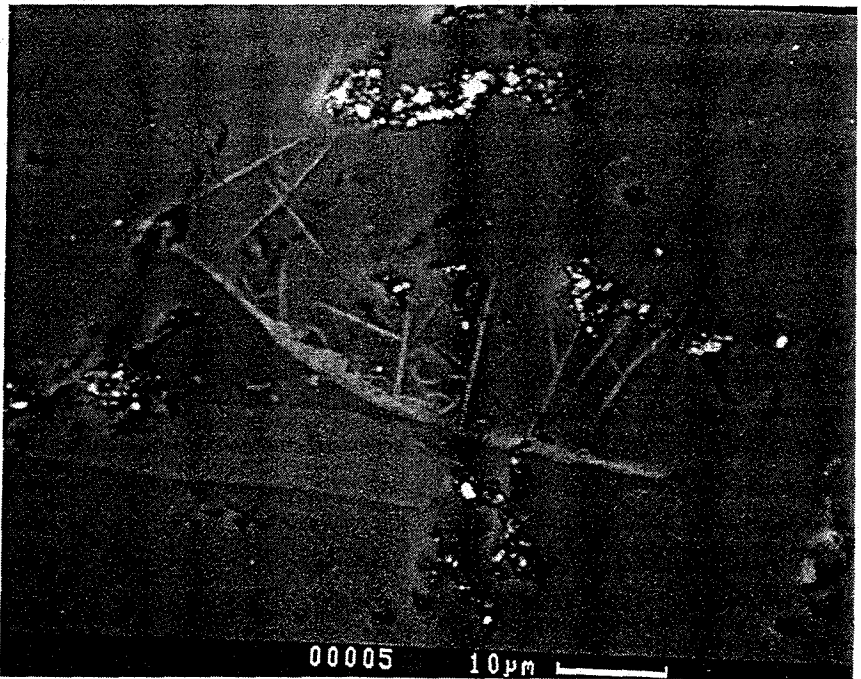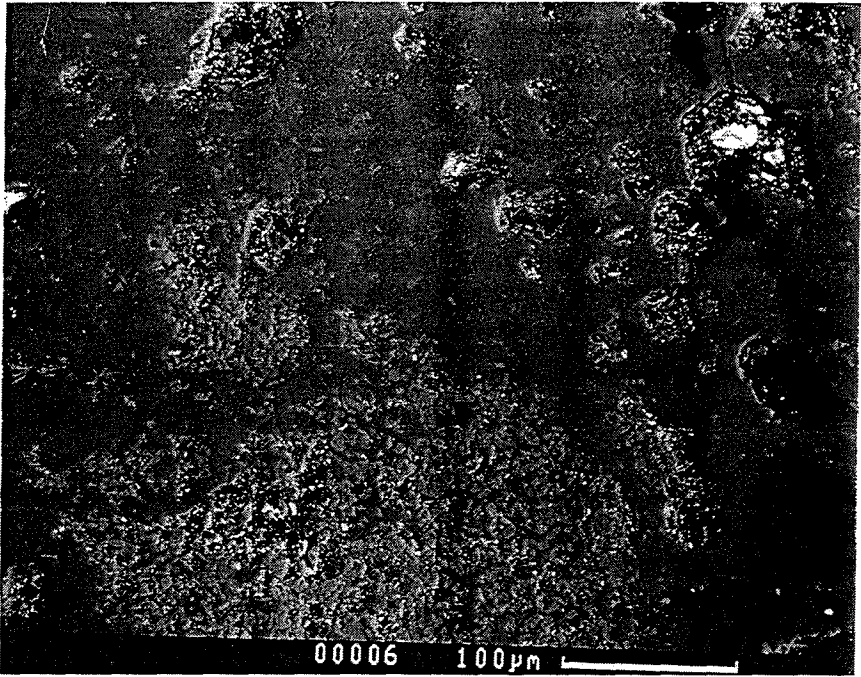
Figure A4-6. Sulfate concentration (wt.% SO_3) vs. melt alkalinity in oxidized silicate glasses. Alkalinity is represented as normative nepheline or normative quartz. Experimental sulfate solubility data from Carroll and Rutherford (1987), abbreviated as "C&R87" in the figure legend, and Luhr (1990), abbreviated as "L90" on calc-alkaline melts, were added. The glasses from Carroll and Rutherford (1987) are dacites, while those of Luhr (1990) are trachyandesites. In order to avoid temperature, pressure and fO_2 effects, only temperatures below 850 ^{0}C, pressures of ~2 kbar and fO_2's below MNO buffer were selected from Carroll and Rutherford (1987) and Luhr (1990). The values obtained in this study represent averages of 8-15 analyses on each glass. The analytical error is ≤10%, while the within-capsule 1σ standard deviation of the SO_3 measurements is much larger (0.033- to 0.111, see Table A4-4), due to sulfur degassing upon quenching.
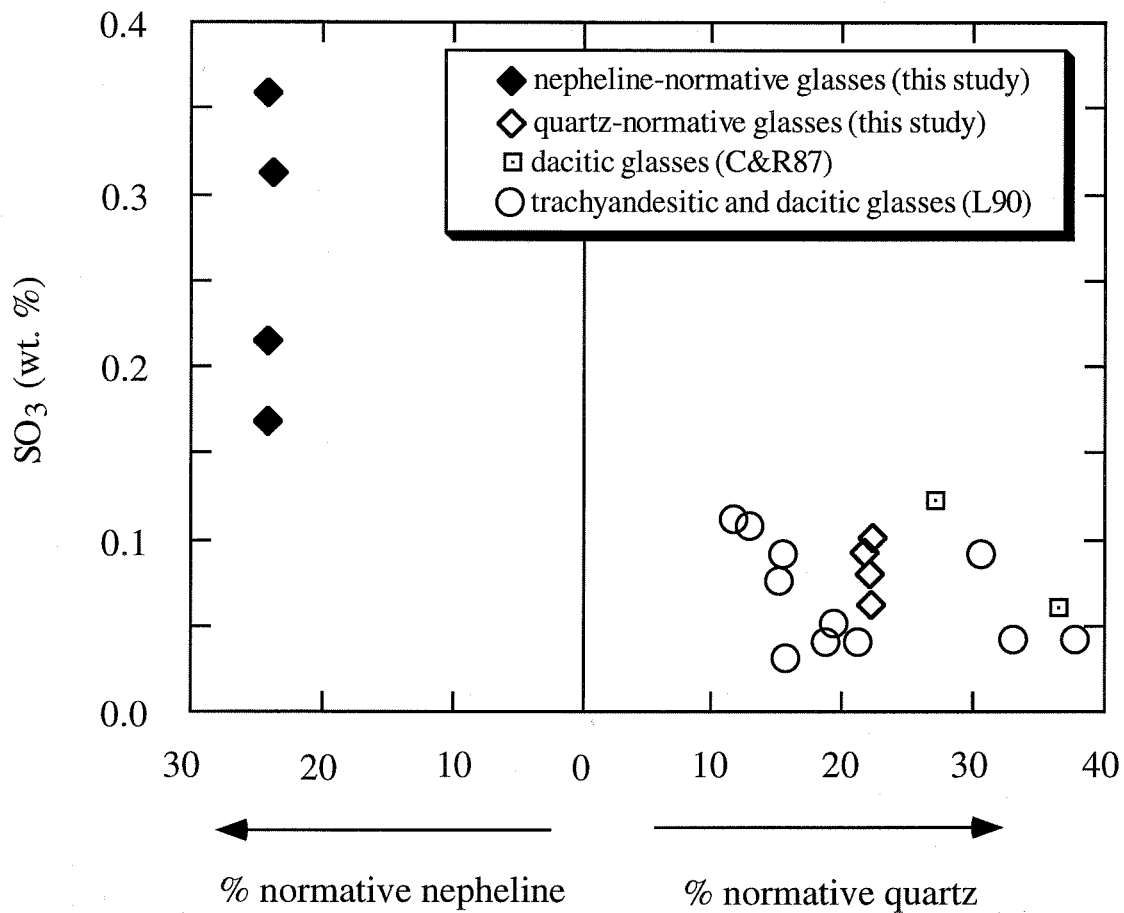
Table A4-3. Selected compositions of silicate glasses from the run products (in wt.%), including sulfur expressed as SO_3.

	Quartz-normative glasses				Nepheline-normative glasses			
Run #	11	22	5	7	55	57	63	58
% $CaSO_4$	1.5	3	10	10	1.5	1.5	3	15
T (°C)	800	800	800	825	800	825	800	825
SiO_2	74.30	73.61	74.34	72.73	59.20	60.51	60.79	60.53
Al_2O_3	12.55	11.72	13.21	12.19	20.18	21.59	22.44	21.54
CaO	0.342	0.991	0.522	0.757	0.240	0.069	0.341	0.170
Na_2O	5.98	5.94	6.55	5.96	13.06	12.25	12.34	11.81
K_2O	0.321	0.331	0.381	0.393	0.620	0.481	0.270	0.230
H_2O*	6.43	7.28	4.96	7.85	6.38	4.92	4.30	5.36
SO_3	0.096 (0.085)	0.078 (0.031)	0.061 (0.045)	0.122 (0.065)	0.321 (0.111)	0.174 (0.033)	0.215 (0.065)	0.364 (0.093)

Reported figures represent averages of 8-15 analyses. Standard deviations (1s) are shown in brackets for SO_3; the large within-capsule variability in sulfur concentration is mainly due to partial sulfur degassing during quenching. * - H_2O concentrations in glasses are calculated by substracting the sum of wt.% oxides from 100%.

solubility in albite-quartz liquids at these conditions is about 6%. Run 8 with assemblage Ab+Qz+L+V̊ about 20 °C above the solidus indicates that mixture M_2 is not quite coincident with the eutectic composition. The liquidus is drawn at about 780 °C, just above run #8. Therefore, experiments at 800 °C and 825 °C with mixture M_2 containing more than 6% H_2O provide the desired starting assemblage of liquid+vapor to which $CaSO_4$ is added, as in Figure A4-4b. Similar experiments with the H_2O-saturated nepheline-normative liquid M_1 (Figure A4-2) define the melting interval within the temperature interval 750 °C and 775 °C (Figure A4-4a), confirming that experiments at 800 °C and 825 °C provide the desired starting assemblage for addition of $CaSO_4$.

The experimental results plotted in Figure A4-4 correspond to the addition of 1.5%, 3% and 10% or 15% $CaSO_4$ to the H_2O-saturated silicate samples #9 and #21 plotted in Figure A4-3 (mixture M_2), and to the corresponding samples at 800 °C and 825 °C on the silicate-H_2O axis (mixture M_1). The conditions were achieved by adding H_2O to the silicate-$CaSO_4$ mixtures. All experiments were H_2O-saturated, but as noted above not every experiment contained the same amount of H_2O, the range being 5-13%. Some SO_2 and possibly alkalies were displaced into the vapor phase.

Figure A4-4 shows that anhydrite crystallized with addition of 10% CaSO4, and the liquidus was bracketed between 800-825 °C. The 1450 °C melting temperature of $CaSO_4$ (Robie et al., 1978) will be lowered with addition of H_2O, but no experimental determination is available. These sparse data permit an outline of the phase boundaries as sketched in Figure A4-4. Liquidus curves for primary silicates and anhydrite must meet at a piercing point for the coprecipitation of silicates and anhydrite, as shown in Figure A4-4, but the composition of the piercing point has not been established. The runs at 750 °C indicate that the solidus is near this temperature, barely distinguishable from that for mixture M_2 (Figure A4-3), and this constrains the temperature of the piercing point. The dacite compositions of Carroll and Rutherford (1985) are similar to the quartz-normative mixture M_2, and their experimental results are consistent with the phase boundaries

sketched in Figure A4-4. For the solubility measurements, the significant experiments are those in the field of liquid+vapor, and those associated with the liquidus for $CaSO_4$.

The results in Figure A4-4 for addition of $CaSO_4$ to the nepheline-normative melt, M_1, show that sulfate mineral saturation is attained at compositions containing less than 1.5% $CaSO_4$, much lower than for the quartz-normative liquids in Figure A4-4. The saturating sulfate mineral was haüyne, $(Na,Ca)_4[Al_6Si_6O_{24}](SO_4)$, rather than anhydrite. Haüyne commonly occurs in mafic to intermediate alkaline rocks (Deer et al., 1992), which is consistent with the phonolitic character of mixture M_1.

At 825 °C, haüyne appears to be replaced by an immiscible sulfate-rich liquid. In runs #57 and 64, the second phase was separated from the silicate glass of the main charge, situated above the glass, and interlayered with vapor rich areas as shown in Figure A4-5f. The compositions of silicate liquid and the second phase are given in Table A4-4. The second phase has a composition similar to that of haüyne (Table A4-4), and thus may be interpreted as representing large crystals of haüyne. The isotropic nature of the sulfur-rich phase was determined microscopically, suggesting strongly a glass origin for this material. Textural evidence also favors an immiscible liquid origin. Liquid immiscibility between silicate and sulfate melt has been documented at 1200 °C and 1 atmosphere in the system Na_2O-SiO_2-$NaSO_4$ (Pearce and Beisler, 1965), and it has been suggested for natural magmas, especially among researchers studying alkaline massifs (Sorensen, 1974).

The crystallization of haüyne and the generation of immiscible sulfate liquid at relatively low $CaSO_4$ contents in Figure A4-4a demonstrates a significant difference in phase relationships between quartz-normative and nepheline-normative systems. The piercing point between silicate and sulfate liquidus curves is constrained to low values of $CaSO_4$ in Figure A4-4a. Run #56 at 750 °C is subsolidus, and the piercing point is thus constrained between 750 °C and 775 °C (run #52), and 0% and 1.5% $CaSO_4$.

A4.5.2. Sulfate concentrations in quartz-normative and nepheline-normative glasses

Table **A4-4**. Major element composition of the two quenched liquids in run #57 (825 ^{0} C, 1.5% anhydrite).

	Liquid 1	Liquid 2 (sulfate-rich)	Haüyne composition*
SiO_2	61.51	34.11	32.18
Al_2O_3	21.59	27.90	27.11
CaO	0.07	8.92	10.26
Na_2O	12.25	15.48	16.34
K_2O	0.48	0.06	0.56
SO_3	0.17	15.81	14.10
H_2O**	6.88	-	0.34

* - from Deer et al., 1992, Table A4-37, analysis #4; ** - H_2O concentrations in glasses are calculated by subtracting the sum of wt.% oxides from 100%.

We selected two simplified compositions at experimental conditions which minimized the effect of all variables other than the variable between quartz-normative and nepheline-normative, or alkalinity, in $Na_2O-Al_2O_3-SiO_2$. The oxygen fugacity was not buffered but we checked that all experiments were carried at fO_2 high enough to ensure the presence of sulfate in melts (Carroll and Rutherford, 1988). The fO_2 effects are small at the temperatures of our experiments (Luhr, 1990).

The sulfate solubility measured in our quartz-normative glass is 0.06-0.12% SO_3, corresponding precisely with the values previously determined for hydrous rocks (Carroll and Rutherford, 1987; Luhr, 1990). The solubility is consistently higher in the nepheline-normative glasses, 0.17- 0.36% SO_3. The immiscible liquid observed in two of the silica-undersaturated runs is very rich in sulfur, ~15% SO_3. Any variations in sulfate solubility as a function of increasing $CaSO_4$ or H_2O contents in experimental mixtures were lost within the error of SO_3 measurements.

Figure A4-6 confirms that under oxidized conditions and moderate temperatures:

1). The sulfur contents of synthetic quartz-normative compositions and the natural quartz-normative, calc-alkaline rock compositions are essentially the same.

2). There is no significant variation in sulfur solubility in the calc-alkaline glasses despite a range of almost 7% in FeO variation among the rocks and our synthetic composition (Carroll and Rutherford, 1987; Luhr, 1990), suggesting that iron content has little influence on sulfur solubility under these conditions.

3). The sulfur contents of synthetic nepheline-normative glasses are significantly higher than those in quartz-normative glasses, and we conclude that this result can be extrapolated to natural nepheline-normative magma compositions, given result 1) above. The results are also consistent with the 1 bar experimental data of Kuznetzova and Krigman (1978) in the system $Na_2O-SiO_2-Al_2O_3$ under reduced conditions, where sulfur dissolved as sulfide, showing sulfur solubility (expressed as SO_3) increasing from 0.035% to 0.075% SO_3 from granitic to nepheline syenite compositions, and reaching 1.87% SO_3 in

agpaitic nepheline syenite composition.

We conclude, on the basis of experimental data at 1 bar (Kuznetzova and Krigman, 1978) as well as at 1.5-4 kbar (Carroll and Rutherford, 1985, 1987; Luhr, 1990 and the present study), under either reducing conditions (Kuznetzova and Krigman, 1978) or oxidizing conditions (the present study), that alkaline melts dissolve more sulfur than do calc-alkaline melts. This suggests that melt alkalinity may control sulfur solubility in magmas as effectively as other variables, regardless of the redox conditions. This conclusion is consistent with the observed higher concentrations of sulfur in natural alkaline volcanic glasses compared to calc-alkaline ones (Ducea et al., 1994).

The solubility mechanism of sulfur (as $SO_4)^{2-}$ in silicate melts at high fO_2 may be similar to that of carbon which dissolves as $(CO_3)^{2-}$ (Carroll and Webster, 1994). By analogy, we might expect higher sulfate solubility in more mafic melts. Figure A4-7 compares SO_3 vs. SiO_2 for the same experimental glasses shown in Figure A4-7. There is a trend toward higher sulfate solubility with decreasing SiO_2 concentrations within the quartz-normative series, although four of Luhr's samples fall below the trend, and the trend is directed toward the nepheline-normative points. Ducea et al. (1994) observed a similar negative S-SiO_2 correlation in naturally-occurring volcanic glasses.

A4.5.3. Igneous anhydrite and haüyne crystallization

Anhydrite can be generated in magmas: (1) by wall-rock contamination (e.g., Arculus et al., 1983), or (2) by saturating an oxidized magma with sulfur (Carroll and Rutherford, 1985, 1987). A phase rich in SO_2, in turn, can form as a product of anhydrite breakdown, perhaps shortly before an eruption (Devine et al., 1984; Sigurdsson, 1990). SO_2 could also be released through long-term degassing of a sulfur-rich magmatic system if magma mixing occurs between a sulfur-rich, more mafic magma and a low-sulfur, silicic crustal melt (Pallister et al., 1992; Wallace and Gerlach, 1994), or through the discharge of a hydrothermal system (Delfin et al., 1992). Therefore, although a clear relation is now

Figure A4-7. Sulfate concentration (wt.% SO_3) vs. SiO_2 (wt.%) in oxidized silicate glasses. This diagram uses the same experimental runs from Figure A4-6, and has the same errors. Symbols are as in Figure A4-6.
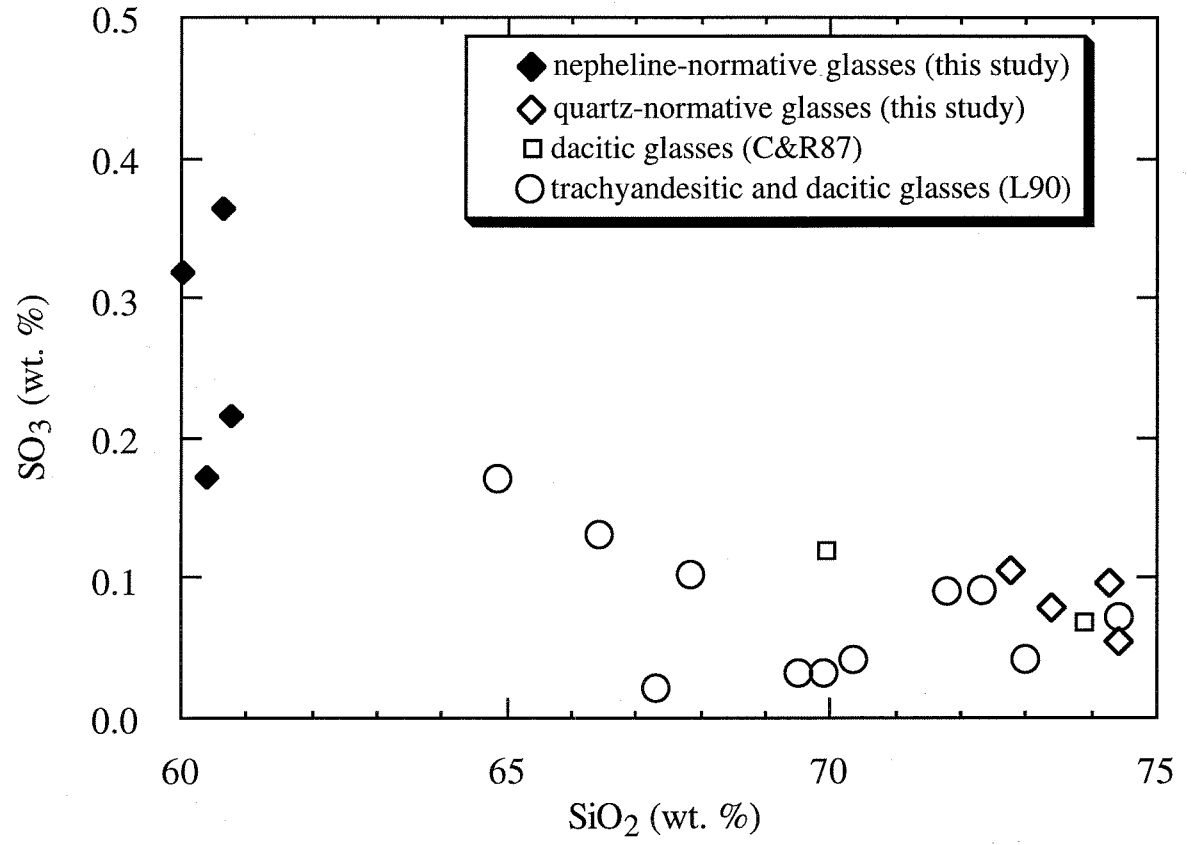
established between SO_2-rich eruptions in arc environments and the presence of igneous anhydrite, it is not clear whether the SO_2 vapor phase forms by anhydrite breakdown, or whether anhydrite crystallizes in a magma with a very high SO_2 fugacity.

The experimental data on the quartz-normative system indicate that anhydrite crystallizes only when the hydrous melt-vapor system contains ~1% S or more. The concentration of sulfur measured in quenched glasses is very small, and therefore most of the sulfur in the system (generally >95%) must be present in the vapor phase in order for anhydrite to crystallize. Anhydrite could break down in the magma chamber due to changes in temperature, pressure, etc. For example, an increase in temperature from 800^0 (run # 5) to 825^0 C (run # 7) in the quartz-normative system charged with 10% $CaSO_4$, leads to anhydrite breakdown, mainly by dissolution in the melt. A rough mass balance calculation shows that a concentration of SO_3 dissolved in melt in run #7 (which is about twice as much as in run #5, Table A4-3) would accomodate ~80% of the anhydrite found in run #5. In both experiments, the gas phase is by far the most significant S carrier. In order to achieve anhydrite saturation in the quartz-normative experiments, a gaseous phase whose S species dominate the mass budget of sulfur in the system (>95 weight%), had to be present. Our experiments suggest that breakdown of anhydrite in the quartz-normative system does not result in a significant increase in SO_2- vapor. If the phase relationships in our quartz-normative system are remotely analogous to a calc-alkaline melt in a shallow magma chamber, and if the melt-vapor magma chamber behaves as a closed system, anhydrite breakdown may not be a quantitatively significant source for the SO_2- vapor budget. We speculate that the most reasonable scenario for anhydrite crystallization in magma chambers is: SO_2-rich gas phase accumulation, perhaps at the top of the magma chamber, causing SO_2 fugacity to increase within that part of the system, and followed by anhydrite crystallization (Westrich and Gerlach, 1992).

In contrast, haüyne can crystallize in a nepheline-normative melt at sulfur concentrations as low as ~0.3-0.4% S. Given the significantly higher sulfur concentration

in nepheline-normative glasses, it is most likely that sulfate can crystallize in a nepheline-normative magma at much lower vapor phase $f(SO_2)$ than in a quartz-normative magma.

References

Barnes HL (1979) Geochemistry of hydrothermal ore deposits. John Willey & Sons New York, 320 p.

Bence AE and Albee AL (1968) Empirical correction factors for the electron microanalysis of silicates and oxides. Jour.. Geol. 76: 382-403.

Carroll MR and Rutherford MJ (1985) Sulfide and sulfate saturation in hydrous silicate melts. Jour. Geophys. Res., 90: C601-C612.

Carroll MR and Rutherford MJ (1987) The stability of igneous anhydrite: experimental results and implications for sulfur behaviour in the 1982 El Chichon trachyandesite and other evolved magmas. Jour. Petrol., 28: 781-801.

Carroll MR and Rutherford MJ (1988) Sulfur speciation in hydrous experimental glasses of varying oxidation state: results from measured wavelength shifts of sulfur X-rays. Amer. Mineral., 73: 845-849.

Carroll MR, and Webster JD (1994) Solubilities of sulfur, noble gases, nitrogen, chlorine, and fluorine in magmas. In Carroll MR and Holloway JR (eds.) Volatiles in magmas, Mineral. Soc. Amer., Reviews in Mineralogy, vol. 30 231-281.

Cavarretta G and Lombardi G (1992) Origin of sulfur in minerals and fluids from Latium (Italy): isotopic constraints. Eur. J. Mineral., 4: 1311-1329.

Deer WA, Howie RA and Zussman J (1992) An introduction to the rock-forming minerals-
    second edition. Longman Scientific and Technical, Essex, 696 pp.

Delfin FG, Sussman D, Ruaya JR, and Reyes AG (1992) Hazard assessment of the
    Pinatubo volcanic-geothermal system: Clues prior to the June 15, 1991 eruption:
    Trans. Geotherm. Res. Council, 16: 519-528.

Devine JD, Sigurdsson H, Davis AN, and Self S (1984) Estimates of S and Cl yields to the
    atmosphere from volcanic eruptions and potential climatic effects. Jour. Geophys.
    Res., 89: 6309-6325.

Dingwell DB, Harris DM, and Scarfe CM (1984) The solubility of H_2O in melts in the
    system SiO_2-Al_2O_3-Na_2O-K_2O at 1 to 2 kbars. Jour. Geol., 92:387-395.

Ducea MN, McInnes BIA, and Wyllie PJ (1994) Sulfur variations in glasses from volcanic
    rocks: Effect of melt composition on sulfur solubility. Int. Geology. Rev., 36: 703-
    714.

Eugster HP and Wones DR (1962) Stability relations of the ferruginous biotite, annite.
    Jour. Petrol 3: 82-125.

Fincham CJB and Richardson FD (1954) The behaviour of sulphur in silicate and
    aluminate melts. Proc. Royal. Soc. London, Ser. A, 223: 40-62.

Haughton DR, Roedder PL and Skinner BJ (1974) Solubility of sulfur in mafic magmas.
    Econ. Geol. 69: 451-467.

Jambon A (1994) Earth degassing and large-scale geochemical cycling of volatile
    elements. In Carroll MR and Holloway JR (eds.) Volatiles in magmas, Mineral.
    Soc. Amer., Reviews in Mineralogy, vol. 30: 479-509.

Katsura T and Nagashima S (1974) Solubility of sulfur in some magmas at 1
    atmosphere. Geochim. Cosmochim. Acta, 38: 517-531.

Kuznetzova SY and Kriegman LD (1978) Solubility of sulfur in silicate melts simulating
    magmas. Geochem. Int., 10: 135-142.

Luhr JF (1990) Experimental phase relations of water- and sulfur-saturated arc magmas

and the 1982 eruption of El Chichon volcano. Jour. Petrol., 31: 1071-1114.

Macmillan PF, and Holloway JR (1987) Water solubility in aluminosilicate melts. Contrib. Mineral. Petrol., 97: 320-332.

Metrich N, and Rutherford MJ (1992) Experimental study of chlorine behaviour in hydrous silicic melts. Geochim. Cosmochim. Acta, 56: 607-616.

Nagashima S and Katsura T (1973) The solubility of sulfur in Na_2O-SiO_2 melts under various oxygen partial pressures at 1200, 1250, and 1300 °C. Bull. Chem. Soc. Japan, 46: 3099-3103.

Nilsson K and Peach CL (1993) Sulfur speciation, oxidation state, and sulfur concentration in backarc magmas. Geochim. Cosmochim. Acta 57: 3807-3813.

Niu YL, and Batiza R (1991) DENSCAL- A program for calculating densities of silicate melts and mantle minerals as a function of pressure, temperature, and composition. Comp. Geosci 17: 679-687.

Pallister JS, Hoblitt RP, and Reyes AG (1992) A basalt trigger for the 1991 eruptions of the Mt. Pinatubo volcano? Nature, 356: 426-428.

Papadopolous K (1973) The solubility of SO_3 in soda-lime-silicate melts. Phys. Chem. Glasses 14: 60-65.

Pearce ML and Beisler JF (1965) Miscibility gap in the system sodium oxide-silica-sodium sulfate at 1200 °C. Jour. Amer. Ceram. Soc. 48: 40-42.

Poulson SR and Ohmoto H (1990) An evaluation of the solubility of sulfide sulfur in silicate melts from experimental data and natural samples. Chem. Geology, 85: 57-75.

Robie RA, Hemingway BS, and Fisher JR (1978) Thermodynamic properties of and related substances at 298.15 K and 1 bar pressure and high temperatures. U. S. Geol. Survey Bull. 1452: 456 pp.

Shima H and Naldrett AJ (1975) Solubility of sulfur in an ultramafic melt and relevance of the Fe-S-O system. Econ. Geol., 70: 960-967.

Sigurdsson H (1990) Assessment of the atmospheric impact of volcanic eruptions. Geol. Soc. Amer. Spec. Pap., 247: 99-110.

Sorensen H (1974) The alkaline igneous rocks. John Wiley & Sons, New York, New York, 622 pp.

Stix J, and 10 others (1993) A model of degassing at Galeras Volcano, Colombia, 1988-1993. Geology, 21: 963-967.

Thibault Y, and Holloway JR (1994) Solubility of CO_2 in Ca-rich leucitite: effects of pressure, temperature and oxygen fugacity. Contrib. Mineral. Petrol., 37: 216-224.

Tuttle OF and Bowen NL (1958) Origin of granite in light of experimental studies in the system $NaAlSi_3O_8$-$KAlSi_3O_8$-SiO_2-H_2O. Geol. Soc. Amer. Mem., 74:153 pp.

Wallace PJ and Gerlach TM (1994) Magmatic vapor source for sulfur dioxide released during volcanic eruptions: Evidence from Mount Pinatubo. Science 265, 497-499.

Wendlandt RF (1982) Sulfide saturation of basalt and andesite melts at high pressure and temperature. Amer. Mineral. 67: 877-885.

Westrich HR, and Gerlach TM (1992) Magmatic gas source for the stratospheric SO_2 cloud from the June 15, 1991 eruption of Mount Pinatubo. Geology, 20: 867-870.

Whitney JA (1975) The effects of pressure, temperature, and x(H_2O) on phase assemblage in four synthetic rock compositions. Jour. Geol. 83: 1-31.